**Tese de Doutorado**

# Métodos Estocásticos e de Teoria de Campos Aplicados a Problemas Motivados na Ecologia e Oncologia

Renato Vieira dos Santos

26 de Julho 2013

*Universidade Federal de Minas Gerais,*
*Instituto de Ciências Exatas,*
*Departamento de Física*

UFMG

Orientador: Ronald Dickman

# Resumo

Esta tese de doutorado utiliza métodos estocásticos e de teoria de campos para tratar dois temas diferentes:

- A dinâmica populacional das células tronco do câncer nos tumores em geral.
- Análises de processos ecologicamente motivados formulados na rede, utilizando técnicas de mecânica estatística de não equilíbrio.

No primeiro caso são aplicadas técnicas estocásticas para obtermos as distribuições de probabilidade para a densidade populacional das chamadas células tronco do câncer, com o objetivo de propor uma explicação para uma controvérsia relacionada à frequência com que estas células aparecem nos tumores. Utiliza-se também, em um outro trabalho e para o mesmo fim, a teoria de campo médio de Weiss, bem como técnicas matemáticas para a obtenção do que às vezes é chamado de tamanho crítico de Kierstead-Skellam-Slobodkin*. Os resultados destes estudos foram aceitos para publicação em [1] e em [2].

No segundo caso utiliza-se técnicas de teoria estatística de campos em modelos inspirados em problemas de ecologia teórica. Primeiramente estudamos um modelo onde dois processos de contato são acoplados por um mecanismo do tipo simbiótico e os expoentes críticos foram obtidos. Este trabalho está publicado em [3]. Posteriormente estudamos um modelo onde, sob certas circunstâncias, populações escassas podem apresentar maiores chances de sobrevivência no longo prazo quando comparadas às chances de populações mais numerosas. A este fenômeno demos o nome de *sobrevivência do mais escasso no espaço*. Este artigo é uma extensão que leva em conta a distribuição espacial para um modelo previamente proposto e seus resultados foram aceitos para publicação em [4].

Temos em seguida um modelo que propõe uma explicação para o problema da existência da reprodução sexuada na natureza, apesar de todos os custos, quando se compara com o método rival de reprodução, a reprodução assexuada. Este artigo foi submetido para publicação em [5].

Finalmente temos um modelo onde o fenômeno da *discreteza induzindo coexistência* ocorre. Neste caso há a indução de coexistência entre duas espécies quando se leva em consideração o caráter discreto das interações e as subsequentes flutuações estatísticas, como modeladas pela equação mestra. Caso contrário, as espécies seriam extintas. Estuda-se também os efeitos das constantes de difusão das espécies. Este trabalho foi submetido para publicação em [6].

Esta tese é organizada como segue: No primeiro capítulo descrevemos de forma geral o método do grupo de renormalização dinâmico utilizado em capítulos posteriores. Utilizamos para isso um exemplo típico que demonstra muitas das características passíveis de serem descritas pelo grupo de renormalização. Utilizamos como exemplo o *processo de aniquilação de pares*. A sequência de capítulos subsequente trata dos diversos artigos publicados e submetidos para publicação. No apêndice foram colocados diversos cálculos detalhadamente feitos no que se refere ao procedimento de Doi-Peliti, que é um procedimento hoje padrão para se mapear a equação mestra de um processo estocástico na rede $d-$dimensional em uma teoria de campos equivalente. Com isso os poderosos métodos analíticos da teoria de campos ficam disponíveis.

*Ou KISS no acrônimo em inglês para Kierstead-Skellam-Slobodkin size.

# Abstract

This thesis uses stochastic and field theory methods to address two different issues:

- The population dynamics of cancer stem cells in tumors in general.
- Analyses of ecologically motivated processes formulated on lattices, using techniques of nonequilibrium statistical mechanics.

In the first case stochastic techniques are applied to obtain the probability distributions for the population density of the so-called cancer stem cells, with the aim to propose an explanation for a controversy related to the frequency with which these cells appear in tumors. In another paper mean-field theory is used to obtain the critical size defined by Kierstead-Skellam-Slobodkin [†]. The results of these studies have been accepted for publication in [1] and [2].

In the second case we use techniques from statistical field theory in models inspired by problems of theoretical ecology. First we study a model where two contact processes are coupled by a symbiotic mechanism and critical exponents were obtained. This work is published in [3]. Subsequently we study a model in which, under certain circumstances, scarce populations may have higher chances of survival in the long run when compared to the chances of the larger populations. This phenomenon was called *survival of scarcer space*. This article is an extension that takes into account the spatial distribution of a model previously proposed and their results were accepted for publication in [4].

We next discuss a model which proposes an explanation for the problem of the existence of sexual reproduction in nature, despite all its costs when compared with the rival method of asexual reproduction. This article was submitted for publication in [5].

Finally we have a model where the phenomenon of *discreteness inducing coexistence* occurs. In this case there is the induction of coexistence between two species when one takes into account the discrete character of the interactions and subsequent statistical fluctuations, as modeled by the master equation. Otherwise, one of the species would be extinct. We also studied the effects of varying diffusion rates of the species. This work was submitted for publication in [6].

This thesis is organized as follows: In the first chapter we describe the method of dynamic renormalization group used in later chapters. We use a typical example, the *process of annihilation of pairs* that demonstrates many of the characteristics that can be described by the renormalization group. The subsequent chapters deals with several articles published and submitted for publication. The Appendix contains details of various calculations using the Doi-Peliti procedure, which today is a standard procedure for map the master equation of a stochastic $d-$dimensional lattice into of a field theory. In this way the powerful analytical methods of field theory are made available.

[†]Or KISS, the acronym for Kierstead-Skellam-Slobodkin size in tumor growth.

# Agradecimentos

Uma das alegrias da conclusão foi olhar para trás e lembrar de todos os amigos e familiares que me ajudaram e me apoiaram ao longo desta longa, mas gratificante estrada.

Eu gostaria de expressar minha sincera gratidão ao Professor Ronald Dickman, que não é apenas meu mentor, sempre solidário e paciente, mas também um querido amigo. Eu não poderia ter pedido por melhores exemplos de competência, profissionalismo e de pessoa, bem como de fonte de inspiração. Eu não poderia estar mais orgulhoso das minhas raízes acadêmicas e espero que eu possa, por sua vez, transmitir os valores da pesquisa que me foram passados.

Gostaria também de agradecer aos meus examinadores, Professor Ricardo Schwartz Schor, Professor João Antônio Plascak, Professor Itzhak Roditi, Professor Allbens Atman Picardi Faria e Professor Welles Antônio Martinez Morgado, que forneceram incentivos e um feedback construtivo. Não é uma tarefa fácil a revisão de uma tese, e eu sou grato por seus comentários inteligentes e detalhados.

Esta tese foi financiada pelo Conselho Nacional de Desenvolvimento Científico e Tecnológico (CNPq), e eu gostaria de agradecer a esta organização por seu apoio generoso.

Para os funcionários, em particular para Shirley Maciel, para os colegas da Universidade Federal de Minas Gerais, e para o nosso grupo de mecânica estatística, Adailton, Alexandre, Bruno, Lobão, Luciana, Marcos e Ricardo: Obrigado por me acolher como um amigo e ajudar a desenvolver as idéias nesta tese. Eu sou grato pela oportunidade de ser parte do grupo.

E por último, mas não menos importante, agradeço imensamente à Linaena, que compartilha minhas paixões, e cujo apoio foi fundamental para que a realização desta tese fosse possível.

Renato Vieira dos Santos
Belo Horizonte, Julho de 2013.

# Sumário

Capítulo 1

# Introdução

A mecânica estatística é um dos mais antigos braços da física teórica e ainda um atual campo de pesquisa da física moderna. Lida com sistemas físicos em que as propriedades macroscópicas podem ser inferidas de uma descrição microscópica [7, 8, 9, 10, 11, 12, 13]. Ela é dividida em mecânica estatística de equilíbrio e mecânica estatística de não equilíbrio. Apesar de muitas técnicas matemáticas terem sido desenvolvidas para estudar sistemas em equilíbrio, o exame de sistemas de muitos corpos em não equilíbrio ainda é uma tarefa desafiadora para a física teórica, pois conceitos mais gerais e mais elaborados são necessários. A necessidade de se estudar física estatística de não equilíbrio surge da sua relevância em descrever os processos da natureza. A maioria dos sistemas são expostos a uma interação com outros sistemas resultando em um fluxo de energia e matéria e portanto não pode ser descrita em termos da termodinâmica de equilíbrio.

O foco deste capítulo será:

- Estudar os sistemas de muitas partículas que se difundem reagindo umas com as outras de uma maneira definida e prover a modelagem correta de tais sistemas com o objetivo de explicar as observações experimentais ou computacionais. Tal estudo fornecerá a base teórica e conceitual necessária ao entendimento de capítulos posteriores.

Em geral estaremos interessados em duas questões relacionadas a estes processos de *reação e difusão:* O primeiro ponto se ocupa da existência de um estado estacionário, ou seja, do estado onde a densidade de partículas não muda com o tempo e, em caso de existência, sua dependência espacial. A segunda questão, sendo naturalmente muito mais difícil de responder, examina a forma com que o sistema se aproxima do estado estacionário. Como estaremos interessados no comportamento assintótico de tais sistemas, poderemos sempre assumir que estes sistemas se encontram no regime limitado por difusão, onde *densidades baixas de partículas estão presentes e a dinâmica será dominada pela taxa de difusão*.

Macroscopicamente, a evolução temporal destes sistemas é às vezes modelada por equações diferenciais ordinárias (EDOs) para a quantidade observável de interesse. Essas variáveis podem ser, por exemplo, a densidade populacional média, concentração química ou a magnetização.

Incluindo também os graus de liberdade espaciais, as variáveis se tornam funções locais e devemos utilizar equações diferenciais parciais (EDPs). Desta forma, comportamentos macroscópicos emergentes podem ser revelados tais como a formação de padrões e a propagação de frentes de onda [14].

Entretanto, devido às interações subjacentes entre os constituintes do sistema, correlações entre as partículas podem surgir, possivelmente induzindo fenômenos coletivos, que envolvem oscilações temporais denominadas quasi-ciclos [15], formação de padrões [16], geração [17] e exacerbação [18] do efeito Allee [19, 20], etc. A importância deste *ruído interno* na dinâmica macroscópica destes sistemas tem sido estudada extensivamente nos anos recentes [21], causando o surgimento de uma enxurrada de artigos nesta

área [22]. Este fato indica uma grande efervescência na pesquisa com fenômenos estocásticos relacionados ao inevitável caráter discreto das interações.

Muitos destes sistemas exibem comportamento de escala universal em sua evolução temporal para o estado estacionário. Este comportamento crítico pode ser descrito por leis de potência, com expoentes críticos para o parâmetro de ordem que caracterizam as propriedades assintóticas do sistema. Por exemplo, a taxa efetiva de reação do processo de reação-difusão pode mudar na presença de flutuações e correlações.

Entretanto, a descrição da dependência temporal de sistemas estocásticos de muitas partículas realizando processos de reação e difusão em termos de EDOs e EDPs, negligenciam inteiramente as correlações e variações espaciais, e são denominadas de *descrições de campo médio.* Às vezes não é possível explicar o comportamento de escala correto para os expoentes críticos aplicando a *teoria de campo médio*, mas o surgimento destes fenômenos sugere o uso de métodos conhecidos da *teoria estatística de campos* [12].

Um dos grandes sucessos da física teórica nas últimas décadas foi a explicação das classes universalidade e leis de escala na física da matéria condensada e física de partículas. A teoria estatística de campos fornece o ferramental matemático para estudar estes sistemas. Tais ferramentas são as técnicas do *grupo de renormalização* e *teoria de perturbação*.

A primeira parte desta tese lida exatamente com a aplicação destas técnicas aos sistemas de reação-difusão de modo a ir além dos métodos baseados em teoria de campo médio. Entretanto, por questões de simplicidade e clareza, iremos nos restringir neste capítulo ao *processo de aniquilação de pares* $A+A \xrightarrow{\lambda} \emptyset$, um processo de reação-difusão específico que será explicado com mais detalhes depois.

Primeiramente, a teoria de campo médio para o processo de aniquilação de pares será utilizada e as suas características serão comparadas aos experimentos e simulações numéricas. Para que possamos generalizar o modelo e aplicar os métodos de teoria estatística de campos, utilizaremos uma abordagem baseada em redes regulares $d-$dimensionais, que serão os ambientes onde os processos de reação-difusão ocorrerão. Baseados na descrição dos processos de reação-difusão na rede, a equação mestra será reformulada em termos de operadores de criação e eniquilação, em analogia com a mecânica quântica no espaço de Fock [23]. Esta formulação fornece uma descrição adequada para sistemas com *número de partículas variáveis.* Esta descrição permite uma formulação em termos de integrais funcionais e uma teoria de campo é obtida. Renormalizando a teoria de campo, o comportamento universal de escala e os expoentes críticos corretos para a forma como o sistema se aproxima do estado estacionário podem ser extraídos.

## 1.1. Processo de reação-difusão de aniquilação de pares

Vamos examinar e exemplificar as características dos problemas que surgem na análise de sistemas de reação-difusão, utilizando o processo de um único tipo de partícula denominado processo de aniquilação de pares

$$A+A \xrightarrow{\lambda} \emptyset \quad + \quad \text{difusão.} \tag{1.1}$$

As partículas da espécie $A$ difundem no espaço e se aniquilam mutuamente com uma taxa de reação $\lambda$. Vamos investigar este sistema simples de reação-difusão porque todas as principais características do comportamento crítico podem ser extraídas analiticamente.

O estado estacionário deste processo é muito simples. Dependendo da condição inicial, se começamos com um número par ou ímpar de partículas, o estado estacionário irá conter 0 partículas (espaço vazio) ou somente uma partícula irá sobrar. O foco da nossa análise estará na questão de *como* o sistema se aproxima do estado estacionário.

## 1.2. Campo médio

Sistemas de reação-difusão são geralmente estudados em termos de equações diferenciais [24, 25]. Em um espaço $d-$dimensional com uma dimensão temporal, elas são equações para a densidade média de partículas e para o processo de aniquilação de pares (em $d = 1$) teremos:

$$\frac{\partial}{\partial t}\rho(x,t) = \underbrace{D\nabla^2\rho(x,t)}_{\text{difusão}} - \underbrace{\lambda\rho^2(x,t)}_{\text{reação}} \tag{1.2}$$

com a condição inicial $\rho(x,0) = f(x)$. O primeiro termo no lado direito está relacionada à difusão e o segundo termo, à aniquilação. Se negligenciarmos momentâneamente o termo difusivo, obteremos a equação cinética

$$\frac{d}{dt}\rho(t) = -\lambda\rho^2(t) \tag{1.3}$$

que é uma equação diferencial ordinária com solução dada por

$$\rho(t) = \frac{1}{\frac{1}{\rho(0)} + \lambda t}, \tag{1.4}$$

onde $\rho(0)$ denota a densidade inicial de partículas no tempo $t_0 = 0$. Esta solução (1.4) se comporta assintoticamente como $\rho \sim t^{-1}$.

Se retornarmos ao sistema não homogêneo, os efeitos da difusão deverão ser levados em conta. Mas os efeitos da difusão tendem a uniformizar a distribuição de partículas e a solução da equação (1.2) irá realizar o mesmo comportamento de escala assintótico para o decaimento temporal na equação (1.4). Afinal, para $\rho \ll 1$ temos $\rho^2 \ll \rho$ de modo que a difusão domina a dinâmica, até o momento em que $\rho$ seja essencialmente uniforme.

Entretanto, resultados rigorosos [26] mostram que o comportamento assintótico depende da dimensão $d$ da rede e portanto tal abordagem via EDPs é uma descrição inerentemente inadequada. Para o processo de aniquilação de pares, encontramos

$$\rho(x,t) \sim \begin{cases} t^{-1/2} & \text{se } d = 1 \quad \text{(descrição em termos de EDPs é incorreta)} \\ \ln t \cdot t^{-1} & \text{se } d = 2 \quad \text{(descrição em termos de EDPs é incorreta)} \\ t^{-1} & \text{se } d > 2 \quad \text{(descrição em termos de EDPs é correta)} \end{cases} \tag{1.5}$$

De fato, tal abordagem de campo médio negligencia quaisquer flutuações e correlações espaciais no sistema. Iremos incluir as flutuações estatísticas na nossa análise e iremos reescrever o processo de aniquilação de pares em termos da teoria estatística de campos. Aplicando os métodos de grupo de renormalização dinâmico [27], obteremos o comportamento assintótico temporal correto.

## 1.3. Descrição em termos da teoria estatística de campos

Seguindo os passos detalhadamente descritos nos apêndices (A) e (B), a ação para o processo de aniquilação de pares pode ser escrita como

$$S[\tilde{\phi}(x,t),\phi(x,t)] = \int d^dx \left\{ \int_0^t d\tau\, \mathcal{L}\left[\tilde{\phi}(x,\tau),\phi(x,\tau)\right] - \rho_0\tilde{\phi}(x,0) \right\}, \tag{1.6}$$

com

$$\mathcal{L}[\tilde{\phi}(x,t),\phi(x,t)] = \underbrace{\tilde{\phi}(\partial_t - D\nabla^2)\phi}_{\text{difusão pura}} + \underbrace{2\lambda\tilde{\phi}\phi^2 + \lambda\tilde{\phi}^2\phi^2}_{\text{reação } A+A\xrightarrow{\lambda}\emptyset}, \tag{1.7}$$

onde a parte bilinear do Lagrangeano $\mathcal{L}$ corresponde ao processo de difusão pura e as interações de maior ordem representam o termo de reação $A+A \xrightarrow{\lambda} \emptyset$. As equações (1.5), (1.6) e (1.7) serão os pontos de partida para a análise posterior. A integral funcional junto com a ação constroem a base da análise via teoria estatística de campos para o processo de aniquilação de pares.

O número médio de partículas $\bar{n}$ no limite contínuo se torna a densidade média de partículas $\rho$ e é igual à média do campo $\rho(x,t) = \langle \phi(x,t) \rangle$,

$$\rho(x,t) = \frac{\int \mathcal{D}[\tilde{\phi}(x,t)]\mathcal{D}[\phi(x,t)]\ \phi(x,t)\ e^{-S[\tilde{\phi}(x,t),\phi(x,t)]}}{\int \mathcal{D}[\tilde{\phi}(x,t)]\mathcal{D}[\phi(x,t)]\ e^{-S[\tilde{\phi}(x,t),\phi(x,t)]}} = \langle \phi(x,t) \rangle \equiv G_1(x,t). \tag{1.8}$$

Mostraremos posteriormente como calcular (1.8) perturbativamente.

Podemos generalizar este procedimento para outras reações. A única mudança necessária é o estabelecimento do Lagrangeano da teoria, o que nos leva a ter de encontrar o Hamiltoniano microscópico na rede.

## 1.4. Observações referentes à teoria de campos

### 1.4.1. Equações de campo clássicas

Vamos obter as equações clássicas de campo referentes à ação (1.6). Para obtermos as soluções estacionárias da ação, devemos calcular

$$\frac{\partial S}{\partial \phi} = \frac{\partial S}{\partial \tilde{\phi}} \equiv 0, \tag{1.9}$$

que são resolvidas por $\tilde{\phi} = 0$ e $(\partial_t - D\nabla^2)\phi + 2\lambda\phi^2 = 0$. Tomando a esperança matemática desta última, temos

$$(\partial_t - D\nabla^2)\langle \phi \rangle + 2\lambda \langle \phi^2 \rangle = 0,$$

$$\Rightarrow \frac{\partial}{\partial t}\rho(x,t) = D\nabla^2 \rho(x,t) - 2\lambda \langle \phi^2 \rangle,$$

que tem a forma parecida com a equação (1.2). A diferença entre estas equações está na diferença entre os termos de reação. Se assumirmos que podemos fatorar o termo $\langle \phi^2 \rangle$ na forma $\langle \phi^2 \rangle = \langle \phi \rangle^2 = \rho^2$, obtemos a equação (1.2). Mas assumir $\langle \phi^2 \rangle = \langle \phi \rangle^2$ é correto somente na ausência de flutuações e correlações espaciais.

## 1.5. Expansão diagramática

Vamos resumir os resultados obtidos na última seção. Reescrevemos a descrição estocástica microscópica da reação de aniquilação de pares (1.1) em termos da equação mestra em uma teoria de campos (1.6, 1.7) utilizando o formalismo da segunda quantização no limite contínuo. Estamos agora na posição de calcular a função de um ponto $\langle \phi(x,t) \rangle$ via equação (1.8), que inclui os efeitos das flutuações estatísticas. Para isso, vamos aplicar os métodos da teoria de campos, em particular, métodos perturbativos e de grupo de renormalização para calcular $\langle \phi(x,t) \rangle$.

Para calcular $\langle \phi(x,t) \rangle$, definimos o funcional gerador $Z[\tilde{h},h]$ introduzindo fontes de campo externas $\tilde{h},h$, linearmente acopladas aos campos $\tilde{\phi},\phi$ na ação:

$$Z[\tilde{h},h] \equiv \int \mathcal{D}[\tilde{\phi}]\mathcal{D}[\phi]\ \exp\left\{ -S[\tilde{\phi},\phi] - \int_{x,\tau} \left( \tilde{h}\tilde{\phi} + h\phi \right) \right\}, \tag{1.10}$$

onde a notação $\int_{x,\tau}\cdots \equiv \int d^dx \int_0^t d\tau \cdots$ foi usada. Então, a função de um ponto pode ser computada tomando a primeira derivada funcional do funcional gerador com relação ao campo de fonte $h$ e fazendo $\tilde{h} = h = 0$,

$$G_1 = \langle \phi \rangle = \frac{1}{Z[0,0]} \frac{\delta}{\delta h} Z[\tilde{h}, h]\Big|_{\tilde{h}=h=0}. \tag{1.11}$$

O objetivo é agora calcular o funcional gerador $Z[\tilde{h}, h]$, o que pode ser feito perturbativamente.

### 1.5.1. Teoria de campo livre: difusão pura

Para calcular o funcional gerador $Z[\tilde{h}, h]$ e então calcular $\rho$ via (1.8) ou (1.11) perturbativamente, temos que estabelecer uma teoria, normalmente denominada teoria de campo livre, que pode ser resolvida exatamente. Usualmente, ela consistirá da parte bilinear na ação, cuja integração funcional pode ser realizada exatamente (pelo menos formalmente) realizando integrações funcionais Gaussianas em torno da qual uma expansão perturbativa pode ser formulada.

Para o processo de aniquilação de pares, a parte bilinear da ação ($S_0[\tilde{\phi}, \phi]$) é a seguinte:

$$S_0[\tilde{\phi}, \phi] = \int d^dx \int_0^t d\tau \, \tilde{\phi} \underbrace{(\partial_t - D\nabla^2)}_{\equiv O(\tau,x)} \phi. \tag{1.12}$$

Na equação acima definimos o operador $O(\tau, x) \equiv \partial_t - D\nabla^2$. O funcional gerador relacionado a esta ação da teoria livre, $Z_0[\tilde{h}, h]$, pode ser escrito como

$$Z_0[\tilde{h}, h] \equiv \int \mathcal{D}[\tilde{\phi}]\mathcal{D}[\phi] \, \exp\left\{ -\int_{x,\tau} \left( \tilde{\phi} O \phi + \tilde{h}\tilde{\phi} + h\phi \right) \right\}. \tag{1.13}$$

Se definirmos o operador inverso $O^{-1}$ do operador difusão como segue,

$$O(x,t) O^{-1}(x',t') = \delta(x - x')\delta(t - t'), \tag{1.14}$$

podemos completar o quadrado na equação (1.13) com a substituição $\phi \to \phi + \int_{x,\tau} O^{-1}\tilde{h}$ e realizar a integração Gaussiana, obtendo

$$\begin{aligned} Z_0[\tilde{h}, h] &= \int \mathcal{D}[\tilde{\phi}]\mathcal{D}[\phi] \, \exp\left\{ -\int_{x,\tau} \tilde{\phi} O \phi + \int_{x,\tau}\int_{x',\tau'} h O^{-1} \tilde{h} \right\} \\ &= Z_0[0,0] \, \exp\left\{ \int_{x,\tau}\int_{x',\tau'} h O^{-1} \tilde{h} \right\}, \end{aligned} \tag{1.15}$$

que é o resultado exato da teoria de campo livre.

#### Propagador: o inverso do operador difusão

A forma explícita do operador inverso $O^{-1}$ precisa ser especificada. Isto pode ser feito aplicando a transformada de Fourier à equação (1.14). Este procedimento é comum em teorias de campos [28]. No espaço de Fourier,

$$O^{-1}(q, \omega) = \frac{1}{Dq^2 - i\omega} \equiv G_0(q, \omega). \tag{1.16}$$

Convenientemente, ao operador inverso da teoria de campo livre é dado um rótulo próprio, aqui $G_0(q,\omega)$. $G_0(q,\omega)$ é o propagador da nossa teoria de campo livre,

$$\langle\phi(q,\omega)\tilde{\phi}(q',\omega')\rangle_0 = (2\pi)^{d+1}\delta(q+q')\delta(\omega+\omega')G_0(q,\omega), \tag{1.17}$$

onde as médias com relação ao campo livre são denotadas como $\langle\rangle_0$.

Se retornarmos ao domínio do tempo aplicando a transformada inversa de Fourier apenas na coordenada temporal, obteremos

$$G_0(q,t) = \frac{1}{2\pi}\int d\omega\, e^{-i\omega t}G_0(q,\omega) = \Theta(t)\, e^{-Dq^2t}, \tag{1.18}$$

com a função de Heaviside definida por

$$\Theta(t) = \begin{cases} 1 & \text{se } t \geq 0, \\ 0 & \text{se } t < 0. \end{cases}$$

Então o propagador $G_0$ inerentemente representa uma ordem causal dos campos $\phi$ e $\tilde{\phi}$, já que somente campos anteriores $\tilde{\phi}$ são conectados a campos posteriores $\phi$,

$$\langle\phi(q,t)\tilde{\phi}(q',t')\rangle_0 \propto \Theta(t-t')\, e^{-D(q-q')^2(t-t')}.$$

Esta é uma característica crucial do propagador da difusão sob a qual a estrutura dos diagramas de Feynman na expansão perturbativa é restringida. Veremos suas consequências na próxima seção.

## 1.6. Perturbação em torno da difusão

Vamos retornar ao nosso objetivo inicial, o cálculo do funcional gerador $Z[\tilde{h},h]$ para a ação (1.6), (1.7) e o respectivo cálculo da função de um ponto $\langle\phi(x,t)\rangle$ via (1.11). O funcional gerador pode ser escrito como segue,

$$\begin{aligned}
Z[\tilde{h},h] &= \int \mathcal{D}[\tilde{\phi}]\mathcal{D}[\phi]\ \exp\left\{-S[\tilde{\phi},\phi] - \int_{x,\tau}(\tilde{h}\tilde{\phi}+h\phi)\right\} \\
&= \int \mathcal{D}[\tilde{\phi}]\mathcal{D}[\phi]\, e^{-S_0}\ \exp\left\{-\int_{x,\tau}\left(2\lambda\tilde{\phi}\phi^2+\lambda\tilde{\phi}^2\phi^2\right)\right\} e^{-\int_{x,\tau}(\tilde{h}\tilde{\phi}+h\phi)} \\
&\quad \text{com condição inicial (c.i.) } \phi(x,0)=\rho_0(x) \\
&= \exp\left\{-\int_{x,\tau}\left(2\lambda\frac{\delta}{\delta\tilde{h}}\frac{\delta^2}{\delta h^2}+\lambda\frac{\delta^2}{\delta\tilde{h}^2}\frac{\delta^2}{\delta h^2}\right)\right\} Z_0[\tilde{h},h] + \text{c.i.} \\
&\overset{1.15}{=} Z_0[0,0]\ \exp\left\{-\int_{x,\tau}\left(2\lambda\frac{\delta}{\delta\tilde{h}}\frac{\delta^2}{\delta h^2}+\lambda\frac{\delta^2}{\delta\tilde{h}^2}\frac{\delta^2}{\delta h^2}\right)\right\} \exp\left\{\int_{x,\tau}\int_{x',\tau'} hG_0\tilde{h}\right\} + \text{c.i.}
\end{aligned} \tag{1.19}$$

A idéia agora é expandir a exponencial com os termos de reação no parâmetro de acoplamento $\lambda$ de acordo com $e^{\lambda x} = \sum_n(\lambda x)^n/n!$. Fazendo isso, teremos uma expansão perturbativa "em torno" do termo de difusão, onde as reações constituem as perturbações.

*Fisicamente, esta forma de expandir o funcional gerador faz sentido, já que estamos interessados no comportamento temporal assintótico da função de um ponto $\langle\phi\rangle$, ou seja, em um regime dominado por difusão. As reações são consideradas pequenas perturbações ao caso da pura difusão.*

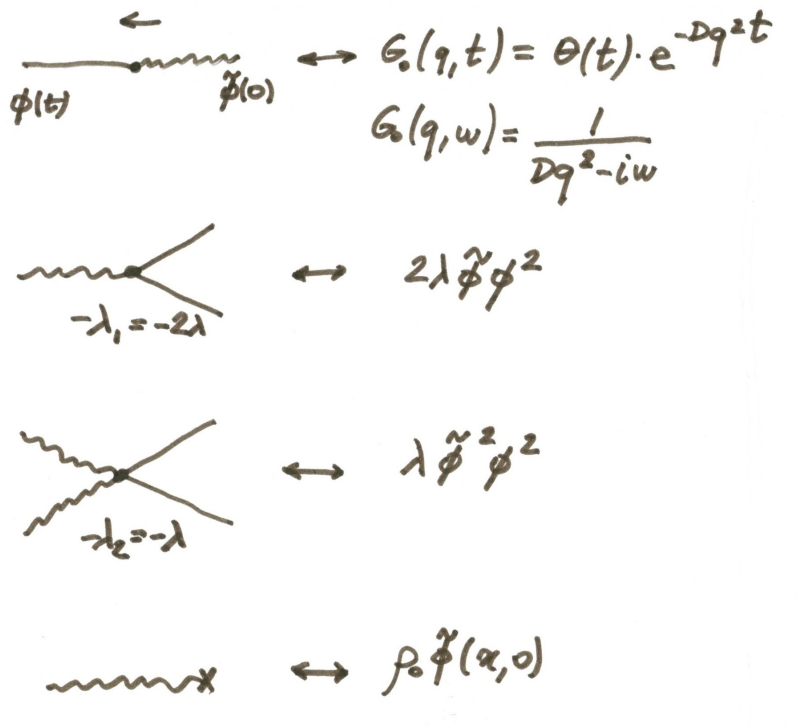


Figura 1.1.: Propagador e vértices para a reação de aniquilação de pares.

Por razões de clareza e simplicidade, usualmente denotamos esta série perturbativa em termos dos chamados diagramas de Feynman [29]. Cada diagrama nesta notação gráfica corresponde a uma expressão em termos de integrais de acordo com a seguinte identificação:

Por exemplo, o termo $2\lambda\tilde{\phi}\phi^2$ corresponde a um vértice que conecta dois propagadores que entram no vértice com um propagador que sai do vértice. A estrutura causal do propagador do processo de reação-difusão assegura ordenamento temporal, já que o tempo aumenta da direita para a esquerda em um diagrama de Feynman.

As regras de Feynman para se construir todos os diagramas que contribuem para $\langle\phi(x,t)\rangle$ são mais convenientemente formuladas no espaço de momentos, já que estamos lidando com um sistema translacionalmente invariante no espaço e no tempo. Elas podem ser resumidas como segue [28]:

- Desenhe todos os diagramas com uma perna externa à esquerda e com pernas iniciais à direita.
- Cada linha corresponde ao propagador $G_0$ (figura (1.1)).
- Os dois vértices (figura (1.1)) conectam linhas internas. Um 3-vértice carrega um fator de $-\lambda_1 = -2\lambda$, e um 4-vértice contribui com um fator $-\lambda_2 = -\lambda$.
- Integramos sobre cada laço de momento $p$ com medida $\frac{1}{(2\pi)^d}\int d^d p\cdots$ e sobre cada tempo indeterminado $t_0$ com medida $\int_{t'}^{t''} dt_0\cdots$.
- Impomos conservação de momento em cada vértice. O propagador final deve ter $q = 0$ (uniformidade espacial) e todos os propagadores conectados com uma perna inicial (figura (1.1)) também deve ter $q = 0$, por causa da condição inicial no espaço de Fourier. Cada perna inicial carrega um fator $\rho_0$.
- Incluir um fator de simetria para cada diagrama sendo igual ao número de possibilidades de conectar um propagador interno a um vértice.

Figura 1.2.: Laços em um instante retornam zero devido à estrutura causal do propagador.

Note que laços em um tempo específico $t'$ não são considerados (1.2), devido ao ordenamento temporal e estrutura causal do propagador $G_0(t) = \Theta(t)\ e^{-Dq^2 t}$. Uma integração sobre cada laço é proporcional à integral

$$\int_{t'}^{t''} dt\ G_0(q,0) = 0.$$

Para a função de um ponto, a expansão diagramática, de acordo com as regras de Feynman, retorna

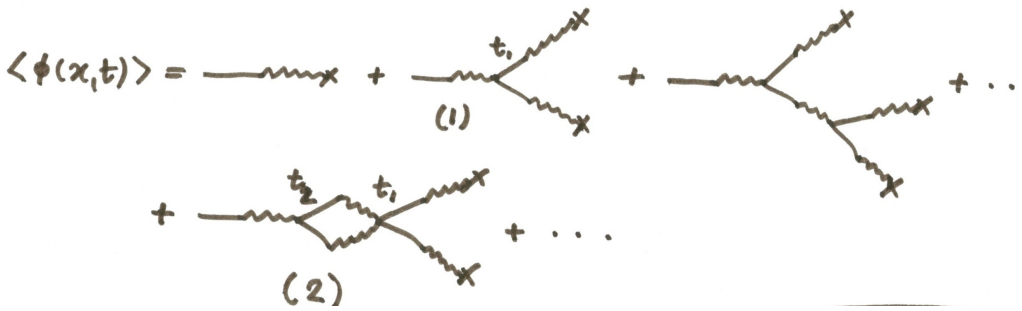


Figura 1.3.: Expansão diagramática para a função de um ponto.

Para exemplificar a correspondência entre os diagramas e as expressões em termos de integrais, vamos olhar mais detalhadamente duas delas, identificadas como (1) e (2) na figura (1.3):

$$(1) = \int_0^t dt_1\ G_0(0,t-t_1)(-\lambda_1)G_0(0,t_1)^2\ \rho_0^2 \propto -\lambda_1 \rho_0^2 t,$$

$$(2) = \int_0^t dt_2 \int_0^{t_2} dt_1\ G_0(0,t-t_2)(-\lambda_1)\times$$

$$\times \int \frac{d^d p}{(2\pi)^d} G_0(p,t_2-t_1)(-\lambda_2)G_0(-p,t_2-t_1)2G_0(0,t_1)^2\rho_0^2.$$

A primeira integral $(1)$ corresponde a um decréscimo linear da densidade inicial no tempo, mas a segunda integral $(2)$ demonstra um problema no nosso procedimento perturbativo, já que ela diverge. Para ver isso, considere um acoplamento efetivo $\lambda_{\rm ef}$, sendo parte da expressão integral acima, dado pela expressão

$$I(t_2) \equiv -\lambda_{\rm ef} = \int_0^{t_2} dt_1 \int \frac{d^d p}{(2\pi)^d} G_0(p,t_2-t_1)(-\lambda_2)G_0(-p,t_2-t_1)2 \propto -\lambda_2\ t_2^{1-d/2}, \quad (d \neq 2,4). \quad (1.20)$$

Temos que distinguir entre dois casos dependendo da dimensão $d$. O comportamento qualitativo muda na dimensão crítica $d_c = 2$ [27].

- $d < d_c = 2$ : Para tempos pequenos $t \to 0$, $I(t)$ é finito e a expansão perturbativa é finita. Este limite é também denominado de *limite ultravioleta* (UV) ($q, \omega \to \infty$). Para tempos longos $t \to \infty$, ($I(t)$) diverge e a teoria de perturbação falha. Este limite é denominado *limite infravermelho* (IV) ($q, \omega \to 0$).
- $d > d_c = 2$ : Teoria de perturbação falha para $t \to 0$, mas funciona para $t \to \infty$.

As divergências UV para $d \geq 2$ são causadas pelo limite contínuo (ver apêndices), onde o espaçamento da rede $a \to 0$. Fisicamente, sempre existirá um corte de curta distância $\Lambda$ que pode ser introduzido "à mão" na análise que resolve a divergência UV.

Em contraste, a divergência IV para $d \leq 2$, que é o caso de interesse, é mais problemática, já que a série perturbativa não pode ser obtida por um argumento físico como feito para o caso UV. Apesar disso, é possível extrair o comportamento de escala correto para a densidade média de partículas mesmo para $d \leq 2$ utilizando os métodos do grupo de renormalização que serão descritos posteriormente.

### 1.6.1. Diagramas em árvore correspondem à teoria de campo médio

Vamos olhar mais de perto para os diagramas em árvore, ou seja, os diagramas de Feynman *sem* laços.

Figura 1.4.: Expressão iterativa para os diagramas em árvore.

Para a soma de todos os diagramas em árvore $\rho_{\text{tree}}$, obtemos a seguinte expressão:

$$\rho_{\text{tree}}(t) = \rho_0 - \lambda_1 \int_0^t dt_1 \, \rho_{\text{tree}}(t_1)^2. \tag{1.21}$$

Tomando a derivada temporal desta equação, obteremos a equação da teoria de campo médio obtida anteriormente para o processo de aniquilação de pares com a condição inicial correta (1.2). Deste modo, toda a análise baseada nos diagramas em árvore corresponde a equação diferencial parcial da teoria de campo médio e as flutuações e correlações são representadas pelas expressões integrais representadas pelos laços nos diagramas. A análise das correções devidas às flutuações terão um importante papel na seção seguinte.

## 1.7. Renormalização

Nas últimas seções vimos como calcular $\langle \phi(x,t) \rangle$ perturbativamente. Entretanto, esta abordagem deu origem a divergências no limite IV para tempos assintóticos abaixo da dimensão crítica $d_c = 2$. Métodos de renormalização conseguirão tornar finitos os resultados para os diagramas em laço que em princípio são divergentes. O custo desta operação é que alguns parâmetros da teoria irão depender de um corte $\Lambda$ introduzido na análise. O comportamento de escala é extraido pelos métodos do *grupo de renormalização dinâmico* [27].

### 1.7.1. Divergências UV primitivas

Queremos investigar as divergências UV primitivas que encontramos na expansão diagramática de $\langle\phi(x,t)\rangle$ em $d=2$. Estas divergências são chamadas de primitivas por serem superficiais e poderem ser removidas por um corte de curta distância $\Lambda^{-1}$. A dependência em $\Lambda^{-1}$ será reescrita em termos da regularização dimensional [28]. Apenas os diagramas conectados amputados serão examinados, já que são os laços contidos neles é que causam as divergências. O "amputado" se refere ao fato que os propagadores das linhas externas são desprezados. A soma de todos os diagramas conectados amputados para a função de $n-$pontos é denotada por $\hat{F}_n(q,\omega)$.

Divergências primitivas tem sua origem nas integrais associadas aos laços, então $\hat{F}$ pode ser escrito como

$$\hat{F} \propto \int dp^{dL} \frac{1}{(Dp^2 - i\omega)^I} \propto \int_0^\infty d|p|\ |p|^{dL-1} \frac{1}{(Dp^2 - i\omega)^I}, \tag{1.22}$$

onde $L$ denota o número de laços no diagrama de Feynman e $I$ o número de linhas internas. O diagrama corresponde a uma integral UV divergente se o grau superficial de divergência $\text{GSD} \equiv dL - 2I \geq 0$. Apenas por razões topológicas, pode ser inferido que o grau superficial de divergência pode ser calculado como [28]

$$\text{GSD} = (d-4)L + \sum_n (n-4)V_n - E + 4. \tag{1.23}$$

$V_n$ denota o número de vértices de valência $n$ e $E$ o número de pernas externas. Entretanto, $\text{GSD} \leq 0$ não garante que um diagrama é finito, já que subdivergências não foram levadas em conta, significando que diagramas com $\text{GSD} \leq 0$ podem possuir subgráficos divergentes. Apesar disso, o grau superficial de divergência é uma ferramenta útil para analisar e resolver divergências via técnicas de renormalização.

No nosso caso, temos $d=2$ e $\text{GSD} \geq 0 \Leftrightarrow -V_3 - E + 4 \geq 2L$. Vemos que quanto mais laçoes estão envolvidos, melhores as chances para um diagrama ser bem definido. Para o pior caso com $L=0$, somente duas situações devem ser consideradas:

- $V_3 = 0$ : No caso de ausência de interações do tipo 3-vértice, segue a condição para divergência superficial: $E \leq 4$. Como a interação envolve vértices sempre com dois campos entrantes, somente diagramas com um ou dois campos que saem são permitidos.
- $V_3 = 1$ : Agora, a condição se torna $E \leq 3$ a apenas diagramas com um campo que sai são permitidos.

Assim somente dois conjuntos de diagramas de Feynman carregam divergências UV, a saber, $\hat{F}_3(q,\omega)$ e $\hat{F}_4(q,\omega)$ (figura (1.5))

Figura 1.5.: $\hat{F}_4(q,\omega)$ (esquerda) e $\hat{F}_3(q,\omega)$ (direita) contém todos os diagramas de Feynman que dão origem aos infinitos na expansão diagramática.

Note que nenhuma divergência superficial pode aparecer em $\hat{F}_2(q,\omega) = Dq^2 - i\omega$ (figura (1.6)). Isto é devido à estrutura de interação do processo de aniquilação de pares e à propriedade de ordenamento temporal do propagador com a consequência de que divergências não podem ocorrer. Portanto, o propagador

permanece inalterado durante o processo de renormalização e a constante de difusão não precisa ser renormalizada. O mesmo vale para os campos $\tilde{\phi}$, $\phi$ e, na linguagem da renormalização, temos $Z_{\tilde{\phi}} = Z_{\phi} = 1$ e $Z_D = 1$. Esta é uma característica do processo de aniquilação de pares e está em contraste com a teoria de campo escalar com interação $\phi^4$, por exemplo, onde o termo de massa precisa ser renormalizado. É então possível fazer $D = 1$ em todas as ordens na teoria de perturbação.


Figura 1.6.: Não é necessária renormalização para o propagador.

Podemos imediatamente escrever as expansões diagramáticas inteiras para $\hat{\Gamma}_3$ e $\hat{\Gamma}_4$, novamente por causa da estrutura dos vértices junto com a estrutura causal do propagador.

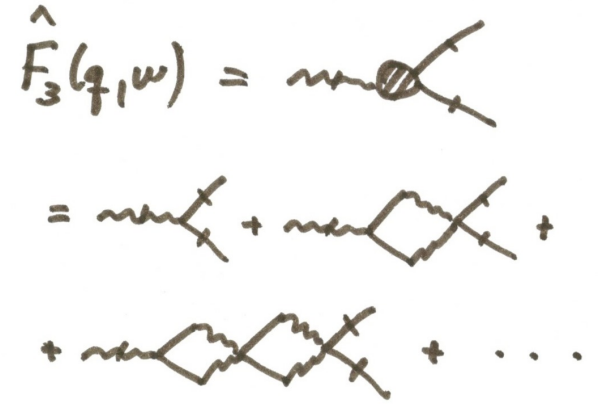


Figura 1.7.: Expansão diagramática para $\hat{\Gamma}_3$.

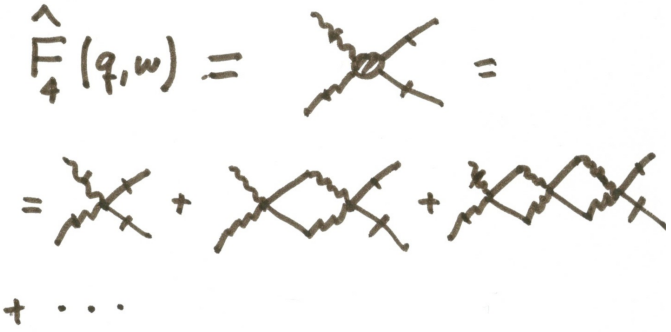


Figura 1.8.: Expansão diagramática para $\hat{\Gamma}_4$.

Denominando de $J(q,\omega)$ a expressão integral para o laço, podemos escrever $\hat{\Gamma}_3(q,\omega)$ como uma série geométrica

$$\begin{aligned}\hat{F}_3 &= -2(-2\lambda) - (-2\lambda)J(-\lambda)2^2 - (-2\lambda)J(-\lambda)J(-\lambda)2^2 \\ &= 4\lambda(1 - 2J\lambda + 2^2J^2\lambda^2 \mp \cdots) \\ &= 4\frac{\lambda}{1+2\lambda J} \equiv 4\lambda_R, \end{aligned} \tag{1.24}$$

que é um resultado exato em todas as ordens na expansão em laço. Este não é o caso na teoria escalar $\phi^4$, onde os cálculos podem ser feitos apenas ordem a ordem na expansão perturbativa.

A integral $J(q,\omega)$ pode ser calculada por regularização dimensional, onde as divergências são transformadas em pólos de funções que dependem de um parâmetro pequeno $\varepsilon \equiv 2-d$, que descreve a distância da dimensão crítica.

Podemos calcular $J(q,\omega)$ da seguinte forma:

$$\begin{aligned} J(q,\omega) &= \int \frac{d^dq'}{(2\pi)^d} \int \frac{d\omega'}{2\pi} \frac{1}{q'^2 - i\omega} \frac{1}{(q'-q)^2 - i(\omega'-\omega)} \\ &\propto \int \frac{d^dq'}{q'^2 + (q'-q)^2 - i\omega} \overset{q'\to q'/\sqrt{2}}{\propto} \int \frac{d^dq'}{q'^2 - 2q'\cdot\frac{q}{\sqrt{2}} + q' - i\omega} \\ &= \frac{\Gamma(1-d/2)}{(4\pi)^{d/2}\Gamma(1)} \cdot \frac{1}{(q^2/2 - i\omega)^{1-d/2}}, \end{aligned} \tag{1.25}$$

onde no último passo a função Gamma foi introduzida ($\Gamma(\alpha) = 1/\alpha\cdot\Gamma(\alpha+1), \Gamma(1)=1, \Gamma(1/2)=\sqrt{\pi}$) e a seguinte identidade [30]

$$\int \frac{d^dk}{(k^2 + 2k\cdot p + m^2)^s} = \frac{\Gamma(s-d/2)}{(4\pi)^{d/2}\Gamma(s)} \cdot \frac{1}{(m^2-p^2)^{s-d/2}}.$$

Com $\varepsilon = 2-d$, obtemos finalmente

$$J(q,\omega) = \frac{1}{(8\pi)^{d/2}} \cdot \Gamma\left(\frac{\varepsilon}{2}\right) \cdot \left(\frac{q^2}{2} - i\omega\right)^{-\varepsilon/2}, \tag{1.26}$$

$$\hat{F}_3 = 4 \cdot \frac{\lambda}{1 + \frac{2\lambda}{(8\pi)^{d/2}} \cdot \Gamma\left(\frac{\varepsilon}{2}\right) \cdot \left(\frac{q^2}{2} - i\omega\right)^{-\varepsilon/2}}. \tag{1.27}$$

Podemos agora reconhecer a divergência olhando para o parâmetro $\varepsilon$. Se $q=0$, a expressão para $\hat{F}_3$ para $\varepsilon > 0$ diverge quando $\omega \to 0$, representando a singularidade IV. A divergência UV é agora expressa pelos pólos da função $\Gamma$ para $\varepsilon = 0, -2, -4, \cdots$, pois $\Gamma\left(\frac{\varepsilon}{2}\right) \sim \frac{2}{\varepsilon}$ para $\varepsilon \to 0$.

## 1.8. O procedimento de renormalização

### 1.8.1. A idéia da renormalização

Começamos com uma teoria de campos cujo Lagrangeano pode ser descrito essencialmente como

$$\mathcal{L} = \mathcal{L}_0 + \mathcal{L}_{\text{int}} = \tilde{\phi}(\partial_t - D\nabla^2)\phi + 2\lambda\tilde{\phi}\phi^2 + \lambda\tilde{\phi}^2\phi^2.$$

Foi visto que em duas dimensões, as funções de $n-$pontos conectadas amputadas $\hat{F}_n(q,\omega;\lambda,\Lambda)$ apresentam divergências IV (para $q \to 0$ e $t \to \infty$) e divergências UV devido ao limite contínuo para $n = 3,4$. As boas notícias são que $\hat{F}_2$ é bem definida e finita e portanto os campos e a constante de difusão não necessitam ser renormalizados. Além disso, é possível calcular $\hat{F}_3$, $\hat{F}_4$ em todas as ordens na expansão em laços.

Foi mostrado nas equações (1.27, 1.25) que se o limite contínuo for tomado (correspondento a fazer $\Lambda \to 0$ ou equivalentemente $\varepsilon \to 0$ na regularização dimensional), o acoplamento efetivo diverge. Entretanto, na teoria, deve existir um acoplamento físico $\lambda_{\text{fis}}$, que pode ser medido em um experimento e corresponde a uma interação efetiva que está representada na figura (1.9).


Figura 1.9.: Constante de acoplamento efetiva $\lambda_{\text{fis}}$.

Então consideramos o *ansatz* $\lambda_{\text{fis}} = \lambda + \bar{\lambda} = \lambda\left(1 + \bar{\lambda}/\lambda\right)$, em que $\lambda$ é o acoplamento que aparece no Lagrangeano e $\tilde{\lambda}$ é um parâmetro introduzido que depende do corte $\Lambda$. Então, a idéia é permitir $\lambda$ depender do corte $\Lambda$, $\lambda \to \hat{\lambda}(\Lambda)$. Queremos realizar um limite mais sofisticado que é fazer $\Lambda \to \infty$ com $\hat{\lambda}(\Lambda)$ variando, mas com $\lambda_{\text{fis}}$ mantido fixo. Devemos obter respostas finitas para todas as quantidades observáveis neste limite. A existência de tal limite não é trivial, mas pode ser atingido para o processo de aniquilação de pares introduzindo um número finito de termos aditivos no Lagrangeano, também conhecidos como contra termos, e tal teoria é dita sob esta condição ser *renormalizável*. Note que, em geral, a constante de difusão $D$ assim como os campos $\tilde{\phi}$ e $\phi$ devem depender do corte $\Lambda$, mas isso não ocorre para o processo de aniquilação de pares como mencionado anteriormente.

Veremos que o procedimento mencionado acima remove as divergências, mas ao custo da variação nos parâmetros (e dos campos, quando for o caso) com o corte $\Lambda$. Na prática, as divergências podem ser canceladas adicionando contra termos ao Lagrangeano $\mathcal{L} \to \mathcal{L} + \mathcal{L}_{c.t.}$. Normalmente isto deve ser feito ordem a ordem na expansão perturbativa, mas aqui nós sabemos que as divergências em todas as ordens e podemos imediatamente escrever os contra termos necessários

$$\mathcal{L}_{c.t.} = A\tilde{\phi}\phi^2 + B\tilde{\phi}^2\phi^2,$$

de modo que novos vértices são introduzidos na expansão de $\mathcal{L} + \mathcal{L}_{c.t.}$, como mostrados na figura (1.10)

Estes novos vértices são construídos e definidos de modo a subtraírem exatamente as divergências que ocorrem no Lagrangeano original $\mathcal{L}$. Assim, levando-se em conta o resultado de (1.20) e (1.22), obtemos

$$A = \lambda_R = \frac{\lambda}{1 + \frac{2\lambda}{(8\pi)^{d/2}} \cdot \Gamma\left(\frac{\varepsilon}{2}\right) \cdot \left(\frac{q^2}{2} - i\omega\right)^{-\varepsilon/2}} = \hat{\lambda}.$$

### 1.8.2. Análise dimensional

Antes de realizar a análise de renormalização, uma análise dimensional mais precisa será feita, pois a expansão perturbativa apenas faz sentido em uma quantidade adimensional. Veremos que, a não ser em

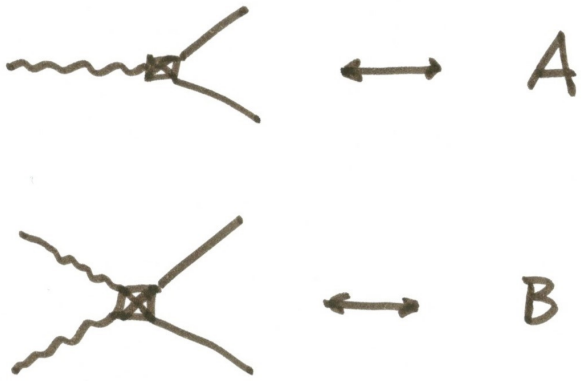


Figura 1.10.: Novos vértices devidos aos contra termos.

duas dimensões, o acoplamento $\lambda$ carrega a dimensão $\varepsilon$ e então, uma quantidade adimensional precisa ser introduzida. Portanto, vamos examinar novamente a ação

$$S[\tilde{\phi}(x,t),\phi(x,t)] = \int d^d x \left\{ \int_0^t d\tau \left[ \tilde{\phi}(\partial_t - D\nabla^2)\phi + 2\lambda\tilde{\phi}\phi^2 + \lambda\tilde{\phi}^2\phi^2 \right] - \rho_0\tilde{\phi}.(x,0) \right\}$$

A ação $S$ aparece na exponencial na integração funcional e portanto possui dimensão 0, onde as quantidades são medidas em unidades de momento, por exemplo, $\Lambda$. Assim, $[S]=0$, $[p]=1$, $[x]=-1$ e estamos livres para escolher $[D]=0$, uma constante de difusão adimensional. Segue do operador de difusão que $[1/x^2]=[1/t] \Rightarrow [t]=-2$. Além disso, temos que $[\tilde{\phi}]=0$, implicando em $[\phi]=d$ e $[\lambda]=2-d=\varepsilon$. Uma constante de acoplamento adimensional $g$ ($[g]=0$) é definida em $d=2-\varepsilon$ dimensiões pela introdução de uma escala arbitrária $\mu$ com $[\mu]=1$, sendo também denominada escala RG,

$$\lambda = g\cdot\mu^{\varepsilon} \quad \text{e} \quad \hat{\lambda} = \hat{g}\cdot\hat{\mu}^{\varepsilon}.$$

### 1.8.3. Equação de Callan-Symanzik e a função Beta

Nesta subseção, a idéia de renormalização e a análise dimensional serão colocadas juntas e as consequências físicas serão inferidas.

Definimos o Lagrangeano despido $\mathcal{L}_B$ como sendo o Lagrangeano $\mathcal{L}+\mathcal{L}_{c.t.}$ escrito agora em termos dos acoplamentos adimensionais,

$$\begin{aligned}
\mathcal{L}_B &= \mathcal{L}+\mathcal{L}_{c.t.} \\
&= \tilde{\phi}\left(\partial_t - D\nabla^2\right)\phi + 2\hat{g}\cdot\hat{\mu}^{\varepsilon}\tilde{\phi}\phi^2 + \hat{g}\cdot\hat{\mu}^{\varepsilon}\tilde{\phi}^2\phi^2 + \hat{A}\cdot\mu^{\varepsilon}\tilde{\phi}\phi^2 + \hat{B}\cdot\mu^{\varepsilon}\tilde{\phi}^2\phi^2 \\
&= \tilde{\phi}_B(\partial_t - D_B\nabla^2)\phi_B + 2\hat{g}_B\cdot\mu^{\varepsilon}\tilde{\phi}_B\phi_B^2 + \hat{g}_B\cdot\mu^{\varepsilon}\tilde{\phi}_B^2\phi_B^2. \qquad (1.28)
\end{aligned}$$

Na segunda linha, os termos dos contra termos $A$, $B$ foram expressos em termos dos acoplamentos adimensionais. Na terceira linha, reescrevemos o Lagrangeano despido na mesma forma do Lagrangeano original definindo os campos despidos ($\tilde{\phi}_B \equiv \tilde{\phi}$, $\phi_B \equiv \phi$) e os parâmetros despidos ($D_B \equiv D$, $\hat{g}_B \equiv \hat{g}+\hat{A}$). Note que os parâmetros despidos e os campos despidos dependem do corte $\varepsilon$, mas são independentes da escala RG $\mu$. Em constraste, o parâmetro renormalizado $\hat{g}=\hat{g}(\mu)$ depende da escala $\mu$, mas não de $\varepsilon$.

Entretanto, a arbitrariedade de $\mu$ irá restringir a teoria. Para vermos como, podemos reescrever a integral funcional em termos das quantidades despidas como segue,

$$S_B[\tilde{\phi}_B,\phi_B] = \int d^dx \left\{ \int_0^t d\tau\ \mathcal{L}_B[\tilde{\phi}_B,\phi_B] - \rho_0 \tilde{\phi}_B(x,0) \right\} \quad \text{e} \quad \mathcal{D}[\phi_B] = \mathcal{D}[\phi]$$

$$\Rightarrow \quad \langle \phi_B(x,t) \rangle = \frac{\int \mathcal{D}[\tilde{\phi}_B]\mathcal{D}[\phi_B]\ \phi_B\ e^{-S_B[\tilde{\phi}_B,\phi_B]}}{\int \mathcal{D}[\tilde{\phi}_B]\mathcal{D}[\phi_B]\ \ e^{-S_B[\tilde{\phi}_B,\phi_B]}} \equiv \rho(x,t). \tag{1.29}$$

O último passo reflete o fato que predições não devem depender da escala RG $\mu$, já que este parâmetro foi introduzido como uma escala arbitrária. Matematicamente, o vínculo se escreve da seguinte forma para a função de um ponto:

$$G_1^B(x,t;\hat{g}_B,\varepsilon) \equiv G_1(x,t;\hat{g},\mu). \tag{1.30}$$

Como o lado esquerdo da equação (1.30) não depende de $\mu$, a dependência explícita de $G_1$ em $\mu$ no lado direito deve ser cancelada pela dependência implícita de $\hat{g}(\mu)$, expressa por

$$\mu \frac{d}{d\mu} G_1(x,t,D,\hat{g},\mu)\Big|_{PN} = 0.$$

O ponto de normalização *PN* é escolhido por conveniência em $q^2 = 0$ e $-i\omega^2 = \mu^2$ e corresponde a manter o parâmetro despido $\hat{g}_B$ fixo. Aplicando a última equação, temos

$$\mu \frac{d}{d\mu}\Big|_{PN} = \mu \frac{\partial}{\partial \mu} + \underbrace{\mu \frac{d\hat{g}}{d\mu}\Big|_{PN}}_{\equiv \beta_g} \cdot \frac{\partial}{\partial \hat{g}},$$

onde a função beta $\beta_g$ foi definida. A função beta pode ser calculada como

$$\beta_g(\hat{g}) = -\varepsilon\hat{g} + \varepsilon\hat{g}^2 \frac{2}{(8\pi)^{d/2}} \cdot \Gamma\left(\frac{\varepsilon}{2}\right). \tag{1.31}$$

Finalmente, a restrição para a função de um ponto pode ser escrita como

$$\left( \mu \frac{\partial}{\partial \mu} + \beta_g(\hat{g}) \frac{\partial}{\partial \hat{g}} \right) G_1 = 0. \tag{1.32}$$

A equação acima é conhecida como equação de Callan-Symanzik.

Como a função beta captura a dependência da constante de acoplamento $\hat{g}$ com a escala $\mu$, suas raízes correspondem às invariâncias de escala da teoria. Se o parâmetro não varia com a mudança de escala, a teoria definida pelo parâmetro $\hat{g}$ se torna invariante de escala. As raízes de $\beta_g(\hat{g})$ estão em $\hat{g}_1 = 0$ e $\hat{g}_2 = \frac{(8\pi)^{d/2}}{2\cdot\Gamma\left(\frac{\varepsilon}{2}\right)}$. A primeira raiz em $\hat{g}_1$ corresponde a $\lambda = 0$, o que significa que existe somente difusão. A segunda raiz, entretanto, não é trivial e corresponde ao ponto fixo estável para o acoplamento. Como $\Gamma\left(\frac{\varepsilon}{2}\right) \sim \frac{1}{\varepsilon}$, obtemos $\hat{g}_2 \sim \varepsilon$ quando $\varepsilon \to 0$. O ponto fixo $\hat{g}_2$ é crucial para o comportamento de escala e determina o comportamento assintótico da função de um ponto como mencionado anteriormente.

Estamos interessados na dependência temporal da função de um ponto $\langle \phi(x,t) \rangle$. Da equação (1.8) e da análise dimensional $[\phi] = d$, segue que $[G_1] = [\phi] = d$. Consequentemente, a função de um ponto pode ser reescrita como segue

$$G_1(t,\hat{g},\mu) = \mu^d \cdot \hat{G}_1(\mu^2 t, \hat{g}).$$

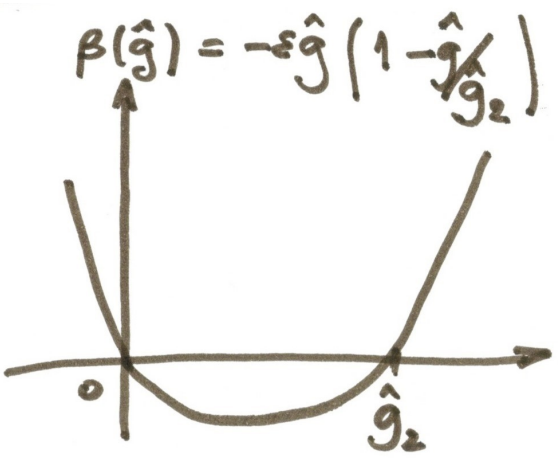


Figura 1.11.: Função beta $\beta(\hat{g}) = -\varepsilon\hat{g}\left(1-\frac{\hat{g}}{\hat{g}_2}\right)$.

Assim, podemos transformar uma derivada em $\mu$ na equação de Callan-Symanzik (1.29) em uma derivada temporal,

$$\mu\frac{\partial}{\partial\mu}G_1(t,\hat{g},\mu) = \mu\frac{\partial}{\partial\mu}\left(\mu^d\cdot\hat{G}_1(\mu^2 t,\hat{g})\right) = \left(d+2t\frac{\partial}{\partial t}\right)G_1(t,\hat{g},\mu).$$

Entretanto, uma sutileza surge por causa do termo de fronteira $\rho_0\tilde{x}(x,0)$ na ação. Uma análise matematicamente rigorosa [27] mostra que um termo adicional aparece na equação de Callan-Symanzik devido à densidade inicial. Finalmente, obtemos a equação completa de Callan-Symanzik,

$$\left(d+2t\frac{\partial}{\partial t}+\beta_g(\hat{g})\frac{\partial}{\partial\hat{g}}-d\phi_0\frac{\partial}{\partial\rho_0}\right)\rho(t,\hat{g},\rho_0,\mu)=0, \tag{1.33}$$

uma equação diferencial parcial de primeira ordem para a densidade de partículas renormalizada $\rho$ que pode ser resolvida pelos métodos das características, um método padrão de análise de equações diferenciais parciais [31]. Introduzimos um parâmetro de fluxo $l$ e escolhemos as curvas corretas (características) onde a equação diferencial parcial pode ser reduzida a um conjunto de equações diferenciais ordinárias. As soluções das equações diferenciais ordinárias podem ser obtidas ao longo das características e resolvem a equação diferencial parcial.

O resultado importante deste procedimento padrão é $\rho(t,\hat{g},\rho_0,\mu)\sim t^{-d/2}$ para $\varepsilon = d_d - d = 2-d > 0$ e uma análise completa (incluindo $d=2$) revela,

$$\rho(t,\hat{g},\rho_0,\mu)\sim t^{-d/2} = \begin{cases} t^{-1/2} & \text{se } d=1, \\ \ln t\cdot t^{-1} & \text{se } d=2, \\ t^{-1} & \text{se } d>2, \end{cases} \tag{1.34}$$

que é exatamente o resultado encontrado em (1.5). A abordagem do grupo de renormalização para o processo de aniquilação de pares reproduz exatamente o comportamento temporal assintótico sugerido por simulações numéricas. O comportamento de longo prazo para a teoria de campo médio se torna exato acima da dimensão crítica $d_c = 2$. Em dimensões menores ($d=1$), a hipótese de campo médio (fatorização da densidade de probabilidade) não descreve o comportamento de escala acuradamente, a solução $\rho\sim t^{-1}$ deve ser renormalizada para $\rho\sim t^{-1/2}$.

## 1.9. Heurística

Apontamos anteriormente que a expansão em laços vai além da descrição de campo médio para a reação de aniquilação. É possível entender fisicamente por que a descrição de campo médio se torna errada para tempos longos em dimensão um?

Considere uma rede uni-dimensional, onde quase todos os sítios da rede são ocupados por partículas da espécie $A$, de modo que a reação de aniquilação $A + A \xrightarrow{\lambda} \emptyset$ pode em princípio acontecer em todo lugar. Então, a dinâmica inicial é acuradamente descrita pela solução da equação de campo médio com $\rho^{-1}$.

À medida que o tempo avança, os sítios da rede se tornam mais e mais diluidos e a taxa de reação fica limitada pelo tempo de primeira passagem (para o encontro de dois agentes na rede) de um passeio aleatório em $d = 1$, que escala exatamente com $t^{-1/2}$. Então, o comportamento para tempos longos de $\rho$ é renormalizado para $\rho \sim t^{-1}/t^{-1/2} = t^{-1/2}$.

Fica claro que a dimensionalidade do sistema é crucial, já que ela determina a dimensionalidade do processo de difusão e portanto o processo de passeio aleatório subjacente. É conhecido que para $d = 1$, um passeio aleatório retorna a um ponto específico no espaço em um tempo finito quase certamente, enquanto que para $d > 2$ isto não ocorre [32]. Portanto, para $d > 2$, as correções devido às correlações e flutuações estatísticas ao comportamento de campo médio $\rho \sim t^{-1}$ se tornam irrelevantes. Estes resultados serão importantes em alguns capítulos posteriores desta tese, em particular no capítulo referente ao artigo de título *A importância de ser discreto no sexo*.

Capítulo 2

# Processo de contato com simbiose

*Esta introdução é baseada nos resultados do artigo [3], publicado em* ***Physical Review E****.*

Neste modelo estuda-se um processo de contato com duas espécies que interagem de maneira simbiótica. Cada sítio da rede pode estar vazio ou hospedar indivíduos de espécie $A$ e/ou $B$. Ocupação múltipla da mesma espécie é proibida. Simbiose é representada por uma taxa de morte reduzida $\mu < 1$ para indivíduos em sítios com ambas as espécies presentes. Caso contrário, a dinâmica é igual à do processo de contato básico, com criação (em sítios vizinhos vazios) à taxa $\lambda$ e morte de indivíduos (isolados) à taxa 1.

Sejam $\sigma_i$ e $\eta_i$ as variáveis indicadoras de ocupação do sítio $i$ pelas espécies $A$ e $B$ respectivamente. Os estados permitidos para um sítio $\sigma_i, \eta_i$ são $(0,0)$, $(0,1)$, $(1,0)$, e $(1,1)$. As transições $(0,0) \to (1,0)$ e $(0,1) \to (1,1)$ ocorrem a taxa $\lambda r_A$, onde $r_A$ é a fração de primeiros vizinhos ocupados pela espécie $A$. De forma semelhante, a taxa para as transições $(0,0) \to (0,1)$ e $(1,0) \to (1,1)$ é $\lambda r_B$, com $r_B$ sendo a fração de primeiros vizinhos ocupados pela partícula $B$. As transições $(0,1) \to (0,0)$ e $(1,0) \to (0,0)$ ocorrem a taxa 1, enquanto $(1,1) \to (1,0)$ e $(1,1) \to (0,1)$ ocorrem à taxa $\mu$. Este conjunto de taxas de transição descrevem um par de processos de contato habitando a mesma rede. Para $\mu = 1$ os dois processos evoluem independentemente, mas para $\mu < 1$ eles interagem simbioticamente já que as taxas de aniquilação são reduzidas em sítios onde ambas as espécies estão presentes.

Para facilitar a construção da teoria de campos pertinente, vamos aqui formular o modelo de processo de contato com simbiose em termos de reações envolvendo processos de Gribov. No processo de Gribov, a aniquilação $A + A \to A$, a divisão $A \to A + A$ e o decaimento $A \to \emptyset$ podem ser intepretados no contexto da teoria de populações com representando nascimentos e mortes de indivíduos da população de interesse. No processo de contato simbiótico, permitimos que outra espécie $B$ participe das interações na rede com a espécie $A$. A maneira com que essas interações se dão deve induzir algum tipo de simbiose entre as entidades que interagem. Nesta seção extenderemos as idéias relacionadas ao clássico processo de percolação direcionada para uma situação onde duas espécies $A$ e $B$ coexistem na rede, de modo que as interações entre espécies diferentes induzam uma diminuição na taxa de morte dos agentes. Uma possibilidade para tal é acoplarmos dois processos de Gribov de modo que as taxas de morte das populações $A$ e $B$ sejam diminuidas com os encontros entre as partículas na rede, de modo que o processo microscópico possa ser descrito por

$$\begin{cases} A \underset{\alpha'}{\overset{\alpha}{\rightleftharpoons}} A + A & B \underset{\beta'}{\overset{\beta}{\rightleftharpoons}} B + B \\ A \overset{\mu e^{-\gamma_B}}{\rightharpoonup} \emptyset & B \overset{\mu e^{-\gamma_A}}{\rightharpoonup} \emptyset \end{cases} \tag{2.1}$$

Desta forma, temos dois processos de Gribov conectados pelas taxas de morte das partículas sendo da forma $\mu e^{-\gamma_B}$ para as partículas $A$ e da forma $\mu e^{-\gamma_A}$ para as partículas $B$. A presença da partícula 'parceira' faz com que a taxa de morte seja reduzida. A idéia aqui é seguir o roteiro em que se mapeia o processo estocástico descrito acima em uma formulação que permite a aplicação das idéias e métodos da teoria quântica de

campos [33]. Nesta formulação fica manifesta a presença de uma ação efetiva que permite desenvolver tais métodos. Partindo desta ação efetiva, métodos perturbativos permitem estimativas dos expoentes críticos com a consequente determinação da classe de universalidade do modelo. Este foi o procedimento realizado em [3], que contemplou também resultados simulacionais obtidos por coautores. Resultados simulacionais para o modelo formulado na rede como descrito acima revelaram que a transição de fase entre estados ativos e absorventes é contínua e que a taxa de criação crítica $\lambda_c$ é reduzida na presença de simbiose. Isto significa que a perda de uma espécie poderá rapidamente levar a extinção já que então o sistema constituirá um processo de contato simples que estará operando com $\lambda < \lambda_c$. A expansão em $\varepsilon$ oriunda do procedimento GR indicou que o modelo se apresenta na classe de universalidade PD, fato consistente com os resultados obtidos numericamente para o comportamento crítico, com algumas anomalias aparecendo no expoente $z$ associadas às flutuações do parâmetro de ordem para tempos longos, onde se espera um desenvolvimento do tipo $\sim t^{1/z}$. Este fenômeno fica mais pronunciado para valores fracos de simbiose, representados por valores de $\mu$ perto de 1. Pode-se conjecturar que com simbiose forte o sistema é atraido rapidamente para o ponto fixo da PD enquanto que para simbiose fraca o sistema executa longas excursões em regimes nos quais o comportamento tipo PD não é evidente, antes de finalmente retornar para as vizinhanças do ponto fixo PD.

PHYSICAL REVIEW E **86**, 011121 (2012)

# Symbiotic two-species contact process

Marcelo Martins de Oliveira,[1,*] Renato Vieira Dos Santos,[2] and Ronald Dickman[2,†]
[1]*Departamento de Física e Matemática, Campus Alto Parapeba, Universidade Federal de São João del Rei, 36420-000 Ouro Branco, Minas Gerais, Brazil*
[2]*Departamento de Física and National Institute of Science and Technology for Complex Systems, Instituto de Ciências Exatas, Universidade Federal de Minas Gerais, 30123-970 Belo Horizonte, Minas Gerais, Brazil*
(Received 24 May 2012; published 19 July 2012)

We study a contact process (CP) with two species that interact in a symbiotic manner. In our model, each site of a lattice may be vacant or host individuals of species A and/or B; multiple occupancy by the same species is prohibited. Symbiosis is represented by a reduced death rate $\mu < 1$ for individuals at sites with both species present. Otherwise, the dynamics is that of the basic CP, with creation (at vacant neighbor sites) at rate $\lambda$ and death of (isolated) individuals at a rate of unity. Mean-field theory and Monte Carlo simulation show that the critical creation rate $\lambda_c(\mu)$ is a decreasing function of $\mu$, even though a single-species population must go extinct for $\lambda < \lambda_c(1)$, the critical point of the basic CP. Extensive simulations yield results for critical behavior that are compatible with the directed percolation (DP) universality class, but with unusually strong corrections to scaling. A field-theoretic argument supports the conclusion of DP critical behavior. We obtain similar results for a CP with creation at second-neighbor sites and enhanced survival at first neighbors in the form of an annihilation rate that decreases with the number of occupied first neighbors.

DOI: 10.1103/PhysRevE.86.011121 PACS number(s): 05.50.+q, 05.70.Ln, 05.70.Jk, 02.50.Ey

## I. INTRODUCTION

Absorbing-state phase transitions have attracted much interest in recent decades, as they appear in a wide variety of problems such as population dynamics, heterogeneous catalysis, interface growth, and epidemic spreading [1–5]. Interest in such transitions has been further stimulated by recent experimental realizations [6,7].

The absorbing-state universality class associated with directed percolation (DP) has proven to be particularly robust. The DP-like behavior appears to be generic for absorbing-state transitions in models with short-range interactions and lacking a conserved density or symmetry beyond translational invariance [8,9]. In contrast, models possessing two absorbing states linked by particle-hole symmetry belong to the voter model universality class [10].

The contact process (CP) [11] is probably the best understood model exhibiting an absorbing-state phase transition; it has been known for many years to belong to the DP class. The CP can be interpreted as a stochastic birth-and-death process with a spatial structure. As a control parameter (the reproduction rate $\lambda$) is varied, the system undergoes a phase transition between extinction and survival. In this context it is natural to seek a manner to include symbiotic interactions in the CP. In the present work, this is done by allowing two CPs (designated as species A and B) to inhabit the same lattice. The two species interact via a reduced death rate $\mu$ at sites occupied by individuals of both species. (Aside from this interaction, the two populations evolve independently.) We find, using mean-field theory and Monte Carlo simulation, that the symbiotic interaction favors survival of a mixed population, in that the critical reproduction rate $\lambda_c$ decreases as we reduce $\mu$. Note that for $\lambda(\mu) < \lambda < \lambda(1)$, *only* mixed populations survive; in isolation, either species must go extinct.

In addition to its interest as a simple model of symbiosis, the critical behavior of the two-species CP is intriguing in the context of nonequilibrium universality classes. By analogy with the (equilibrium) $n$-vector model, in which the critical exponents depend on the number of spin components $n$, one might imagine that the presence of two species would modify the critical behavior. Using extensive simulations, we find that the critical behavior is consistent with that of DP, although with surprisingly strong corrections to scaling. An argument based on field theory supports the conclusion of DP scaling. We note that our result agrees with that of Janssen, who studied general multispecies DP processes [12]. Similar conclusions apply to a related model, a CP with creation at second-neighbor sites and enhanced survival at first neighbors, in the form of an annihilation rate that decreases with the number of occupied first neighbors. (In this case the two species inhabit distinct sublattices.)

The balance of this paper is organized as follows. In Sec. II we define the models and analyze them using mean-field theory. In Sec. III we present our simulation results and in Sec. IV we discuss a field-theoretic approach. Section V is devoted to discussion and conclusions.

## II. MODELS AND MEAN-FIELD THEORY

To begin we review the definition of the basic contact process. Following the usual nomenclature, we refer to an active site as being occupied by a particle and an inactive one as vacant. The CP [11] is a stochastic interacting particle system defined on a lattice, with each site $i$ either occupied by a particle $[\sigma_i(t) = 1]$ or vacant $[\sigma_i(t) = 0]$. Transitions from $\sigma_i = 1$ to 0 occur at a rate of unity, independent of the neighboring sites. The reverse transition, a vacant site becoming occupied, is possible only if at least one of its nearest neighbors (NNs) is occupied: The transition from $\sigma_i = 0$ to 1

*mmdeoliveira@ufsj.edu.br
†dickman@fisica.ufmg.br

 

occurs at rate $\lambda r$, where $r$ is the fraction of NNs of site $i$ that are occupied. Thus the state $\sigma_i = 0$ for all $i$ is absorbing. At a certain critical value $\lambda_c$ the system undergoes a phase transition between the active and the absorbing state [11]. The CP has been studied intensively via series expansion and Monte Carlo simulation and its critical properties are known to high precision [1,3–5,13].

We now define a two-species symbiotic contact process (2SCP). Let the indicator variables for occupation of site $i$ by species A and B be $\sigma_i$ and $\eta_i$, respectively. The allowed states for a site $(\sigma_i,\eta_i)$ are (0,0), (0,1), (1,0), and (1,1). The transitions $(0,0) \to (1,0)$ and $(0,1) \to (1,1)$ occur at rate $\lambda r_A$, with $r_A$ the fraction of NNs bearing a particle of species A. Similarly, the rate for the transitions $(0,0) \to (0,1)$ and $(1,0) \to (1,1)$ is $\lambda r_B$, with $r_B$ the fraction of NNs bearing a particle of species B. The transitions $(0,1) \to (0,0)$ and $(1,0) \to (0,0)$ occur at a rate of unity, whereas $(1,1) \to (1,0)$ and $(1,1) \to (0,1)$ occur at rate $\mu$. This set of transition rates describes a pair of contact processes inhabiting the same lattice. For $\mu = 1$ the two processes evolve independently, but for $\mu < 1$ they interact symbiotically since the annihilation rates are reduced at sites with both species present. We note that the rates are symmetric under exchange of species labels A and B.

We also study a CP with creation at second-neighbor sites. In Ref. [14] a modified CP was defined as follows.

(i) In addition to creation at NNs, at rate $\lambda_1$, we allow creation at *second neighbors*, at rate $\lambda_2$. For bipartite lattices such as the ring or the square lattice, $\lambda_1$ is the rate of creation in the opposite sublattice, while $\lambda_2$ is the rate in the same sublattice as the replicating particle.

(ii) The annihilation rate at a given site is $1 + \nu n^2$, with $n$ denoting the number of occupied NNs.

For $\nu > 0$, the presence of particles in one sublattice tends to suppress their survival in the other, leading to the possibility of sublattice ordering, as discussed in Ref. [14].

Suppose now that $\lambda_1 = 0$, and let $\lambda_2 \equiv \lambda$. Then the populations in the two sublattices constitute distinct species since creation is always in the same sublattice. For $\nu < 0$ moreover, the two species interact in a symbiotic manner, analogous to that in the two-species CP defined above. (For $\nu = 0$ the two sublattices evolve independently.) We call this process the symbiotic sublattice contact process (SSLCP).

Both the 2SCP and SSLCP possess four phases: the fully active phase (nonzero populations of both species), a symmetric pair of partly active phases (only one species present), and the inactive phase (all sites inactive). The latter is absorbing while the partly active phases represent absorbing subspaces of the dynamics. (That is, a species cannot reappear once it goes extinct.) Let $\lambda_{c,0}$ denote the critical creation rate of the basic CP. In the 2SCP with $\mu = 1$ (or the SSLCP with $\nu = 0$), the critical creation rate must be $\lambda_{c,0}$. The same applies for the transitions from the partly active phases to the absorbing one, regardless of the value of $\mu$ or $\nu$. Intuitively, in the presence of symbiotic interactions, one expects the transition from the fully active to the absorbing phase to occur at some $\lambda_c < \lambda_{c,0}$ since the annihilation rate is reduced. Since this expectation is borne out numerically, the partly active phases are of little interest as they are not viable in the vicinity of the fully active-absorbing phase transition. Understanding the latter transition is the principal objective of this study.

As a first step in characterizing the phase diagrams of the models, we develop mean-field approaches. The derivation of a dynamic mean-field theory (MFT) for an interacting particle system begins with the equations of motion for the set of one-site probabilities (or, more generally, the $n$-site joint probability distribution) [1]. In this equation, the $n$-site probability distribution is inevitably coupled to the distribution for $n+1$ or more sites. An $n$-site MFT is obtained by estimating the latter distribution(s) in terms of that for $n$ sites. Here we consider the simplest cases, $n = 1$ and 2.

Consider the 2SCP in the one-site approximation. Denoting the probabilities for a given site to be vacant, occupied by species A only, by species B only, and doubly occupied by $p_0$, $p_A$, $p_B$, and $p_{AB}$, respectively, assuming spatial homogeneity, and factorizing two-site joint probabilities $(p[(\sigma_i,\eta_i),(\sigma_j,\eta_j)] = p[(\sigma_i,\eta_i)]p[(\sigma_j,\eta_j)])$ one readily obtains the equations

$$\begin{aligned}
\frac{dp_0}{dt} &= -\lambda p_0(\rho_A + \rho_B) + p_A + p_B, \\
\frac{dp_A}{dt} &= \lambda p_0 \rho_A + \mu p_{AB} - (1 + \lambda\rho_B)p_A, \\
\frac{dp_B}{dt} &= \lambda p_0 \rho_B + \mu p_{AB} - (1 + \lambda\rho_A)p_B, \\
\frac{dp_{AB}}{dt} &= \lambda(p_A\rho_B + p_B\rho_A) - 2\mu p_{AB},
\end{aligned} \tag{1}$$

where $\rho_A = p_A + p_{AB}$ and $\rho_B = p_B + p_{AB}$. If one species is absent (so that, say, $p_B = p_{AB} = 0$) this system reduces to the MFT for the basic contact process $\dot{p}_A = \lambda p_A(1 - p_A) - p_A$ with a critical point at $\lambda = 1$. To study the effect of symbiosis we seek a symmetric solution $p_A = p_B = p$. In this case one readily finds the stationary solution

$$\overline{p} = \frac{\mu}{2\lambda(1-\mu)}[2(1-\mu) - \lambda + \sqrt{\lambda^2 - 4\mu(1-\mu)}] \tag{2}$$

and

$$\overline{p}_{AB} = \frac{\lambda p^2}{\mu - \lambda p}. \tag{3}$$

For $\mu \geqslant 1/2$, $p$ grows continuously from zero at $\lambda = 1$, marking the latter value as the critical point. The activity grows linearly, $p \simeq [\mu/(2\mu - 1)](\lambda - 1)$, in this regime. For $\mu < 1/2$, however, the expression is already positive for $\lambda = \sqrt{4\mu(1-\mu)} < 1$ and there is a *discontinuous* transition at this point. The value $\mu = 1/2$ may be viewed as a tricritical point; here $p \sim \sqrt{\lambda - 1}$ for $\lambda > 1$. Numerical integration of the MFT equations confirms the above results. For $\mu < 1/2$, MFT in fact furnishes the *spinodal* values of $\lambda$. For a given set of initial probabilities, the numerical integration converges to the active stationary solution for $\lambda \geqslant \lambda^*$ and to the absorbing state for smaller values of $\lambda$. For the most favorable initial condition, i.e., $p_{AB}(0) \to 1$, $\lambda^* \to \lambda^{(-)} = \sqrt{4\mu(1-\mu)}$, the lower spinodal, while for a vanishing initial activity $\rho_A$, $\rho_B \to 0$, $\lambda^* \to \lambda^{(+)} = 1$. The stationary activity at $\lambda^*$ is nonzero. Figure 1 shows the stationary probabilities versus $\lambda$ for $\mu = 1/4$.

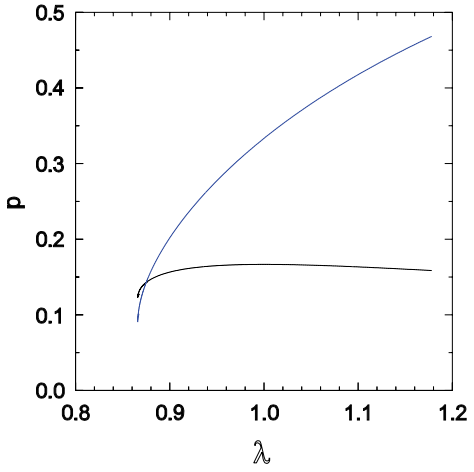


FIG. 1. (Color online) Density $p$ of species A (bottom curve) and of doubly occupied sites $p_{AB}$ (top curve) in the one-site approximation for the 2SCP, with $\mu = 0.25$.

The two-site MFT for the one-dimensional 2SCP involves ten pair probabilities and a set of 32 transitions. The resulting phase diagram is qualitatively similar to that of the one-site MFT. For $\mu > 0.75$, the transition is continuous and occurs at $\lambda = 2$, the same value as for the basic CP at this level of approximation. There is a tricritical point at $\mu = 0.75$, below which the transition is discontinuous; Fig. 2 shows the phase boundary.

The one-site MFT for the SLCP was developed in Ref. [14]. Adapted to the present case (creation only in the same sublattice, symbiotic interaction), the equation is

$$\frac{d\rho_A}{dt} = -\left(1 - \nu q^2 \rho_B^2\right)\rho_A + \lambda_2 \rho_A (1 - \rho_A) \qquad (4)$$

and similarly for $\rho_A \leftrightharpoons \rho_B$, on a lattice of coordination number $q$. (Here $\rho_j$ denotes the fraction of occupied sites in sublattice $j$.) As we seek a symmetric solution, we set $\rho_A = \rho_B$. The resulting equation yields a continuous phase transition at $\lambda = 1$, independent of $\nu$. (Note that $\nu$ must be greater than $-1/16$; smaller values correspond to a *negative* annihilation rate, for $\rho$ near unity.) The two-site approximation is likely

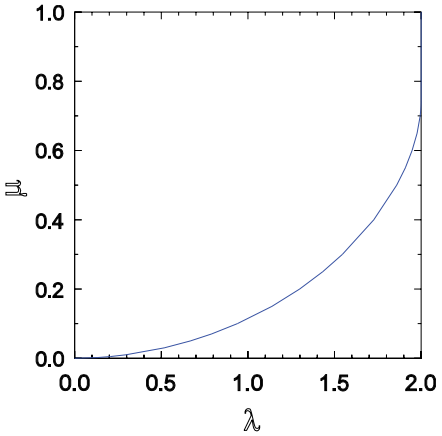


FIG. 2. (Color online) Phase boundary in the $\lambda$-$\mu$ plane as given by two-site MFT for the 2SCP on the line. The curved portion represents the lower spinodal $\lambda^{(-)}(\mu)$.

to provide a better description of the SSLCP since in this case the nearest-neighbor double occupancy probability is an independent variable, analogous to $p_{AB}$ in the one-site MFT of the 2SCP. Since such an analysis is unlikely to result in additional insights, we shall not pursue it here.

Although MFT predicts a discontinuous phase transition in the 2SCP in any number of dimensions, such a transition is not possible in one-dimensional systems with short-range interactions and free of boundary fields [15]. In one dimension the active-absorbing transition should be continuous, as we have indeed verified in simulations. Although our simulations show no evidence of a discontinuous transition in two dimensions ($d = 2$), such a transition remains a possibility for $d \geqslant 2$, for small values of $\mu$. A discontinuous transition might also arise under rapid particle diffusion, as this generally favors mean-field-like behavior.

## III. SIMULATIONS

We performed extensive Monte Carlo simulations of the 2SCP on rings and the square lattice (with periodic boundaries) and of the SSLCP on rings. A general observation is that both models appear to be more strongly affected by finite-size corrections than is the basic CP.

In the simulation algorithm for the two-species CP, we maintain two lists, i.e., of singly and doubly occupied sites. Let $N_s$ and $N_d$ denote, respectively, the numbers of such sites, so that $N_p = N_s + 2N_d$ is the number of particles. The total rate of (attempted) transitions is $\lambda N_p + N_s + 2\mu N_d \equiv 1/\Delta t$, where $\Delta t$ is the time increment associated with a given step in the simulation. At each such step, we choose among the events: (i) creation attempt by an isolated particle, with probability $\lambda N_s \Delta t$; (ii) creation attempt by a particle at a doubly occupied site, with probability $2\lambda N_d \Delta t$; (iii) annihilation of an isolated particle, with probability $N_s \Delta t$; and (iv) annihilation of a particle at a doubly occupied site, with probability $2\mu N_d \Delta t$. Once the event type is selected we choose a site $i$ from the appropriate list. In the case of annihilation, a particle is simply removed, while creation requires the choice of a neighbor $j$ of site $i$ and can proceed only if $j$ is not already occupied by a particle of the species to be created. For creation by a particle at a doubly occupied site, the species of the daughter particle is chosen to be A or B with equal probability and similarly for annihilation at a doubly occupied site.

In simulations of the SSLCP we maintain a list of occupied sites. At each step a site is selected from the list; an attempt to create a new particle, at one of the second-neighbor sites, is chosen with probability $p = \lambda/(1 + \lambda_2 + \mu n_1^2)$; the site is vacated with the complementary probability $1 - p$. The time increment associated with each event is $\Delta t = 1/N_p$, with $N_p$ the number of particles just prior to the event.

### A. Results: The 2SCP in one dimension

We studied the 2SCP using three values of $\mu$: 0.9, 0.75, and 0.25. While the first case may be seen as a relatively small perturbation of the usual CP ($\mu = 1$), the third represents a very strong departure from the original model. We perform three kinds of studies: quasistationary (QS) [16], initial decay (starting from a maximally active configuration), and

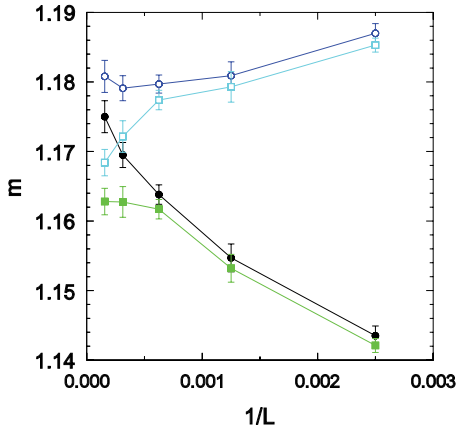


FIG. 3. (Color online) Quasistationary simulation of the one-dimensional 2SCP: moment ratios $m_\rho$ (solid symbols) and $m_q$ (open symbols) versus $1/L$ for the one-dimensional model with $\mu = 0.75$. The top curve in each pair is for $\lambda = 3.0336$ and the bottom is for $\lambda = 3.0337$.

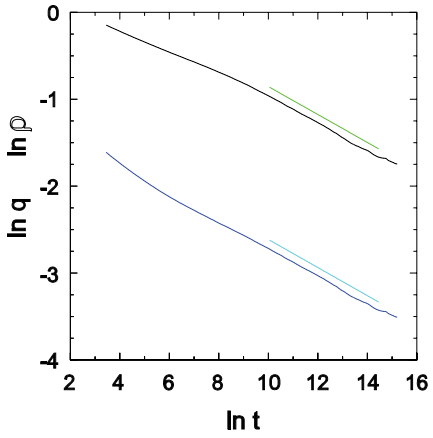


FIG. 4. (Color online) Initial-decay simulation of the 2SCP in one dimension: decay of the particle density $\rho$ (upper curve) and the density $q$ of doubly occupied sites in initial-decay studies with $\mu = 0.9$, $\lambda = 3.2273$, and system size $L = 51\,200$. The slopes of the regression lines are $-0.161$ ($\rho$) and $-0.162$ ($q$).

spreading, in which the initial condition is a doubly occupied site in an otherwise empty lattice. Although the critical value $\lambda_c(\mu)$ can be estimated using each method, spreading simulations proved the most effective in this regard.

In the QS simulations, we study system sizes 800, 1600, 3200, 6400, and 12800, with each run lasting $10^7$ time units; averages and uncertainties are calculated over 10–80 runs. We use three well established criteria to estimate the critical value: (i) power-law dependence of the order parameter on system size $\rho \sim L^{-\beta/\nu_\perp}$, (ii) power-law dependence of the lifetime $\tau \sim L^z$, and (iii) convergence of the moment ratio $m_\rho(L)$ to a finite limit $m_c$ as $L \to \infty$ [17]. Here $m_\rho \equiv \langle\rho^2\rangle/\langle\rho\rangle^2$. The order parameter is defined as the density of individuals, i.e., $\rho = (N_A + N_B)/L$. A related quantity of interest is the density $q$ of doubly occupied sites; the moment ratio $m_q$ is defined in a manner analogous to $m_\rho$. Two further quantities of interest are the scaled variances of $\rho$ and $q$; we define $\chi_\rho \equiv L^d\,\mathrm{var}(\rho)$ and similarly for $\chi_q$. The expected critical behavior is $\chi \sim L^{\gamma/\nu_\perp}$, where the critical exponent $\gamma$ satisfies the hyperscaling relation $\gamma = d\nu_\perp - 2\beta$ [1].

A preliminary estimate of $\lambda_c$ is obtained from the crossings of $m_\rho$ for successive system sizes $L$ and $2L$. For $\mu = 0.75$, for example, this yields $\lambda_c = 3.0337$. The plot of $m_\rho$ and $m_q$ (see Fig. 3) indicates that $\lambda_c > 3.0336$ (since $m_\rho$ curves upward), while the slight downward curvature for $\lambda = 3.0037$ suggests that this value may be slightly above critical. This graph also suggests that $m_\rho$ and $m_q$ approach the same limiting value, despite marked differences for smaller system sizes. Table I summarizes our findings for the critical parameters obtained from QS simulations.

The initial-decay studies use, as noted above, an initial configuration with all sites doubly occupied. The activity then decays, following a power law $\rho \sim t^{-\delta}$ at the critical point [18] until it saturates at its QS value. The larger the system size, the longer the period of power-law decay and the more precise the resulting estimate for the critical exponent $\delta$; here we use $L = 25\,600$ or $51\,200$. Averages are calculated over 500–3000 realizations. As the order parameter decays, its fluctuations build up; at the critical point, the moment ratio is expected to follow $m - 1 \sim t^{1/z}$ [19]. Since we expect $\rho$ and $q$ to scale in the same manner, we define exponents $\delta_\rho$ and $\delta_q$, and similarly $z_\rho$ and $z_q$, based on the behavior of $m_\rho$ and $m_q$, respectively. Figure 4 shows, for $\mu = 0.9$, that $\rho$ and $q$ decay in an analogous manner and follow power laws at long times, although there are significant deviations from a simple power law at short times; the decay exponents are consistent with the value of $\delta$ for directed percolation in one space and one time dimension (see Table II). The growth of fluctuations follows a more complicated pattern, as shown in Fig. 5. At relatively short times, $m_\rho - 1 \sim t^{1/z_\rho}$, with $z_\rho = 1.63(2)$, which is not very different from the DP value; $m_q - 1$ also grows as a power law in this regime, but with an apparent exponent of $z_q = 2.06(1)$. At longer times $z_\rho$ appears to take a smaller value [1.31(1) for $7.5 < \ln t < 10.5$], while $z_q$ shifts to a value close to that of DP [1.61(1) for $10 < \ln t < 14$]. The reason for the distinct behaviors of $m_\rho$ and $m_q$, in marked contrast

TABLE I. Two-species symbiotic CP in one dimension: results from QS simulations, with $L = 800$, 1600, 3200, 6400, and 12800. For $\mu = 0.25$ the maximum size is 6400.

| $\mu$ | $\lambda_c$ | $\beta/\nu_\perp$ | $z$ | $m_\rho$ | $m_q$ | $(\gamma/\nu_\perp)_\rho$ | $(\gamma/\nu_\perp)_q$ |
|---|---|---|---|---|---|---|---|
| 0.9 | 3.2273(1) | 0.25(2) | 1.50(5) | 1.168(12) | 1.164(4) | 0.627(20) | 0.474(7) |
| 0.75 | 3.03370(5) | 0.241(6) | 1.64(5) | 1.163(10) | 1.166(2) | 0.528(6) | 0.486(1) |
| 0.25 | 1.76297(1) | 0.248(3) | 1.56(4) | 1.168(3) | 1.169(3) | 0.500(1) | 0.492(2) |
| CP or DP | 3.29785 | 0.25208(5) | 1.5807(1) | 1.1736(1) | | 0.49584(9) | |

TABLE II. Two-species symbiotic CP in one dimension: results from initial-decay studies.

| $\mu$ | $L$ | $\lambda_c$ | $\delta$ | $z_\rho$ | $z_q$ |
|---|---|---|---|---|---|
| 0.9 | 51200 | 3.2273 | 0.161(1) | 1.44(1) | 1.54(2) |
| 0.75 | 25600 | 3.0337 | 0.1625(10) | 1.48(4) | 1.55(4) |
| 0.25 | 51200 | 1.76297 | 0.1581(3) | 1.56(1) | 1.58(1) |
| DP | | | 0.1599 | 1.5807(1) | |

with the similar scaling of $\rho(t)$ and $q(t)$, is unclear. While scaling anomalies are observed in the initial-decay studies for $\mu = 0.9$ and 0.75, for strong symbiosis ($\mu = 0.25$) they are absent, as seen in Table II, which summarizes the results of the initial-decay studies. (In this table, the values listed for $z_\rho$ and $z_q$ reflect the latter part of the evolution, during which the order parameter decays in the expected manner.)

In the spreading studies, each realization runs to a maximum time of $t_m$ (unless it falls into the absorbing state prior to this). The system size is taken large enough so that activity never reaches the boundary. Here we use $t_m = 2 \times 10^6$ and $L = 10^5$; averages are calculated over $10^4$ or $2 \times 10^4$ realizations. At the critical point, one expects to observe power-law behavior of the survival probability $P(t) \sim t^{-\delta}$, the mean number of particles $n(t) \sim t^{\eta}$, and the mean-square distance of particles from the initial seed $R^2(t) \sim t^{z_s}$ [18]. Here $\delta$ is the same exponent as governs the initial decay of the activity and $z_s$ is related to the dynamic exponent $z$ via $z_s = 2/z$. Deviations from asymptotic power laws, indicating off-critical values of the control parameter $\lambda$, are readily identified in spreading simulations, leading to precise estimates for $\lambda_c$.

The spreading behavior is characterized by clean power laws, as illustrated in Fig. 6. As this plot makes clear, the mean particle number $n_p$ and the mean number of doubly occupied sites $n_2$ grow with the same critical exponent. Precise estimates of the spreading exponents are obtained via analysis of local slopes such as $\delta(t)$, defined as the inclination of a

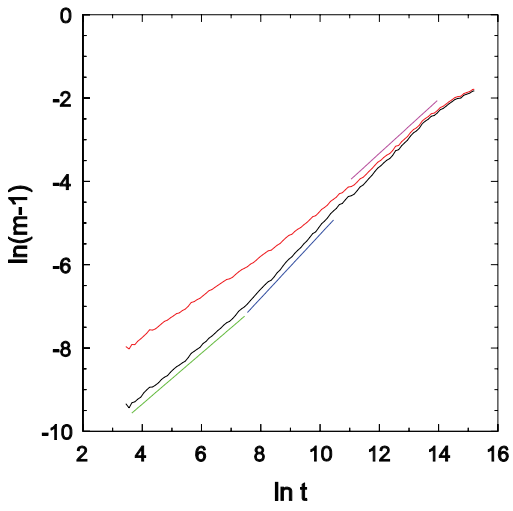


FIG. 5. (Color online) Initial-decay simulation of the 2SCP in one dimension: growth of fluctuations in $\rho$ (bottom curve) and $q$ (top curve) for the same parameters as in Fig. 4. The slopes of the regression lines are (from left to right) 0.613, 0.694, and 0.649.

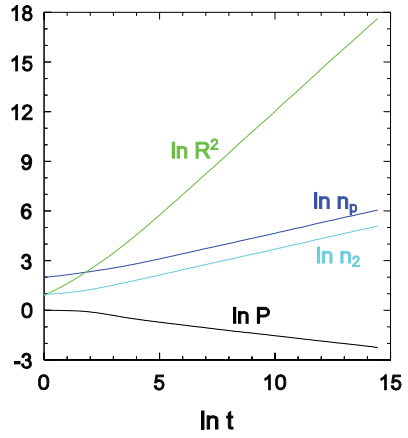


FIG. 6. (Color online) Spreading simulation of the 2SCP in one dimension: survival probability $P(t)$, total particle number $n_p(t)$, number of doubly occupied sites $n_2(t)$, and mean-square distance from seed $R^2(t)$. The parameters are $\mu = 0.25$ and $\lambda = 1.76\,297$.

least-square linear fit to the data (on logarithmic scales), on the interval $[t/a, at]$. (The choice of the factor $a$ represents a compromise between high resolution, for smaller $a$, and insensitivity to fluctuations, for larger values; here we use $a = 4.59$.) Curvature in a plot of a local slope versus $1/t$ signals an off-critical value. Figure 7 shows the behavior of $\delta(t)$ for $\mu = 0.25$. The spreading exponents, summarized in Table III, are in good agreement with the values for DP in 1+1 dimensions. (We note that in all three cases, $\eta_p = \eta_2$ to within uncertainty.)

### B. Contact process with creation at second neighbors

We studied the SSLCP using QS and initial-decay simulations. The results from the former, based on finite-size scaling analysis of studies using $L = 800$, 1600, 3200, 6400, and 12 800, are summarized in Table IV. The value of $\nu_\perp$ was estimated (for $\nu = -0.1$ only) via analysis of the derivatives $|dm/d\lambda|$, $d \ln \tau/d\lambda$, and $d \ln \rho_p/d\lambda$ in the neighborhood of the critical point. Finite-size scaling implies that the derivatives follow $|dx/dp| \propto L^{1/\nu_\perp}$ (here $x$ stands for any of the quantities

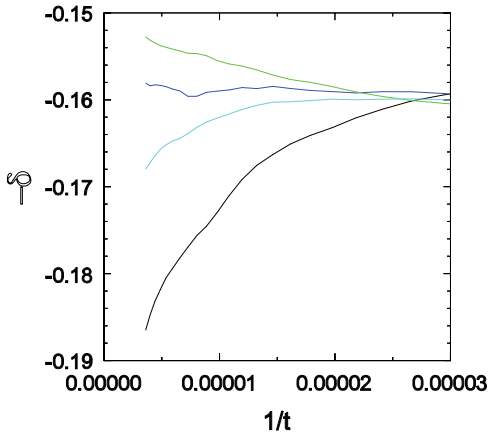


FIG. 7. (Color online) Spreading simulation of the 2SCP in one dimension: local slope $\delta(t)$ versus $1/t$ for $\mu = 0.25$ and (from bottom to top) $\lambda = 1.7629$, 1.762 95, 1.762 97, and 1.7630.

TABLE III. One-dimensional 2SCP: results from spreading simulations.

| $\mu$ | $\lambda_c$ | $\delta$ | $\eta$ | $z_s$ |
|---|---|---|---|---|
| 0.9 | 3.2273 | 0.165(1) | 0.310(1) | 1.257(2) |
| 0.75 | 3.0337 | 0.1595(5) | 0.3180(5) | 1.265(5) |
| 0.25 | 1.76297 | 0.158(1) | 0.315(3) | 1.265(10) |
| DP | 3.29785 | 0.15947(5) | 0.31368(4) | 1.26523(3) |

mentioned). We estimate the derivatives via least-squares linear fits to the data on an interval that includes $\lambda_c$. (The intervals are small enough that the graphs show no significant curvature.) Linear fits to the data for $m$, $\ln \rho_p$, and $\ln \tau$ yield $1/\nu_\perp = 0.94(2)$, 0.92(3), and (again) 0.92(3), respectively, leading to the estimate $\nu_\perp = 1.08(3)$.

Results of the initial-decay studies are summarized in Table V. As in the two-species CP, the value of $z$ obtained from analysis of $m(t)$ appears to be smaller than the DP value, whereas the result obtained from the QS simulations is consistent with that of DP.

### C. Two-species contact process in two dimensions

We performed extensive Monte Carlo simulations of the 2SCP on square lattices using both initial-decay and QS simulations. In order to locate the critical point with good precision, we study the initial decay of the particle density, starting from a maximally active initial condition (all sites doubly occupied). We use lattices of linear size $L = 4000$ and average over at least 20 different realizations. Figure 8 shows the decay of $\rho(t)$ for $\mu = 0.1$. After an initial transient, during which the density evolves slowly, the particle density follows a power law with $\delta = 0.46(1)$, which is compatible with the value $[\delta = 0.4523(10)]$ for the DP class in $2+1$ dimensions. The transient behavior lasts longer the larger is $\mu$, as shown in Fig. 9. However, the relaxation is seen to cross over to DP-like behavior for all values studied, except for $\mu = 0.9$, for which the transient regime persists throughout the entire simulation.

Having determined $\lambda_c$ to good precision in the initial-decay studies, we perform QS simulations of the model on square lattices of linear size $L = 20,40,\ldots,320$ with periodic boundaries. Figure 10 shows moment-ratio crossings and the finite-size scaling behavior of the density and lifetime for $\mu = 0.1$. For the larger sizes we obtain $\beta/\nu_\perp = 0.78(1)$ and $z = 1.74(2)$, in good agreement with the best estimates for DP in $2+1$ dimensions. Simulation results for the two-dimensional model are summarized in Table VI.

TABLE IV. One-dimensional SSLCP: results from quasistationary simulations.

| $\nu$ | $\lambda_c$ | $\beta/\nu_\perp$ | $z$ | $m_c$ | $\nu_\perp$ |
|---|---|---|---|---|---|
| −0.05 | 3.1489(1) | 0.235(8) | 1.63(5) | 1.154(5) | |
| −0.1 | 2.8878(1) | 0.242(1) | 1.612(12) | 1.161(3) | 1.08(3) |
| −0.2 | 2.0502(1) | 0.253(6) | 1.59(1) | 1.170(6) | |
| DP | 3.29785 | 0.25208(5) | 1.5807(1) | 1.1736(1) | 1.096854(4) |

TABLE V. One-dimensional SSLCP: results from initial-decay simulations.

| $\mu$ | $L$ | $\lambda_c$ | $\delta$ | $z$ |
|---|---|---|---|---|
| −0.05 | 50000 | 3.1489 | 0.1458(5) | 1.45(2) |
| −0.1 | 50000 | 2.8878 | 0.1484(7) | 1.45(3) |
| −0.2 | 20000 | 2.0503 | 0.1597(3) | 1.53(1) |
| DP | | | 0.1599 | 1.5807(1) |

## IV. FIELD-THEORETIC ANALYSIS

In this section we extend the field theory or continuum representation of DP to the two-species case to determine whether the presence of additional species changes the scaling behavior. Since the theory of DP has been known for some time, we give a bare outline of this analysis, referring the reader to Refs. [20–24] for details. To begin, we modify the lattice model so as to facilitate the definition of a continuum description following the Doi-Peliti formalism [20,21], which has been applied to DP in Refs. [22,24]. (The latter study applies the Wilson renormalization group to the problem.)

In the Doi-Peliti formalism, the master equation governing the evolution of the probability vector $|P(t)\rangle \equiv \sum_{\mathcal{C}} p(\mathcal{C},t)|\mathcal{C}\rangle$ (the sum is over all configurations) is written in the form $d|P\rangle/dt = L|P\rangle$, where the evolution operator $L$ is composed of creation and annihilation operators. Starting from this "microscopic" description, one derives an effective action $\mathcal{S}$ via a path-integral mapping. Then, taking the continuum limit, one arrives at a field theory for the model. Of the many lattice models that belong to the DP universality class, the simplest to analyze in this manner is the Malthus-Verhulst process (MVP). Here, each site $i$ of a lattice hosts a number $n_i \geqslant 0$ of particles. The transitions at a given site are creation $(n_i \to n_1 + 1)$ at rate $\lambda n_i$ and annihilation $(n_i \to n_1 - 1)$ at rate $\mu n_i + \nu n_i(n_i - 1)$. In addition, particles hop between nearest-neighbor sites at rate $D$.

For the MVP on a ring of $\ell$ sites, one has the set of basis configurations $|n_1,\ldots,n_\ell\rangle$. Letting $c_i$ and $c_i^\dagger$ denote, respectively, annihilation and creation

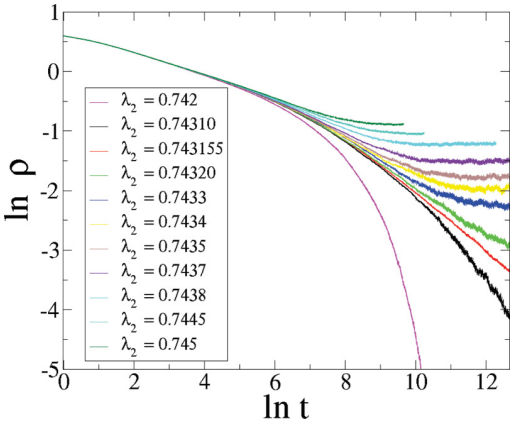


FIG. 8. (Color online) The 2SCP in two dimensions: density of active sites starting from a maximally active initial condition for $\mu = 0.1$ and $\lambda$ values increasing from $\lambda = 0.742$ (bottom curve) to from $\lambda = 0.745$ (top curve). The system size is $L = 4000$.

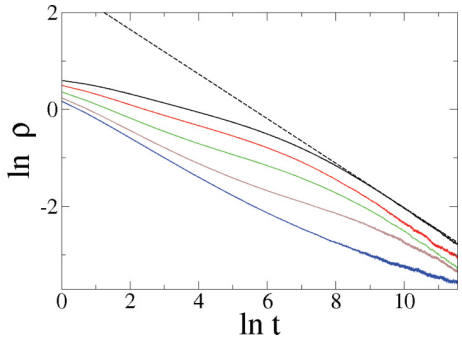


FIG. 9. (Color online) The 2SCP in two dimensions: density of active sites starting from a maximally active initial condition for $\mu = 0.1$, 0.25, 0.5, 0.75, and 0.9 (from top to bottom) and $\lambda = \lambda_c(\mu)$ (see Table VI). The slope of the dashed line is $-0.45$. The system size is $L = 4000$.

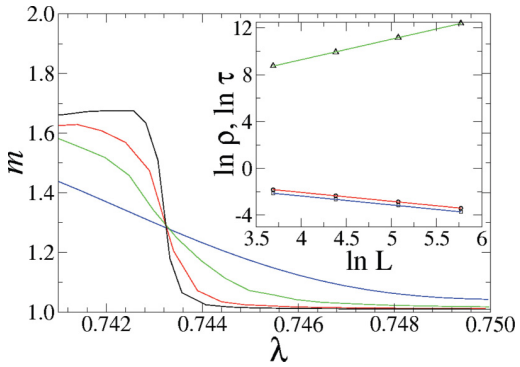


FIG. 10. (Color online) The 2SCP in two dimensions: QS moment ratio of particles vs $\lambda$ for $\mu = 0.1$ (the system sizes are $L = 40$, 80, 160, and 320 in order of steepness). The inset shows the QS density of active sites (circles), density of doubly occupied sites (squares), and lifetime of the QS state (triangles) for $\mu = 0.1$.

operators associated with site $i$, we have, by definition, $c_i|n_1,\ldots,n_i,\ldots,n_\ell\rangle = n_i|n_1,\ldots,n_i-1,\ldots,n_\ell\rangle$ and $c_i^\dagger|n_1,\ldots,n_i,\ldots,n_\ell\rangle = |n_1,\ldots,n_i+1,\ldots,n_\ell\rangle$. Then the evolution operator for the MVP is

$$L_{\rm MVP} = \sum_i [\lambda(c_i^\dagger - 1)c_i^\dagger c_i + (1-c_i^\dagger)(\mu + \nu c_i)c_i] + \frac{D}{2}\sum_i [(c_i^\dagger - c_{i+1}^\dagger)c_{i+1} + (c_i^\dagger - c_{i-1}^\dagger)c_{i-1}]. \quad (5)$$

Following the steps detailed in Ref. [22], one arrives at the effective action for the MVP,

$$\mathcal{S}_{\rm MVP} = \int dt \int dx [\hat\psi(\partial_t + w - D\nabla^2)\psi + \nu\hat\psi\psi^2 - \lambda\hat\psi^2\psi], \quad (6)$$

where $w \equiv \mu - \lambda$, the continuum limit has been taken, and terms higher than third order have been discarded, as they are irrelevant to critical behavior. (We recall that $\hat\psi(x,t)$ is an auxiliary field that arises in the mapping. The operator that governs the evolution of the probability generating function is given by the functional integral $U_t = \int \mathcal{D}\psi \int \mathcal{D}\hat\psi \exp[-\mathcal{S}(\psi,\hat\psi)]$; see Refs. [21,22].)

The action of Eq. (6) is equivalent that of DP and serves as the starting point for renormalization-group (RG) analyses [8,9,24]. (One usually imposes the relation $\nu = \lambda$ via a rescaling of the fields, but this is not needed here.) In the RG analysis the bilinear term naturally defines the propagator, while the cubic terms correspond to the vertices shown in Fig. 11. These terms lead, via diagrammatic analysis, to a nontrivial DP fixed point below $d_c = 4$ dimensions. The one-loop diagrams that yield, to lowest order, the recursion relations for parameters $w$, $\lambda$, and $\nu$ are shown in Fig. 12.

Now consider the two-species CP. To formulate a minimal field theory, we consider a two-species MVP; call it MVP2. Let $m_i$ and $n_i$ denote, respectively, the number of particles of species A and B at site $i$ and let $a_i$ and $a_i^\dagger$, and $b_i$ and $b_i^\dagger$, denote the associated annihilation and creation operators. We require the annihilation rate for species A to be a decreasing function of $n_i$ and vice versa; a simple choice for the annihilation rate of an A particle at site $i$ is $\mu\exp[-\gamma n_i]$, where $\gamma$ is a positive constant, and similarly for B particles, with $n_i$ replaced by $m_i$. This corresponds to the evolution operator

$$L_{\rm MVP2} = \sum_i [\lambda(a_i^\dagger - 1)a_i^\dagger a_i + (1-a_i^\dagger)(\mu e^{-\gamma b_i^\dagger b_i} + \nu a_i)a_i] + \frac{D}{2}\sum_i [(a_i^\dagger - a_{i+1}^\dagger)a_{i+1} + (a_i^\dagger - a_{i-1}^\dagger)a_{i-1}] + \sum_i [\lambda(b_i^\dagger - 1)b_i^\dagger b_i + (1-b_i^\dagger)(\mu e^{-\gamma a_i^\dagger a_i} + \nu b_i)b_i] + \frac{D}{2}\sum_i [(b_i^\dagger - b_{i+1}^\dagger)b_{i+1} + (b_i^\dagger - b_{i-1}^\dagger)b_{i-1}]. \quad (7)$$

To avoid ambiguity, we interpret the exponentials as being in *normal order*, i.e., all creation operators to the left of annihilation operators. Recalling that terms with four or more fields are irrelevant, we may expand the exponentials, retaining only the terms proportional to $b_i^\dagger b_i$ and $a_i^\dagger a_i$. Using $:X:$ to denote the normal-ordered expression of $X$, it is

TABLE VI. Simulation: critical parameters for the two-dimensional 2SCP.

| $\mu$ | $\lambda_c$ | $\beta/\nu_\perp$ | $z$ | $\delta$ | $m_p$ | $m_q$ |
|---|---|---|---|---|---|---|
| 0.9 | 1.64515(5) | 0.63(5) | 1.95(5) | >0.35 | 1.40(2) | 1.52(2) |
| 0.75 | 1.61640(5) | 0.73(5) | 1.78(6) | 0.44(3) | 1.32(3) | 1.33(3) |
| 0.5 | 1.47290(5) | 0.74(3) | 1.72(3) | 0.46(2) | 1.298(8) | 1.322(8) |
| 0.25 | 1.13730(5) | 0.76(2) | 1.73(2) | 0.45(2) | 1.30(2) | 1.31(2) |
| 0.1 | 0.743160(5) | 0.78(1) | 1.73(2) | 0.46(1) | 1.305(10) | 1.315(12) |
| CP or DP | 1.64874(4) | 0.797(3) | 1.7674(6) | 0.4523(10) | 1.3264(5) | |

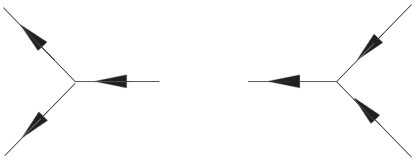

FIG. 11. Two three-field vertices in the field theory of DP. Lines exiting a vertex correspond to $\hat{\psi}$, while those entering correspond to $\psi$.

straightforward to show that

$$: e^{-\gamma b^\dagger b} := 1 - (1 - e^{-\gamma}) b^\dagger b + I \equiv 1 - \bar{\gamma} b^\dagger b + I, \quad (8)$$

where $I$ consists of terms with four or more operators. (With the truncation comes the possibility of a negative rate, but this is of no consequence in the RG analysis.) Now, following the usual procedure, we obtain the effective action for the two-species MVP:

$$\begin{aligned} \mathcal{S}_{\mathrm{MVP2}} = & \int dt \int dx [\hat{\psi}(\partial_t + w - D\nabla^2)\psi + \nu \hat{\psi}\psi^2 - \lambda \hat{\psi}^2 \psi] \\ & + \int dt \int dx [\hat{\varphi}(\partial_t + w - D\nabla^2)\varphi + \nu \hat{\varphi}\varphi^2 - \lambda \hat{\varphi}^2 \varphi] \\ & - \bar{\nu} \int dt \int dx [\hat{\varphi}\varphi\psi + \hat{\psi}\psi\varphi], \end{aligned} \quad (9)$$

where $\bar{\nu} = \bar{\gamma}\mu$. Here $\psi$ and $\hat{\psi}$ are fields associated with species A; $\varphi$ and $\hat{\varphi}$ are associated with species B. The first two lines of expression (9) correspond to independent MVPs; the third represents the symbiotic interaction between them. [While such a minimal action could have been "postulated" directly, we prefer to start with the microscopic expression of Eq. (7) since it describes a valid stochastic process.]

There are two cubic terms in the action involving only species A (i.e., the vertices shown in Fig. 11), two involving only B (those of Fig. 11 drawn, say, with dashed lines), and two vertices with a *mixed pair* of incoming lines as well as a single outgoing line that may belong to either species. One readily identifies the one-loop diagrams leading to renormalization of the parameter $\bar{\nu}$. In contrast, *no* diagrams (at any order) involving mixed-species vertices can affect the recursion relations for the DP parameters $w$, $\nu$, and $\lambda$. The reason is that the presence of a mixed-species vertex anywhere in a diagram implies that the lines entering the diagram are mixed, so that it can only contribute to the recursion relation for $\bar{\nu}$. We conclude that the interaction between species cannot alter the scaling behavior, which must therefore remain that of DP. At one-loop order, there are two fixed-point values for $\bar{\nu}$, namely, $2\lambda$ and zero, the latter corresponding to independent processes.

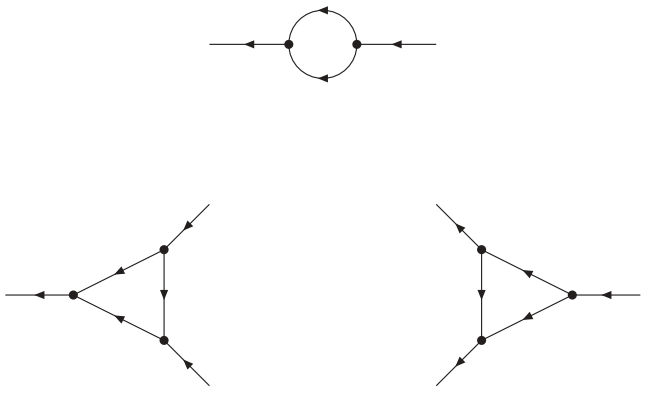

FIG. 12. One-loop diagrams in the field theory of DP, leading to renormalization of $w$, $\mu$, and $\lambda$, respectively.

## V. CONCLUSION

We study symbiotic interactions in contact-process-like models in one and two dimensions. For this purpose, we propose a two-species model (2SCP), in which the death rate is reduced (from unity to $\mu$) on sites occupied by both species. A related model (SSLCP), in which each species is confined to its own sublattice, is also studied in one dimension and found to exhibit similar behavior. Simulations reveal that the phase transition between active and absorbing states is continuous and that the critical creation rate $\lambda_c$ is reduced in the presence of symbiosis. This means that the loss of one species will rapidly lead to extinction since the system is then a basic contact process operating at $\lambda < \lambda_c$. Although this might suggest identifying the density $q$ of doubly occupied sites as the order parameter, we find that the particle density $\rho$ (which includes a large contribution from singly occupied sites) scales in the same manner as $q$.

Mean-field theory (in both the one- and two-site approximations) predicts a discontinuous phase transition in any number of dimensions for $\mu$ sufficiently small. A discontinuous transition between an active and an absorbing phase is not expected in one-dimensional systems of the kind studied here [15], nor do our simulations show any evidence of a discontinuous transition in two dimensions. Nevertheless, we cannot discard the possibility of such a transition for $d \geqslant 2$, for small values of $\mu$, or under rapid particle diffusion, which generally favors mean-field-like behavior.

Overall, the critical behavior of the symbiotic models is consistent with that of directed percolation. Corrections to scaling are, however, more significant than in the basic CP, so that a study restricted to smaller systems, or to only one kind of simulation, could easily suggest non-DP behavior. These corrections are stronger, and of longer duration, the *smaller* the intensity of symbiosis. Thus, in the two-dimensional case, the decay of $\rho$ (in initial-decay studies) attains the expected power-law regime (with a DP value for the decay exponent), *except* for $\mu = 0.9$, the weakest symbiosis studied. A similar tendency is observed in the QS simulations of the one-dimensional 2SCP, for which the estimates for critical exponents and the critical moment ratio $m_c$ differ most from DP values for $\mu = 0.9$.

In the initial-decay studies in one dimension, for smaller intensities of symbiosis (i.e., $\mu = 0.9$ and 0.75), we observe anomalous growth of fluctuations in the order parameter. The latter are characterized by $m_\rho - 1 = \mathrm{var}(\rho)/\rho^2$, which is expected to grow $\sim t^{1/z}$, before saturating at its QS value. The growth at long times corresponds to a $z$ value significantly smaller than that of DP. The exponent $z_q$ associated with the growth of $m_q$ is substantially larger, though still slightly below the DP value. In contrast with these anomalies, the spreading exponents are found to take DP values in one dimension,

*independent* of the degree of symbiosis. Thus we are inclined to regard the asymptotic scaling of the symbiotic models as being that of DP and to interpret the deviations as arising from finite-time and finite-size corrections. One might conjecture that under strong symbiosis, the critical system is rapidly attracted to the DP fixed point (although not as rapidly as is the basic CP), whereas for weak symbiosis, it makes a long excursion into a regime in which DP-like scaling is not evident before finally returning to the vicinity of the DP fixed point. The asymptotic scaling behavior is presumably associated with large, sparsely populated but highly correlated regions of doubly occupied sites, which, for reasons of symmetry, behave analogously to DP space-time clusters. The presence of isolated particles, which are relatively numerous and long lived for weak symbiosis, could mask the asymptotic critical behavior, on short scales. We defer further analysis of these questions to future work.

Extending the field theory of DP to the two-species case, we find that the irrelevance of four-field terms makes DP extremely robust since the only possible three-field vertices are already present in the single-species theory. This means that the interaction between species cannot alter the scaling behavior, as already noted by Janssen in the case of multispecies DP processes [12]. Our simulation results, as noted, support this conclusion. A more detailed field-theoretic analysis, including the evolution of the lowest-order irrelevant terms, might shed some light on the scaling anomalies observed in the simulations.

## ACKNOWLEDGMENTS

We are grateful to Miguel A. Muñoz for helpful comments. This work was supported by Conselho Nacional de Desenvolvimento Científico e Tecnológico and Fundação de Amparo à Pesquisa do Estado de Minas Gerais, Brazil.

[1] J. Marro and R. Dickman, *Nonequilibrium Phase Transitions in Lattice Models* (Cambridge University Press, Cambridge, 1999).
[2] M. A. Muñoz *et al*., in *Procedings of the 6th Granada Seminar on Computational Physics*, edited by J. Marro and P. L. Garrido, AIP Conf. Proc. No. 574 (AIP, New York, 2001).
[3] G. Ódor, *Universality in Nonequilibrium Lattice Systems: Theoretical Foundations* (World Scientific, Singapore, 2007).
[4] M. Henkel, H. Hinrichsen, and S. Lübeck, *Non-Equilibrium Phase Transitions: Absorbing Phase Transitions* (Springer, Dordrecht, 2008).
[5] G. Ódor, Rev. Mod. Phys. **76**, 663 (2004).
[6] K. A. Takeuchi, M. Kuroda, H. Chaté, and M. Sano, Phys. Rev. Lett. **99**, 234503 (2007).
[7] L. Corté, P. M. Chaikin, J. P. Gollub, and D. J. Pine, Nat. Phys. **4**, 420 (2008).
[8] H. K. Janssen, Z. Phys. B **42**, 151 (1981).
[9] P. Grassberger, Z. Phys. B **47**, 365 (1982).
[10] I. Dornic, H. Chaté, J. Chave, and H. Hinrichsen, Phys. Rev. Lett. **87**, 045701 (2001).
[11] T. E. Harris, Ann. Probab. **2**, 969 (1974).
[12] H. K. Janssen, J. Stat. Phys. **103**, 801 (2001).
[13] H. Hinrichsen, Adv. Phys. **49**, 815 (2000).
[14] M. M. de Oliveira and R. Dickman, Phys. Rev. E **84**, 011125 (2011).
[15] H. Hinrichsen, arXiv:cond-mat/0006212.
[16] M. M. de Oliveira and R. Dickman, Phys. Rev. E **71**, 016129 (2005); R. Dickman and M. M. de Oliveira, Physica A **357**, 134 (2005).
[17] R. Dickman and J. Kamphorst Leal da Silva, Phys. Rev. E **58**, 4266 (1998).
[18] P. Grassberger and A. de la Torre, Ann. Phys. (NY) **122**, 373 (1979).
[19] R. da Silva, R. Dickman, and J. R. Drugowich de Felicio, Phys. Rev. E **70**, 067701 (2004).
[20] M. Doi, J. Phys. A **9**, 1465 (1976); **9**, 1479 (1976).
[21] L. Peliti, J. Phys. **46**, 1469 (1985).
[22] R. Dickman and R. Vidigal, Braz. J. Phys. **33**, 73 (2003).
[23] U. C. Täuber, in *Field-Theory Approaches to Nonequilibrium Dynamics*, edited by M. Henkel, M. Pleimling, and R. Sanctuary, Lecture Notes in Physics, Vol. 716 (Springer, Heidelberg, 2007), pp. 295–348.
[24] F. van Wijland, K. Oerding, and H. J. Hilhorst, Physica A **251**, 179 (1998).

Capítulo 3

# Sobrevivência do mais escasso no espaço

*Esta introdução é baseada nos resultados do artigo [4], publicado em* ***Journal of Statistical Mechanics****.*

É comum se afirmar que populações grandes de espécies interagentes tendem a ser menos susceptíveis à extinção quando em competição com populações mais escassas. Seria interessante nos questionar se é possível o contrário e, se a resposta for sim, sob quais condições.

Em um artigo recente [34] foi proposto um modelo em que há a possibilidade de a espécie mais escassa ser menos susceptível à extinção quando em competição com uma espécie mais numerosa, com características análogas. Os autores utilizaram um modelo $0-$dimensional e tal fenômeno foi denominado de *sobrevivência do mais escasso* (SE). A condição para que o fenômeno SE ocorra é que a espécie mais escassa precisa ser *mais competitiva* na interação com a mais abundante. Mais competitiva quer dizer que na maioria das vezes que um ser da espécie mais rara luta pela sobrevivência com um ser da espécie mais abundante, a primeira vence.

Até aqui, não há nenhuma surpresa. Porém, o interessante é que há um regime de equilíbrio onde a descrição feita em termos de equações diferenciais (descrição contínua), que indica a prevalência de uma dada espécie, fica em explícito contraste com a descrição discreta feita através da equação mestra, que indica uma maior chance de extinção da espécie prevalente. A descrição probabilística em termos da equação mestra leva em conta a finitude das populações e a discreteza das interações entre as espécies. E o resultado obtido nas duas descrições, contínua e discreta, são conflitantes. Estamos diante de um típico exemplo onde uma descrição feita em termos de equações diferenciais (às vezes denominada descrição em termos da *teoria de campo médio*) está em pleno contraste com a descrição mais detalhada e realista da equação mestra. Tal descrição em termos probabilísticos que leva em consideração a intrínseca aleatoriedade das interações entre os agentes tem tido um papel muito relevante no desenvolvimento de vários ramos da biologia teórica. E este fato representa e espinha dorsal de todo a minha pesquisa de doutorado.

O artigo que expõe o fenômeno SE não considera a possibilidade de as espécies se difundirem no espaço. É conhecida a importância que o fenômeno da difusão pode ter nas dinâmicas populacionais de espécies interagentes. Alguns fenômenos conhecidos que decorrem desta extensão espacial são a formação de padrões espaciais e temporais, a formação de frentes de onda de invasão de uma espécie sobre a outra, o surgimento de um tamanho crítico mínimo para sustentar uma população em um ambiente hostil, etc.

Em um artigo publicado em *Journal of Statistical Mechanics* [4], extendemos o modelo original à situação onde as espécies podem se difundir pelo espaço $d-$dimensional e verificamos que o fenômeno da *sobrevivência do mais escasso no espaço* (SEE) se verifica, com algumas diferenças. Utilizamos as técnicas de mapeamento do processo estocástico subjacente em uma teoria de campos via procedimento de Doi-Peliti [27]. Subsequentemente utilizamos os conceitos da teoria do grupo de renormalização para inferirmos como as intensidades das interações variam com a escala de observação. Construímos um diagrama que mostra as regiões no espaço de parâmetros onde há coexistência entre as espécies. Constatamos

que este diagrama é fundamentalmente diferente do diagrama proposto no artigo original [34]. Uma das principais conclusões é que para qualquer vantagem competitiva que uma espécie tenha sobre a outra, não importa o quão pequena ela seja, no *longo prazo* e para escalas de observação grandes*, teremos que a espécie menos abundante, *se* mais competitiva, *sobrepuja* a espécie mais numerosa. De certa forma o fenômeno SE ficou muito mais evidente e robusto na nova versão SEE quando consideramos a possibilidade de difusão.

Simulações de Monte Carlo confirmaram a existência do fenômeno SEE e detalhes a respeito dele foram obtidos numericamente, como algumas características relacionadas às velocidades de propagação das frentes de onda das populações no espaço e as distribuições de probabilidade quase-estacionárias.

*Suponhamos, por exemplo, na escala de dezenas ou centenas de quilômetros.

# Survival of the scarcer in space



J. Stat. Mech. (2013) P07004

(http://iopscience.iop.org/1742-5468/2013/07/P07004)

Journal of Statistical Mechanics: Theory and Experiment
An IOP and SISSA journal

# Survival of the scarcer in space

**Renato Vieira dos Santos**[1] **and Ronald Dickman**[1,2]

[1] Departamento de Física, Instituto de Ciências Exatas, Universidade Federal de Minas Gerais, CP 702, CEP 30161-970, Belo Horizonte, Minas Gerais, Brazil
[2] National Institute of Science and Technology for Complex Systems, Universidade Federal de Minas Gerais, CP 702, CEP 30161-970, Belo Horizonte, Minas Gerais, Brazil
E-mail: econofisico@gmail.com and dickman@fisica.ufmg.br

Received 13 April 2013
Accepted 16 June 2013
Published 4 July 2013

Online at stacks.iop.org/JSTAT/2013/P07004
doi:10.1088/1742-5468/2013/07/P07004

**Abstract.** The dynamics leading to extinction or coexistence of competing species is of great interest in ecology and related fields. Recently a model of intra- and interspecific competition between two species was proposed by Gabel *et al*, in which the scarcer species (i.e., with smaller stationary population size) can be more resistant to extinction when it holds a competitive advantage; the latter study considered populations without spatial variation. Here we verify this phenomenon in populations distributed in space. We extend the model of Gabel *et al* to a $d$-dimensional lattice, and study its population dynamics both analytically and numerically. Survival of the scarcer in space is verified for situations in which the more competitive species is closer to the threshold for extinction than is the less competitive species, when considered in isolation. The conditions for survival of the scarcer species, as obtained applying renormalization group analysis and Monte Carlo simulation, differ in detail from those found in the spatially homogeneous case. Simulations highlight the speed of invasion waves in determining the survival times of the competing species.

**Keywords:** renormalization group, stochastic particle dynamics (theory), population dynamics (theory), stochastic processes



 1742-5468/13/P07004+19$33.00

## Contents



## 1. Introduction

Coexistence of species and maintenance of species diversity are key issues in ecology as well as in conservation and restoration. A key idea in this context is the competitive exclusion principle, which asserts that similar species competing for a limited resource cannot coexist [1]. Individual-based stochastic models, both with and without spatial structure, are useful for analyzing these questions [2]. There is some evidence [3] to suggest that spatial structure should facilitate coexistence of similar competitors. This is because when dispersal and interactions are localized, individuals tend to interact with conspecific neighbors more frequently than would be suggested by the overall densities at the landscape level; this is a common pattern in natural communities [4]. Computer simulations suggest that such spatial structures could lead to the long-term coexistence of similar competitors and hence to the maintenance of high levels of biodiversity [5]. This mechanism has been encapsulated in the segregation hypothesis [6], which states that intraspecific spatial aggregation promotes stable coexistence by reducing interspecific competition.

In the context of competition and extinction, the question of population size plays a fundamental role. In the simplest birth-and-death models, for example, the extinction probability of a viable, but initially small population is high, but decreases rapidly with population size.[3] Recently, Gabel *et al* [7] proposed a stochastic model of two-species competition in which the species with smaller population size is, under certain conditions, less susceptible to extinction than the more populous species. This phenomenon, dubbed

[3] See chapter 2 of [2].



J. Stat. Mech. (2013) P07004

survival of the scarcer (SS) in [7], is somewhat surprising since conventional wisdom on population dynamics suggests that a smaller population is more susceptible to extinction due to demographic fluctuations. The authors of [7] use a variant of the Wentzel–Kramers–Brillouin–Jeffreys (WKBJ) approximation to obtain the tails of the quasi-stationary (QS) probability distribution [8, 9]. (Here and below, the quasi-stationary regime characterizes the behavior at long times, conditioned on survival.) They show that asymmetry in interspecific competition can induce survival of the scarcer species.

While the analysis of [7] holds for well mixed (spatially uniform) populations, in view of the above-mentioned segregation hypothesis it is natural to inquire whether the same conclusions apply for populations distributed in space. In this paper we study a stochastic model similar to that of [7], but with organisms located on a $d$-dimensional lattice, and investigate the conditions required for survival of the scarcer in space (SSS). On reproduction, a daughter organism appears at the same site as the mother; competition only occurs between organisms at the same site. In addition to these reactions, organisms also diffuse on the lattice. We study the model using two complementary approaches: field-theoretic analysis and direct numerical (Monte Carlo) simulation.

Since the field-theoretic study requires specialized techniques, we summarize the method for readers less familiar with this approach. Starting from the master equation, we construct a representation involving creation and annihilation operators. This allows us to obtain a functional integral formulation, that is, a mapping of the stochastic process to a field theory. This now standard procedure is known as the Doi–Peliti mapping [10]–[12]. We consider the population dynamics in a critical situation, i.e., competing populations close to extinction. The dynamic renormalization group (DRG) is used to study the nonequilibrium critical dynamics of the populations, specifically, to determine how the model parameters transform under rescaling of length and time. The analysis furnishes a set of reduced stochastic evolution equations that describe the population dynamics for parameters close to those of a fixed point of the DRG. Analysis of these equations lets us map out regions of coexistence and of single-species survival in the space of reproduction and competition rates. In particular, we find regions in which the species predicted by mean-field theory to have the larger population in fact goes extinct.

We use Monte Carlo simulations to probe the QS population densities and lifetimes of the two species. We find SSS in a small but significant region of parameter space, in which the less populous species is more competitive. The simulations yield insights into the spatiotemporal pattern of population growth and decay, the speed of species invasion, and the QS probability distribution.

The remainder of this paper is organized as follows. In section 2 we describe the model and write the effective action associated with the stochastic process. A brief analysis of mean-field theory, valid in dimensions greater than the critical dimension is performed. In section 3 we use some known results on multispecies directed percolation to obtain the renormalization group flow in parameter space. This analysis, combined with numerical simulations of the associated stochastic partial differential equations, allows us to determine the regions in parameter space in which SSS occurs. Results of Monte Carlo simulations are presented in section 4. Section 5 closes the paper with our conclusions.

J. Stat. Mech. (2013) P07004

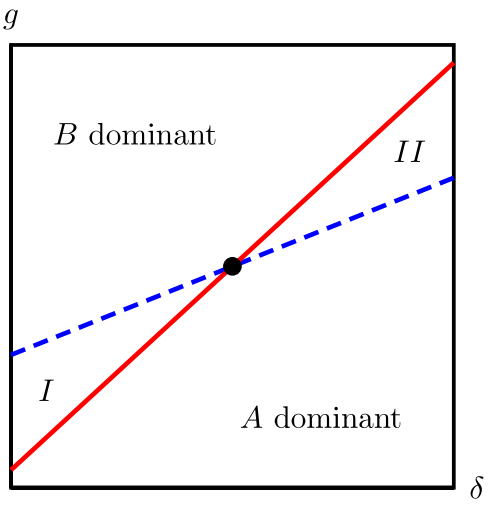


**Figure 1.** Phase diagram of a well mixed system in the $g$–$\delta$ plane, as furnished by the analysis of [7]. Dashed blue curve: $g_{\rm mf} = (1+\delta\epsilon)/(1+\epsilon)$. Full red curve: $g_{\rm sw} = (1+m\delta\epsilon)/(1+m\epsilon)$.

## 2. Model

The model proposed in [7] may be described, with some minor modifications in the rates as specified below, by the following set of reactions:

$$\begin{array}{ll} \mathrm{A} \xrightarrow{\alpha} \mathrm{A}+\mathrm{A} & \mathrm{B} \xrightarrow{\beta} \mathrm{B}+\mathrm{B} \\ \mathrm{A}+\mathrm{A} \xrightarrow{\alpha'} \emptyset(\mathrm{A}) & \mathrm{B}+\mathrm{B} \xrightarrow{\beta'} \emptyset(\mathrm{B}) \\ \mathrm{A}+\mathrm{B} \xrightarrow{\zeta} \mathrm{B} & \mathrm{A}+\mathrm{B} \xrightarrow{\xi} \mathrm{A}. \end{array} \tag{1}$$

The reactions in the first line correspond to reproduction of species A and B. Those in the second line describe intraspecific competition resulting in the death of one individual (A/B) or of both ($\emptyset$), while the third line represents interspecific competition. $\alpha$ ($\beta$), $\alpha'$ ($\beta'$) and $\zeta$ ($\xi$) are the rates of the reactions associated with species A (B).

The relation between the rates in equation (1) and those of the original model [7] is (in the case of mutual annihilation): $\alpha \leftrightarrow 1$, $\beta \leftrightarrow g$, $\alpha' \leftrightarrow 1/K$, $\beta' \leftrightarrow 1/K$, $\zeta \leftrightarrow \epsilon/K$, and $\xi \leftrightarrow \delta\epsilon/K$. $\delta < 1$ implies an asymmetry in competition between species that favors B at the expense of A. In this case species B is *more competitive* than A; the opposite occurs if $\delta > 1$.

The authors of [7] constructed a phase diagram in the $g$–$\delta$ plane (shown schematically in figure 1). The phase diagram includes results of both mean-field theory (MFT) and analysis of the master equation for a stochastic population model in a well mixed system, i.e., without spatial structure. In MFT, the populations of the two species are equal when $g_{\rm mf}(\delta) = (1+\delta\epsilon)/(1+\epsilon)$. Analysis of the master equation in the QS regime yields equal extinction probabilities when $g_{\rm sw}(\delta) = (1+m\delta\epsilon)/(1+m\epsilon)$ with $m \equiv [(\ln 2)^{-1} - 1]^{-1}$. These conditions are plotted in figure 1; they intersect at the point $(g, \delta) = (1, 1)$. The phase diagram includes two 'normal' regions, in which the more populous species is less likely to go extinct, and two 'anomalous' regions, in which the scarcer species is more likely to survive. Thus in region I (where $\delta < 1$ and B is more competitive in the sense defined



J. Stat. Mech. (2013) P07004

above), species A is more numerous in the quasi-stationary state and simultaneously more susceptible to extinction, while in region II (where $\delta > 1$ and A is more competitive), species B is more numerous, yet more likely to go extinct first. Regions I and II are anomalous since they correspond to an inversion of the usual dictum that susceptibility to extinction grows with diminishing population size. Our goal in this work is to determine whether a stochastic model of two-species competition with spatial structure, in which organisms diffuse in $d$-dimensional space, exhibits a similar phenomenon. In section 2.1 we develop a continuum description for this spatial stochastic process.

### 2.1. Effective action

We consider a stochastic implementation of the reactions of equation (1) on a $d$-dimensional lattice, adding diffusion (nearest-neighbor hopping) of individuals of species A and B at rates $D_{\rm A}$ and $D_{\rm B}$ respectively. Following the standard Doi–Peliti procedure mentioned in section 1, ignoring irrelevant terms (in the renormalization group sense) and with the so-called Doi shift [12] already performed, we obtain the following effective action:

$$\begin{aligned} S(\bar{\phi},\phi,\bar{\psi},\psi) = & \int \mathrm{d}^{\mathrm{d}}x \int \mathrm{d}t \left\{ \bar{\phi}[\partial_t + D_{\rm A}(\sigma_{\rm A} - \nabla^2)]\phi - \alpha\bar{\phi}^2\phi + j\alpha'\bar{\phi}\phi^2 + \alpha'\bar{\phi}^2\phi^2 + \zeta\psi\phi\bar{\phi} \right\} \\ & + \int \mathrm{d}^{\mathrm{d}}x \int \mathrm{d}t \left\{ \bar{\psi}[\partial_t + D_{\rm B}(\sigma_{\rm B} - \nabla^2)]\psi - \beta\bar{\psi}^2\psi + j\beta'\bar{\psi}\psi^2 + \beta'\bar{\psi}^2\psi^2 \right. \\ & \left. + \xi\phi\psi\bar{\psi} \right\}, \end{aligned} \tag{2}$$

where $\sigma_{\rm A} \equiv -\alpha/D_{\rm A}$, $\sigma_{\rm B} \equiv -\beta/D_{\rm B}$ and $j \equiv 1$ (2) for individual death (mutual annihilation). Action $S$ has four fields. The expected values of the fields $\phi$ and $\psi$ (evaluated by performing functional integrals over the four fields, using the weight $\exp[-S]$), represent the mean population densities of species A and B, respectively. The fields with overbars have no immediate physical interpretation, but are related to intrinsic fluctuations of the stochastic dynamics. In particular, terms quadratic in $\bar{\phi}$ and $\bar{\psi}$ correspond to *noise* in the associated stochastic evolution equations [13]. The terms $\propto \phi\bar{\phi}^2$ and $\psi\bar{\psi}^2$ correspond, respectively, to intrinsic fluctuations of species A and B. In the expansion of the action in powers of the fields, the lowest order term involving the product $\bar{\phi}\bar{\psi}$ would be $\phi\psi\bar{\phi}\bar{\psi}$. Since it is of fourth order in the fields, this term is *irrelevant*, that is, the coefficient of this term flows to zero under repeated renormalization group transformations; it has therefore been excluded from the action. Fluctuations of one species nevertheless affect the other species via the coupling terms $\propto \zeta$ and $\xi$ in equation (2).

Using the definitions of $\sigma_{\rm A}$ and $\sigma_{\rm B}$ and the change of variables $\bar{\phi} \to \theta_{\rm A}\bar{\phi}$, $\phi \to \theta_{\rm A}^{-1}\phi$, $\bar{\psi} \to \theta_{\rm B}\bar{\psi}$, and $\psi \to \theta_{\rm B}^{-1}\psi$, where $\theta_{\rm A} \equiv \sqrt{j\alpha'/\alpha}$, $\theta_{\rm B} \equiv \sqrt{j\beta'/\beta}$, we can write the effective action in the form:

$$\begin{aligned} S(\bar{\phi},\phi,\bar{\psi},\psi) \quad = & \int \mathrm{d}^{\mathrm{d}}x \int \mathrm{d}t \Big\{ \bar{\phi}[\partial_t + D_{\rm A}(\sigma_{\rm A} - \nabla^2)]\phi \\ & + \bar{\psi}[\partial_t + D_{\rm B}(\sigma_{\rm B} - \nabla^2)]\psi \\ & + g_{\rm A}\phi\bar{\phi}(\phi - \bar{\phi}) + g_{\rm B}\psi\bar{\psi}(\psi - \bar{\psi}) + h_{\rm B}\phi\psi\bar{\psi} + h_{\rm A}\phi\psi\bar{\phi} \Big\}, \end{aligned} \tag{3}$$

with

$$g_{\rm A} \equiv \sqrt{j\alpha\alpha'} \qquad h_{\rm A} \equiv \theta_{\rm A}^{-1}\zeta \qquad g_{\rm B} \equiv \sqrt{j\beta\beta'} \qquad h_{\rm B} \equiv \theta_{\rm B}^{-1}\xi. \tag{4}$$



J. Stat. Mech. (2013) P07004

Dimensional analysis yields

$$[h_{\rm A}] = [h_{\rm B}] = p^{2-d/2} = [g_{\rm A}] = [g_{\rm B}],$$

where $[X]$ denotes the dimensions of $X$, and $p$ has dimensions of momentum [12]. The upper critical dimension is therefore $d_{\rm c} = 4$, as for single-species processes such as the contact process and directed percolation.

### 2.2. Mean-field approximation

For $d \geq d_{\rm c}$, mean-field analysis, which ignores fluctuations in $\phi$ and $\psi$, yields the correct critical behavior. Imposing the conditions $\delta S/\delta\phi = 0$, $\delta S/\delta\bar{\phi} = 0$, $\delta S/\delta\psi = 0$ and $\delta S/\delta\bar{\psi} = 0$, we obtain the mean-field equations

$$\begin{aligned} \frac{\partial\phi}{\partial t} &= D_{\rm A}\nabla^2\phi + \alpha\phi - g_{\rm A}\phi^2 - h_{\rm B}\phi\psi \\ \frac{\partial\psi}{\partial t} &= D_{\rm B}\nabla^2\psi + \beta\psi - g_{\rm B}\psi^2 - h_{\rm A}\phi\psi. \end{aligned} \tag{5}$$

Let $L$ be a typical length scale and define $X = g_{\rm A}\phi/\alpha$, $Y = g_{\rm B}\psi/\beta$, $s = D_{\rm A}t/L^2$, and define a rescaled coordinate $x' = x/L$. Then equation (5) can be written in dimensionless form as

$$\begin{aligned} \frac{\partial X}{\partial s} &= \nabla^2 X + \gamma\left(X - X^2 - aXY\right) \equiv \nabla^2 X + f(X,Y) \\ \frac{\partial Y}{\partial s} &= D\nabla^2 Y + \gamma\left(cY - cY^2 - bXY\right) \equiv D\nabla^2 Y + g(X,Y) \end{aligned} \tag{6}$$

with $\gamma \equiv \alpha L^2/D_{\rm A}$, $a \equiv \beta h_{\rm B}/(\alpha g_{\rm B})$, $b \equiv \beta h_{\rm A}/(\alpha g_{\rm B})$, $c \equiv g_{\rm A}\beta^2/(g_{\rm B}\alpha^2)$, $D \equiv D_{\rm B}\beta g_{\rm A}/(D_{\rm A}\alpha g_{\rm B})$, $f(X,Y) \equiv \gamma(X - X^2 - aXY)$ and $g(X,Y) \equiv \gamma(cY - cY^2 - bXY)$. Coexistence is possible in the stationary state if the conditions $c > b$ and $a < 1$ hold, implying $h_{\rm A} < \beta g_{\rm A}/\alpha$ and $h_{\rm B} < \alpha g_{\rm B}/\beta$. These conditions depend monotonically on parameters $\alpha, \beta, g_{\rm A}$ and $g_{\rm B}$, analogous to the coexistence conditions found in [7]. The same is not true in spatial stochastic theory, as we shall see in section 3.

## 3. Renormalization group (RG) flow

In this section we apply a renormalization group analysis to determine regions of coexistence and of single-species survival in the space of reproduction and competition rates. Some years ago, Janssen analyzed a class of reactions of the kind defined in equation (1) [14]. This work considered multispecies reactions of the form

$$X_i \leftrightarrow 2X_i \qquad X_i \to \emptyset \qquad X_i + X_j \to kX_i + lX_j, \tag{7}$$

where $i$ and $j$ are species indices and $k, l$ are either zero or unity; this process is called multicolored directed percolation (MDP), with different colors referring to different species. The RG analysis of [14] shows that knowledge of the directed percolation fixed points is sufficient to determine the fixed points of the full MDP. As shown in that work, the parameter combinations $g_{\rm A}/D_{\rm B} \equiv u_{\rm A}$ and $g_{\rm B}/D_{\rm A} \equiv u_{\rm B}$, related to intraspecific competition, flow under renormalization group transformations to the stable DP fixed point $u^*_{\rm A} = u^*_{\rm B} = u^* = 2\epsilon/3$ with $\epsilon = 4 - d > 0$.[4] Therefore, regarding the renormalization

[4] Not to be confused with parameter $\epsilon$ used in equation (1).



J. Stat. Mech. (2013) P07004

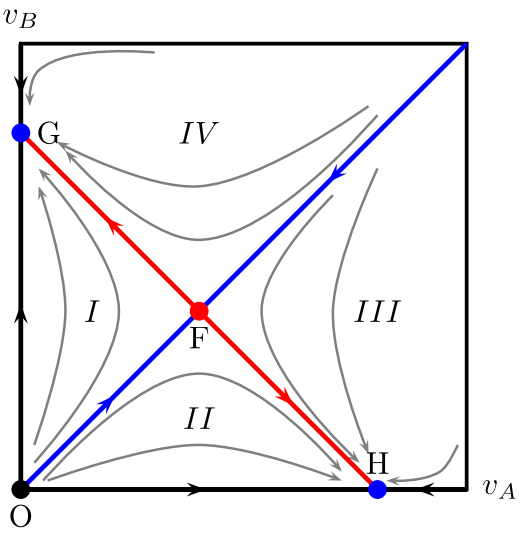


**Figure 2.** RG flow of the interspecific competition parameters $v_\mathrm{B}$ and $v_\mathrm{A}$. Only the first quadrant is relevant due to the requirement of positive rates. There is an unstable fixed point **O** at $(v_\mathrm{A}, v_\mathrm{B}) = (0, 0)$ (black dot); a hyperbolic fixed point **F** at $(v_\mathrm{A}, v_\mathrm{B}) = (u^*, u^*)$ (red dot), and two stable fixed points **G** and **H**, located at $(v_\mathrm{A}, v_\mathrm{B}) = (0, 2u^*)$ and $(v_\mathrm{A}, v_\mathrm{B}) = (2u^*, 0)$ respectively (blue dots). The separatrix $v_\mathrm{A} = v_\mathrm{B}$ is the boundary between the basins of attraction of **G** and **H**.

of intraspecific competition parameters, inclusion of other species behaving as in DP does not alter the fixed point.

Janssen's analysis shows that there are four fixed points for interspecific competition parameters $h_\mathrm{A}/D_\mathrm{A} \equiv v_\mathrm{A}$ and $h_\mathrm{B}/D_\mathrm{B} \equiv v_\mathrm{B}$, which from reactions (1) are related to $\xi$ and $\zeta$. The first two are $(v_\mathrm{A}^*, v_\mathrm{B}^*) = (0, 0)$, which is unstable, and

$$(v_\mathrm{A}^*, v_\mathrm{B}^*) = \left( \frac{D_\mathrm{A} + D_\mathrm{B}}{D_\mathrm{A}} \frac{2}{3}\epsilon, \frac{D_\mathrm{A} + D_\mathrm{B}}{D_\mathrm{B}} \frac{2}{3}\epsilon \right) \tag{8}$$

which is a hyperbolic fixed point if $D_\mathrm{A} = D_\mathrm{B}$.[5] For $D_\mathrm{A} \neq D_\mathrm{B}$, it was conjectured [14] that the stability of the fixed points remains the same despite small changes in the renormalization group flow diagram topology. The other two fixed points for $D_\mathrm{A} = D_\mathrm{B}$ are stable; they are given by $(v_\mathrm{A}^*, v_\mathrm{B}^*) = (0, 2u^*)$ and $(v_\mathrm{A}^*, v_\mathrm{B}^*) = (2u^*, 0)$. To summarize, for $D_\mathrm{A} = D_\mathrm{B} \equiv D_0$, the interspecies competition parameters flow to one of the following four $d$-dependent fixed points (denoted as **O**,**F**,**G**, and **H** below),

$$\begin{aligned} (v_\mathrm{A}, v_\mathrm{B}) &= \left( \frac{\theta_\mathrm{A}^{-1}\zeta}{D_0}, \frac{\theta_\mathrm{B}^{-1}\xi}{D_0} \right) \\ &\to \{ \mathbf{O} : (0, 0), \qquad \mathbf{F} : (u^*, u^*), \\ &\quad \mathbf{G} : (2u^*, 0), \qquad \mathbf{H} : (0, 2u^*) \}. \end{aligned} \tag{9}$$

Figure 2 shows the renormalization group flow diagram. The unstable fixed point **O** corresponds to complete decoupling between the two species, and the hyperbolic point **F** to

[5] In the nomenclature of [14], if species are of the same flavor.



J. Stat. Mech. (2013) P07004

symmetric coupling. In the symmetric subspace, any nonzero initial value of $v \equiv v_A = v_B$, flows to **F**. For $v_B > v_A$ ($\delta > 1$), $(v_A, v_B)$ flows to **G**, so that species A is effectively unable to compete with B. Similarly, if $v_A > v_B$ ($\delta < 1$), the flow attains point **H**. In section 3.1 we discuss the stationary states associated with these fixed points.

### 3.1. Steady state close to critical points

Population dynamics in the critical regime is governed by a pair of coupled stochastic partial differential equations (SPDE), which are readily deduced from the action of equation (3) [12]:

$$\frac{\partial \phi}{\partial t} = D_0 \nabla^2 \phi + \alpha \phi - g_A \phi^2 - h_B \phi \psi + \eta_1 \tag{10}$$

and

$$\frac{\partial \psi}{\partial t} = D_0 \nabla^2 \psi + \beta \psi - g_B \psi^2 - h_A \psi \phi + \eta_2 \tag{11}$$

where the noise terms $\eta_1(\mathbf{x}, t)$ and $\eta_2(\mathbf{x}, t)$ satisfy $\langle \eta_1(\mathbf{x}, t) \rangle = \langle \eta_2(\mathbf{x}, t) \rangle = 0$, and

$$\langle \eta_1(\mathbf{x}, t) \eta_1(\mathbf{x}, t) \rangle = 2 g_A \phi(\mathbf{x}, t) \delta^d(\mathbf{x} - \mathbf{x}') \delta(t - t'), \tag{12}$$

$$\langle \eta_2(\mathbf{x}, t) \eta_2(\mathbf{x}, t) \rangle = 2 g_B \psi(\mathbf{x}, t) \delta^d(\mathbf{x} - \mathbf{x}') \delta(t - t'). \tag{13}$$

Note that these multiplicative noise terms depend on the square root of their respective fields, and were obtained directly from the action, without any additional hypotheses.

*3.1.1. SPDE in the vicinity of point **F**.* In the symmetric subspace, $\delta = 1$, the RG flow is to the fixed point **F**, and parameters $g_A/D_0$, $g_B/D_0$, $h_A/D_0$, and $h_B/D_0$ take the associated values. Therefore the SPDEs in (10) and (11) can be written as [15]:

$$\frac{\partial \phi}{\partial t} = D_0 \nabla^2 \phi + \phi - D_0 u^* \phi^2 - D_0 u^* \phi \psi + \eta_1, \tag{14}$$

$$\frac{\partial \psi}{\partial t} = D_0 \nabla^2 \psi + g \psi - D_0 u^* \psi^2 - D_0 u^* \psi \phi + \eta_2 \tag{15}$$

where we set $\alpha = 1$ and $\beta = g$. With the rescaling $\phi \to \phi/(D_0 u^*)$, $\psi \to \psi/(D_0 u^*)$ and $x \to (1/D_0)^{1/2} x$, we can write equations (14) and (15) in the form:

$$\frac{\partial \phi}{\partial t} = \nabla^2 \phi + \phi - \phi^2 - \phi \psi + \eta_1, \tag{16}$$

$$\frac{\partial \psi}{\partial t} = \nabla^2 \psi + g \psi - \psi^2 - \psi \phi + \eta_2 \tag{17}$$

with rescaled noise

$$\langle \eta_1(\mathbf{x}, t) \eta_1(\mathbf{x}, t) \rangle = 2 (D_0)^{2-d/2} (u^*)^2 \phi(\mathbf{x}, t) \delta^d(\mathbf{x} - \mathbf{x}') \delta(t - t') \tag{18}$$

$$\langle \eta_2(\mathbf{x}, t) \eta_2(\mathbf{x}, t) \rangle = 2 (D_0)^{2-d/2} (u^*)^2 \psi(\mathbf{x}, t) \delta^d(\mathbf{x} - \mathbf{x}') \delta(t - t'). \tag{19}$$

For $d < 4$, the rescaled noise intensity $\sigma$ grows with diffusion rate $D_0$; for $d = 1$ we have $\sigma^2 = 2 D_0^{3/2} u^{*2}$ with $u^{*2} \approx 2$. Figures 3(a) and (b) show results of numerical simulations of equations (16) and (17) in $d = 1$ with $g = 1$. They show, for a one-dimensional lattice of



J. Stat. Mech. (2013) P07004

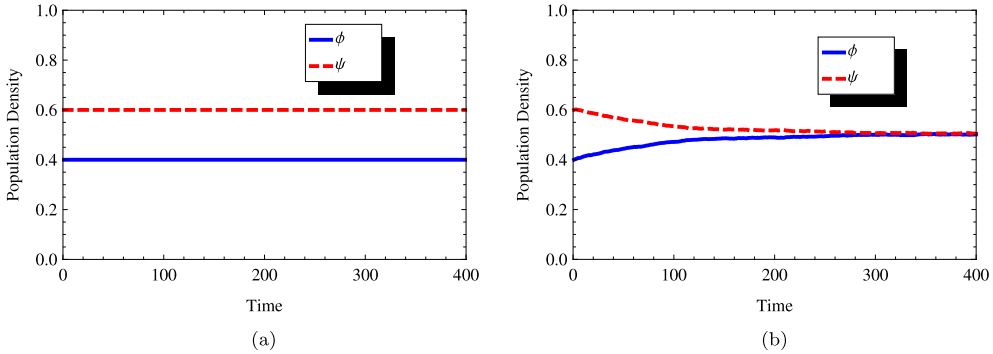


**Figure 3.** Numerical simulations symmetric SPDE. (a) Symmetric case with $\sigma = 0.0$ and $g = 1$. Initial populations are $\phi(x, 0) = 0.4$ and $\psi(x, 0) = 0.6$. (b) Symmetric case with $\sigma = 0.03$ and $g = 1$. Initial populations are $\phi(x, 0) = 0.4$ and $\psi(x, 0) = 0.6$.

$L = 128$ sites in the interval $(-1, 1)$, the population densities averaged over 1000 Monte Carlo realizations for two different values of the noise intensity. The time interval $T$ is $T = 400$, partitioned into $N = 40\,000$ steps so that $\Delta t \equiv T/N = 400/40\,000 = 0.01$. Initial conditions are $\phi(x, 0) = 0.4$ and $\psi(x, 0) = 0.6$. For $\sigma = 0$, population densities are almost time-independent, as shown in figure 3(a). This is not the case for larger noise values. In this case, the two populations tend to the same value (see figure 3(b)). Although figures 3(a) and (b) represent averages over many realizations, we have verified coexistence in individual runs.

These simulations were performed using standard integration techniques for the Langevin equation with the XMDS2 software [16]. Since we are interested in showing only the initial temporal trends of the two population densities in the vicinity of fixed points, the use of standard techniques of integrating the Langevin equations is sufficient to reveal the qualitative nature of the solutions. Near a phase transition to an absorbing state, one of the population densities tends to zero and the standard numerical integration scheme fails. This standard algorithm is not suitable for extracting the more accurate results associated with critical exponents or asymptotic decays. In this case we would have to use more sophisticated algorithms, such as those proposed in [17]–[19].

*3.1.2. SPDE in the vicinity of a stable fixed point.* Now consider the case $\delta \neq 0$. With $\delta > 1$, the parameters flow to point **G** and equations (10) and (11) become

$$\frac{\partial \phi}{\partial t} = D_0 \nabla^2 \phi + \phi - u^* \phi^2 + \eta_1, \tag{20}$$

$$\frac{\partial \psi}{\partial t} = D_0 \nabla^2 \psi + g\psi - u^* \psi^2 - 2u^* \psi\phi + \eta_2, \tag{21}$$

where we put $\alpha = 1$ and $\beta = g$. With a rescaling similar to that used above, we have

$$\frac{\partial \phi}{\partial t} = \nabla^2 \phi + \phi - \phi^2 + \eta_1, \tag{22}$$

$$\frac{\partial \psi}{\partial t} = \nabla^2 \psi + g\psi - \psi^2 - 2\phi\psi + \eta_2 \tag{23}$$



J. Stat. Mech. (2013) P07004

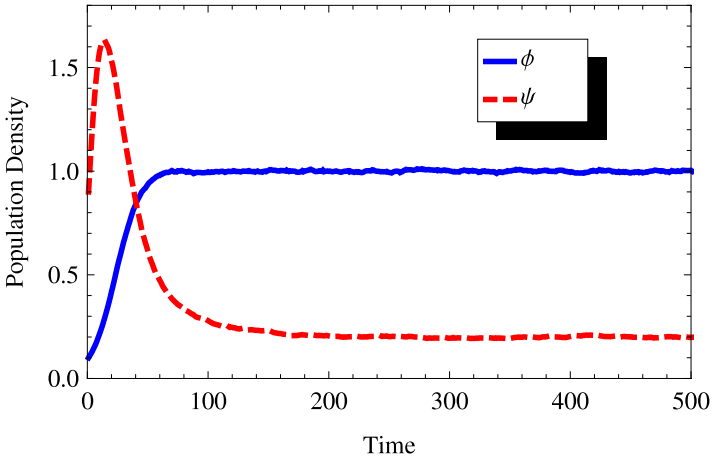


**Figure 4.** Asymmetric case ($\delta = 1.5$) with $\sigma = 0.03$ and $g = 2.2$. Initial populations for A and B species are $\phi(x, 0) = 0.1$ and $\psi(x, 0) = 0.9$, respectively.

with $\eta_1$ and $\eta_2$ satisfying (18) and (19), respectively. For $\delta < 1$ the situation is completely analogous to the case $\delta > 1$, and the resulting equations are as above, with the exchange of $\phi$ and $\psi$ and changing the position of the factor $g$ accordingly.

If we neglect diffusion and noise terms, we have a system of ordinary differential equations having a fixed point associated with the stable coexistence state given by $(\phi^*, \psi^*) = (1, g - 2)$.[6] Therefore, the condition for coexistence is $g > 2$. If $g < 2$, only species A survives for $\delta > 1$. Figure 4 shows the result of a simulation with $g = 2.2$ in which the equations are integrated including both diffusion and noise. Numerical experiments indicate that the effect of these terms is to increase the value of $g \gtrapprox 2$ for coexistence. Higher noise values imply higher thresholds $g$ for coexistence.

For $\delta < 1$ similar reasoning applies. The results are summarized in the phase diagram of figure 5. There are four stationary phases: a pure-A phase for $\delta > 1$ and $g < 2$, a symmetric pure-B phase for $\delta < 1$ and $g < 1/2$, and two (disjoint) coexistence phases. The latter arise when the less competitive species proliferates sufficiently faster than the more competitive one.

*3.1.3. Nature of phase transitions.* From the equations that omit the diffusion and noise terms, one may infer the nature of the phase transitions in the diagram of figure 5. From table 1, which shows the fixed points of the equations for different values of $\delta$, we see that in general the values in the final column do not match for $\delta \neq 1$. This fact indicates that the vertical blue line in the diagram (5), i.e., the line $\delta = 1$, is a line of discontinuous phase transitions. Similarly, examining the expressions in the final column of table 1, we infer the nature of phase transitions along the horizontal lines at $g = 1/2$ and 2. In regions of coexistence, the densities of the minority species grow continuously from zero; thus these transitions are continuous. One should of course recognize that the predictions for the phase diagram are essentially qualitative; quantitative predictions for nonuniversal properties such as phase boundaries are not possible once irrelevant terms have been discarded. Regarding the nature of the transitions, we expect the continuous ones, as

[6] For the case $\delta < 1$, the fixed points are $(\phi^*, \psi^*) = (1 - 2g, g)$, and the coexistence condition is $0 < g < 1/2$.



J. Stat. Mech. (2013) P07004

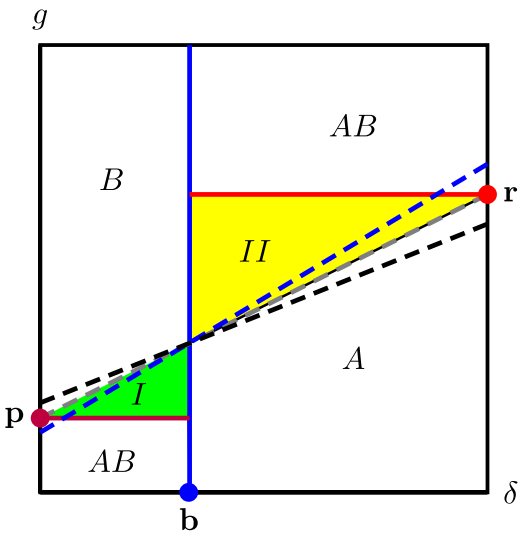


**Figure 5.** Stationary phase diagram in the $g$–$\delta$ plane for the stochastic model with spatial structure. The reference points have coordinates: $\mathbf{b} = (1, 0)$, $\mathbf{p} = (0, 1/2)$, $\mathbf{r} = (3, 2)$. For $\delta > 1$, when $g < 2$ only species A is present, while for $g > 2$ there is coexistence. Similarly, for $\delta < 1$, when $g > 1/2$ only species B is present, and for $g < 1/2$ there is coexistence. The diagonal line connecting points **p** and **r** is the equal-population criterion furnished by mean-field theory, $g_{\rm mf}(\delta) = (1+\epsilon\delta)/(1+\epsilon)$, with $\epsilon = 1$. In regions I and II, the more populous species (A or B, respectively), as predicted by mean-field theory, in fact goes extinct. The thick, dashed, blue and black curves represent $g_{\rm mf}$ and $g_{\rm sw}$ for the value of $\epsilon$ that maximizes the area between them, i.e., $\epsilon = 1/\sqrt{m} \approx 0.66$.

**Table 1.** Simplified equations and their fixed points for different values of $\delta$.

| $\delta$ | Equation | Fixed Point |
|---|---|---|
| $= 1$ | $\dot{\phi} = \phi - \phi^2 - \phi\psi$ and $\dot{\psi} = g\psi - \psi^2 - \phi\psi$ | $(\phi^*, \psi^*) = (0, g)$ |
| $> 1$ | $\dot{\phi} = \phi - \phi^2$ and $\dot{\psi} = g\psi - \psi^2 - 2\phi\psi$ | $(\phi^*, \psi^*) = (1, 2 - g)$ |
| $< 1$ | $\dot{\phi} = g\phi - \phi^2$ and $\dot{\psi} = \psi - \psi^2 - 2\phi\psi$ | $(\phi^*, \psi^*) = (g, 1 - 2g)$ |

furnished by this mean-field-like analysis, do in fact belong to the DP universality class [14]. The line of discontinuous transitions contains a portion (between levels p and r) that is between absorbing subspaces (only on species present in each phase), and other portions that separate (from the viewpoint of the species undergoing extinction) an active and an absorbing phase. Discontinuous transitions of this nature are not expected to occur in one dimension [20].

According to mean-field theory, a point in region II corresponds to $\rho_{\rm B} > \rho_{\rm A}$. If we increase the competitiveness of species A, increasing $\delta$ while maintaining $g$ fixed, there will be a point beyond which species B no longer has the greater population density. Improvement of the competitiveness of species A will make it the more populous species if organisms are well mixed. In the case of a spatially structured population, by contrast, *any* competitive advantage of species A, no matter how small, is sufficient to dominate the B population (if the latter does not proliferate very rapidly) when the population densities



J. Stat. Mech. (2013) P07004

are very low, as is the case near criticality. Thus in a situation in which mean-field theory predicts species B to be the majority, we can have species A *exclusively*. This can be seen as a strong version of the survival of the scarcer phenomenon.

To compare the predictions of the mean-field and spatially structured descriptions, a pair of dashed lines are plotted in figure 5, representing equations for $g_{\rm mf}$ and $g_{\rm sw}$ as defined previously, for parameters such that the area between them is maximum, thereby maximizing the region in which SS occurs. (The maximum area is obtained using $\epsilon = 1/\sqrt{m}$ with $m = [(\ln 2)^{-1} - 1]^{-1}$, in equation (1)). Given the much larger area of the region exhibiting SS in the spatial model, compared with that in the mean-field analysis (i.e., the area between the two dashed lines for $1 < \delta < 3$,) we see that the SS phenomenon can be greatly intensified when spatial structure is included. Analogous reasoning applies for region I (green). (For the parameter values used, however, this reasoning does not apply for $\delta > 3$, since in this case the area between the dashed lines can be arbitrarily large. Also we no longer have a region analogous to region II with species A only.) In this way we see that the phase diagram for the spatial stochastic model is rather different from that found in [7]. Moreover, under certain conditions, the survival of the scarcer phenomenon is strengthened.

## 4. Simulations

Since the preceding analysis involves approximations whose reliability is difficult to assess, we perform simulations of a simple lattice model to verify SSS. This approach permits us to access the QS regime of the spatial model, in finite systems. We consider the following spatial stochastic process, defined on a lattice of $L^d$ sites. Each site $i$ is characterized by nonnegative occupation numbers $a_i$ and $b_i$ for the two species. The organisms (hereafter 'particles') of the two species evolve according to the following rates.

- Particles of either species hop to a neighboring site at rate $D$.
- Particles of species A(B) reproduce at rate $\lambda_{\rm A}(\lambda_{\rm B})$.
- At sites with two or more A particles, mutual annihilation occurs at rate $\alpha_{\rm A} a_i(a_i - 1)$, and similarly for B particles, at rate $\alpha_{\rm B} b_i(b_i - 1)$.
- At sites having both A and B particles, the competitive reaction $\mathrm{B} \to 0$ occurs at rate $\zeta_{\rm A} a_i b_i$ and the reaction $\mathrm{A} \to 0$ occurs at rate $\zeta_{\rm B} a_i b_i$.

The model is implemented in the following manner. In each time step, of duration $\Delta t$, each process is realized, at all sites, in the sequence: hopping, reproduction, annihilation, competition.

In the hopping substep, each site is visited, and the probability of an A particle hopping to the right (under periodic boundaries) is set to $p_{\rm h} = D a_i \Delta t/(2d)$. A random number $z$, uniform on $[0, 1)$ is generated, and if $z < p_{\rm h}$ the site is marked to transfer a particle to the right. Once all sites have been visited, the transfers are realized. The same procedure is applied, in parallel, for B particles hopping to the right. Subsequently, hopping in the other $2d - 1$ directions is realized in the same manner.

In the reproduction substep, the A particle reproduction probability at each site $i$ is taken as $p_{\rm c} = \lambda_{\rm A} a_i \Delta t$. A random number $z$ is generated and a new A particle created at this site if $z < p_{\rm c}$. An analogous procedure is applied for reproduction of B particles.



J. Stat. Mech. (2013) P07004

In the annihilation substep, a probability $p_a = \alpha_A a_i(a_i - 1)\Delta t$ is defined at each site, and mutual annihilation ($a_i \to a_i - 2$) occurs if a random number is $< p_a$. Again, an analogous procedure is applied for annihilation of B particles.

Finally, at sites harboring both A and B particles, probabilities $p_A = \zeta_A a_i b_i \Delta t$ and $p_B = \zeta_B a_i b_i \Delta t$ are defined. The process B $\to 0$ occurs if a random number $z < p_A$, while the complementary process A $\to 0$ occurs if $p_A \leq z < p_A + p_B$. Note that at most one of the processes (A $\to 0$ and B $\to 0$) can occur at a given site in this substep.

The time step $\Delta t$ is chosen to render the reaction probabilities relatively small. To do this, before each step we scan the lattice and determine the maximum, over all sites, of $a_i$, $b_i$, and $a_i b_i$. With this information we can determine the maximum reaction rate over all sites and all reactions. Then $\Delta t$ is taken such that the maximum reaction probability (again, over sites and reactions) be 1/5. In this way, the probability of multiple reactions (e.g., two A particles hopping from $i$ to $i + 1$, etc) is at most 1/25, and can be neglected to a good approximation, particularly in the regime in which occupation numbers are typically small.

We simulate the process on a ring ($d = 1$) using quasi-stationary (QS) simulations, intended to sample the QS probability distribution [21, 22]. In these studies the system is initialized with one A and one B particle at each site. When either species goes extinct (an absorbing subspace for the process), the simulation is reinitialized with one of the active configurations (having nonzero populations for both species) saved during the run. Following a brief transient, the particle densities fluctuate around steady values. We search for parameter values such that species A is more numerous, despite being much less competitive than species B (i.e., $\zeta_B \gg \zeta_A$).

Given the large parameter space, certain rates are kept fixed in the study. We set $D = \alpha_A = \alpha_B = 1/4$. To understand the competitive dynamics we first need to determine the conditions for *single-species* survival. We use QS simulations as well as spreading simulations [23] to estimate the critical value of $\lambda$ for survival of a single species, given $\alpha = 1/4$. In spreading simulations the initial configuration is that of a single site with one particle, and all other sites empty. We search for the value of $\lambda$ associated with a power-law behavior of the survival probability $P(t)$ and the mean population size $n(t)$. These studies yield $\lambda_c = 1.267(1)$ as the critical point for survival of a single species, i.e., without interspecies competition. (Here and in the following, figures in parentheses denote statistical uncertainties in the final digit.) The phase transition is clearly continuous; details on scaling behavior will be reported elsewhere.

In the two-species studies we set $\lambda_A = 1.6$ and $\zeta_A = 0.005$, so that species A is well above criticality but weakly competitive. We then vary $\lambda_B$ and $\zeta_B$, monitoring the QS population densities $\rho_A$ and $\rho_B$ of the two species, as well as their QS lifetimes, $\tau_A$ and $\tau_B$. The latter are estimated by counting the number of times, in a long QS simulation, that one or the other species goes extinct. Survival of the scarcer is then characterized by the conditions $\rho_A > \rho_B$ and $\tau_A < \tau_B$. For the parameter values studied, we observe SSS for $\lambda_B \approx \lambda_c$ and $\zeta_B \gg \zeta_A$. Figure 6 illustrates the variation of the population densities, and of the ratio $\tau_A/\tau_B$, as $\zeta_B$ is varied for fixed $\lambda_B = 1.25$, on a ring of 200 sites. In this case, $\rho_A > \rho_B$ throughout the range of interest; the scarcer species, B, survives longer than A for $\zeta_B \geq 0.25$. Figure 7 shows a typical evolution, for $\zeta_B = 2$ and other parameters as in figure 6. (The spatiotemporal pattern observed for other parameter sets exhibiting SSS is qualitatively similar.) The system is divided into A-occupied regions, B-occupied



J. Stat. Mech. (2013) P07004

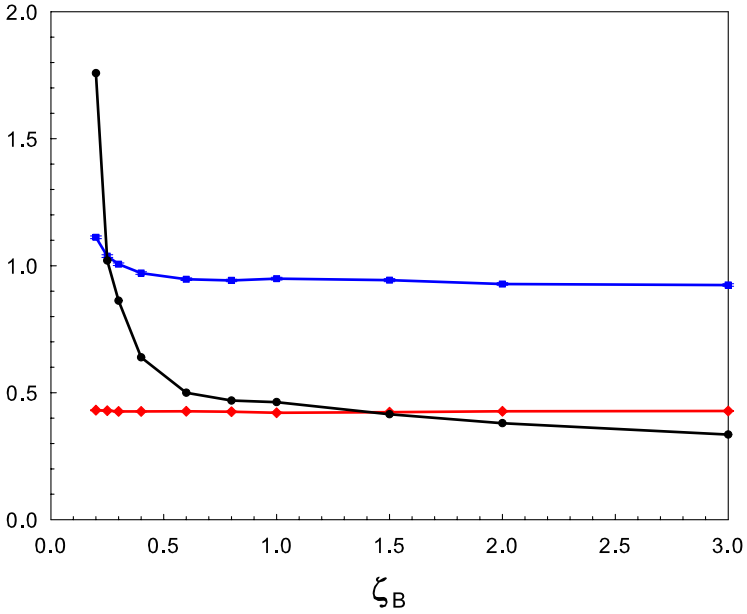


**Figure 6.** Quasi-stationary population densities $\rho_A$ (blue) and $\rho_B$ (red), and lifetime ratio $\tau_A/\tau_B$ (black) versus $\zeta_B$, for parameters as specified in the text.

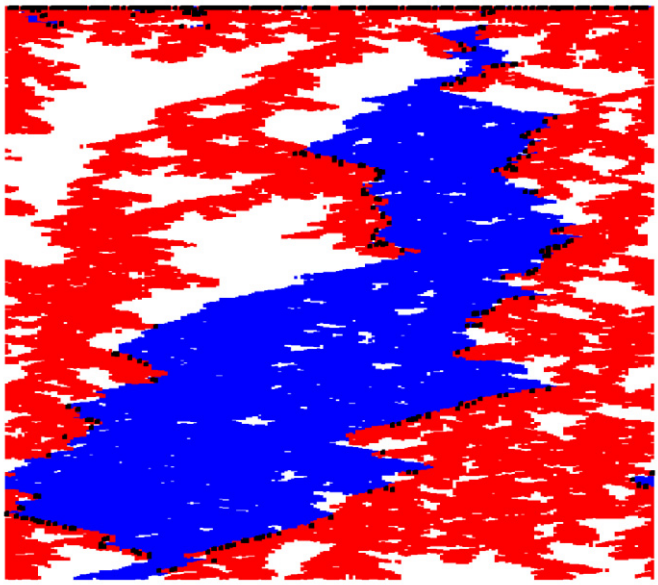

**Figure 7.** A sample evolution on a ring of 200 sites, of duration 4000 time units (with time increasing downward). Blue: sites with $a_i > 0$ and $b_i = 0$; red: sites with $a_i = 0$ and $b_i > 0$; black: sites with both species present.

regions, and voids. The voids arising in B-occupied regions are larger, as this species is nearer criticality. Species A, which is well above criticality, rapidly invades empty regions, but is in turn subject to invasion by the more competitive species B. Sites bearing both species are quite rare, occurring only at the frontiers between regions occupied by a single species.

J. Stat. Mech. (2013) P07004

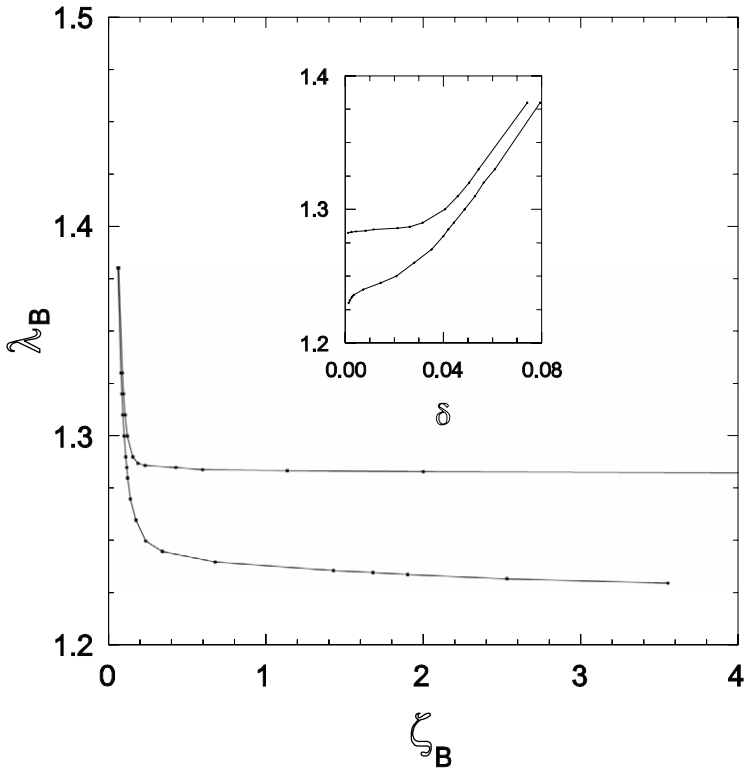


**Figure 8.** Simulations in one dimension: SSS is observed in the region bounded by the two curves; see text for parameters. Inset: the same data plotted using $\delta = \zeta_A/\zeta_B$ instead of $\zeta_B$ on the horizontal axis.

Figure 8 shows the result of a systematic search in the $\zeta_B$–$\lambda_B$ plane on a ring of $L = 200$ sites. These data represent averages of 200 realizations, each lasting $10^5$ time units. SSS is observed in the region bounded by the two curves; the lower curve corresponds to $\tau_A = \tau_B$ while on the upper we have $\rho_A = \rho_B$. There is an interval of $\lambda_B$ values, including $\lambda_c$, on which SSS is observed for *any* value of $\zeta_B$ greater than a certain minimum. For larger values of $\lambda_B$, SSS occurs only within a narrow range of $\zeta_B$. In the latter region we have $\alpha > \zeta_B > \zeta_A$, so that intraspecies competition is stronger than competition between species. Although we use a rather small system to facilitate the search, SSS is not restricted to this system size. For $L = 800$, for example, the range of $\lambda_B$ values admitting SSS is more restricted (from about 1.24 to 1.27) but at the same time the effect can be more dramatic. For $\lambda_B = 1.27$ and $\zeta_B = 0.2$, for example, we find $\rho_A = 0.74$, $\rho_B = 0.49$, and $\tau_B \approx 100\tau_A$. Studies using $\lambda_A = 1.35$ and $\zeta_A = 0.01$ yield a qualitatively similar diagram, leading us to conjecture that the form of the region exhibiting SSS in one dimension is generically that shown in figure 8. To summarize, we verify SSS in a limited but significant region of parameter space.

In the inset of figure 8 the data are plotted in the $\delta$–$\lambda_B$ plane, for comparison with the theoretical predictions shown in figure 5. (Recall that parameter $g$ corresponds to the ratio $\lambda_B/\lambda_A$, which is smaller than unity here. The parameter $\delta = \zeta_A/\zeta_B$, i.e., the ratio of the interspecies competition rates.) The region exhibiting SSS is rather different from the predictions of both MFT and stochastic field theory. In particular the lower



J. Stat. Mech. (2013) P07004

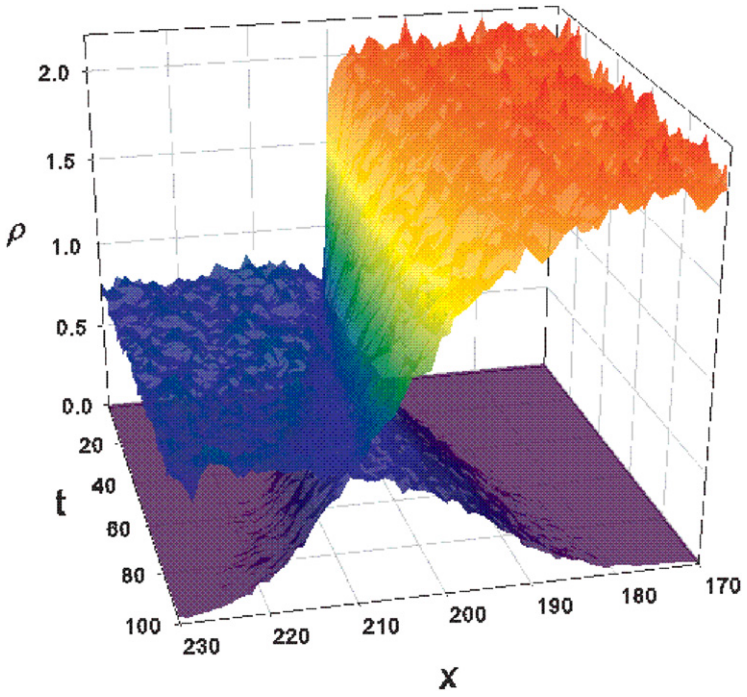


**Figure 9.** Mean density profiles $\rho_A(x,t)$ (maximum at right) and $\rho_B(x,t)$ (maximum at left) starting from neighboring single-species domains. Parameters: $\lambda_A = 1.6$, $\lambda_B = 1.29$, $\zeta_A = 0.005$, $\zeta_B = 0.16$.

boundary in the $\delta$-$\lambda_B$ plane is not horizontal and it is unclear whether the SSS region extends to $\delta = 1$. (As $\lambda_B$ is increased, SSS is observed in an ever more limited range of $\zeta_B$ values, making numerical work quite time-consuming.) Here it is important to recall that irrelevant terms (in the renormalization group sense) are discarded in the theoretical analysis, so that predictions for the phase diagram are only qualitative.

The evolution shown in figure 7 suggests that survival of a given species depends on the speed of invasion into territory occupied by the competing species; we study this issue via the following procedure. We first use simulations to prepare collections of configurations drawn from the QS distribution for each species in isolation. (We saved 1000 such configurations, on a ring of $L = 200$ sites, for each $\lambda$ value of interest.) To determine the speed of invasion we prepare initial configurations for the two-species system by placing a randomly chosen, saved configuration with species A only at sites $1, \ldots, L$, beside a similar configuration, with species B only, occupying sites $L+1, \ldots, 2L$. In the subsequent dynamics, the two species interact at the boundary, leading to invasion by one species or the other in different realizations. Figure 9 shows the evolution of the A and B density profiles, averaged over many realizations (3000 or more). Given the average density profiles $\rho_A(x,t)$ and $\rho_B(x,t)$ we identify the interface position $X_i(t)$ of species $i$ via the condition $\rho_i[X_i(t),t] = \bar{\rho}_i/2$, with $\bar{\rho}_i$ the QS density of species $i$ in isolation. Plotting the interface positions versus time, we find that they attain steady velocities after a certain initial transient; the velocities are plotted versus $\zeta_B$ in figure 10. (For the system size used here, steady velocities are attained after about 500 time units.) The interface velocity $v_B$ of species B increases slowly with $\zeta_B$, but that of species A ($v_A$) falls rapidly, becoming



J. Stat. Mech. (2013) P07004

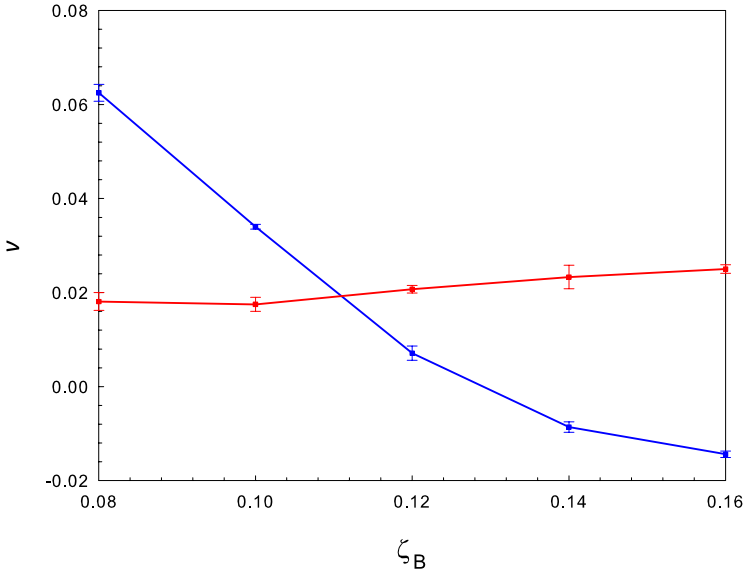


**Figure 10.** Steady state interface velocities for species A (blue) and B (red) versus $\zeta_B$; other parameters as in figure 9.

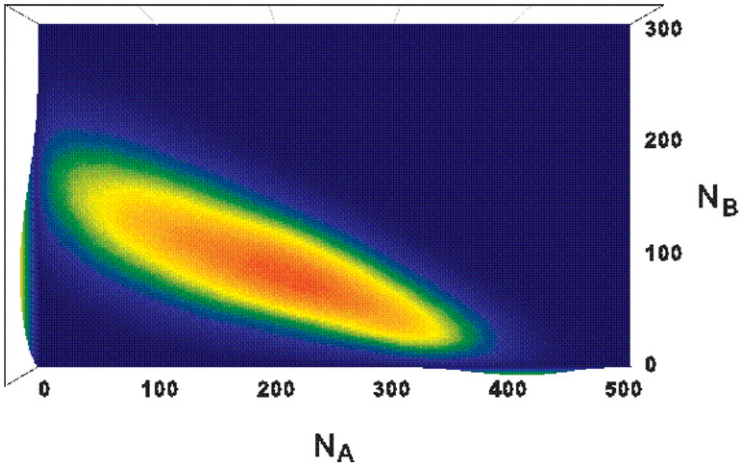


**Figure 11.** Quasi-stationary probability distribution for parameters $\lambda_A = 1.6$, $\lambda_B = 1.26$, $\zeta_A = 0.005$, and $\zeta_B = 0.3$, system size $L = 200$. Red corresponds to maximum and violet to zero probability. The maxima along the $x$ and $y$ axes correspond to the single-species QS distributions.

negative for $\zeta_B$ greater than about 0.13. For the parameters considered here, the mean lifetime of the scarcer species (B) is longer for $\zeta_B \geq 0.113$; very near this value, $v_A$ becomes smaller than $v_B$. This suggests that, as one would expect, the preferential extinction of the more populous species is associated with a smaller rate of spreading, so that A domains eventually die out due to invasion by B.

To close this discussion of simulation results, we present in figure 11 a portrait of the QS probability distribution in the SSS region. The basic features identified in the spatially uniform case (i.e., a well defined maximum corresponding to coexistence with $N_A > N_B$, as well as single-species QS distributions), persist in the presence of spatial structure. We may

speculate that the higher extinction probability for species A is associated with the more diffuse barrier in the small-$N_A$ region (near the $y$-axis) as compared with the corresponding barrier near the $x$ axis. More detailed simulations, including other parameter sets, larger systems, and simulations on the square lattice, are planned for future work.

## 5. Conclusion

We study a spatial stochastic model of two-species competition, inspired by the spatially uniform system analyzed in [7]. Based on Janssen's results for multicolored directed percolation [14], we find that the flow of parameters under the renormalization group is such that a small competitive advantage may be amplified to the point of excluding the more numerous, but less competitive species, unless the latter reproduces rapidly. Thus the less competitive population can go extinct, regardless of its size as given by mean-field theory. These effects tend to be stronger, the smaller the dimensionality $d$ of the system. Our result shows that the survival of the scarcer phenomenon observed in [7] persists, in some cases in a stronger form, in the presence of spatial structure. These differences are evident when comparing figures 1 and 5.

Monte Carlo simulations of a one-dimensional lattice model verify the existence of SSS when the more competitive species has a reproduction rate near the critical value, while that of the less competitive one is above criticality. The latter species, although more numerous in the quasi-stationary regime, loses out due to invasion by the more competitive species.

Our results suggest that, in an ecological setting, a species with smaller population density can in fact out-compete one with a higher density, even when the populations are not well mixed, so that the spatiotemporal pattern is one of shifting domains. Under conditions that favor survival of the scarcer, when both species are present in the same niche, the more competitive species (B) tends to survive longer, even if its density is smaller than that of the less competitive species (A). In isolation, however, species A is *less* susceptible to extinction than is species B, again considered in isolation. This suggests that, as long as both species are present globally, a cyclical dynamics of the form $A \to B \to 0 \to A, \ldots$, may be observed in localized regions. That is, a region occupied by species A is susceptible to invasion by B, which in turn is susceptible to extinction, permitting the return of species A, and so on. Sequences of this kind are indeed seen in figure 7. Given the simplicity of the model and the limitations of the present theoretical and numerical analysis, the above conclusions should be seen as preliminary at best. They may nevertheless suggest directions for further research in ecological modeling.

## Acknowledgment

This work is supported by CNPq, Brazil.

## References

[1] Hardin G, 1960 *Science* **131** 1292
[2] Renshaw E, 1991 *Modelling Biological Populations in Space and Time* (Cambridge: Cambridge University Press)
[3] Murrell D J, Purves D W and Law R, 2001 *Trends Ecol. Evol.* **16** 529

[4] Condit R *et al,* 2000 *Science* **288** 1414
[5] Silander J A Jr and Pacala S W, 1985 *Oecologia* **66** 256
[6] Pacala S W and Deutschman D H, 1995 *Oikos* **74** 357
[7] Gabel A, Meerson B and Redner S, 2013 *Phys. Rev.* E **87** 010101
[8] Assaf M and Meerson B, 2006 *Phys. Rev.* E **74** 041115
[9] Assaf M and Meerson B, 2010 *Phys. Rev.* E **81** 021116
[10] Doi M, 1976 *J. Phys. A: Math. Gen.* **9** 1479
[11] Peliti L, 1985 *J. Physique* **46** 1469
[12] Tauber U C, Howard M and Vollmayr-Lee B P, 2005 *J. Phys. A: Math. Gen.* **38** 79
[13] Cardy J, 1996 *Scaling and Renormalization in Statistical Physics* (Cambridge: Cambridge University Press)
[14] Janssen H, 2001 *J. Stat. Phys.* **103** 801
[15] Barabasi A L and Stanley E, 1995 *Fractal Concepts in Surface Growth* (Cambridge: Cambridge University Press)
[16] Dennis G R, Hope J J and Johnsson M T, 2013 *Comput. Phys. Commun.* **184** 201
[17] Dickman R, 1994 *Phys. Rev.* E **50** 4404
[18] Moro E, 2004 *Phys. Rev.* E **70** 045102
[19] Dornic I, Chaté H and Muñoz M A, 2005 *Phys. Rev. Lett.* **94** 100601
[20] Hinrichsen H, 2000 *Adv. Phys.* **49** 815
[21] De Oliveira M M and Dickman R, 2005 *Phys. Rev.* E **71** 016129
[22] Dickman R and De Oliveira M M, 2005 *Physica* A **357** 134
[23] Grassberger P and De La Torre A, 1979 *Ann. Phys., NY* **122** 373

J. Stat. Mech. (2013) P07004

Capítulo 4

# A importância de ser discreto no sexo

*Esta introdução é baseada nos resultados do artigo [5].*

Uma das mais fascinantes questões da biologia evolutiva envolve as razões da manutenção da reprodução sexuada entre os seres vivos. Esse processo está associado a um elevado dispêndio energético (disputas territoriais, acasalamento e meiose) e expõe os indivíduos a uma série de riscos, como predação, parasitismo e ferimentos causados em disputas por fêmeas. Apesar disso, esse mecanismo é adotado pela maioria das espécies multicelulares e apenas poucas espécies conhecidas de vertebrados adotam normalmente a reprodução assexuada [35, 36, 37].

A onipresença da reprodução sexuada é especialmente intrigante quando consideramos que este modo de reprodução está associado a diversos custos [38][39]. Em primeiro lugar, existem os vários custos associados ao acasalamento. Em muitas espécies, é preciso tempo e energia para garantir um companheiro. Por exemplo, para garantir a polinização, muitas plantas investem recursos substanciais na exposição floral e nas recompensas de néctar. Além disso, o ato de reprodução sexuada é muitas vezes mais lento do que o ato de reprodução assexuada, como pode ser visto em muitos micróbios. Durante o acasalamento, os indivíduos normalmente são menos capazes de reunir recursos e fugir de predadores. O acasalamento também introduz o risco de doenças sexualmente transmissíveis e elementos genéticos parasitas.

Nas espécies com sexos separados ou com tipos de acasalamento distintos, podem surgir conflitos sexuais dispendiosos - Por exemplo, o fluido seminal da *Drosophila* contém toxinas que reduzem a aptidão das fêmeas acasaladas. Também existem, na reprodução sexuada, os custos de produção dos vários descendentes, tais como o custo duplo do sexo: na reprodução sexuada, a unidade de reprodução é o casal, enquanto que na reprodução assexuada, é o indivíduo. A não ser que o casal que se reproduz sexualmente possa produzir o dobro de descendentes do indivíduo assexuado, os indivíduos sexuados terão necessariamente uma produção reprodutiva *per capita* menor. Em um extremo, se os casais sexuados e indivíduos assexuados produzem o mesmo número médio de descendentes, devido ao fato de um parceiro sexuado não contribuir com recursos para a prole, a produção por indivíduo reprodutivo nas espécies assexuadas é o dobro das espécies sexuadas, portanto, o custo duplo do sexo. Por último, é arriscado produzir descendentes misturando aleatoriamente genes com os de outro indivíduo. Por todas as contas, o sexo deveria ser um beco sem saída evolutivo, uma relíquia que deveria ser observada apenas raramente.

A teoria da evolução tem, em sua maior parte, mostrado que a resposta para o paradoxo do sexo é mais elusiva do que inicialmente se pensava. A maioria dos biólogos está confortável com a idéia de que o sexo evoluiu para fornecer variabilidade, mas modelos matemáticos provaram que esse conforto é injustificado: o sexo não precisa aumentar a variabilidade, a variabilidade não precisa ser benéfica e a evolução não precisa ser a favor do sexo, mesmo quando ela faz aumentar a variabilidade e variabilidade é benéfica [40]. Resolver o paradoxo do sexo exige que abracemos mais as complexidades do mundo real, e que utilizemos modelos evolutivos de *populações finitas*, que são distribuídas no *espaço*, e que estão sujeitas à seleção

gerada por várias forças ecológicas, incluindo espécies co-evoluindo como predadores, competidores e parasitas.

Neste artigo [5] apresento uma possível explicação para esse aparente "paradoxo do sexo". Proponho que uma das razões possíveis para a predominância da reprodução sexuada na natureza se encontra no caráter discreto das interações entre os indivíduos (sexuados) e entre os indivíduos e seus parasitas/predadores. Tal caráter induz flutuações estatísticas endógenas* na dinâmica populacional que, por sua vez, induzem a emergência de fenômenos a primeira vista inesperados. Devido a discreteza das interações, que está intimamente associada à finitude das populações, os seres sexuados tendem a agir coletivamente e um agrupamento entre os agentes emerge em dimensões espaciais menores que $d = 3$.† Este fato decorre diretamente da propriedade recorrente dos passeios aleatórios em baixas dimensões.‡ Consequência imediata desta propriedade é que a densidade populacional *localmente* elevada favorece os encontros entre os indivíduos sexuados, fazendo sua população florescer. O contrário ocorre para populações assexuadas: densidade elevada localmente favorece encontros entre os indivíduos e seus parasitas/predadores. Encontros entre os indivíduos sexuados e seus parasitas/predadores também ocorrem, mas seus efeitos são amenizados por uma espécie de *blindagem* que os indivíduos das camadas mais externas do aglomerado exercem sobre os indivíduos mais internos. Desta forma, a existência de sexo na natureza seria uma consequência puramente física da natureza discreta das interações e pode não ter nada a ver com genética.

*Endógeno: diz-se de uma causa interna.

†Esta dependência na dimensão espacial nos leva a uma conjectura: As espécies assexuadas tendem a existir nos oceanos, na atmosfera, ou em algum outro meio "efetivo" tridimensional.

‡Para $d < 3$, dois indivíduos perfazendo passeios aleatórios devem necessariamente se encontrar para tempos suficientemente longos.

# The Importance of Being Discrete in Sex

**Renato Vieira dos Santos***
UFLA - Universidade Federal de Lavras
DEX - Departamento de Ciências Exatas
CEP: 37200-000, Lavras, Minas Gerais, Brazil.

*econofisico@gmail.com

**Abstract**

**The puzzle associated with the cost of sex, an old problem of evolutionary biology, is discussed here from the point of view of nonequilibrium statistical mechanics. The results suggest, in a simplified model, that the prevalence of sexual species in nature can be a natural and necessary consequence of the discrete character of the nonlinear interactions between couples and their pathogens/parasites. Mapped into a field theory, the stochastic processes performed by the species are described by continuous fields in space and time. The way that the model's parameters scale with subsequent iterations of the renormalization group gives us information about the stationary emergent properties of the complex interacting systems modeled. We see that the combination of one aspect of the Red Queen theory with the stochastic processes theory, including spatiotemporal interactions, provides interesting insights into this old Darwinian dilemma.**

| Paradox of sex | Red Queen theory | Stochastic processes | Renormalization group

# 1 Introduction

Sex is an evolutionary puzzle. In several ways, sexual reproduction is less efficient when compared with the asexual method [1]. All offspring produced by asexual individuals will be able to reproduce, whereas sexual beings need to spend energy on creating males and females that do not reproduce separately. Hence the resources spent on producing sons are a cost of sexual reproduction and asexual species economize on males. John Maynard Smith [2] summarized this argument as follows:

> *"Suppose a population consists of a mixture of sexual and parthenogenetic females, the former producing equal numbers of male and (sexual) female offspring, and the latter only parthenogenetic females like themselves. If the two kinds of female lay equal numbers of eggs, and if survival probabilities are equal, then the parthenogenetic type will have a twofold selective advantage, and will increase in frequency very rapidly. Sexual reproduction means that a female wastes half her energy producing males."*

He also noted that a sexual individual uses only half of its genetic material on its descendents, while an asexual individual uses all his sexless genes. That is, in the evolutionary race where passing on genes to the next generation is one of the greatest goals, sexual organisms starts with a disadvantage of almost 50%, which is known as the *cost of meiosis* [1]. There is also the risk of infection by sexually transmitted diseases, the fact that sexual reproduction is often slower than asexual reproduction, and that during mating, individuals are typically less able to gather resources and evade predators. In addition to these disadvantages, and perhaps more important, is the cost of having to find a mate [3]. If insects are excluded, approximately one-third of animal species are hermaphrodites [4]. Hermaphroditism is even more widespread in plants. The difficulty of finding mates is widely implicated in the evolution of hermaphroditism, so its widespread occurrence suggests that sexual organisms incur significant costs to locate mates [5]. Sex, therefore, seems to be a luxury that should not exist. Consequently, many works about its evolution look for it's compensatory benefits.

Since sexual reproduction exists, biologists try to find out what great benefit it brings to living beings. Maynard Smith argued that sex could only have evolved if this mysterious benefit at least outweighed the great cost of meiosis. But what, after all, could this benefit be? To answer this question, an audacious theory about the origin and perpetuation of sex was proposed in [6]. According to this work, the parasites *are everywhere and will always seek, by their nature, to explore their hosts.* As the generation time of parasites is many times smaller than that of hosts,

and their evolution rates therefore many times higher, the only way out for the hosts is to produce offspring with greater genetic variability through sexual reproduction. Therefore, competition with parasites that develop very fast genetically, favors sexual reproduction, which enables a more efficient genetic evolution [7, 8].

The world in which this model is inserted became known as the Red Queen's world, a name given in [9] in reference to a passage in the fable Alice in the mirrors [10]. In this passage, Alice flees the army (of cards) of the Red Queen, but can not distance herself from her pursuers. The Red Queen then says: "Now, here, you see, it takes all the running you can do, to keep in the same place". Alice would be caught only if she stopped running. Things have to change to remain the same.

According to [6], an arms race has been underway between hosts and parasites since life appeared on Earth. The parasites are always breaking the defensive barriers imposed by the host's genotype, while the host, with the help of sex, continually creates new defenses. In the absence of sex, the hosts would remain essentially the same, while the parasites would accumulate adaptations that would enable them to break all the defensive systems of the former. Sooner or later, the hosts would be virtually devoured from the inside out. To escape the parasite army besieging them, the only remaining option is to just keep running. The coevolutive cycle of parasites and hosts reflects this eternal pursuit. For criticism to the Red Queen theory, see [11, 12].

The aim of this paper is to investigate the prevalence of sexual reproduction observed in nature through simple models of reaction-diffusion inspired by the Red Queen theory, but *not* fully equivalent to it. The role of the parasite may be replaced by any pathogen which diffuses through space and fatally harms the species. There is also no need for any aspect related to genetics [13].

Over the years, evolutionary theory has shown that the answer to the paradox of sex is more elusive than we initially thought. While most biologists are comfortable with the idea that sex exists to provide genetic variability, several mathematical models have shown that this comfort is unjustified. According to [14], *"...the theory of population genetics, as complete as it may be in itself, fails to deal with many problems of primary importance for an understanding of evolution."* After all, it is risky to produce offspring by randomly mixing genes with those of another individual. In the words of [15]:

> *"... sex need not increase variability, variability need not be beneficial and evolution need not favour sex, even when it does increase variability and variability is beneficial."*

There is also a well-documented pattern of high frequency of sex in undisturbed, biologically complex habitats [16, 17, 18, 19] where disease and other

"natural enemies" are prevalent [16, 17, 20]. The recognition of the predominance of sex in stable communities has devalued models hypothesizing that sex is common because it provides a selective advantage when abiotic conditions are unpredictable [17, 21, 22].

Moreover, the need to take into account aspects of complexity that are routinely neglected is widely recognized [15]. One reason that an answer to the paradox of sex has been so elusive is that many mathematical models have focused on populations that are infinite in size, unstructured, and isolated from other species. Satisfactory explanations for the paradox of sex should consider *finite* populations of agents that interact in an environment where *structure* and *complexity* are able to *emerge*.

To incorporate a few of these elements, we take into account the *discrete* nature of the species interactions with itself and with its pathogens/parasites, in a $d-$dimensional space. Discreteness of the interactions is a consequence of the *finiteness* of the populations, interactions with parasites characterize the *non*-insulation explicitly, and a $d-$dimensional space enables *structure* and *complexity to emerge*.

We know that if we want information about the emergent aggregate macroscopic behavior of complex systems, we'll need to consider the corpuscular character of interacting species [23]. We will achieve this goal by employing dynamic renormalization group (DRG) theory to obtain the renormalization group (RG) flow in the parameter space [24, 25]. Starting from the microscopic formulation of the model described by reactions, this RG flow will allow us to understand *how the model parameters scale in space and time*. In turn, this information will be helpful in determining the final equilibrium state of the aggregates of interacting species. Such aggregates imply the advantage of sex on the population- or group-level [26, 27, 28, 29]. This approach is consistent with the perspective of extensive time and space scales taken by macroecology and biogeography [30, 31, 32]. Large-scale spatial correlations are likely to be important for understanding the evolutionary influence of predator and prey or host and pathogen ecology [33].

It's worth noting that it is not our intention to refute the wide existing knowledge of population genetics about the paradox of sex. It is intended only to call attention to an intrinsic feature of sexual reproduction that's been neglected so far. The longevity of the problem indicates that the solution requires a variety of causal effects, and what we propose here could be just one of these effects.

## 1.1 Models

In this subsection we present the two models used. They are simplified models that attempt to capture only the essential aspects of population dynamics. The first refers to the competition between an asexual species and a pathogen that can

harm it, eventually inducing death. The second is the analogous model for the sexual species. The incorporation of the pathogen in interactions was inspired by the Red Queen theory regarding the host's parasites. In principle, however, any other death-inducing agent can be imagined. The models are as follows:

### Asexual species model

The model for asexual species is described by the following reactions, occurring in a $d-$dimensional lattice:

$$A \xrightarrow{\lambda} 2A \qquad\qquad A + B \xrightarrow{\mu} B \tag{1}$$

The first reaction on the left describes the reproduction of species $A$ which occurs at rate $\lambda$ per time unit, at a given site of the lattice. The second reaction describes the attack that species $A$ suffers from its pathogen $B$. In this attack, species $A$ will always be annihilated at a rate of $\mu$ per time unit per population size unit. Note that in a model that takes the spatial character of the interactions in a $d$ dimensional lattice, pathogen/parasites only diffuse.* They are not created or annihilated. This captures their essence of *being everywhere and always seeking, by their nature, to exploit their hosts,* as mentioned above.

### Sexual species model

The model for sexual species is described by the following reactions:

$$2A \xrightarrow{\lambda} 3A \qquad\qquad A + B \xrightarrow{\mu} B \tag{2}$$

The first reaction describes species $A's$ reproduction that occurs at rate $\lambda$ per time unit per population size unit, always at a given site of the lattice. Because two agents are required to reproduce a third, this reaction captures the cost of finding a mate. Everything else is as in the previous model.

This is not the first time that a model of this type is proposed for population dynamics incorporating the *Allee effect*† [34, 35, 36] on the lattice. For recent references, see [37, 38]. In the process known as the quadratic contact process (QCP) [39], we also have similar reactions. QCP is sometimes called the process of sexual reproduction [40].

It is very important to keep in mind that we are considering the critical situation where the concentration of species in the lattice is initially very small and

*This diffusion process (for the species $B$, for example) could be represented by $B+\emptyset \rightarrow \emptyset+B$, where $\emptyset$ is an empty site of the lattice.

†For all sexual populations, there is a density threshold below which the probability of finding a mate is too low to ensure sufficient reproduction for the population to remain viable.

the dynamics is dominated by diffusion [41]. The average number of agents per site is initially much lower than 1 and sexual reproduction is therefore penalized. Only in this critical regime does it make sense to use the renormalization group techniques.

# 2 Results

In the following subsection (2.1) we consider $A$ or $B$ as the *average* density of agents in the sites of the lattice.

## 2.1 Mean field theory

### Asexual model

Using the law of mass action, we obtain the differential equations for asexual species: $\dot{A} = D_A\nabla^2 A + \lambda A - \mu AB$ and $\dot{B} = D_B\nabla^2 B$ with $D_A$ and $D_B$ being diffusion coefficients. The diffusion processes only tend to homogenize populations in space and nabla operators will be neglected from now on in this subsection. The $B$ population is a constant on average denoted by $\langle N_B\rangle$ and therefore $\dot{A} = (\lambda - \mu\langle N_B\rangle)A \equiv mA$, which defines $m = \lambda - \mu\langle N_B\rangle$. We see that if $\mu\langle N_B\rangle < \lambda$, $m > 0$ and the $B$ population tends exponentially to infinity. Otherwise, $m < 0$ and the $B$ population becomes extinct. If $m = 0$, the $A$ population remains constant.

### Sexual model

In this case, the equation for population dynamics already disregards diffusion terms and settings $\kappa \equiv \mu\langle N_B\rangle$ is $\dot{A} = \lambda A^2 - \kappa A \equiv -dV/dA$ with $V \equiv -\lambda A^3/3 + \kappa A^2/2$. $V$ is an effective potential that allows a pictorial view of the dynamics, as illustrated in Figure (1). The point $P$ on the potential maximum has coordinates $(A_{\max}, V_{\max}) = (\kappa/\lambda, \kappa^3/6\lambda^2)$. For any initial population $A(0) < \kappa/\lambda$, the population tends to be extinct. This fact is illustrated in figure (1) by the tendency of the red ball to moves down the curve to the origin, and characterizes the aforementioned Allee effect. If $A(0) > \kappa/\lambda$, population tends to infinity, a fact represented by the tendency of the green ball to get lost in the bottomless potential hole.

In the next subsections we will see how the $\kappa$, $\lambda$ and $\mu$ parameters change with successive renormalization group iterations, or, in other words, how the discrete nonlinear species interactions in space-time induce variations in the numerical parameter values. These changes can transform very significantly the potential barrier to be overcome (given by $\kappa^3/6\lambda^2$) by the population.

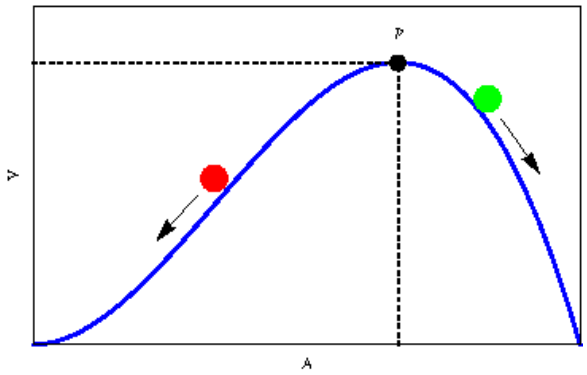


Figure 1: **Effective potential** $V(A)$. The black point $P$ has coordinates $(A_{\max}, V_{\max}) = (\kappa/\lambda, \kappa^3/6\lambda^2)$.

## 2.2 Statistical Field Theory

### Asexual model

We are interested in the way the parameters $\lambda$ and $m$ vary when we increase the observation scales of time and space. Using the results of statistical field theory [42, 43, 44], we get the following flow equations for these parameters in the asexual model (see section 5):

$$\frac{d\mu}{dl} = \epsilon\mu + \frac{\mu^2}{2\pi\bar{D}} \tag{3a}$$

$$\frac{dm}{dl} = 2m - \frac{\langle N_B\rangle\mu^2}{2\pi\bar{D}}, \tag{3b}$$

where $\epsilon = 2-d$ ($d$ is the dimension of space), $l = \ln(s)$ ($s$ is the escale parameter, see section 5), and $\bar{D} \equiv (D_A + D_B)/2$. Competition parameter $\mu$ increases indefinitely with the renormalization group iterations, favoring the extinction of the asexual species. This fact is interpreted in section 3 using the re-entrant property of diffusive systems in low dimensions.

Equations (3) are identical to those obtained in [23, 45] for the reactions $B \xrightarrow{\mu} \emptyset, A + B \xrightarrow{\lambda} 2B + A$, with bare mass $m_{AB} \equiv \mu - \lambda\langle N_A\rangle$, with $\langle N_A\rangle$ representing the average number of $A$. This model is known as the $AB$ model [46]. It has been originally proposed in [23, 47, 46, 48, 45] to discuss the origin of life in terms of auto-catalysis, and it has been applied in some research areas such as ecology and economy [49, 50, 51]. The spatial version of this model shows that self-replication can be locally maintained with $B$ growing exponentially, even when average $A$

concentration would not be sufficient to sustain growth in a homogeneous vessel. This fact is a consequence of the tendency of $\mu$ to grow with the scale $s$, as shown by the equations (6), and from the definition of $m_{AB}$. Exactly the opposite will occur in the case of the model with asexual population, since in this case $m = \lambda - \mu\langle N_B\rangle$ and therefore $\mu$ is subtracted rather than added.

Figures (2a) and (2b) show the RG flow diagrams associated with equations (6) for $\mu \geq 0$. On the left we have the case of $\epsilon < 0$ (or $d > 2$). The black dot is the fixed point given by $(\mu^*, m^*) = (2\pi\bar{D}\epsilon, \bar{D}\pi\epsilon^2\langle N_B\rangle)$. The diagonal line represents an eigenvector indicating two distinct behaviors of the diagram near the fixed point. The horizontal dotted line represents $m = 0$. Above the straight line and for $m > 0$, the RG flow tends to take $m$ to *infinity*. In this case the asexual species population explodes. This happens for a sufficiently small $\mu$. The opposite occurs below the line (*i.e.*, for sufficiently large $\mu$), with the RG flow inducing $m$ to negative values, inducing the population to extinction, even with the mean field theory indicating explosion. We may call this phenomenon *Discreteness Inducing Extinction* (DIE).

More interesting is the figure on the right, where the DIE phenomenon is certain across the parameter space (for $\mu > 0$) for $d \leq 2$ (or $\epsilon \geq 0$). *On the surface, asexual species always die.*

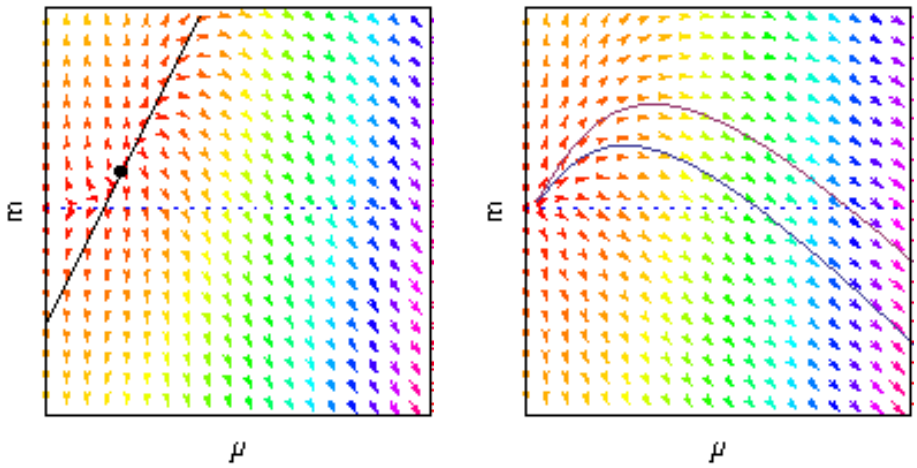


(a) **RG flow for** $\epsilon < 0$. (b) **RG flow for** $\epsilon \geq 0$.

Figure 2: **RG flow asexual model**

### Sexual model

Let's compare the effects caused by the discrete character of the interactions in asexual and sexual reproduction. For the model of sexual reproduction, there is

one more parameter ($\lambda$) flowing due to the iterations of the renormalization group. This is due to the nonlinearity of the process $2A \xrightarrow{\lambda} 3A$. The flow equations are:

$$\frac{d\mu}{dl} = \epsilon\mu + \frac{\mu^2}{2\pi\bar{D}} \tag{4a}$$

$$\frac{d\kappa}{dl} = 2\kappa - \frac{\langle N_B\rangle\mu^2}{2\pi\bar{D}} \tag{4b}$$

$$\frac{d\lambda}{dl} = \epsilon\lambda + \frac{\lambda^2}{\pi\bar{D}} \tag{4c}$$

where $\epsilon = 2 - d$, $l = \ln(s)$, and $\bar{D} \equiv (D_A + D_B)/2$. The new $\lambda$ RG flow does not influence $\kappa$ and therefore RG flows involving $\kappa$ and $\mu$ are as shown in figures (2a) and (2b) by replacing $m$ with $\kappa$ in the vertical axes. We can now examine how the potential barrier (given by $V_{\max} = \kappa^3/6\lambda^2$) in figure (1) varies when the parameters are renormalized. We see that on the surface (or in smaller dimensions: $\epsilon \geq 0$), this potential barrier disappears quickly, *favoring* the sexual species. This happens because of how quickly $\lambda$ approaches infinity (with decreasing $\kappa$), making $V_{\max} \to 0$. The barrier that prevented the sexual population's development is increasingly transposable if there is enough space and time for the interactions to occur. And this fact arises from the interaction's discreteness. This is *the importance of being discrete in sex*. Furthermore, according to our simplified models, the only chance for an asexual species to exist in nature, is in a three dimensional space. This finding leads to the conjecture that most asexual species existing today, live in the oceans, in the air, or in other "effective" three-dimensional media.

# 3 Discussion

## 3.1 General discussion

A possible objection to the sexual model is that various particles can accumulate in one lattice site, leading to a divergence in the population due to the reaction $2A \xrightarrow{\lambda} 3A$. In principle, the amount of particles per site can be infinite, but for our purposes, it does not matter. One possible argument goes as follows:

If we establish the same initial conditions[‡] for the two models, with both species on the verge of extinction, the sexuated species will win unequivocally, after a transient. And this occurs twice: once because of the certainty of extinction of the asexual species (at least for $d = 2$) and once because of the trend of

[‡]Random initial positions of individuals in the lattice, without the overlapping of two or more individuals at the same site.

sexuated species to diverge. It does not matter if ultimately the amount of individuals per site becomes greater than one. From this point on, our minimal model is no longer valid and constraints must be added, but the battle has already been won by the sexuated species.

Is it possible to understand physically why the description based on differential equations (or mean field theory) becomes invalid for long timeframes and large scales in lower dimensions? To answer this question, let's first consider a different situation, for the sake of simplicity. Consider a one-dimensional lattice, where nearly all lattice sites are populated by particles of species A, such that the only reaction occurring is the *annihilation* reaction $A + A \xrightarrow{\alpha} \emptyset$. In principle, this reaction can take place everywhere. The initial dynamics is therefore accurately described by the solution of the kinetic rate equation $\frac{\partial \rho}{\partial t} = D_A \nabla^2 \rho - \alpha \rho^2$, where $\rho(x,t)$ is the concentration of $A$ individuals in the lattice and $D_A$ is the diffusion constant. Therefore, initially, $\rho \propto t^{-1}$. At later times, the lattice becomes more and more diluted and the reaction rate is limited by the first passage time of a random walk in $d = 1$, scaling exactly with $t^{-1/2}$. Hence, the long time behavior of $\rho$ is renormalized to $\rho \propto t^{-1}/t^{-1/2} = t^{-1/2}$. This is a simple example of how the reactions limited by diffusion might provide different results from the equivalent models described in terms of differential equations.

The probability of species $B$ (the parasites) finding species $A$ is 1 for $d < 3$ for asexual species at the limit of the reaction limited by diffusion because of the re-entrant property of random walks in low dimensions. Physically, this means that the diffusing particle will thoroughly sweep its neighborhood. It's therefore highly probable that it will react with another particle in its vicinity. Hence, it is reasonable to expect that after a short period of time, the system will be in a state where there are almost *no* individuals of species $A$. This phenomenon no longer occurs in $d > 2$ and asexual species may exist.

In the case of sexual reproduction, two nonlinear phenomena are in competition: $2A \xrightarrow{\lambda} 3A$ and $A + B \xrightarrow{\mu} \emptyset$. As we have seen, however, the former wins from the latter and the tendency to form clusters of sexed individuals predominates. *This is due to the "shielding" effects that the boundaries of the clusters have on the individuals within it.* It is therefore reasonable to expect that after a short period of time the system will be in a state where there are a lot of isolated particles. This leads to the interesting question whether "ancestral" sexed reproductions are responsible for habitat heterogeneity (through the formation of clusters of individuals) rather than the heterogeneity of the environment inducing mating [52, 53, 54, 55]. We are referring to the chicken or the egg causality dilemma. Taking this idea to the extreme, we might ask: is there sex *because* of demographic noise?

## 3.2 Some remarks

Some specific comments related to our results and to the literature.

**Importance of the space**

Several authors have indicated the importance of considering spatial distribution to explain the paradox of sex [56, 57, 58, 59, 52, 60, 61]. A population's spatial structure is well known to have significant evolutionary consequences [62]. For prey-predator or host-pathogen interactions, theory has convincingly shown that spatial structure can lead to the evolution of a reduced predator-pathogen attack rate [63, 64, 65]. This involves mechanisms that are analogous to the shielding mentioned before.

The evolutionary influence of a population's spatial structure is particularly compelling because it bears on the fundamental evolutionary question of the emergence of cooperation. Theory suggests that spatial structure is a key requirement for the emergence of cooperation [66, 67, 68, 69, 70, 71]. Notably, spatial structure appears to resolve the tragedy of the commons [72, 73, 74]. Spatial structure also seems to imply biodiversity and species coexistence [75, 76, 77, 78, 79].

**Importance of Discreteness**

Many fields of science have come to the realization that complex phenomena can be explained by supposing the existence of discrete underlying levels that can be described using integers. Atomic theory is perhaps the best example. In biology, a consistent theory of evolution was developed by introducing the concept of genes as the quantum of inheritance information [80]. Various phenomena of modern physics, such as the photoelectric effect, the radiation spectrum of stars, the universal temperature dependence of the specific heat of solids, can be explained assuming an underlying discrete level of some physical quantity.

Demographic stochasticity, which that in this paper emerges from the discreteness of the interactions, is known to be important in population dynamics [81]. The inclusion of stochasticity into non-linear mathematical models affects the mean dynamics [62, 82, 83]. We can cite as example the ability of demographic stochasticity to excite macroscopic-scale coherent oscillations, known as quasi-cycles [84]. An extension to the spatial case where spatiotemporal patterns are induced by demographic noise has also been observed [85]. Generation [86] and exacerbation [87] of the Allee effect are also consequences of the discrete character of the interactions associated with demographic noise, which can even induce survival when mean field theory indicates extinction [23]. The importance of this intrinsic noise in the microscopic dynamics of cellular systems has also

been studied intensively in recent years [88], leading to a flurry of papers in this area [89]. These facts indicate a considerable effervescence in research associated with stochastic phenomena related to the inevitable discrete character of the interactions [90].

**Sex and density**

Our results suggest that in the long term the sexual species agglomerate in regions of high relative density. Some experimental studies have associated high population density to an advantage for sexual reproduction. In [91], the frequency of sexual reproduction in a population is found to increase with the intensity of intraspecific competition in a lichen species. Several mathematical models indicate positive dependence between density and sexual reproduction [92]. Many of them are related to the Tangled Bank hypothesis [93], an idea based on previous studies about the role of spatial heterogeneity in the maintenance of sex [94, 95].

**Geographic Parthenogenesis**

There is some observational evidence of the phenomenon which we call shielding [96]. One of the characteristics of so-called *geographic parthenogenesis* (GP) is *adaptation at the margin*. Geographical parthenogenesis is a term that describes the phenomenon that related sexual and asexual organisms have different distribution areas, and adaptation at the margin of asexual species is one of their characteristics. The sexual species tends to concentrate in the central regions, being surrounded by the asexual species [96]. A mathematical model [97] suggests that asexuals could more easily adapt to environmental conditions in boundary areas.

Another characterization is that GP is the phenomenon where sexual populations are restricted to a core area while parthenogenetic lineages occupy a wider geographic range [96]. Such segregation is not always complete. Sometimes there is coexistence between the two reproduction modes as is common in freshwater ostracods [98, 99]. Understanding the coexistence of sexuals and asexuals on a local scale is not simple because of the *competitive exclusion principle* [100, 101]. However, there are theoretical indications that the discreteness of interactions between individuals in populations can also induce coexistence [79].

# 4 Conclusion

Understanding how complex ecosystems work often relies on simplified models that disregard many details of the actual system while retaining the essential information [102, 103]. In this paper we propose a simplified model that can shed some

light on the question of the predominance and maintenance of sexual reproduction in nature despite all its costs. Sex is a reproductive ritual that is inherently more complex than its rival asexual method. And this inherent complexity gives rise to some counterintuitive features. The complexity aspect discussed here refers only to the nonlinear interactions between species and their pathogens/parasites, and to the cost of finding a mate in the case of sexual selection. Mathematically, this cost implies a nonlinearity (coming from the reaction $2A \to 3A$) which is absent in the asexual reproduction model. And from this nonlinearity in the interactions, *purely physical* conditions emerge that favor sexual reproduction. We need not consider anything about genetics for example.

Another important actor in this context of complexity is the discrete character of the interactions. This actor is solely responsible for the DIE phenomenon in asexual species, where the extinction is possible for $d < 2$ and certain for $d \geq 2$, even if the mean field theory indicates otherwise. The intrinsic stochasticity induced by this discreteness is also responsible for effectively raising the $\lambda$ parameter, as seen through the RG flow for the sexual model. This fact allows for the development of sexual populations, despite its considerable costs for finding a mate, even in situations not covered by the mean field theory. A phenomenon able to induce this increase is the aggregation in clusters of interacting agents. A well-known property of diffusion is the re-entrancy of the visited sites in low space dimensions. In particular, for $d = 1$ and $d = 2$, the probability that the diffusing particle will ever return ($t \to \infty$) to the starting point is equal to 1. Physically, it means that the diffusing particle thoroughly sweep its neighborhood and thus it is highly probable that it will react with another particle in its vicinity. Hence, it is reasonable to expect that after short period of time the system will be in a state where there is a lot of isolated particles.[§] The clustering of sexual agents favors a localized increase in the $\lambda$ reproduction rate, allowing their permanence and development. These aggregates, emergent phenomena in our model, helps to explain the group-level advantage of sex and their associated experimental observations [104, 105]. We must not forget that an individual cannot reproduce arbitrarily fast. This imposes an upper limit for $\lambda$. Briefly, I propose that:

*One aspect of the explanation for the maintenance of sexual reproduction in nature is in the scale of populations, far above the molecular scale of the gene, and manifests itself as an* ***emergent property*** *of the discrete interactions in the intermediate scale of the individuals.*

[§]A similar phenomenon also occurs among species and their pathogens/parasites, making the death rate also rises, explaining the extinction of asexual species in $d \leq 2$. However, this increase is insufficient to overcome the increased of the sexual species for $d \leq 2$.

# 5 Materials and Methods

### Asexual model

In the Doi-Peliti theory, the master equation which describes the evolution of the probability vector $|P(t)\rangle \equiv \sum_C p(C,t)|C\rangle$, with the sum being performed over all configurations, is written in the form $d|P\rangle/dt = H|P\rangle$, where the Hamiltonian operator $H$ is composed of creation and destruction operators. Starting from this "microscopic" description, one derives an effective action $S$ via a path-integral representation [24]. Then, taking the continuum limit, one arrives at a field theory for the model.

For the asexual model, Doi-Peliti action, already with the following Doi shifts $\tilde{\phi} \to 1 + \bar{\phi}, \tilde{\psi} \to 1 + \bar{\psi}, \psi \to \psi + \langle N_B \rangle$, and $\phi \to \phi$, is

$$\begin{aligned} S[\bar{\phi},\phi,\bar{\psi},\psi] &= \int d^d x \int dt \Big[ \bar{\phi}(\partial_t - m - D_A \nabla^2)\phi \\ &+ \bar{\psi}(\partial_t - D_B \nabla^2)\psi - \lambda \bar{\phi}^2 \phi + \mu \bar{\phi}\phi\psi \\ &+ \mu \langle N_B \rangle \bar{\phi}\bar{\psi}\phi + \mu \bar{\phi}\bar{\psi}\phi\psi \Big] \end{aligned} \tag{5}$$

where $m \equiv \lambda - \mu\langle N_B \rangle$ is the bare mass. $\phi$ and $\psi$ are fields associated with the populational densities of $A$ and $B$ respectively, while $\bar{\phi}$ and $\bar{\psi}$ are related to their statistical fluctuations.

Let us assume that the parameters $\mu$ and $\lambda$ are adjusted so that the species are on the verge of extinction for perturbation theory to be valid [106]. Feynman diagrams associated with the action (5) are shown in Figure (2).

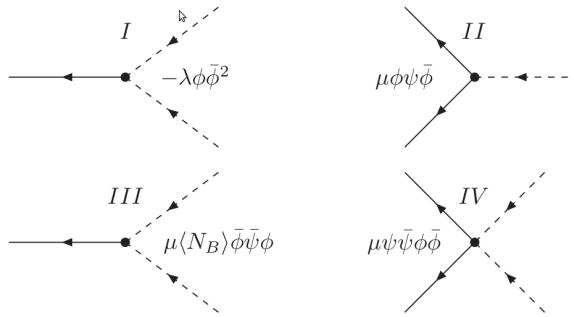


Figure 3: Feynman diagrams

## 5.1 Dynamical renormalization group

We use the field theory techniques to find the renormalization group flow in the parameter space. The system will be analyzed using the standard renormalization group technique, imposing the change of scale $x \to sx, t \to s^z t, \phi \to s^{-d-\eta}\phi, \psi \to s^{-d-\eta}\psi$ (similarly to $\bar{\phi}, \bar{\psi}$), and $\Lambda \to \Lambda/s$, where $s$ is the renormalization group scale factor, $\eta$ is a critical exponent, and $\Lambda$ is a momentum cuttoff. Performing the standard perturbation theory procedures [107], using the diagrams combinations $II$ and $III$ (propagator renormalization, see Figure (3) left) and $II$ and $IV$ (vertice renormalization, see Figure (3) right), we find the following flow equations for the model parameters in the limit of $\Lambda \to \infty$ [23]:

$$\frac{d\mu}{dl} = \epsilon\mu + \frac{\mu^2}{2\pi\bar{D}} \tag{6a}$$

$$\frac{dm}{dl} = 2m - \frac{\langle N_B\rangle\mu^2}{2\pi\bar{D}}, \tag{6b}$$

where $\epsilon = 2 - d, l = \ln(s)$, and $\bar{D} \equiv (D_A + D_B)/2$.

Figure 4: Propagator renormalization diagram $II + III$ (left) and vertice renormalization diagram $II + IV$ (right).

### Sexual model

The Doi-Peliti effective action for the sexual reproduction model is:

$$\begin{aligned} S[\bar{\phi},\phi,\bar{\psi},\psi] &= \int d^dx \int dt \Big[\bar{\phi}(\partial_t + \kappa - D_A\nabla^2)\phi \\ &+ \bar{\psi}(\partial_t - D_B\nabla^2)\psi - \lambda\bar{\phi}\phi^2 + \mu\bar{\phi}\phi\psi \\ &+ \mu\langle N_B\rangle\bar{\phi}\bar{\psi}\phi + \mu\bar{\phi}\bar{\psi}\phi\psi 2\lambda\bar{\phi}^2\phi^2 \\ &- \lambda\bar{\phi}^3\phi^2\Big] \end{aligned} \tag{7}$$

where $\kappa \equiv \mu\langle N_B\rangle$. Field interpretations are as before.

An important feature of this model is the diagram $V$ in figure (5). We also should replace the diagram $I$ in figure (2) with the diagram $VI$ in figure (5).

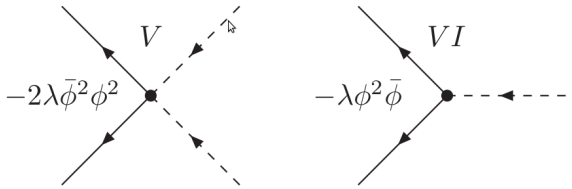


Figure 5: Some Feynman diagrams in sexual model.

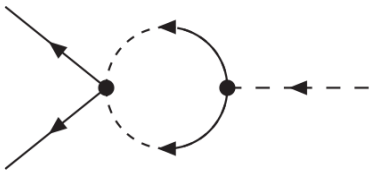

Figure 6: Vertice renormalization (Feynman diagram $V + VI$) for sexual model.

Now, the crucial point is that the parameter $\lambda$ can be explicitly renormalized using diagrams $V$ and $VI$ (see Figure (6)). Performing the basic steps mentioned before, we have the following RG flow equations for the sexual species model:

$$\frac{d\mu}{dl} = \epsilon\mu + \frac{\mu^2}{2\pi\bar{D}} \tag{8a}$$

$$\frac{d\kappa}{dl} = 2\kappa - \frac{\langle N_B\rangle\mu^2}{2\pi\bar{D}} \tag{8b}$$

$$\frac{d\lambda}{dl} = \epsilon\lambda + \frac{\lambda^2}{\pi\bar{D}} \tag{8c}$$

where $\epsilon = 2-d, l = \ln(s)$, and $\bar{D} \equiv (D_A+D_B)/2$. The diagram in Figure (6) which renormalizes $\lambda$ is equal to the diagram in Figure (4) at right, which renormalizes $\mu$, with the difference of a factor 2 in the former. Associating this similarity to the fact that the propagators are also very similar,[¶] the results are almost identical and we obtain an expression for the RG flow for $\lambda$ very similar to the expression of $\mu$.

[¶]The propagator for the field $\phi$ in equation (7) is given by $G_{\phi\phi}[k,\omega] = (Dk^2 + \kappa - i\tau\omega)^{-1}$. Replacing $\kappa$ by $-m$ we obtain the propagator for the field $\phi$ in equation (5). The propagators for the fields $\psi$, $G_{\psi\psi}[k,\omega]$, are identical for both models.

# 6 Acknowledgments

RVS is grateful to Linaena Méricy da Silva for helpful comments. This work was supported by the Conselho Nacional de Desenvolvimento Científico e Tecnológico, Brazil.

# Bibliography


[1] Lehtonen J, Jennions MD, Kokko H (2012) The many costs of sex. Trends in ecology & evolution 27: 172–178.

[2] Smith J, Dawkins R (1993) The Theory of Evolution. Canto Series. Cambridge University Press.

[3] Daly M (1978) The cost of mating. The American Naturalist 112: 771–774.

[4] Jarne P, Auld J (2006) Animals mix it up too: the distribution of self-fertilization among hermaphroditic animals. Evolution 60: 1816–1824.

[5] Eppley S, Jesson L (2008) Moving to mate: the evolution of separate and combined sexes in multicellular organisms. Journal of evolutionary biology 21: 727–736.

[6] Hamilton W, Zuk M (1982) Heritable true fitness and bright birds: a role for parasites? Science .

[7] Lively CM (2010) A review of red queen models for the persistence of obligate sexual reproduction. Journal of Heredity 101: S13–S20.

[8] Liow LH, Van Valen L, Stenseth NC (2011) Red queen: from populations to taxa and communities. Trends in ecology & evolution 26: 349–358.

[9] van Valen L (1973) A new evolutionary law. Evolutionary Theory 1: 1–30.

[10] Carroll L (2000) Alice's Adventures in Wonderland and Through the Looking Glass. Perma-Bound Books.

[11] Otto SP, Nuismer SL (2004) Species interactions and the evolution of sex. Science 304: 1018–1020.

[12] Elzinga J, Chevasco V, Mappes J, Grapputo A (2012) Low parasitism rates in parthenogenetic bagworm moths do not support the parasitoid hypothesis for sex. Journal of evolutionary biology 25: 2547–2558.

[13] Agrawal AF (2006) Evolution of sex: why do organisms shuffle their genotypes? Current Biology 16: R696–R704.

[14] Lewontin RC (1961) Evolution and the theory of games. J Theor Biol 1: 382-403.

[15] Otto SP, Lenormand T (2002) Resolving the paradox of sex and recombination. Nature Reviews Genetics 3: 252–261.

[16] Levin DA (1975) Pest pressure and recombination systems in plants. American Naturalist : 437–451.

[17] Glesener RR, Tilman D (1978) Sexuality and the components of environmental uncertainty: clues from geographic parthenogenesis in terrestrial animals. American Naturalist : 659–673.

[18] BARRETT SC, ECKERT CG (1990) 14 variation and evolution of mating systems in seed plants. Biological approaches and evolutionary trends in plants : 229.

[19] Hamilton WD, Axelrod R, Tanese R (1990) Sexual reproduction as an adaptation to resist parasites (a review). Proceedings of the National Academy of Sciences 87: 3566–3573.

[20] Bell G (1982) The masterpiece of nature: the evolution and genetics of sexuality. CUP Archive.

[21] Smith JM, Maynard-Smith J (1978) The evolution of sex. Cambridge Univ Press.

[22] Price MV, Waser NM (1982) Population structure, frequency-dependent selection, and the maintenance of sexual reproduction. Evolution : 35–43.

[23] Shnerb N, Louzoun Y, Bettelheim E, Solomon S (2000) The importance of being discrete: Life always wins on the surface. Proceedings of the National Academy of Sciences 97: 10322.

[24] Tauber UC, Howard M, Vollmayr-Lee BP (2005) Applications of field-theoretic renormalization group methods to reaction-diffusion problems. J Phys A-Math Gen 38: 79.

[25] Santos RV, Dickman R (2013) Survival of the scarcer in space. Journal of Statistical Mechanics: Theory and Experiment 2013: P07004.

[26] Rice WR, Chippindale AK (2001) Sexual recombination and the power of natural selection. Science 294: 555–559.

[27] Colegrave N (2002) Sex releases the speed limit on evolution. Nature 420: 664–666.

[28] Poon A, Chao L (2004) Drift increases the advantage of sex in rna bacteriophage $\phi 6$. Genetics 166: 19–24.

[29] Goddard MR, Godfray HCJ, Burt A (2005) Sex increases the efficacy of natural selection in experimental yeast populations. Nature 434: 636–640.

[30] Beck J, Ballesteros-Mejia L, Buchmann CM, Dengler J, Fritz SA, et al. (2012) What's on the horizon for macroecology? Ecography 35: 673–683.

[31] Loreau M (2010) From Populations to Ecosystems: Theoretical Foundations for a New Ecological Synthesis (MPB-46). Monographs in Population Biology. Princeton University Press.

[32] Brown J (1995) Macroecology. Biology/Ecology. University of Chicago Press.

[33] Messinger SM, Ostling A (2013) Predator attack rate evolution in space: The role of ecology mediated by complex emergent spatial structure and self-shading. Theoretical Population Biology 89: 55 - 63.

[34] Allee W, Bowen ES (1932) Studies in animal aggregations: mass protection against colloidal silver among goldfishes. Journal of Experimental Zoology 61: 185–207.

[35] Allee W, Park O, Emerson A, Park T, Schmidt K (1949) Principles of animal ecology. WB Saunders London.

[36] Courchamp F, Berec L, Gascoigne J (2008) Allee effects in ecology and conservation. Oxford University Press, Oxford , New York.

[37] Windus A, Jensen H (2007) Allee effects and extinction in a lattice model. Theoretical population biology 72: 459–467.

[38] Gastner MT, Oborny B, Ryabov AB, Blasius B (2011) Changes in the gradient percolation transition caused by an allee effect. Physical Review Letters 106: 128103.

[39] Durrett R (1999) Stochastic spatial models. Siam Review 41: 677–718.

[40] Preece T, Mao Y (2009) Sustainability of dioecious and hermaphrodite populations on a lattice. Journal of theoretical biology 261: 336–340.

[41] Mattis DC, Glasser ML (1998) The uses of quantum field theory in diffusion-limited reactions. Reviews of Modern Physics 70: 979.

[42] Parisi G (1988) Statistical Field Theory. Frontiers in Physics. Addison-Wesley. URL http://books.google.com.br/books?id=0F8sAAAAYAAJ.

[43] Mussardo G (2010) Statistical Field Theory: An Introduction to Exactly Solved Models in Statistical Physics. Oxford Graduate Texts. OUP Oxford. URL http://books.google.com.br/books?id=JnLnXmBmCzsC.

[44] Täuber UC (2007) Field-theory approaches to nonequilibrium dynamics. In: Ageing and the Glass Transition, Springer. pp. 295–348.

[45] Shnerb N, Bettelheim E, Louzoun Y, Agam O, Solomon S (2001) Adaptation of autocatalytic fluctuations to diffusive noise. Phys Rev E 63: 021103.

[46] Louzoun Y, Shnerb N, Solomon S (2007) Microscopic noise, adaptation and survival in hostile environments. The European Physical Journal B-Condensed Matter and Complex Systems 56: 141–148.

[47] Agranovich A, Louzoun Y, Shnerb N, Moalem S (2006) Catalyst-induced growth with limited catalyst lifespan and competition. Journal of theoretical biology 241: 307–320.

[48] Louzoun Y, Solomon S, Atlan H, Cohen I (2003) Proliferation and competition in discrete biological systems. Bulletin of mathematical biology 65: 375–396.

[49] Challet D, Solomon S, Yaari G (2009) The universal shape of economic recession and recovery after a shock. Economics: The Open-Access, Open-Assessment E-Journal 3.

[50] Solomon S, Goldenberg J, Mazursky D (2003) World-size global markets lead to economic instability. Artificial life 9: 357–370.

[51] Yaari G, Nowak A, Rakocy K, Solomon S (2008) Microscopic study reveals the singular origins of growth. The European Physical Journal B 62: 505–513.

[52] Becks L, Agrawal AF (2010) Higher rates of sex evolve in spatially heterogeneous environments. Nature 468: 89–92.

[53] Candolin U, Salesto T, Evers M (2007) Changed environmental conditions weaken sexual selection in sticklebacks. Journal of Evolutionary Biology 20: 233–239.

[54] Candolin U, Heuschele J (2008) Is sexual selection beneficial during adaptation to environmental change? Trends in Ecology & Evolution 23: 446–452.

[55] Myhre LC, Forsgren E, Amundsen T (2013) Effects of habitat complexity on mating behavior and mating success in a marine fish. Behavioral Ecology 24: 553–563.

[56] Peck JR, Jonathan Y, Barreau G (1999) The maintenance of sexual reproduction in a structured population. Proceedings of the Royal Society of London Series B: Biological Sciences 266: 1857–1863.

[57] Barraclough TG, Herniou E (2003) Why do species exist? insights from sexuals and asexuals. Zoology 106: 275–282.

[58] Halkett F, Kindlmann P, Plantegenest M, Sunnucks P, Simon J (2006) Temporal differentiation and spatial coexistence of sexual and facultative asexual lineages of an aphid species at mating sites. Journal of evolutionary biology 19: 809–815.

[59] Hartfield M, Keightley PD (2012) Current hypotheses for the evolution of sex and recombination. Integrative Zoology 7: 192–209.

[60] Ament I, Scheu S, Drossel B (2008) Influence of spatial structure on the maintenance of sexual reproduction. Journal of theoretical biology 254: 520–528.

[61] Kokko H, Heubel KU, Rankin DJ (2008) How populations persist when asexuality requires sex: the spatial dynamics of coping with sperm parasites. Proceedings of the Royal Society B: Biological Sciences 275: 817–825.

[62] Houchmandzadeh B, Vallade M (2003) Clustering in neutral ecology. Physical Review E 68: 061912.

[63] Pels B, de Roos AM, Sabelis MW (2002) Evolutionary dynamics of prey exploitation in a metapopulation of predators. The American Naturalist 159: 172–189.

[64] Van Baalen M, Sabelis MW (1995) The milker-killer dilemma in spatially structured predator-prey interactions. Oikos : 391–400.

[65] Rauch E, Sayama H, Bar-Yam Y (2002) Relationship between measures of fitness and time scale in evolution. Physical Review Letters 88: 228101.

[66] Doebeli M, Knowlton N (1998) The evolution of interspecific mutualisms. Proceedings of the National Academy of Sciences 95: 8676–8680.

[67] Killingback T, Doebeli M, Knowlton N (1999) Variable investment, the continuous prisoner's dilemma, and the origin of cooperation. Proceedings of the Royal Society of London Series B: Biological Sciences 266: 1723–1728.

[68] Nowak MA, May RM (1992) Evolutionary games and spatial chaos. Nature 359: 826–829.

[69] Lion S, Gandon S (2009) Habitat saturation and the spatial evolutionary ecology of altruism. Journal of evolutionary biology 22: 1487–1502.

[70] Lehmann L, Keller L, Sumpter DJ (2007) The evolution of helping and harming on graphs: the return of the inclusive fitness effect. Journal of evolutionary biology 20: 2284–2295.

[71] Hauert C, Doebeli M (2004) Spatial structure often inhibits the evolution of cooperation in the snowdrift game. Nature 428: 643–646.

[72] Hardin G (1968) The tragedy of the commons. New York .

[73] J Rankin D, López-Sepulcre A (2005) Can adaptation lead to extinction? Oikos 111: 616–619.

[74] Bargum K, Sundström L (2007) Multiple breeders, breeder shifts and inclusive fitness returns in an ant. Proceedings of the Royal Society B: Biological Sciences 274: 1547–1551.

[75] Ai D, Gravel D, Chu C, Wang G (2013) Spatial structures of the environment and of dispersal impact species distribution in competitive metacommunities. PloS one 8: e68927.

[76] Hugueny B, Cornell HV, Harrison S (2007) Metacommunity models predict the local-regional species richness relationship in a natural system. Ecology 88: 1696–1706.

[77] Leibold MA, Holyoak M, Mouquet N, Amarasekare P, Chase J, et al. (2004) The metacommunity concept: a framework for multi-scale community ecology. Ecology letters 7: 601–613.

[78] Logue JB, Mouquet N, Peter H, Hillebrand H (2011) Empirical approaches to metacommunities: a review and comparison with theory. Trends in ecology & evolution 26: 482–491.

[79] Santos RV (2013) Discreteness inducing coexistence. Physica A: Statistical Mechanics and its Applications 392: 5888 - 5897.

[80] Fisher RA (1999) The genetical theory of natural selection: a complete variorum edition. Oxford University Press.

[81] Black A, McKane A (2012) Stochastic formulation of ecological models and their applications. Trends in ecology & evolution .

[82] Houchmandzadeh B (2008) Neutral clustering in a simple experimental ecological community. Physical review letters 101: 078103.

[83] Houchmandzadeh B (2009) Theory of neutral clustering for growing populations. Physical Review E 80: 051920.

[84] McKane A, Newman T (2005) Predator-prey cycles from resonant amplification of demographic stochasticity. Physical review letters 94: 218102.

[85] Butler T, Goldenfeld N (2011) Fluctuation-driven turing patterns. Physical Review E 84: 011112.

[86] Lande R (1998) Demographic stochasticity and allee effect on a scale with isotropic noise. Oikos : 353–358.

[87] Dennis B (2002) Allee effects in stochastic populations. Oikos 96: 389–401.

[88] Paulsson J (2004) Summing up the noise in gene networks. Nature 427: 415–418.

[89] Thattai M, Van Oudenaarden A (2001) Intrinsic noise in gene regulatory networks. Proceedings of the National Academy of Sciences 98: 8614–8619.

[90] Houchmandzadeh B (2013) The remarkable discreteness of being. arXiv preprint arXiv:13064535 .

[91] Hestmark G (1992) Sex, size, competition and escape—strategies of reproduction and dispersal in lasallia pustulata (umbilicariaceae, ascomycetes). Oecologia 92: 305–312.

[92] Song Y, Drossel B, Scheu S (2011) Tangled bank dismissed too early. Oikos 120: 1601–1607.

[93] Bell G (1982) The Masterpiece of Nature: The Evolution and Genetics of Sexuality. Croom Helm applied biology series. Croom Helm. URL http://books.google.com.br/books?id=q5g9AAAAIAAJ.

[94] Williams G (1975) Sex and Evolution. Monographs in population biology. Princeton University Press.

[95] Smith JM (1976) A short-term advantage for sex and recombination through sib-competition. Journal of theoretical biology 63: 245–258.

[96] Schmit O, Adolfsson S, Vandekerkhove J, Rueda J, Bode S, et al. (2013) The distribution of sexual reproduction of the geographic parthenogen eucypris virens (crustacea: Ostracoda) matches environmental gradients in a temporary lake. Canadian Journal of Zoology 91: 660–671.

[97] Peck JR, Yearsley JM, Waxman D (1998) Explaining the geographic distributions of sexual and asexual populations. Nature 391: 889–892.

[98] Chaplin JA, Havel JE, Hebert PD (1994) Sex and ostracods. Trends in ecology & evolution 9: 435–439.

[99] Horne D, Baltanás A, Paris G (1998) Geographical distribution of reproductive modes in living non-marine ostracods. Sex and parthenogenesis: evolutionary ecology of reproductive modes in non-marine ostracods Backhuys, Leiden, the Netherlands : 77–99.

[100] Hardin G (1960) The competitive exclusion principle. Science 131: 1292.

[101] Hutchinson G (1961) The paradox of the plankton. American Naturalist : 137–145.

[102] Levin SA (1992) The problem of pattern and scale in ecology: the robert h. macarthur award lecture. Ecology 73: 1943–1967.

[103] Bascompte J, Solé R (1998) Modeling spatiotemporal dynamics in ecology. Environmental intelligence unit. Springer.

[104] Greig D, Borts RH, Louis EJ (1998) The effect of sex on adaptation to high temperature in heterozygous and homozygous yeast. Proceedings of the Royal Society of London Series B: Biological Sciences 265: 1017–1023.

[105] Becks L, Agrawal AF (2012) The evolution of sex is favoured during adaptation to new environments. PLoS biology 10: e1001317.

[106] van Wijland F, Oerding K, Hilhorst HJ (1998) Wilson renormalization of a reaction–diffusion process. Physica A: Statistical and Theoretical Physics 251: 179–201.

[107] Zinn-Justin J (2002) Quantum Field Theory and Critical Phenomena (International Series of Monographs on Physics). Clarendon Press, 4 edition.

Capítulo 5

# Uma possível explicação para a frequência variável das células tronco do câncer nos tumores

*Esta introdução é baseada nos resultados do artigo [1], publicado em* ***PLoS ONE****.*

O ressurgimento de tumores tempos depois de eles terem sido combatidos pelos tratamentos convencionais (cirurgia, quimioterapia e radioterapia) é um dilema que aflige há muito tempo médicos e pesquisadores que lidam com câncer. Estudos recentes [41, 42] conseguiram mostrar a ação de células-tronco tumorais* na retomada desse crescimento, oferecendo um novo alvo para a luta contra a doença.

Uma controvérsia existe no que se refere à frequência com que estas células aparecem nos mais diversos tumores [43, 44, 45, 46, 47, 48, 49, 50]. No início, cogitou-se que esta frequência era muito baixa, indo de 0,0001% a 0,1% do total de células [51]. Posteriormente foi verificada a possibilidade de esta frequência ser bem maior, com experimentos indicando uma fração de até 41% [52]. A relevância da determinação da quantidade de células tronco do câncer (CTCs) nos tumores se faz perceber da necessidade de se focar os tratamentos clínicos na eliminação destas células. Se for percebido que as CTCs representam grande parte dos tumores, tais tratamentos deverão atuar sobre todo o tumor como sempre foi feito. Caso contrário, técnicas mais específicas para tratar células específicas deverão ser desenvolvidas. A importância deste aspecto fica evidente em [53], onde os pesquisadores da área afirmam que o trabalho mais importante nos últimos anos anteriores a 2011 foi [54], o pioneiro na identificação de grandes populações de CTCs nos tumores sólidos.

Neste primeiro artigo, de uma sequência de dois nesta tese, propomos um modelo estocástico simples, sem estrutura espacial, que tem como hipóteses fundamentais os mecanismos conhecidos de divisão celular [55], bem como de plasticidade celular [56, 57, 58]. Este modelo apresenta a propriedade de transição induzida por ruído† em sua distribuição estacionária de probabilidade $P_{st}$. Este ruído tem origem nos eventos complexos aos quais as células estão inevitavelmente expostas no microambiente celular, e a bimodalidade de $P_{st}$ é interpretada de acordo com as observações experimentais. Desta forma, se as perturbações estatísticas com origem no microambiente não são suficientemente intensas, a população de CTCs adquire uma distribuição unimodal. Caso contrário, a distribuição é bimodal e, como tal, pode justificar as discrepâncias observadas nos experimentos, às vezes indicando frações pequenas, às vezes frações grandes.

Considerações a respeito da heterogeneidade dos tumores bem como implicações clínicas dos resultados são feitas. Em particular, conclui-se que, dentro das hipóteses do modelo, os tratamentos convencionais

*Células com características de células tronco, ou seja, grande capacidade de renovação e diferenciação, que seriam responsáveis pelo desenvolvimento e manutenção dos tumores.

†Modelado como um processo Gaussiano conhecido como ruído branco.

contra o câncer podem não apenas ser ineficazes, como podem *estimular* o desenvolvimento das CTCs. Esta conclusão depende da interpretação atribuída a tais formas de tratamento como fontes de variabilidade estatística no microambiente celular. Se estes resultados estiverem corretos, pode ser que as recidivas muitas vezes fatais da doença, às vezes na forma de metástazes, possam ser explicadas pelo estímulo fornecido às células tronco do câncer no estágio inicial dos tratamentos convencionais.

OPEN ACCESS Freely available online

PLOS | ONE

# A Possible Explanation for the Variable Frequencies of Cancer Stem Cells in Tumors

**Renato Vieira dos Santos**[1]*, **Linaena Méricy da Silva**[2]*

**1** Departamento de Física, Instituto de Ciências Exatas, Universidade Federal de Minas Gerais, Belo Horizonte, Minas Gerais, Brasil, **2** Laboratório de Patologia Comparada, Instituto de Ciências Biológicas, Universidade Federal de Minas Gerais, Belo Horizonte, Minas Gerais, Brasil

## Abstract

A controversy surrounds the frequency of cancer stem cells (CSCs) in solid tumors. Initial studies indicated that these cells had a frequency ranging from 0.0001 to 0.1% of the total cells. Recent studies have shown that this does not always seem to be the case. Some of these studies have indicated a frequency of 40%. In this paper we propose a stochastic model that is able to capture this potential variability in the frequency of CSCs among the various type of tumors. Considerations regarding the heterogeneity of the tumor cells and its consequences are included. Possible effects on conventional treatments in clinical practice are also described. The model results suggest that traditional attempts to combat cancer cells with rapid cycling can be very stimulating for the cancer stem cell populations.

**Citation:** dos Santos RV, da Silva LM (2013) A Possible Explanation for the Variable Frequencies of Cancer Stem Cells in Tumors. PLoS ONE 8(8): e69131. doi:10.1371/journal.pone.0069131

**Editor:** Jérémie Bourdon, Université de Nantes, France

**Received** March 9, 2013; **Accepted** June 4, 2013; **Published** August 7, 2013



**Funding:** This work was supported by the Conselho Nacional de Desenvolvimento Científico e Tecnológico, Brazil. The funders had no role in study design, data collection and analysis, decision to publish, or preparation of the manuscript.

**Competing Interests:** The authors have declared that no competing interests exist.

* E-mail: econofisico@gmail.com; linaena.mericy@gmail.com

## Introduction

In recent years there has been increasing evidence for the *Cancer Stem Cell* (CSC) hypothesis [1–4], according to which tumor formation is a result of genetic and epigenetic changes in a subset of stem-like cells, also known as *tumor-forming* or *tumor-initiating* cells [5]. *Cancer stem cells* (CSCs) were first identified in leukemia and more recently in several solid tumors such as brain, breast, cervix and prostate tumors [4]. It has been suggested that these are the cells responsible for initiating and maintaining tumor growth [6]. In this paper, we study a model for tumor growth assuming the existence of cancer stem cells, or *tumor initiating cells* [6–8].

The conceptual starting point relevant to the CSC theory is constructed from the known tumor heterogeneity. We now know that cells in a tumor aren't all identical copies of each other, but that they display a striking array of characteristics [9–13]. The CSC theory recognizes this fact and develops its consequences. And one of the most immediate consequences for clinical practice is that conventional treatments can attack the wrong cell type. The appeal of the CSC idea can be described through the following analogy: just as killing the queen bee will lead to the demise of the hive, destroying cancer stem cells, should, in theory, stop the tumor from renewing itself. Unfortunately, things are never that simple. In the hive, workers react quickly to the death of queen by replacing her with a new one. And there is some evidence [8,14] suggesting that the same may occur in a tumor due to a phenomenon known as *cell plasticity*, which allows differentiated tumor cells to turn into cancer stem cells, should the situation call for this. One goal of the present study is to evaluate the possible effects of this plasticity. Analogies with super organisms such as bee colonies are taken much more seriously in [15].

Stem cells in general (the same applies to CSCs) tend to be found on specific areas of a tissue where one particular microenvironment, called *niche* [16,17], promotes the maintenance of their vital functions. Such a niche is specialized in providing factors that prevent differentiation and thus maintain the stemness of CSCs and, ultimately, the tumor's survival. Stem cells and niche cells interact with each other through adhesion molecules and paracrine factors. This complex network of interactions exchanges molecular signals and maintains the unique characteristics of stem cells, namely, pluripotency and self-renewal.

In this paper, we are interested in investigating a controversy related to the frequency in which CSCs appear in various tumors [18–25]. In the initial version of the CSC theory, it was believed that these cells were a tiny fraction of the total, ranging from 0.0001 to 0.1 % [26]. However, more recent studies have shown a strong dependence of the number of CSCs present in the tumor with the experimental xenograft model used. In explicit contrast to what was previously thought, in [27] a proportion of CSCs of approximately 25% was observed. Other studies have confirmed this observation [26,28,29] with the possibility of a proportion of up to 41% [30]. In [31] the authors provide evidence that this discrepancy may be due to the possibility of phenotypic switching between different tumor cells. Phenotypic switching is interpreted as the possibility of a more differentiated cancer cell being able to, under the appropriate conditions, dedifferentiate into cancer stem cell. This is the cellular plasticity mentioned above.

In [32] it is suggested that inconsistencies in the numbers of cancer stem cells reported in the literature can also be explained as a consequence of the different definitions used by different researchers. Different assays will give different numbers of cells, which can be orders of magnitude away from each other. Articles [31] and [32] provide different explanations for the discrepancy in

the frequency of CSCs. Our arguments are consistent with the results of [31].

Considering that the complexity of the cellular microenvironment can be modeled by the insertion of a Gaussian noise into the equation that describes the population dynamics, we show that a noise-induced transition occurs. That corresponds to the emergence of a bimodal stationary probability distribution. This happens when the noise intensity $\sigma$ exceeds a critical limit value $\sigma_{cr}$.

In this paper we show that *cell plasticity* [14,33,34], combined with a complex network of interactions modeled as noise, can induce discrepant (too small or too large) stationary CSC populations. Effects related to tumor heterogeneity and clinical treatments will be discussed at the end, occasion in which the model parameters possess the appropriate biological interpretations.

## Methods

### Model Assumptions

In the model used in this paper, cancer stem cells can perform three types of divisions, according to [35]:

- **symmetric self-renewal:** cell division in which both daughter cells have the characteristics of the mother stem cell, resulting in an expanding population of stem cells;
- **symmetric differentiation:** a stem cell divides into two progenitor cells;
- **asymmetric self-renewal** a cancer stem cell (denoted by $C$) is generated and a progenitor cell (mature cancer cell, denoted by $P$) is also produced;

We have developed a simple mathematical model for the stochastic dynamics of CSCs in which the three division types possess intrinsic replication rates, which are assumed to be time-independent. We assume, therefore, that besides the three described types of division, there is also the possibility of a transformation in which a progenitor cell can acquire characteristics of stem cells where, for all practical purposes, we may regard it as having become a dedifferentiated CSC. This hypothesis has experimental support [36]. These dedifferentiated cells do not become cancer stem cells, but rather develop CSC like behavior by re-activating a subset of genes highly expressed in normal hematopoietic stem cells [14]. The biological mechanisms underlying this transformation are described in [31], for example. As mentioned previously, we refer to this process as *cell plasticity*. Finally, we assume that cells are well mixed, so that we can ignore spatial effects.

The model proposed is a natural extension of what is proposed in [37]. We also incorporates the possibility of competition between CSCs and between the progenitor cells in order to limit the exponential growth of the linear model in [37]. This is described in the next subsection.

### The basic model

We assume that the dynamics of cancer stem cells ($C$) and progenitor cells ($P$) are governed by the following reactions:

$$
\begin{aligned}
&C \underset{k'_2/\Omega_2}{\overset{k_1}{\rightleftharpoons}} C+C\\
&P \underset{k'_4/\Omega_4}{\overset{k_3}{\rightleftharpoons}} P+P\\
&C \xrightarrow{k_5} C+P\\
&C \xrightarrow{k_6} P+P\\
&P \xrightarrow{k_7} \varnothing\\
&P \xrightarrow{k_8} C
\end{aligned}
\tag{1}
$$

The first and second reactions, in the forward sense, models cell proliferation, which occurs at a rate of $k_1$ and $k_3$, respectively. The constants $k'_2$ and $k'_4$ are associated with the reverse process and describe the intensity of competition between the CSCs and progenitors cells, respectively, and prevents their unlimited exponential growth. Many studies, experimental and theoretical, justify this approach [38–47]. As long as no mechanical nor nutritional restrictions apply, the tumor cells go on replicating with a constant duplication time. After a while, however, several constraints force the development of a necrotic core, and growth slows down towards some asymptotic level of saturation. $\Omega_2$ and $\Omega_4$ are constants related to the carrying capacity of the model. The third reaction involving $k_5$ originates from the asymmetric transformation of CSCs in CSC daughter and progenitor cell types. The reaction involving the $k_6$ rate is related to a symmetrical division of the stem cell, which gives rise to two progenitor cells. The penultimate reaction is associated with the progenitor cell's death at rate $k_7$. Finally, $k_8$ is the rate of dedifferentiation. All rates have dimension $(\text{time})^{-1}$. The specific time unit (months, quarters, years, etc.) will depend on the type and aggressiveness of the tumor.

Using the law of mass action, we can write

$$
\begin{cases}
\dfrac{dC}{dt} = k_1 C - k_2 C^2 - k_6 C + k_8 P\\
\dfrac{dP}{dt} = k_3 P - k_4 P^2 + (k_5 + 2k_6) C - (k_7 + k_8) P
\end{cases}
\tag{2}
$$

with $k_2 \equiv k_{2'}/\Omega_2$, $k_4 \equiv k_{4'}/\Omega_4$. Setting $\Omega_C \equiv k_1/k_2$, $\Omega_P \equiv k_3/k_4$, $k_9 \equiv k_5 + 2k_6$ and $k_{10} \equiv k_7 + k_8$ and making the substitutions $C = \Omega_C x$, $P = \Omega_C \sqrt{k_9/k_2}\, y$ and $t = \tau/k_6$, equation (2) can be written as (see Appendix S1)

$$
\begin{cases}
\dfrac{dx}{d\tau} = Ax(1-x) - x + By \equiv f(x,y)\\
\dfrac{dy}{d\tau} = Ey(1-Fy) + Bx - Gy \equiv g(x,y)
\end{cases}
\tag{3}
$$

with

$$\begin{cases} A \equiv \dfrac{k_1}{k_6} \\ B \equiv \dfrac{\sqrt{k_8 k_9}}{k_6} \\ E \equiv \dfrac{k_3}{k_6} \\ F \equiv \dfrac{\Omega_C}{\Omega_P}\sqrt{\dfrac{k_9}{k_8}} \\ G \equiv \dfrac{k_{10}}{k_6} \end{cases} \quad (4)$$

As $\partial f/\partial y = \partial g/\partial x = B$, equation (3) represents a gradient system [48] with potential $V(x,y)$ given by (see Appendix S1)

$$V(x,y) = \frac{1}{6}(3 - 3A + 2Ax)x^2 - Bxy + \frac{1}{6}(3G - 3E + 2EFy)y^2. \quad (5)$$

As a consequence [49]:

1. The eigenvalues of the linearization of equation (3) evaluated at equilibrium point are real.
2. If $(x_0; y_0)$ is an isolated minimum of $V$ then $(x_0; y_0)$ is an asymptotically stable solution of (3).
3. If $(x(\tau); y(\tau))$ is a solution of (3) that is not an equilibrium point then $V(x(\tau),y(\tau))$ is a strictly decreasing function and is perpendicular to the level curves of $V(x,y)$.
4. There are no periodic solutions of (3).

Sufficiently small $F$ ($\Omega_P \gg \Omega_C$) implies large differences in $C$ and $P$ equilibrium populations. For parameters $A = B = G = 1$, $E = 3$ and $F = 0.01$, $(x_0; y_0) = (8.4; 70.6)$. If we set $F = 0.0001$ keeping the other parameters fixed, we have $(x_0; y_0) = (82; 6710)$.

## Adiabatic elimination

The proposed model in (1) is in fact a general model of stem cells and does not carry any specific characteristic of cancer stem cells. All properties considered, such as plasticity and changes in the microenvironment conditions (to be included later), are also found in normal, stem cell tissue systems. The features associated with cancer stem cells are related to the large carrying capacity of progenitor cells when compared with the carrying capacity of CSCs. This fact is represented numerically by the choice of model parameters made below and is important because it allows a simplification using the adiabatic approximation.

We can write (2) as (see Appendix S1)

$$\begin{cases} x' = A'x(1-x) - x + B'y \\ y' = E'y(1-y) + F'x - G'y \end{cases} \quad (6)$$

with $x' \equiv \dfrac{dx}{dt'}$, $y' \equiv \dfrac{dy}{dt'}$, $t' \equiv t/k_6$ and

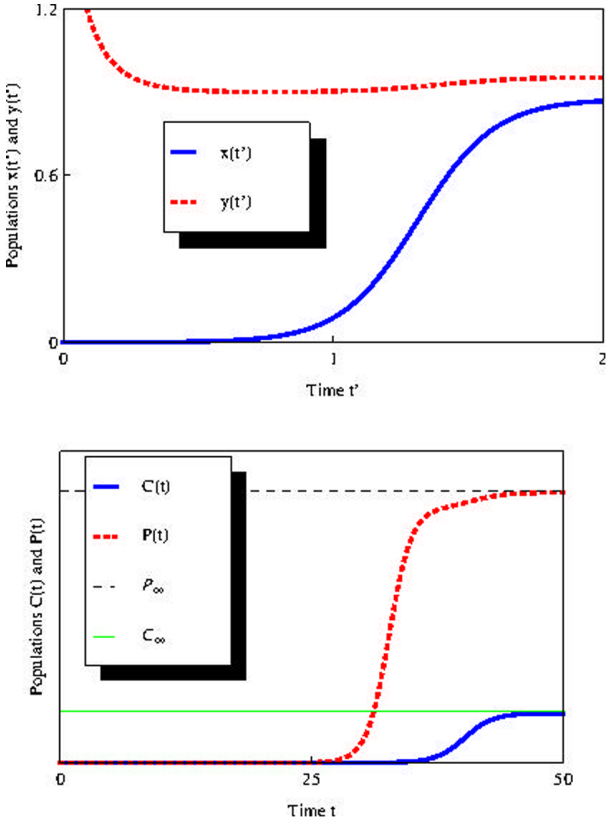


**Figure 1. Numerical solutions of differential equations. Top:** Numerical solution for reescaled equation (6). Horizontal axis is time $t$. $x(t)$ and $y(t)$ represent the rescaled population of cancer stem cells and progenitor cells, respectively. **Bottom:** Numerical solution for equation (2). $C(t)$ and $P(t)$ represent he population of cancer stem cells and progenitor cells, respectively. $P_\infty$ and $C_\infty$ represent the limits of $C(t)$ and $P(t)$ when $t \to \infty$, respectively. Parameters values: $k_1 = 1 - k_5 - k_6$, $k_2 = 4 \times 10^{-13}$, $k_3 = 1$, $k_4 = 10^{-13}$, $k_5 = 0.1$, $k_6 = 0.1$, $k_7 = 0.1$ and $k_8 = 0.00001$. $P_\infty = 9.6 \times 10^{12}$ and $C_\infty = 1.8 \times 10^{12}$. $C_\infty/P_\infty = 0.1875$.
doi:10.1371/journal.pone.0069131.g001

$$\begin{cases} A' \equiv \dfrac{k_1}{k_6} \\ B' \equiv \dfrac{k_2 k_3 k_8}{k_1 k_4 k_6} \\ E' \equiv \dfrac{k_3}{k_6} \\ F' \equiv \dfrac{k_1 k_4 k_9}{k_2 k_3 k_6} \\ G' \equiv \dfrac{k_{10}}{k_6} \end{cases} \quad (7)$$

Figure (1) shows the numerical solutions of equations (6, Top) (the rescaled equation) and (2, Bottom) for the parameter values shown in table 1 (which correspond to $A' = 8$, $B' = 5 \times 10^{-4}$, $E' = 10$, $F' = 0.6$ and $G' = 1$, and $\beta$ is a general parameter with dimension $time^{-1}$ required for dimensional consistency in the following analysis):

Considering the global rate $\beta$ (we use $\beta \equiv 1$ throughout the text) and assuming $k_5 = r_5\beta$, $k_6 = r_6\beta$, we make the usual assumption

**Table 1.** Parameter Values.

| Parameters | $k_1$ | $k_2$ | $k_3$ | $k_4$ | $k_5$ | $k_6$ | $k_7$ | $k_8$ | β |
|---|---|---|---|---|---|---|---|---|---|
| Values | β-$k_5$-$k_6$ | $4\times10^{-13}$ | 1 | $10^{-13}$ | 0.1 | 0.1 | 0.1 | $10^{-5}$ | 1 |

doi:10.1371/journal.pone.0069131.t001

$r_1+r_5+r_6=1$ [50] and write $k_1=r_1\beta=(1-r_5-r_6)\beta=\beta-k_5-k_6$, where $r_1$, $r_2$, and $r_3$ are probabilities. The values for $r_5$ and $r_6$ are consistent with those estimated in [50]. For these parameter values, $\Omega_C\equiv\frac{k_1}{k_2}=2\times10^{12}$ and $\Omega_P\equiv\frac{k_3}{k_4}=1\times10^{13}$ (see Appendix S1). These are rescaled parameters in $x$ and $y$ variables, respectively. Stationary values for $P(t)$ and $C(t)$ are $P_\infty=9.6\times10^{12}$ cells and $C_\infty=1.8\times10^{12}$ cells, respectively. Adjusting the $k_2$ and $k_4$ parameters, we can easily obtain more suitable values for the CSC and progenitor cell equilibrium populations, according to possible new experimental results.

Employing standard adiabatic elimination methods, we can write equation (6) as

$$\begin{cases} x'=A'\left[x(1-x)-\frac{x}{A'}+\frac{B'}{A'}y\right] \\ \epsilon y'=y(1-y)+\epsilon F'x-G'y \end{cases} \quad (8)$$

where $\equiv1/E'$. If we consider $\ll1$ (this is equivalent to considering the progenitor cell division rate sufficiently large) we can perform adiabatic approximation [51,52] in (8) and, setting $y'=0$, we obtain the following equation for $x$, expanding in Taylor series up to first order in :

$$x'=\chi-\mu x+\alpha x(1-x) \quad (9)$$

where $\chi\equiv B'(1-G')=\frac{k_8k_2(k_3-k_{10})}{k_1k_4k_6}$, $\mu\equiv1-\epsilon B'F'=1-\frac{k_8k_9}{k_3k_6}$ and $\alpha\equiv A'=\frac{k_1}{k_6}$. Note that $\chi$ can be positive or negative depending on the magnitude of $k_3$ and $k_{10}$.

If we set a small enough value for with respect to $G'$, $B'$ and $F'$, we can further simplify and write $\chi=B'$ and $\mu=1$. We observe that the plasticity phenomenon (associated with $k_8$) is crucial for the existence of the constant term $\chi$. For this reason, from now on we will consider the parameter $\chi$ as representing the plasticity phenomenon in the reduced equation (9).

## The deterministic equation

For comparison with the stochastic study of the next section, we will briefly review the deterministic analysis of the problem. An analytic solution of Eq. (9) is possible. For the initial condition $x(0)=N_0$, one has

$$x(t)=\frac{1}{2\alpha}\left\{\delta-\sqrt{\kappa}\,\mathrm{Tan}\left[\frac{1}{2}t\sqrt{\kappa}+\mathrm{ArcTan}\left(\frac{\delta-2N_0\alpha}{\sqrt{\kappa}}\right)\right]\right\} \quad (10)$$

with $\delta\equiv\alpha-\mu$ and $\kappa\equiv-\delta^2-4\alpha\chi$. The physically relevant stable fixed point is

$$x^*=\frac{\alpha-\mu+\sqrt{\alpha^2-2\alpha\mu+\mu^2+4\alpha\chi}}{2\alpha}. \quad (11)$$

The $x$ scaled population size dynamics can be thought of as analogous to the motion of a particle in a potential $V_0(x)$, seeking its minimum point, with $V_0(x)\equiv-\int\zeta(x)dx$ with $\zeta(x)=\chi+\delta x-\alpha x^2$ from (9). Thus, $V_0$ is given by the cubic polinomial,

$$V_0(x)=\frac{x^3\alpha}{3}-\frac{\delta x^2}{2}-x\chi.$$

We see from (11) that by increasing either $\chi$ or $\delta$, the minimum $x^*$ of $V_0$ moves to the right in the potential, thus favoring CSCs population. Such behavior, of course, is expected, since an increase of $\chi$ means an increase in frequency in which the induced plasticity mechanism occurs, and an increase of $\delta$ is an increase of the symmetric renewal rate of cancer stem cells, both of which increase the population.

# Results

## Noise in the CSCs niche

**Environmental noise.** In tumor tissue, the growth rate and other parameters are influenced by many environmental factors, *e.g.*, degree of vascularization of tissues, supply of oxygen and nutrients, immunological state of the host, chemical agents, gene expression, protein synthesis, mechanical stress, temperature, radiation, etc [50,53–55]. Given the many perturbations affecting the CSC niche, we expect parameters such as growth rate to be random, rather than fixed, to give a more reliable description. We propose a simplification in the interaction mechanisms between cancer stem cells and their niche by adding an external Gaussian white noise in an attempt to capture the essential aspects of this complexity in a mathematically tractable way.

It is worth noting that in conjunction with nonlinear interactions, noise can induce many interesting phenomena, such as stochastic resonance [56], noise-induced phase transitions [57], noise-induced pattern formation, and noise-induced transport [51,58].

**Including external noise.** To model the effect of external noise, focusing initially on the CSCs proliferation rate (by making $\alpha\rightarrow\alpha+\xi(t)$, $\xi(t)$ is the noise with the statistical properties described below), we modify the deterministic equation (9) as follows:

$$x'=\chi-\mu x+(\alpha+\xi)x(1-x)=\chi-\mu x+\alpha x(1-x)+x(1-x)\xi, \quad (12)$$

where $\xi\equiv\xi(t')$ is a Gaussian white noise with statistical properties $\langle\xi(t')\rangle=0$ and $\langle\xi(t')\xi(t'')\rangle=\sigma^2\delta(t'-t'')$, $\sigma^2$ is the variance of $\xi(t')$. Furthermore, $\chi$ is considered a constant related to the plasticity phenomenon and $\alpha$,$\mu$ have interpretations similar to those of equation (9), where $\alpha$ now represents the average symmetric division rate. The noise term in equation (12) represents fluctuations in parameter $\alpha$, due to the complexity of the microenvironment, as discussed above. We include noise in this

term because it is more important in the CSCs population dynamics, since it is this parameter that regulates symmetric reproduction ($C \rightarrow C+C$). Later on we will add yet another noise in the plasticity constant.

We can write the Langevin equation (12) as a stochastic differential equation (considerations concerning the interpretation of the multiplicative term, *i.e.*, if Itô or Stratonovich or other, will be made below) in the form of

$$\begin{aligned} dx_t &= \zeta(x_t,t)dt + \sigma D(x_t,t)dB_t \\ &\equiv [\chi - \mu x_t + \alpha x_t(1-x_t)]dt + \sigma x_t(1-x_t)dB_t, \end{aligned} \tag{13}$$

where we define the drift $\zeta(x_t,t)$ and diffusion $D(x_t,t)$ functions and where $dB_t$ is the Wiener process increment [52,59,60]. The stationary probability distribution $P_{st}(x)$ of the stochastic process defined by (13) is given by [52]

$$P_{st}(x) = N \exp\left(-2\frac{V(x)}{\sigma^2}\right) \tag{14}$$

where $N$ is a normalization constant and $V(x)$ is the stochastic effective potential defined by

$$V(x) = -\int \frac{\zeta(x)}{D(x)^2}dx + \theta\frac{\sigma^2}{2}\ln[D(x)]. \tag{15}$$

Here $\theta=1$ refers to the Stratonovich interpretation of (13) and $\theta=2$ to the Itô version. Substituting the drift and diffusion functions, we get

$$V(x) = \frac{x\mu+\chi-2x\chi}{x-x^2} + (\alpha-\mu+2\chi)\ln\left(\frac{x-1}{x}\right) + \frac{\theta}{2}\sigma^2\ln[x(1-x)] \tag{16}$$

and

$$P_{st}(x) = Ne^{-\frac{2\left(\frac{x\mu+\chi-2x\chi}{x-x^2} + (\alpha-\mu+2\chi)\ln\left(\frac{x-1}{x}\right) + \frac{1}{2}\theta\sigma^2\ln[x(1-x)]\right)}{\sigma^2}}. \tag{17}$$

The maximum $x_m$ of $P_{st}$, which corresponds to the minimum of $V(x)$, can be obtained from the following equation [61]:

$$\zeta(x_m) - \theta\frac{\sigma^2}{2}D(x_m)\frac{d[D(x_m)]}{dx_m} = 0. \tag{18}$$

We see that for $\sigma=0$, $x_m$ corresponds to the value given by $x^*$ in eq. (11). From the drift and diffusion functions, we get:

$$-x^3\theta\sigma^2 - \frac{1}{2}x^2(2\alpha-3\theta\sigma^2) + \frac{1}{2}x(2\alpha-2\mu-\theta\sigma^2) + \chi = 0. \tag{19}$$

The condition for (19) possessing three real roots (corresponding to the two extremes of $P_{st}$) is [62]:

$$\frac{1}{16}(2\mu+\theta\sigma^2-2\alpha)^2(4\alpha^2+4\theta(\alpha-4\mu)\sigma^2+\theta^2\sigma^4) + (2\alpha-3\theta\sigma^2)(2\alpha^2+3\theta(\alpha-3\mu)\sigma^2)\chi - 27\theta^2\sigma^4\chi^2 > 0. \tag{20}$$

For example, for the parameters values $\theta=2$, $\alpha=8$, $\mu=1$ and $\chi=0.00045$, the critical value $\sigma_{cr}$ above which a transition is induced in $P_{st}$ is $\sigma_{cr}=2.68$.

Figures (2) show, in Stratonovich interpretation ($\theta=1$), (the results do not change qualitatively if we use Itô. For a discussion quite enlightening about the controversial dilemma Itô/Stratonovich, see [63]) the effect of increasing the noise intensity in the stochastic effective potential $V(x)$ (Top) and in the stationary probability distribution $P_{st}(x)$ (Middle). Below is the $\chi-\sigma$ plane. The shaded region corresponds to high values of $\sigma$ where $P_{st}$ is bimodal. Note that the presence of plasticity (represented by $\chi>0$) implies the survival of cells populations regardless of noise intensity. Inclusion of external noise can induces the appearance of a bimodal stationary probability distribution, which leads to a result quite different from the deterministic case: while the population in the deterministic case will necessarily reach the value $x^*$, in the stochastic case the population is unlikely to reach $x^*$ if $\sigma$ is above its critical value $\sigma_{cr}$. It is much more likely to possess a nonzero (if $\chi>0$), very small population (left peak of $P_{st}$) or a very large one (right peak of $P_{st}$). This peak positioned to the right is associated with a population near the maximum value $x\approx 1$ in the rescaled variable $x=C/\Omega_C$. It stands for the possibility that the population of cancer stem cells possess a value close to $C=\Omega_C x^* \approx 2\times 10^{12}$. This represents a significant fraction of the population of progenitor cells $P$, a fraction that depends mainly on the equilibrium value $x^*$ of the deterministic equation given by (11), never exceeding this threshold. When we insert noise in the plasticity $\chi$ this is no longer the case.

The inhibition of the host's immune system, which can result in a decrease of the microenvironmental complexity, is equivalent in our model to a decrease of $\sigma$. Therefore, a xenograft performed in immunosuppressed mice may, over time, present significantly large CSC populations. This may have been the case for the experiments conducted in [27]. On the other hand, the left peak in $P_{st}$ may represent a tiny fraction of the CSCs population, as commonly reported in the pioneering experiments mentioned in the introduction, in which less immunosuppressed mice were used. If $\chi=0$ and $\sigma>\sigma_{cr}$, it is much more likely that the population becomes extinct as shown in figure (3).

Figures (4) and (5) show five trajectories of the relevant stochastic process, constructed using the Euler algorithm [64], with initial condition $x(0)=0.1$, for $\sigma<\sigma_{cr}$ and $\sigma>\sigma_{cr}$, respectively. The black curve represents the solution for $\sigma=0$. We see in Figure (5) that for high values of $\sigma$, some trajectories can exhibit spontaneous regression of the CSCs. This seems plausible in light of the supporting evidence from many clinical reports [65].

Figure (6) shows the effect of $\alpha$ on $V(x)$ (Top) and $P_{st}$ (Middle). Sufficiently small values of $\alpha$ refer to unimodal distributions with left asymmetry (blue curve/dot). Intermediate values correspond to bimodal distributions (shaded area in the $\alpha-\sigma$ plane, red curve/dot). Sufficiently high levels of $\alpha$ correspond to unimodal distributions with right asymmetry (black curve/dot).

We conclude in this section that the cell plasticity phenomenon is necessary for the existence of a cancer stem cell population as a small fraction of total tumor cells. Of course, microenvironmental conditions consistent with high noise levels are also necessary.

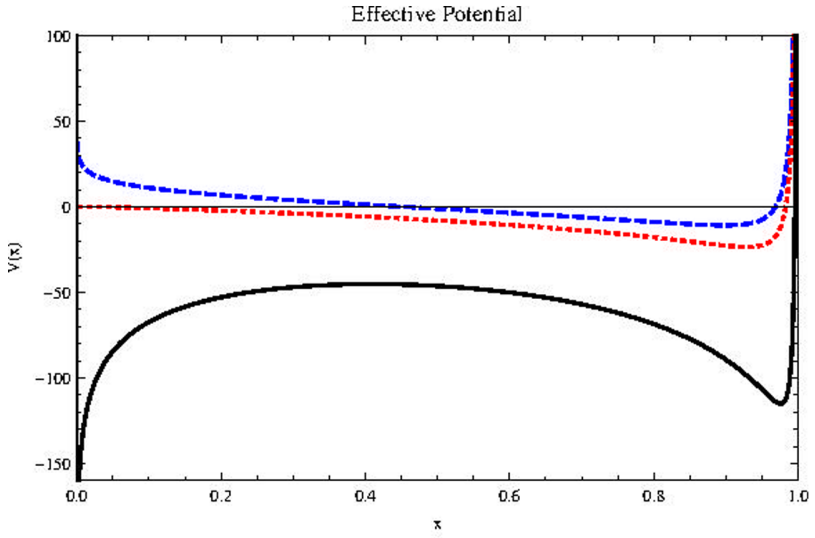
Effective Potential
V(x)
x

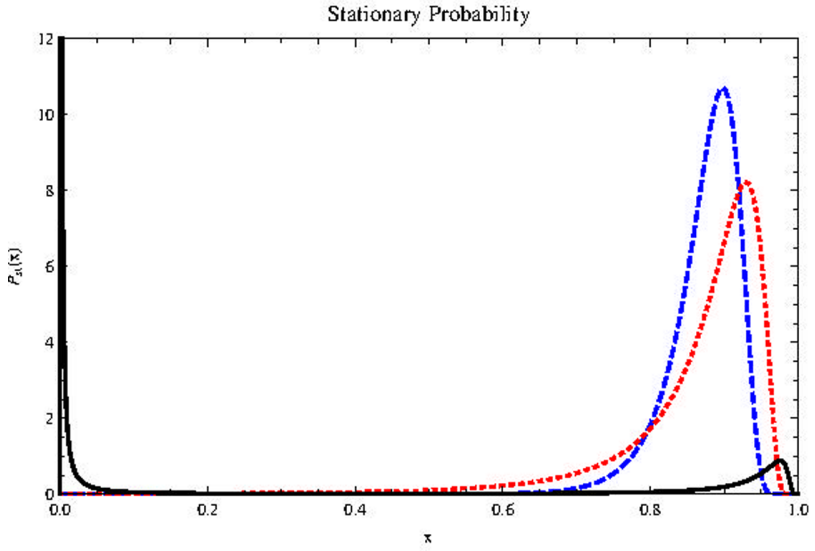
Stationary Probability
$P_{st}(x)$
x

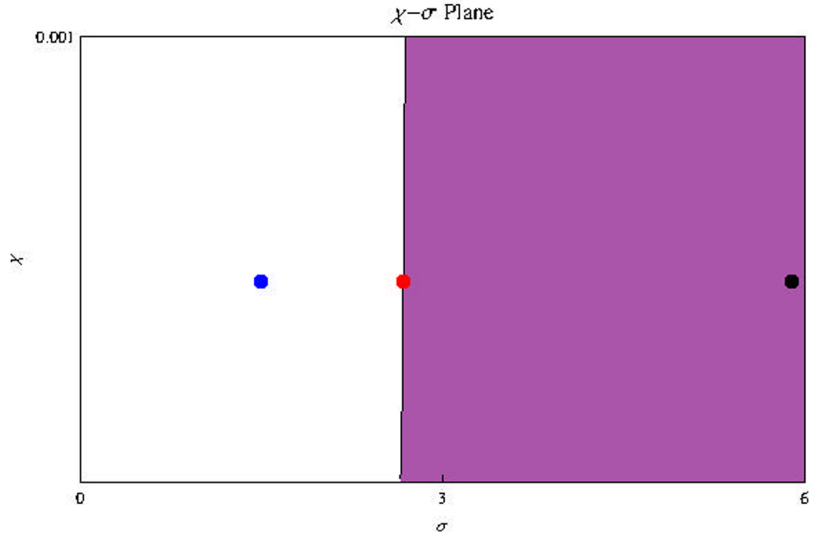
$\chi-\sigma$ Plane
$\chi$
$\sigma$

**Figure 2. Effects of noise intensity on $V(x)$ and $P_{st}(x)$.** Effect of $\sigma$ on $V(x)$ (on the top) and $P_{st}(x)$ (in the middle) for parameters $k_1=1-k_5-k_6$, $k_2=4\times10^{-13}$, $k_3=1$, $k_4=10^{-13}$, $k_5=0.1$, $k_6=0.1$, $k_7=0.1$ and $k_8=0.00001$. Horizontal axis represents population size $x$. Blue, dashed curve: $\sigma=1.5$. Red, dotted: $\sigma=2.68$. Black, thick: $\sigma=5.9$. Below we also show the $\chi-\sigma$ plane with $\sigma$ in the horizontal axis.
doi:10.1371/journal.pone.0069131.g002

## Colorful background noise

We can ask ourselves what effects the variability induced by noise in $P$ cells produce in the $C$ population. In equation (9), reminiscences of the presence of $P$ cells are manifested by the presence of $\chi$. We can imagine this term as representing a source of background noisy for $C$ cells. The question that immediately arises is: what are the effects of a noise on the proliferation rate $\alpha$ combined with other noise related to the plasticity in constant $\chi$?

To answer this question, let's add the noise $\xi(t)$ and $\eta(t)$ as $\chi\to\chi+\xi(t)$ and $\alpha\to\alpha+\eta(t)$ and write the equations

$$\begin{aligned}\dot{x}&=\chi-\mu x+\alpha x(1-x)+\xi(t)+\eta(t)x(1-x)\\&\equiv h(x)+g_1(x)\xi(t)+g_2(x)\eta(t)\end{aligned}\tag{21}$$

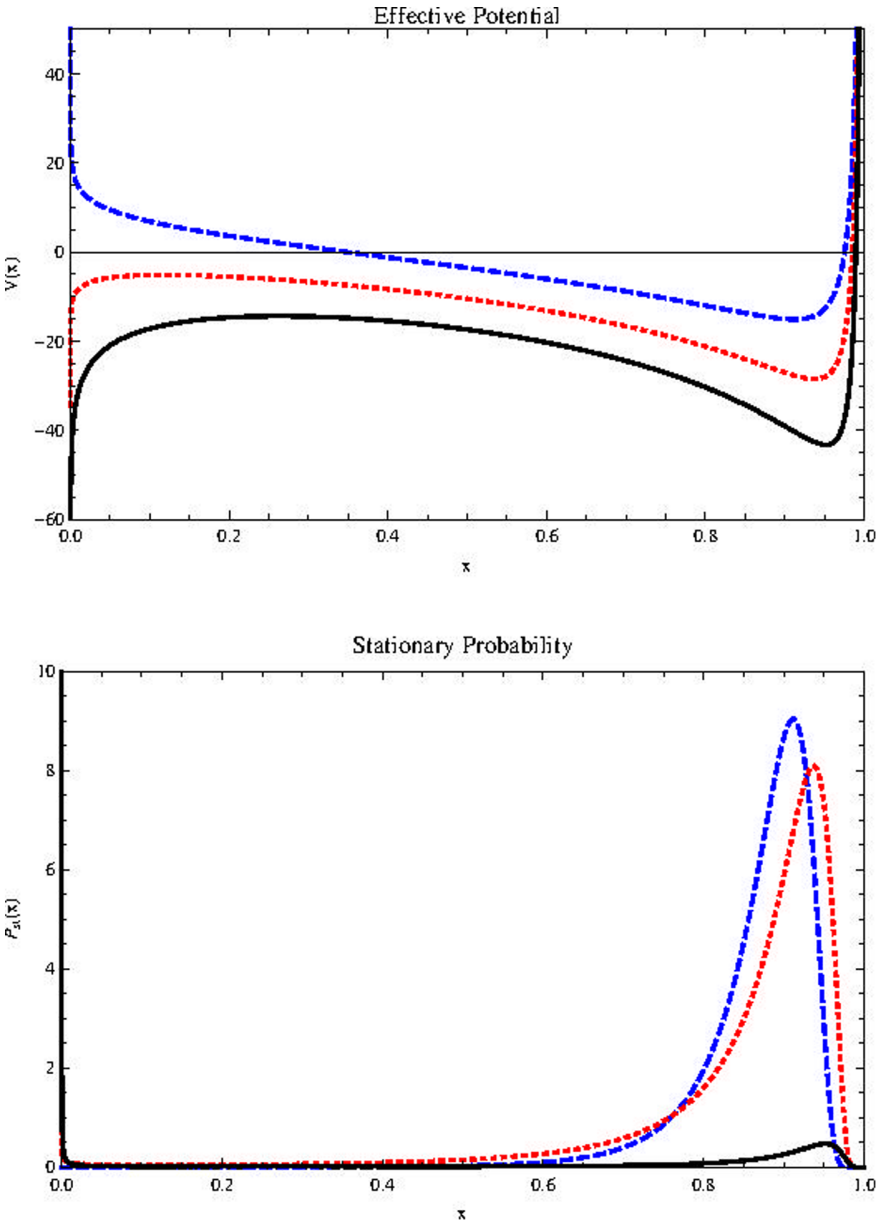


**Figure 3. Effects of noise intensity on $V(x)$ and $P_{st}(x)$.** Effect of $\sigma$ on $V(x)$ (on the top) and $P_{st}(x)$ (at bottom) for $\chi=0$. Horizontal axis represents population size $x$. Blue, dashed curve: $\sigma=2$. Red, dotted: $\sigma=3$. Black, thick: $\sigma=3.74$. Other parameters are as in figure (2). For sufficiently high values of $\sigma$, the CSCs population is extinguished.
doi:10.1371/journal.pone.0069131.g003

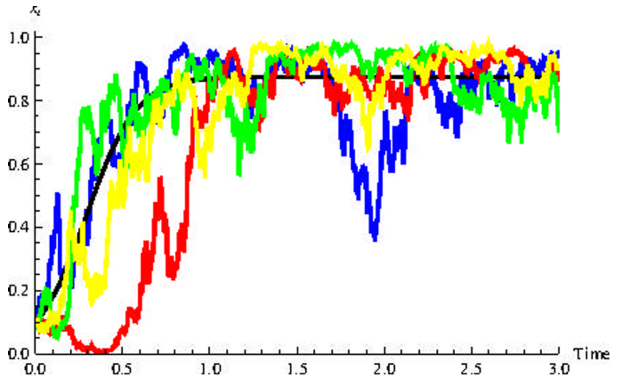


**Figure 4. Some possible trajectories for the population dynamics with weak noise.** The rugged curves show four realizations of stochastic process (13) with $\sigma=1.0$. The black curve shows the deterministic case, $\sigma=0$.
doi:10.1371/journal.pone.0069131.g004

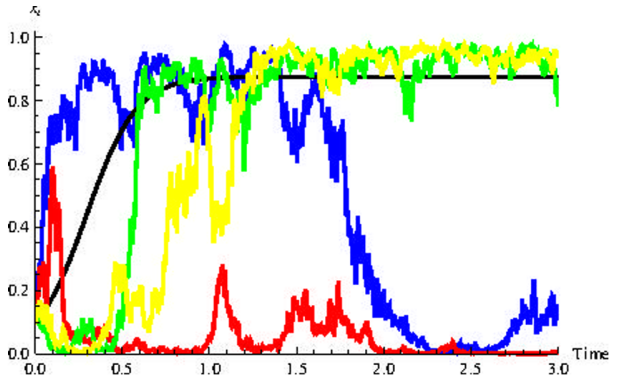


**Figure 5. Some possible trajectories for the population dynamics with strong noise.** The rugged curves show four realizations of stochastic process (13) with $\sigma=6.0$. The black curve shows the deterministic case, $\sigma=0$. Some cases demonstrate the possibility of spontaneous remission.
doi:10.1371/journal.pone.0069131.g005

$$\dot{\xi}=-\frac{1}{\tau}\xi+\frac{1}{\tau}\zeta(t) \tag{22}$$

where $h(x)\equiv\chi-\mu x+\alpha x(1-x)$, $g_1(x)\equiv 1$ and $g_2(x)\equiv x(1-x)$ and $\eta(t)$ and $\zeta(t)$ are white noises with the following properties

$$\langle\zeta(t)\rangle=\langle\eta(t)\rangle=0 \tag{23}$$

$$\langle\zeta(t)\zeta(t')\rangle=2\sigma\delta(t-t') \tag{24}$$

$$\langle\eta(t)\eta(t')\rangle=2\Gamma\delta(t-t') \tag{25}$$

$$\langle\zeta(t)\eta(t')\rangle=\langle\eta(t)\zeta(t')\rangle=2\lambda\sqrt{\sigma\Gamma}\delta(t-t'), \tag{26}$$

where $\sigma$ and $\Gamma$ are the noise intensity of $\zeta(t)$ and $\eta(t)$ respectively, and $\lambda$ is the correlation between noises. Equation (22) represents the Ornstein-Uhlenbeck process that displays exponential correlation function described in equation (27) below with correlation time $\tau$. This stochastic process is called "colored noise".

The two dimensional Markovian process defined by equations (21)–(26) is stochastically equivalent to the one-dimensional non-Markovian process described by (21), (24) and (25), with Gaussian colored noise $\xi(t)$ [52]:

$$\langle\xi(t)\rangle=0,\quad \langle\xi(t)\xi(t')\rangle=\frac{\sigma}{\tau}\exp\left(-\frac{1}{\tau}|t-t'|\right). \tag{27}$$

We are considering the possibility of a colored noise in $\chi$ (for correlation time $\tau>0$). Thus we intend to capture the effects of noise in the plasticity more realistically.

Following [66], the stationary probability distribution is given by

$$P_{st}(x)=N\frac{C(\tau,x)}{\sqrt{B(x)}}\exp\left[\int^{x}\frac{h(x')C(\tau,x')}{B(x')}dx'\right] \tag{28}$$

where $N$ is a normalization constant and $B(x)$ and $C(\tau,x)$ are given by

$$B(x)=\Gamma[g_1(x)]^2+2\lambda\sqrt{\Gamma\sigma}g_1(x)g_2(x)+\sigma[g_2(x)]^2$$

and

$$C(\tau,x)=1-\tau\left(h'(x)-\frac{g'_1(x)}{g_1(x)}h(x)\right).$$

In figure (7) we show the stationary probability distribution with $\lambda=0.9$, $\tau=0$, $\sigma=1\times10^{-9}$, $\Gamma=5$ (blue), $\Gamma=10$ (red, dotted) and $\Gamma=15$ (black, dashed). Now we see that even for very small $\sigma$ (the background noise intensity due to $\chi$), extinction of CSCs is possible for sufficiently high $\Gamma$ (the noise due to $\alpha$), which does not occur when $\chi$ is deterministic. For $\tau\neq0$ this statement becomes more evident, as shown in figure (8) where we used the same parameter values of previous figure with $\Gamma=10$ except that $\tau=0.1$ for blue thick curve and $\tau=0$ for red dotted curve. The conclusion is that the induction of fluctuations in the population of progenitor cells (represented by the background noise due to $\chi$) can promote CSC extinction.

## Some remarks on the interpretation of $\sigma$, $\Gamma$ and $\lambda$.

Before we continue the discussion about the effects of background noise, we will make some considerations about the interpretation that we assign to the parameters $\sigma$, $\Gamma$ and $\lambda$.

**About** $\sigma$ : Given equation (9), we can interpret the system formed by CSCs as an isolated system that exchanges "particles" ($P$ cells) with the external environment and "feels" the disturbances of the medium through the parameter $\chi$, the window of communication with the outside. The intensity of these external disturbances is represented by parameter $\sigma$, and $\xi(t)$ can therefore be interpreted as an external noise, external to the system formed by CSCs. When the body of the tumor is subjected to the effects of clinical treatments such as radiotherapy, chemotherapy or thermotherapy [67], the increase in the intensity of this parameter can be considerable.

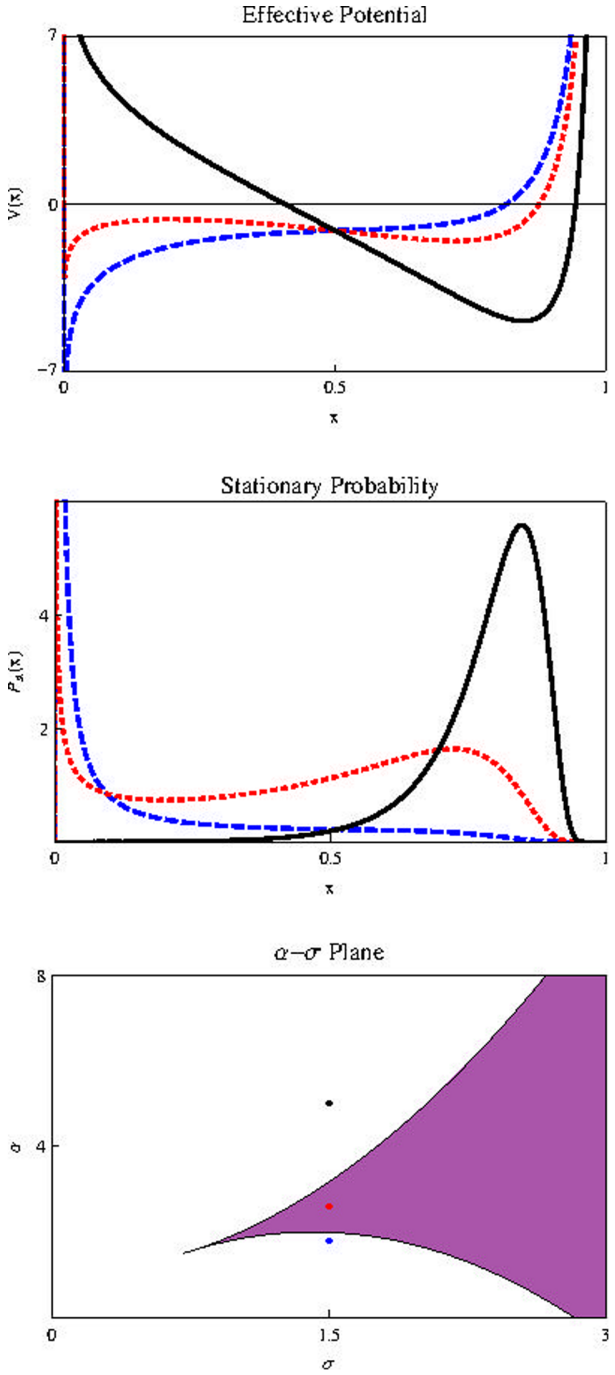


**Figure 6. Effect of $\alpha$ on $V(x)$ (on the top) and $P_{st}(x)$ (in the middle) and the $\alpha-\sigma$ plane at bottom ($\alpha$ on the vertical axis and $\sigma$ on the horizontal axis).** The parameters are: $\sigma=1.5$ in all figures. Blue-dashed: $\alpha=2.2$. Red-dotted: $\alpha=2.6$ and Black-thick: $\alpha=5$.
doi:10.1371/journal.pone.0069131.g006

**About** $\Gamma$ : The direct contact of CSCs with their immediate microenvironment (their niche) is what enables exchange of nutrients and complex biochemical interactions that allow for cell life. Variability in this context represented by $\Gamma$, can be interpreted as an internal noise (internal noise here is not related in any way to the internal demographic noise as modeled by master equations). This internal noise affects the cell proliferation rate $\alpha$.

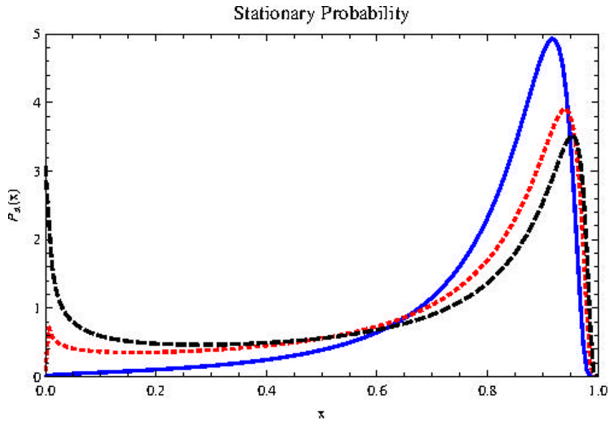


**Figure 7. Stationary probability distribution for different values of $\Gamma$.** $P_{st}(x)$ with parameters $\lambda=0.9$, $\tau=0$, $\sigma=1\times10^{-9}$, $\Gamma=5$ (blue), $\Gamma=10$ (red dotted) and $\Gamma=15$ (black, dashed). Horizontal axis represents population size $x$. Fluctuations in the progenitor population $P$ can stimulate CSCs extinction.
doi:10.1371/journal.pone.0069131.g007

**About** $\lambda$ : A very important aspect about cancer, as mentioned in the introduction, is that tumors contain heterogeneous populations of cells, which may contribute differently in extent and mechanism to the progression of malignancy [68]. Tumor heterogeneity is possibly one of the most significant factors that most treatment methods fail to address sufficiently. While a particular drug may exhibit initial success, the eventual relapse into tumor growth is due in many cases to subpopulations of cancer cells that are either not affected by the drug mechanism, possess or acquire a greater drug resistance, or have a localized condition in their microenvironment that enables them to evade or withstand the treatment. These various subpopulations may include cancer stem cells, mutated clonal variants, and tumor-associated stromal cells, in addition to cells experiencing a spatially different condition such as hypoxia within a diffusion-limited tumor region.

This important aspect is related to different forms in which the various sub-populations respond to various types of internal and external stimuli. Thus, we argue that the correlation coefficient $\lambda$

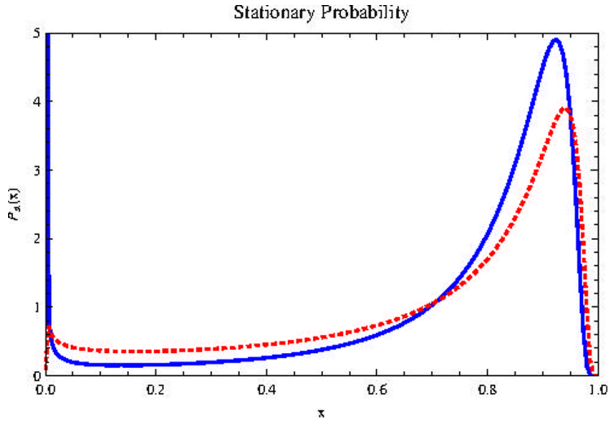


**Figure 8. Dependence of $P_{st}$ with $\tau$.** $P_{st}(x)$ with parameters $\lambda=0.9$, $\tau=0$ (red curve), $\tau=0.1$ (blue curve), $\sigma=1\times10^{-9}$, $\Gamma=10$. Horizontal axis represents population size $x$. High values of $\tau$ facilitates CSCs extinction.
doi:10.1371/journal.pone.0069131.g008

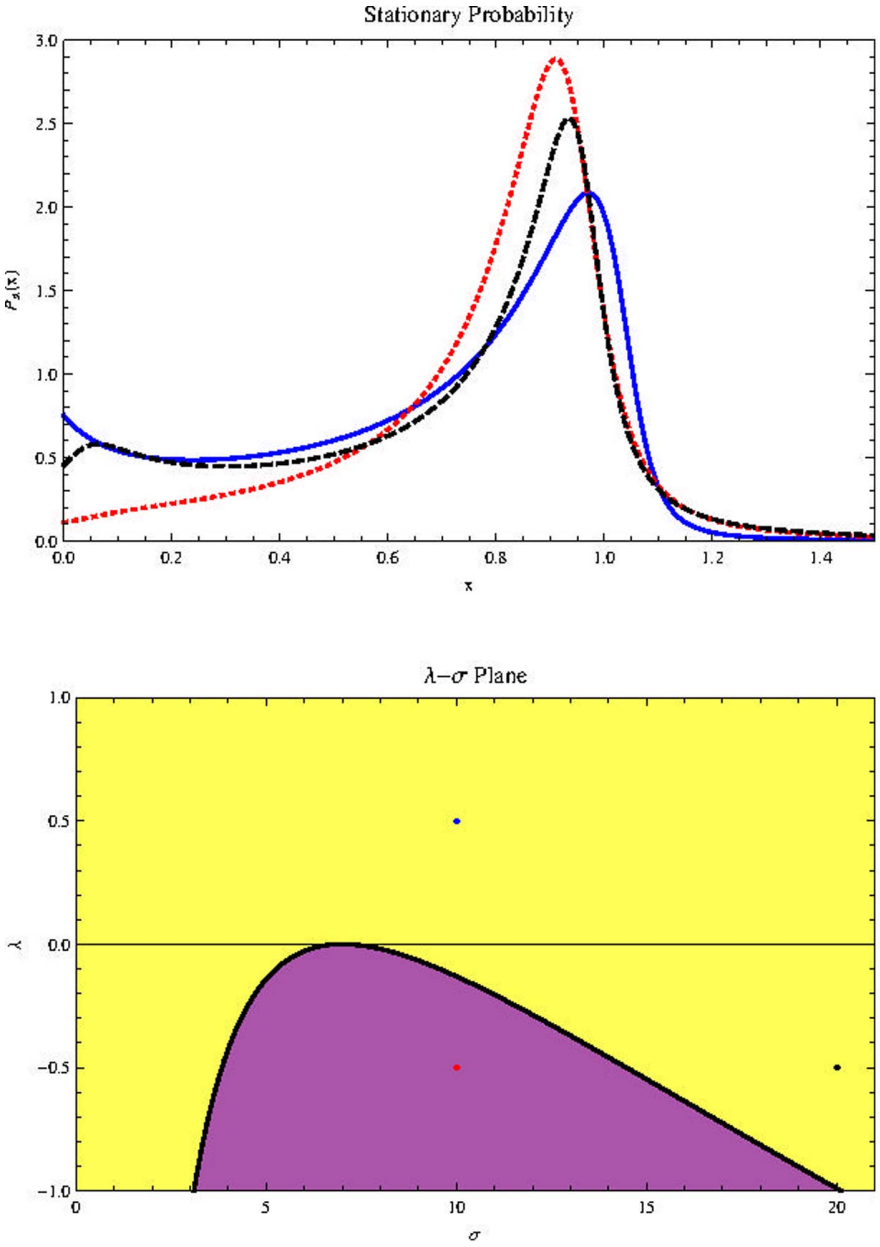


**Figure 9. Effect of $\lambda$ on $P_{st}(x)$ (top) with parameters $\sigma=10$, $\lambda=0.5$ (Blue, thick line), $\sigma=10$, $\lambda=-0.5$ (Red, dotted line), $\sigma=20$, $\lambda=-0.5$ (Black, dashed line),** $\tau=0$, $\Gamma=10^{-1}$, $\mu=1$, $\alpha=8$, $\chi=0.00045$. Horizontal axis represents population size $x$. Bottom: $\lambda-\sigma$ plane with $\sigma$ in the horizontal axis.
doi:10.1371/journal.pone.0069131.g009

between the noise acts as a measure of this heterogeneity between the two populations we are considering. Since each noise is related primarily to a specific cell type, we have that parameter $\lambda$ "measured" different responses of these cells to these stimuli. If the different subpopulations behave more or less in the same manner when subjected to various stimuli (low heterogeneity), $\lambda$ tends to approach 1. If the behaviors are independent, $\lambda\approx 0$. If the responses to the stimuli tend to be opposite (great heterogeneity), $\lambda$ tends to approach $-1$.

Figure (9) (Top) shows the possible effect of changes in $\lambda$ in stationary probability distribution for the parameters values shown in the description. The results for $\tau\neq 0$ are analogous. Below is the $\lambda-\sigma$ diagram. In the yellow region the stationary probability distribution is bimodal. We see that negative values of $\lambda$ favor the survival of cancer stem cells. This result is no surprise, since it is known that the heterogeneity of the tumor provides the phenotypic variation required for natural selection to act to increase the robustness (a property that allows a system to mantain its function despite internal and external perturbations) of the tumor [10].

## Possible effect of conventional treatments

The proposed model in this paper is idealized and highly simplified. In addition, it does not rely on biological data for some

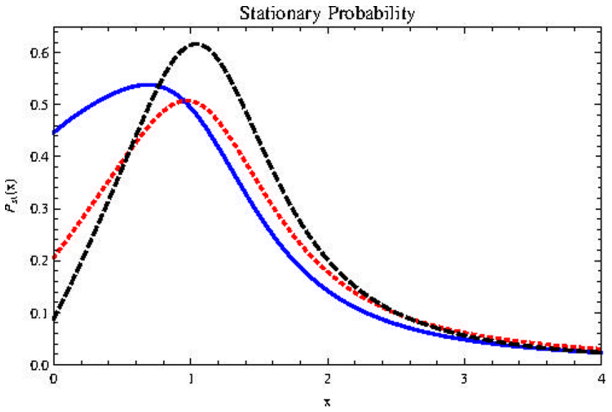


**Figure 10. Effect of $\tau$ on $P_{st}(x)$ with parameters $\tau=0.0$ (Blue, thick line), $\tau=0.05$ (Red, dotted line), $\tau=0.1$ (Black, dashed line), $\Gamma=10$, $\sigma=10$, $\lambda=-0.5$ $\mu=1$, $\alpha=8$, $\chi=0.0$.** Horizontal axis represents population size $x$.
doi:10.1371/journal.pone.0069131.g010

values of the $k$ parameters. Therefore, the conclusions we can get from it in this section are merely theoretical speculations. Having said this, let's try to estimate the effects that conventional treatments may have on the CSC population.

In the proposed model we imagine that such treatments work directly on progenitor cells, since such treatments are designed to act mainly in cells that reproduce faster [69]. Thus, the effect on CSCs is indirect via background noise in a manner that is analogous to what was discussed above. Now we have the possibility of noise intensity $\sigma$ being much larger. Treatments act to eliminate progenitor cells and the tendency, therefore, is for parameter $\chi$ to approach zero. Since this is the parameter that connects the "underlying world" of cancer stem cells to the world of progenitor cells, we could imagine that the contact between the worlds is lost. This is no problem, however, because now we think of the background noise as an additive noise that arises as a result of external perturbations to the CSCs. Thus, we can consider equation (21) with $\chi=0$ and think about the noise $\xi(t)$ as is commonly understood when you introduce an additive noise in the equations "phenomenologically" or "by hand".

For large values of $\sigma$, the parameter of greater relevance is $\tau$. Figure (10) shows the effect on the stationary probability distribution: Positive values, even small ones, help cancer stem cells considerably not going extinct. The most important, however, is another fact, which is explicitly shown in this figure: The main consequence of exploring the possibility of an intense additive noise is that the population of cancer stem cells may be considerably greater than the maximum population of the deterministic model $C_\infty=\Omega_C x^*$. This means that the effects of conventional treatments that act primarily in the fast cycling cells, here represented by progenitor cells, can be extremely exciting for CSC proliferation. *Cancer stem cells enjoy noise.*

## Discussion

The importance of cellular plasticity in the conclusions we have drawn so far, is evident. In [32] the authors point out potential conceptual difficulties associated with the phenotypic switching hypothesis. They argue that if cancer cells can turn into cancer stem cells, then the very notion of CSC becomes blurred, since in this way the cancer cells could dedifferentiate at any time and acquire the potential immortality of CSCs. In the authors words, "the distinction between phenotypic switching and the original conventional model, run the risk of becoming purely semantic." From a clinical perspective, this means that the existence or not of the CSCs is irrelevant, since we must try to kill all tumor cells and not just focus on tumor initiating cells. However, the fact that we have to kill the greatest possible amount of tumor cells does not mean that we have to try to do it in the same way for all of them. In [70], a near-twofold reduction in the density of brain tumors in mice was observed when authors combined standard anticancer drugs with the selective killing of CSCs, if compared with standard agents alone. With regard to the phenotypic switching property, selectively killing a population of CSCs can make room for progenitor cells to dedifferentiate and occupy this vacant niche space. Trying to limit "stemness" instead, by changing conditions of the niche that supports the life of CSCs, may be a more promising therapeutic strategy. This idea is in line with what is thought to be necessary for major mass extinctions [71].

Until now the properties of cancer stem cells were tested only in transplantation assays and their very existence have been questioned several times [6–8]. In [72], the authors use a lineage tracing technique that allows permanent, *in vivo* fluorescent marking of stem cells and their progeny, trying to put an end to the controversy of the existence of cancer stem cells in solid tumors. They unraveled the *in vivo* mode of tumor growth in its native environment and found that the majority of labeled tumor cells in benign skin tumors have only limited proliferative potential, whereas a fraction has the capacity to persist in the long term, giving rise to progeny that occupies a significant part of the tumor. Progression to cancer in benign skin tumors was associated with expansion of the CSC population and a decrease in the production of non-stem cells. This suggests that tumor evolution enriches the CSC population. Designing therapies that prevent increases in stemness may be a means to restrict tumor progression into cancer.

## Conclusion

We propose a model to describe the population dynamics of cancer cells, using the theory of cancer stem cells (CSCs). Our analysis allows us to address a controversy related to the frequency of such cells in tumors. Initially it was thought that these cells were relatively rare, comprising at most $\sim 1\%$ of the cancer cell population. More recent experiments, however, suggest that the CSC population need not be small. Taking into account the cellular plasticity property, which permits more mature cells to dedifferentiate into cells with characteristics of stem cells, we show that the discrepancy observed in the frequency of these cells is entirely consistent with the original hypothesis of the existence of cancer stem cells, as long as favorable conditions related to the complexity of the microenvironment are met. We assume that these conditions can be described by the inclusion of noise in the rate of tumor growth or in the rate at which the plasticity phenomenon occurs.

In the model where we take into account only the noise in the rate of CSC proliferation, we conclude that there is the possibility of the stationary probability distribution being bimodal. In the model that also incorporates noise in parameter $\chi$ associated to the cellular plasticity phenomenon, the possibility of extinction arises and the fraction of CSCs in the tumor can assume quite high values, exceeding the threshold $C_\infty$. The "color" of this noise stimulates the CSC population. The correlation coefficient between noises is interpreted as a measure of heterogeneity between progenitor cells and cancer stem cells, since different cells respond to stimuli in different ways. This heterogeneity also excites the CSC population.

In future work we plan to extend the model to include spatial distribution. We will also investigate the possibility of a model based on a master equation to investigate the effects of demographic stochasticity.

## Supporting Information

**Appendix S1 Appendix to a possible explanation for the variable frequencies of cancer stem cells in tumors.**
(PDF)

## Acknowledgments

RVS is grateful to Ronald Dickman for his helpful comments. We thank the referees of PLOS ONE for the rigorous and competent reviewing.

## Author Contributions

Conceived and designed the experiments: RVS LMS. Analyzed the data: RVS. Wrote the paper: RVS LMS.

## References


1. Reya T, Morrison SJ, Clarke MF, Weissman IL (2001) Stem cells, cancer, and cancer stem cells. Nature 414: 105–111.
2. Clarke MF, Fuller M (2006) Stem cells and cancer: Two faces of eve. Cell 124: 1111–1115.
3. Vermeulen L, Sprick MR, Kemper K, Stassi G, Medema JP (2008) Cancer stem cells – old concepts, new insights. Cell Death and Differentiation aop.
4. Dalerba P, Cho RW, Clarke MF (2007) Cancer stem cells: models and concepts. Annual review of medicine 58: 267–284.
5. Bomken S, Fišer K, Heidenreich O, Vormoor J (2010) Understanding the cancer stem cell. British journal of cancer 103: 439–445.
6. Lewis M (2008) Faith, heresy and the cancer stem cell hypothesis. Future oncology (London, England) 4: 585.
7. Hill RP (2006) Identifying cancer stem cells in solid tumors: case not proven. Cancer Research 66: 1891–1895; discussion 1890.
8. Welte Y, Adjaye J, Lehrach HR, Regenbrecht CR (2010) Cancer stem cells in solid tumors: elusive or illusive? Cell Commun Signal 8: 6.
9. Denison TA, Bae YH (2012) Tumor heterogeneity and its implication for drug delivery. Journal of Controlled Release.
10. Tian T, Olson S, Whitacre J, Harding A (2011) The origins of cancer robustness and evolvability. Integr Biol 3: 17–30.
11. Shackleton M, Quintana E, Fearon E, Morrison S (2009) Heterogeneity in cancer: cancer stem cells versus clonal evolution. Cell 138: 822–829.
12. Marusyk A, Polyak K (2010) Tumor heterogeneity: causes and consequences. Biochimica et Biophysica Acta (BBA)-Reviews on Cancer 1805: 105–117.
13. Marusyk A, Almendro V, Polyak K (2012) Intra-tumour heterogeneity: a looking glass for cancer? Nature Reviews Cancer.
14. Rapp UR, Ceteci F, Schreck R (2008) Oncogene-induced plasticity and cancer stem cells. Cell Cycle 7: 45.
15. Grunewald T, Herbst S, Heinze J, Burdach S (2011) Understanding tumor heterogeneity as functional compartments-superorganisms revisited. Journal of translational medicine 9: 79.
16. Lander A, Kimble J, Clevers H, Fuchs E, Montarras D, et al. (2012) What does the concept of the stem cell niche really mean today? BMC biology 10: 19.
17. Iwasaki H, Suda T (2009) Cancer stem cells and their niche. Cancer science 100: 1166–1172.
18. Ishizawa K, Rasheed Z, Karisch R, Wang Q, Kowalski J, et al. (2010) Tumor-initiating cells are rare in many human tumors. Cell stem cell 7: 279–282.
19. Stewart J, Shaw P, Gedye C, Bernardini M, Neel B, et al. (2011) Phenotypic heterogeneity and instability of human ovarian tumor-initiating cells. Proceedings of the National Academy of Sciences 108: 6468.
20. Vargaftig J, Taussig D, Griessinger E, Anjos-Afonso F, Lister T, et al. (2011) Frequency of leukemic initiating cells does not depend on the xenotransplantation model used. Leukemia.
21. Sarry J, Murphy K, Perry R, Sanchez P, Secreto A, et al. (2011) Human acute myelogenous leukemia stem cells are rare and heterogeneous when assayed in nod/scid/il2rāc-deficient mice. The Journal of Clinical Investigation 121: 384.
22. Zhong Y, Guan K, Zhou C, Ma W, Wang D, et al. (2010) Cancer stem cells sustaining the growth of mouse melanoma are not rare. Cancer letters 292: 17–23.
23. Baker M (2008) Melanoma in mice casts doubt on scarcity of cancer stem cells. Nature 456: 553.
24. Johnston M, Maini P, Jonathan Chapman S, Edwards C, Bodmer W (2010) On the proportion of cancer stem cells in a tumour. Journal of theoretical biology 266: 708–711.
25. Baker M (2008) Cancer stem cells, becoming common. Nature Reports Stem Cells.
26. Schatton T, Murphy G, Frank N, Yamaura K, Waaga-Gasser A, et al. (2008) Identification of cells initiating human melanomas. Nature 451: 345–349.
27. Quintana E, Shackleton M, Sabel M, Fullen D, Johnson T, et al. (2008) Efficient tumour formation by single human melanoma cells. Nature 456: 593–598.
28. Kelly P, Dakic A, Adams J, Nutt S, Strasser A (2007) Tumor growth need not be driven by rare cancer stem cells. Science 317: 337.
29. Williams R, Den Besten W, Sherr C (2007) Cytokine-dependent imatinib resistance in mouse bcr-abl+, arf-null lymphoblastic leukemia. Genes & development 21: 2283.
30. Boiko A, Razorenova O, van de Rijn M, Swetter S, Johnson D, et al. (2010) Human melanomainitiating cells express neural crest nerve growth factor receptor cd271. Nature 466: 133–137.
31. Gupta P, Chaffer C, Weinberg R (2009) Cancer stem cells: mirage or reality? Nature medicine 15: 1010–1012.
32. Zapperi S, La Porta CAM (2012) Do cancer cells undergo phenotypic switching? the case for imperfect cancer stem cells markers. Scientific reports.
33. Chaffer C, Brueckmann I, Scheel C, Kaestli A, Wiggins P, et al. (2011) Normal and neoplastic nonstem cells can spontaneously convert to a stem-like state. Proceedings of the National Academy of Sciences 108: 7950.
34. Strauss R, Hamerlik P, Lieber A, Bartek J (2012) Regulation of stem cell plasticity: Mechanisms and relevance to tissue biology and cancer. Molecular Therapy.
35. Morrison S, Kimble J (2006) Asymmetric and symmetric stem-cell divisions in development and cancer. Nature 441: 1068–1074.
36. Leder K, Holland E, Michor F (2010) The therapeutic implications of plasticity of the cancer stem cell phenotype. PloS one 5: e14366.
37. Turner C, Stinchcombe AR, Kohandel M, Singh S, Sivaloganathan S (2009) Characterization of brain cancer stem cells: a mathematical approach. Cell Prolif 42: 529–40.
38. Laird AK (1964) Dynamics of tumour growth. British journal of cancer 18: 490.
39. Choe SC, Zhao G, Zhao Z, Rosenblatt JD, Cho HM, et al. (2011) Model for in vivo progression of tumors based on co-evolving cell population and vasculature. Scientific reports 1.
40. Gliozzi AS, Guiot C, Delsanto PP (2009) A new computational tool for the phenomenological analysis of multipassage tumor growth curves. PloS one 4: e5358.
41. Herman AB, Savage VM, West GB (2011) A quantitative theory of solid tumor growth, metabolic rate and vascularization. PloS one 6: e22973.
42. Vaidya VG, Alexandro FJ Jr (1982) Evaluation of some mathematical models for tumor growth. International Journal of Bio-Medical Computing 13: 19–35.
43. Weedon-Fekjær H, Lindqvist BH, Vatten LJ, Aalen OO, Tretli S, et al. (2008) Breast cancer tumor growth estimated through mammography screening data. Breast Cancer Res 10: R41.
44. Guiot C, Delsanto PP, Carpinteri A, Pugno N, Mansury Y, et al. (2006) The dynamic evolution of the power exponent in a universal growth model of tumors. Journal of theoretical biology 240: 459–463.
45. Guiot C, Degiorgis PG, Delsanto PP, Gabriele P, Deisboeck TS (2003) Does tumor growth follow a universal law? Journal of theoretical biology 225: 147–151.
46. Castorina P, Zappalà D (2006) Tumor gompertzian growth by cellular energetic balance. Physica A: Statistical Mechanics and its Applications 365: 473–480.
47. Von Bertalanffy L (1957) Quantitative laws in metabolism and growth. The quarterly review of biology 32: 217–231.
48. Perko L (2000) Differential Equations and Dynamical Systems. Texts in Applied Mathematics. Springer.
49. Hirsch M, Smale S, Devaney R (2004) Differential Equations, Dynamical Systems, and an Introduction to Chaos. Pure and Applied Mathematics. Academic Press.
50. Tomasetti C, Levy D (2010) Role of symmetric and asymmetric division of stem cells in developing drug resistance. Proceedings of the National Academy of Sciences 107: 16766–16771.
51. Berglund N, Gentz B (2006) Noise-induced phenomena in slow-fast dynamical systems: a samplepaths approach. Probability and its applications. Springer.
52. Gardiner C (2009) Stochastic methods: a handbook for the natural and social sciences. Springer series in synergetics. Springer.
53. Burness M, Sipkins D (2010) The stem cell niche in health and malignancy. In: Seminars in cancer biology. Elsevier, volume 20, 107–115.
54. Whiteside T (2008) The tumor microenvironment and its role in promoting tumor growth. Oncogene 27: 5904–5912.
55. Maffini M, Soto A, Calabro J, Ucci A, Sonnenschein C (2004) The stroma as a crucial target in rat mammary gland carcinogenesis. Journal of cell science 117: 1495–1502.
56. Gammaitoni L, Hänggi P, Jung P, Marchesoni F (1998) Stochastic resonance. Reviews of Modern Physics 70: 223.
57. Van den Broeck C, Parrondo J, Toral R, Kawai R (1997) Nonequilibrium phase transitions induced by multiplicative noise. Physical Review E 55: 4084.
58. Ridolfi L, D'Odorico P, Laio F (2011) Noise-Induced Phenomena in the Environmental Sciences. Cambridge University Press.
59. Oksendal B (2003) Stochastic differential equations: an introduction with applications. Universitext (1979). Springer.

60. Karlin S, Taylor H (2000) A second course in stochastic processes. Academic Press.
61. Horsthemke W, Lefever R (1984) Noise-induced transitions: theory and applications in physics, chemistry, and biology. Springer series in synergetics. Springer.
62. Kavinoky R, Thoo J (2008) The number of real roots of a cubic equation. The AMATYC Review 29: 3–8.
63. Braumann CA (2007) Harvesting in a random environment: It or stratonovich calculus? Journal of Theoretical Biology 244: 424–432.
64. Kloeden P, Platen E (1992) Numerical solution of stochastic differential equations. Applications of mathematics. Springer-Verlag.
65. Kalialis L, Drzewiecki K, Klyver H (2009) Spontaneous regression of metastases from melanoma: review of the literature. Melanoma research 19: 275.
66. Da-jinW, Li C, Sheng-zhi K (1994) Bistable kinetic model driven by correlated noises: Steady-state analysis. Phys Rev E 50: 2496–2502.
67. Atkinson R, Zhang M, Diagaradjane P, Peddibhotla S, Contreras A, et al. (2010) Thermal enhancement with optically activated gold nanoshells sensitizes breast cancer stem cells to radiation therapy. Science translational medicine 2: 55ra79–55ra79.
68. Pietras A (2011) Cancer stem cells in tumor heterogeneity. Advances in Cancer Research 112: 256.
69. Chow E (2012) Implication of cancer stem cells in cancer drug development and drug delivery. Journal of Laboratory Automation.
70. Chen J, Li Y, Yu TS, McKay RM, Burns DK, et al. (2012) A restricted cell population propagates glioblastoma growth after chemotherapy. Nature 488: 522–526.
71. Arens N, West I (2008) Press-pulse: a general theory of mass extinction? Paleobiology 34: 456–471.
72. Driessens G, Beck B, Caauwe A, Simons BD, Blanpain C (2012) Defining the mode of tumour growth by clonal analysis. Nature 488: 527–530.

# Appendix to
# *A possible explanation for the variable frequencies of cancer stem cells in tumors*

## Rescale transformations

In this appendix we detail the rescales made throughout the main text. The general model written in terms of the reactions is

$$\begin{gathered} C \underset{k_2'/\Omega_2}{\overset{k_1}{\rightleftharpoons}} C+C \\ P \underset{k_4'/\Omega_4}{\overset{k_3}{\rightleftharpoons}} P+P \\ C \xrightarrow{k_5} C+P \\ C \xrightarrow{k_6} P+P \\ P \xrightarrow{k_7} \emptyset \\ P \xrightarrow{k_8} C \end{gathered} \tag{1}$$

Using the law of mass action we have

$$\begin{cases} \dot{C}=k_1 C\left(1-\frac{C}{\Omega_C}\right)-k_6 C+k_8 P \\ \dot{P}=k_3 P\left(1-\frac{P}{\Omega_P}\right)+k_9 C-k_{10} P \end{cases} \tag{2}$$

with $k_9 \equiv k_5+2k_6$, $k_{10} \equiv k_7+k_8$, $\Omega_C \equiv \frac{k_1}{k_2}$, $\Omega_P \equiv \frac{k_3}{k_4}$ and $k_2 \equiv k_2'/\Omega_2$, $k_4' \equiv k_4'/\Omega_4$. Using the reescale $C \equiv \Omega_C x$ and $P \equiv \Omega_P y$ :

$$\begin{cases} \dot{x}=k_1 x\left(1-x\right)-k_6 x+\frac{k_8 \Omega_P}{\Omega_C} y \\ \dot{y}=k_3 y\left(1-y\right)+\frac{k_9 \Omega_C}{\Omega_P} x-k_{10} y \end{cases} \tag{3}$$

Using $t \equiv k_6 t'$ and $\Omega \equiv \frac{\Omega_P}{\Omega_C}$ :

$$\begin{cases} \frac{dx}{dt'}=\frac{k_1}{k_6} x\left(1-x\right)-x+\frac{k_8 \Omega}{k_6} y \\ \frac{dy}{dt'}=\frac{k_3}{k_6} y\left(1-y\right)+\frac{k_9}{k_6 \Omega} x-\frac{k_{10}}{k_6} y \end{cases} \tag{4}$$

or

$$\begin{cases} x'=Ax(1-x)-x+By \\ y'=Ey(1-y)+Fx-Gy \end{cases} \tag{5}$$

with $x' \equiv \frac{dx}{dt'}$, $y' \equiv \frac{dy}{dt'}$ and

$$\begin{cases} A \equiv \frac{k_1}{k_6} \\ B \equiv \frac{k_2 k_3 k_8}{k_1 k_4 k_6} \\ E \equiv \frac{k_3}{k_6} \\ F \equiv \frac{k_1 k_4 k_9}{k_2 k_3 k_6} \\ G \equiv \frac{k_{10}}{k_6} \end{cases} \tag{6}$$

# Gradient system

Starting from (30) and carrying out the transformation $C = s_1 c$, $P = s_2 p$ and $t = s_3 \tau$, we can write

$$\begin{cases} \frac{dc}{d\tau} = k_1 s_3 c \left(1 - \frac{s_1}{\Omega_C} c\right) - k_6 s_3 c + \frac{k_8 s_2 s_3}{s_1} p \\ \frac{dp}{d\tau} = k_3 s_3 p \left(1 - \frac{s_2}{\Omega_P} p\right) + \frac{k_9 s_1 s_3}{s_2} c - k_{10} s_3 p \end{cases} \tag{7}$$

Imposing $\frac{k_8 s_2 s_3}{s_1} = \frac{k_9 s_1 s_3}{s_2}$, $k_6 s_3 = 1$ and $s_1 = \Omega_C$, we obtain $s_1 \equiv \frac{k_1}{k_2}$, $s_2 \equiv \Omega_C \sqrt{\frac{k_9}{k_8}}$ and $s_3 = \frac{1}{k_6}$.

In this way we obtain

$$\begin{cases} \frac{dc}{d\tau} = \frac{k_1}{k_6} c\,(1 - c) - c + \frac{\sqrt{k_8 k_9}}{k_6} p \\ \frac{dp}{d\tau} = \frac{k_3}{k_6} p \left(1 - \frac{\Omega_C}{\Omega_P} \sqrt{\frac{k_9}{k_8}} p\right) + \frac{\sqrt{k_8 k_9}}{k_6} c - \frac{k_{10}}{k_6} p. \end{cases} \tag{8}$$

# Potential $V(x, y)$

We want to write the equation (3) in the form $\dot{\mathbf{x}} = -\nabla V(x, y)$, where $\mathbf{x} = (x(t), y(t))^T$ ($T$ means transpose), $\nabla$ is the nabla operator. Integrating $f(x, y)$ from (3) with respect to $x$ gives

$$V(x, y) = \int f(x, y) dx = -\frac{x^2}{2} + \frac{Ax^2}{2} - \frac{Ax^3}{3} + Bxy + f_0(y). \tag{9}$$

We must now obtain $f_0(y)$. Imposing $\partial_y V(x, y) = g(x, y)$, we obtain $Bx + f_0'(y) = g(x, y)$ and then $f_0(y) = \int [Ey(1 - Fy) - Gy] dy = \frac{Ey^2}{2} - \frac{Gy^2}{2} - \frac{1}{3} EFy^3$. This provides the equation (5).

Capítulo 6

# O ruído e o KISS no nicho das células tronco do câncer

*Esta introdução é baseada nos resultados do artigo [2], publicado em* ***Journal of Theoretical Biology****.*

No artigo anterior propusemos um modelo estocástico $0-$dimensional para estudarmos a dinâmica populacional das células tronco do câncer (CTC). Neste segundo artigo, publicado em *Journal of Theoretical Biology*, [2] ampliamos a análise do anterior a uma situação onde as células podem se difundir em um espaço $1-$dimensional. Mudamos o tratamento das equações diferenciais ordinárias estocásticas para as equações diferenciais parciais estocásticas. Verificamos que um fenômeno análogo à transição induzida por ruído, *i.e.*, uma *transição de fase*, ocorre no caso $1-$dimensional: para valores suficientemente elevados das flutuações estatísticas no microambiente celular, a distribuição estacionária de probabilidades sofre uma transição de fase e se torna bimodal. Alguns estudos associaram esta transição na distribuição estacionára a uma transição do caráter benigno para o maligno dos tumores.

Neste artigo também estávamos especialmente interessados no estudo do tamanho crítico mínimo necessário $L_c$ para que uma população possa se desenvolver quando cercada por um ambiente hostil. Tal tamanho crítico mínimo às vezes é denominado na literatura *Kierstead-Skellam-Slobodkin size* (KISS).

Estudamos os efeitos da plasticidade celular e do ruído do microambiente em $L_c$, através dos chamados diagramas de bifurcação. Concluímos mais uma vez que os efeitos das perturbações estatísticas podem ser benéficos às células tronco do câncer, diminuindo o tamanho crítico mínimo necessário ao seu desenvolvimento. Também estudamos os efeitos do ruído combinados com os efeitos da difusão celular. Concluímos que a difusão compete com as flutuações estatísticas fazendo com que os efeitos destas (por exemplo, indução de transição de fase em $P_{st}$) sejam amenizados.

Journal of Theoretical Biology 335 (2013) 79–87

Contents lists available at SciVerse ScienceDirect

Journal of Theoretical Biology

journal homepage: www.elsevier.com/locate/yjtbi

# The noise and the KISS in the cancer stem cells niche

Renato Vieira dos Santos [a,*], Linaena Méricy da Silva [b,c]

[a] Departamento de Física, Instituto de Ciências Exatas, Universidade Federal de Minas Gerais, CP 702, CEP 31270-901 Belo Horizonte, Minas Gerais, Brasil
[b] Centro Universitário Metodista Izabela Hendrix, Núleo de Biociências, Rua da Bahia 2020, CEP 30160-012, Belo Horizonte, Minas Gerais, Brasil
[c] Laboratório de Patologia Comparada, Instituto de Ciências Biológicas, Universidade Federal de Minas Gerais, CP 702, CEP 31270–901 Belo Horizonte, Minas Gerais, Brasil

## HIGHLIGHTS

- Possible explanation for wide variability observed in cancer stem cells frequency.
- Plasticity is necessary for maintenance of cancer stem cell populations.
- Cell population may exhibit a noise-induced transition.

## ARTICLE INFO

*Article history:*
Received 15 December 2012
Received in revised form
8 May 2013
Accepted 21 June 2013
Available online 1 July 2013

*Keywords:*
Cancer stem cells
Stochastic modeling
Minimal patch size
Plasticity
Diffusion

## ABSTRACT

There is a persistent controversy regarding the frequency of cancer stem cells (CSCs) in solid tumors. Initial studies indicated that these cells had a frequency ranging from 0.0001% to 0.1% of total cells. Recent studies have shown that this does not seem to be always the case. Some of these studies have indicated a frequency of 40%. Through a simple population dynamics model, we studied the effects of stochastic noise and cellular plasticity in the minimal path size of a cancer stem cells population, similar to what is done in what is sometimes called the Kierstead–Skellam–Slobodkin (KISS) Size analysis. We show that the possibility of large variations in the results obtained in the experiments may be a consequence of the different conditions under which the different experiments are submitted, specifically regarding the effective cell niche size where stem cells are transplanted. We also show the possibility of a noise induced transition where the stationary probability distribution of the CSC population can present bimodality.



## 1. Introduction

In recent years there has been increasing evidence for the *Cancer Stem Cell* (CSC) hypothesis (Reya et al., 2001; Clarke and Fuller, 2006; Vermeulen et al., 2008; Dalerba et al., 2007), according to which tumor formation is a result of genetic and epigenetic changes in a subset of stem-like cells, also known as *tumor-forming* or *tumor-initiating* cells (Bomken et al., 2010). Cancer stem cells were first identified in various leukemias and, more recently, in several solid tumors such as brain, breast, cervix and prostate tumors (Dalerba et al., 2007).

It has been suggested that these are the cells responsible for initiating and maintaining tumor growth. In this paper, we study a model for tumor growth that assumes the existence of *cancer stem cells* (CSCs), or *tumor initiating cells*.

The conceptual starting point relevant to CSC theory is constructed from the known heterogeneity of tumors. We now know that cells in a tumor are not all identical copies of each other, but that they display a striking array of characteristics (Denison, 2012; Tian et al., 2011; Shackleton et al., 2009; Marusyk and Polyak, 2010; Marusyk et al., 2012). CSC theory recognizes this fact and develops its consequences. And one of the most immediate implications for clinical practice is that conventional treatments can generally attack the wrong cell type. The appeal of the CSC idea can be described by the following analogy: just as killing the queen bee leads to the demise of the hive, destroying cancer stem cells, should, in theory, stop a tumor from renewing itself. Unfortunately, things are never that simple. In the hive, workers react quickly to the death of the queen by replacing her with a new one. And there is some evidence (Welte et al., 2010; Rapp et al., 2008) to suggest that could also happen in tumors due to a phenomenon known as *cell plasticity*, which allows normal tumor cells to turn into cancer stem cells, should the situation call for it. One goal of this study is to evaluate the possible effects of this

* Corresponding author. Tel.: +51 3133737186.
*E-mail addresses:* econofisico@gmail.com (R.V. dos Santos), linaena.mericy@gmail.com (L.M. da Silva).

0022-5193/$ - see front matter © 2013 Elsevier Ltd. All rights reserved.
http://dx.doi.org/10.1016/j.jtbi.2013.06.025

plasticity. Analogies with superorganisms such as bee colonies are taken much more seriously in Grunewald et al. (2011).

Stem cells in general (the same applies to CSCs) tend to be found on specific areas of a tissue where one particular microenvironment, called *niche* (Lander et al., 2012), promotes the maintenance of its vital functions. This niche has specialized in providing factors that prevent differentiation and thus maintain the stemness of CSCs and, ultimately, the tumor's survival. Stem cells and niche cells interact with each other via adhesion molecules and paracrine factors. This complex network of interactions exchanges molecular signals and maintains the unique characteristics of stem cells, namely, pluripotency and self-renewal.

Given the extreme complexity of the cellular microenvironment in general and of the niche in particular (Iwasaki and Suda, 2009; Lander et al., 2012), we will formulate an effective stochastic theory for the population dynamics of CSCs. We are especially interested in investigating a controversy related to the frequency with which CSCs appear in various tumors (Ishizawa et al., 2010; Stewart et al., 2011; Vargaftig et al., 2011; Sarry et al., 2011; Zhong et al., 2010; Baker, 2008a,b; Johnston et al., 2010). In the initial version of CSC theory, it was believed that these cells were a tiny fraction of the total, ranging from 0.0001% to 0.1% (Schatton et al., 2008; Quintana et al., 2008). However, more recent studies have shown a strong dependence on the number of stem cells present in a tumor with the xenograft experimental model used. In explicit contrast to what was previously thought, in Quintana et al. (2008) a CSC proportion of approximately 25% was observed. Other studies have confirmed this observation (Kelly et al., 2007; Williams et al., 2007; Schatton et al., 2008), with the proportion potentially reaching 41% (Boiko et al., 2010). In Gupta et al. (2009) the authors provide evidence that this discrepancy may be caused by the possibility of phenotypic switching between different tumor cells. By phenotypic switching we mean that a more differentiated cancer cell can, under appropriate conditions, de-differentiate into a cancer stem cell. This is the cellular plasticity mentioned above.

In Zapperi and La Porta (2012), it is suggested that inconsistencies in the numbers of cancer stem cells reported in the literature can also be explained as a consequence of the different definitions used by different researchers. Different assays will give different numbers of cells, which can be orders of magnitude away from each other.

In this paper we are also interested in knowing what are the possible effects of cells diffusion in space. For this, we constructed bifurcation diagrams that show how the population size of CSCs varies when the size of the niche cells changes. We consider the effects that the plasticity phenomenon as well as spatio-temporal noise can have in these diagrams. Finally we studied the effects of the spatial distribution of cells in stationary probability distributions.

The paper is organized as follows: in Section 2 we explain the basic assumptions of our model of CSC population dynamics. In Section 3 we describe the set of reactions we use in the models. The effects of inclusion of spatial structure in the analysis are considered in Section 4. Section 5 closes the paper with conclusions.

## 2. Assumptions

Mathematical modeling has made significant contributions to our understanding of the biology of cancer since the pioneering work of Nordling (1953) and Armitage and Doll (1954), in which the authors proposed that multiple mutations may explain the data on the incidence of cancer and its correlation with age (Chen et al., 2005; Horov et al., 2009). For historical reviews on the subject, see McElwain and Araujo (2004) and Byrne et al. (2006).

In the model used in this paper, cancer stem cells can perform three types of divisions, according to Morrison and Kimble (2006):

- *Symmetric self-renewal*: Cell division in which both daughter cells have the characteristics of the stem cell mother, resulting in an expanding population of stem cells.
- *Symmetric differentiation*: A stem cell divides into two progenitor cells.
- *Asymmetric self-renewal*: A cancer stem cell (denoted by $C$) is generated and a progenitor cell (mature cancer cell, denoted by $P$) is also produced.

We developed a simple mathematical model for the stochastic dynamics of CSCs in which the three division types possess intrinsic replication rates, which are assumed to be time-independent. Therefore, besides these division types, we assume that there is also the possibility of a transformation in which a progenitor cell can acquire characteristics of stem cells where, for all practical purposes, we may regard it as having become a de-differentiated stem cell. In mixed lineage leukemia cells, it was recently shown that committed myeloid progenitor cells acquire properties of leukemia stem cells without changing their overall identity (Leder et al., 2010). These cells do not become stem cells, but rather develop stem cell like behavior by re-activating a subset of genes highly expressed in normal hematopoietic stem cells (Rapp et al., 2008). The biological mechanisms underlying this transformation are described in Gupta et al. (2009), for example. As mentioned previously, we refer to this process as *cell plasticity*.

## 3. Model

This section describes the basic model investigated in this paper. It is based on the cell division mechanism and the plasticity property. We will use the language of stochastic differential equations (Karlin and Taylor, 2000; Schuss, 2010; Oksendal, 2003).

The model is a natural extension of the one proposed in Turner et al. (2009). This extension refers to the inclusion of competition between cells because of the scarcity of resources when populations become large enough. This new possibility in relation to the model proposed in Turner et al. (2009) makes the model nonlinear and prevents that the populations tend to infinity. The model is described in the next subsection.

### 3.1. The basic model

We assume that the population dynamics of cancer stem cells and progenitor cells are governed by the following reactions:

$$
\begin{aligned}
&C \underset{k'_2/\Omega_2}{\overset{k_1}{\rightleftharpoons}} C+C\\
&P \underset{k'_4/\Omega_4}{\overset{k_3}{\rightleftharpoons}} P+P\\
&C \xrightarrow{k_5} C+P\\
&C \xrightarrow{k_6} P+P\\
&P \xrightarrow{k_7} \varnothing\\
&P \xrightarrow{k_8} C
\end{aligned}
\tag{1}
$$

The first and second reactions, in the forward sense, model cell proliferation, which occurs at a rate $k_1$ and $k_3$, respectively. Constants $k'_2$ and $k'_4$ are associated to the reverse process and describe the intensity of competition between the CSC and progenitor cells, respectively, and prevents their unlimited exponential growth; $\Omega_2$ and $\Omega_4$ are constants related to the model's carrying capacity. The third reaction involving $k_5$ originates from the asymmetric transformation of CSCs in CSC daughter and progenitor cell types. The reaction involving the rate $k_6$ is related

to a symmetrical division of stem cells, which gives rise to two progenitor cells. The penultimate reaction is associated with progenitor cell death at rate $k_7$. Finally, $k_8$ is the de-differentiation rate. All rates have dimension (time)$^{-1}$. The specific unit of time (months, quarters, years, etc.) will depend on the type and aggressiveness of the tumor.

Using the law of mass action, we can write

$$\begin{cases} \dfrac{dC}{dt} = k_1 C - k_2 C^2 - k_6 C + k_8 P \\ \dfrac{dP}{dt} = k_3 P - k_4 P^2 + (k_5 + 2k_6) C - (k_7 + k_8) P \end{cases} \tag{2}$$

with $k_2 \equiv k'_2/\Omega_2$, $k_4 \equiv k'_4/\Omega_4$. Setting $\Omega_C \equiv k_1/k_2$, $\Omega_P \equiv k_3/k_4$, $k_9 \equiv k_5 + 2k_6$ and $k_{10} \equiv k_7 + k_8$ and making the substitutions $C = \Omega_C x$, $P = \Omega_C \sqrt{k_9/k_2}\, y$ and $t = \tau/k_6$, Eq. (2) can be written as (see Appendix A)

$$\begin{cases} \dfrac{dx}{d\tau} = Ax(1-x) - x + By \equiv f(x,y) \\ \dfrac{dy}{d\tau} = Ey(1-Fy) + Bx - Gy \equiv g(x,y) \end{cases} \tag{3}$$

with

$$\begin{cases} A \equiv \dfrac{k_1}{k_6} \\ B \equiv \dfrac{\sqrt{k_2 k_9}}{k_6} \\ E \equiv \dfrac{k_3}{k_6} \\ F \equiv \dfrac{\Omega_C}{\Omega_P}\sqrt{\dfrac{k_9}{k_2}} \\ G \equiv \dfrac{k_{10}}{k_6} \end{cases} \tag{4}$$

As $\partial f/\partial y = \partial g/\partial x = B$, Eq. (3) represents a gradient system (Perko, 2000) with potential $V(x,y)$ given by

$$V(x,y) = \frac{1}{6}(3 - 3A + 2Ax)x^2 - Bxy + \frac{1}{6}(3G - 3E + 2EFy)y^2. \tag{5}$$

As a consequence (Hirsch et al., 2004):

1. The eigenvalues of the linearization of Eq. (3) evaluated at equilibrium point are real.
2. If $(x_0; y_0)$ is an isolated minimum of $V$ then $(x_0; y_0)$ is an asymptotically stable solution of (3).
3. If $(x(\tau); y(\tau))$ is a solution of (3) that is not an equilibrium point then $V(x(\tau), y(\tau))$ is a strictly decreasing function and is perpendicular to the level curves of $V(x,y)$.
4. There are no periodic solutions of (3).

Fig. 1 shows the potential function $V(x,y)$. Sufficiently small $F$ ($\Omega_P \gg \Omega_C$) implies large differences in equilibrium populations of $C$ and $P$. For parameters $A = B = G = 1$, $E = 3$ and $F = 0.01$, $(x_0; y_0) = (8.4; 70.6)$. If we set $F = 0.0001$, keeping the other parameters fixed, we get $(x_0; y_0) = (82; 6710)$.

### 3.2. Adiabatic elimination

The proposed model in (1) is in fact a general model of stem cells and does not even carry any specific characteristic of cancer stem cells. All properties considered, such as plasticity and changes in the microenvironment conditions (to be included later), are also found in stem cell systems of normal tissue. The features associated with cancer stem cells are related to the large carrying capacity of progenitor cells when compared with the carrying capacity of cancer stem cells. This fact is represented

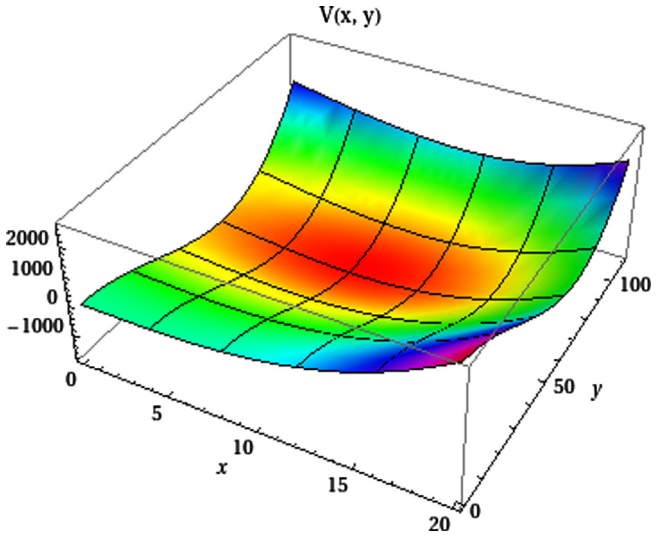


**Fig. 1.** Potential $V(x,y)$ from Eq. (5) for parameters $A = B = G = 1$, $E = 3$ and $F = 0.01$.

numerically by the choice of model parameters made below, which results in this discrepancy.

We can write (2) in the form (see Appendix A)

$$\begin{cases} x' = A'x(1-x) - x + B'y \\ y' = E'y(1-y) + F'x - G'y \end{cases} \tag{6}$$

with $x' \equiv dx/dt'$, $y' \equiv dy/dt'$, $t' \equiv t/k_6$ and

$$\begin{cases} A' \equiv \dfrac{k_1}{k_6} \\ B' \equiv \dfrac{k_2 k_3 k_8}{k_1 k_4 k_6} \\ E' \equiv \dfrac{k_3}{k_6} \\ F' \equiv \dfrac{k_1 k_4 k_9}{k_2 k_3 k_6} \\ G' \equiv \dfrac{k_{10}}{k_6} \end{cases} \tag{7}$$

Fig. 2 shows the numerical solutions of Eqs. (6) (the rescaled equation) and (2) for the following parameter values: $k_1 = 1 - k_5 - k_6$, $k_2 = 4 \times 10^{-13}$, $k_3 = 1$, $k_4 = 10^{-13}$, $k_5 = 0.1$, $k_6 = 0.1$, $k_7 = 0.1$ and $k_8 = 0.00001$.[1] We make the usual assumption $(k_1 + k_5 + k_6)\beta = 1$ (Tomasetti and Levy, 2010), where $\beta \equiv 1$ is a general parameter with dimension time$^{(-1)}$ required for dimensional consistency in the following analysis. The values for $k_5$ and $k_6$ are consistent with those estimated in Tomasetti and Levy (2010). For these parameter values, $\Omega_C \equiv k_1/k_2 = 2 \times 10^{12}$ and $\Omega_P \equiv k_3/k_4 = 1 \times 10^{13}$ (see Appendix A). These are rescaling parameters for $x$ and $y$ variables, respectively. Stationary values for $P(t)$ and $C(t)$ are $P_\infty = 9.6 \times 10^{12}$ cells and $C_\infty = 1.8 \times 10^{12}$ cells, respectively. By adjusting the $k_2$ and $k_4$ parameters we can easily obtain more suitable values for the CSC and progenitor cell equilibrium populations, according to possible new experimental results.

By using standard adiabatic elimination methods, one can write Eq. (6) as

$$\begin{cases} x' = A'\left[x(1-x) - \dfrac{x}{A'} + \dfrac{B'}{A'}y\right] \\ \epsilon y' = y(1-y) + \epsilon F'x - \epsilon G'y \end{cases} \tag{8}$$

[1] These values correspond to $A' = 8$, $B' = 5 \times 10^{-4}$, $E' = 10$, $F' = 0.6$ and $G' = 1$.

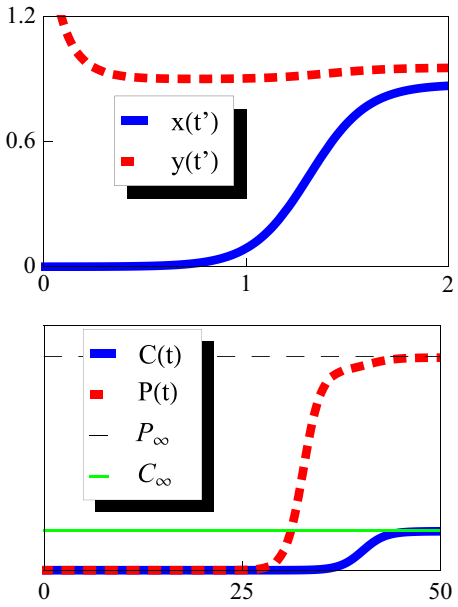


**Fig. 2.** Top: numerical solution for rescaled Eq. (6). $x(t)$ and $y(t)$ represent the rescaled population of cancer stem cells and progenitor cells, respectively. Bottom: numerical solution for Eq. (2). $C(t)$ and $P(t)$ represent the population of cancer stem cells and progenitor cells, respectively. $P_\infty$ and $C_\infty$ represent the limits of $C(t)$ and $P(t)$ when $t\to\infty$, respectively. Parameters values: $k_1=1-k_5-k_6$, $k_2=4\times10^{-13}$, $k_3=1$, $k_4=10^{-13}$, $k_5=0.1$, $k_6=0.1$, $k_7=0.1$ and $k_8=0.00001$. $P_\infty=9.6\times10^{12}$ and $C_\infty=1.8\times10^{12}$. $C_\infty/P_\infty=0.1875$.

where $\epsilon\equiv1/E'$. If we consider $\epsilon\ll1$ (this is equivalent to considering the progenitor cell division rate sufficiently large) we can perform adiabatic approximation (Berglund and Gentz, 2006; Gardiner, 2009) in (8) and, setting $y'=0$, we obtain the following equation[2] for $x$:

$$x'=\chi-\mu x+\alpha x(1-x) \tag{9}$$

where $\chi\equiv B'(1-\epsilon G')=k_8k_2(k_3-k_{10})/k_1k_4k_6$, $\mu\equiv1-\epsilon B'F'=1-k_8k_9/k_3k_6$ and $\alpha\equiv A'=k_1/k_6$. Note that $\chi$ can be positive or negative depending on the magnitudes of $k_3$ and $k_{10}$.

If we consider $\epsilon$ to be small enough with respect to $G'$, $B'$ and $F'$, we further simplify and write $\chi=B'$ and $\mu=1$. We can observe that the plasticity phenomenon (associated with $k_8$) is crucial for the existence of the constant term $\chi$. For this reason, from now on we will consider the parameter $\chi$ as representing the plasticity phenomenon in the reduced equation (9).

### 3.3. The deterministic equation

We will briefly review the deterministic analysis of the problem. An analytic solution of Eq. (9) is possible. For the initial condition $x(0)=N_0$, we get

$$x(t)=\frac{1}{2\alpha}\left\{\delta-\sqrt{\kappa}\,\tan\left[\frac{1}{2}t\sqrt{\kappa}+\arctan\left(\frac{-2N_0\alpha+\delta}{\sqrt{\kappa}}\right)\right]\right\} \tag{10}$$

with $\delta\equiv\alpha-\mu$ and $\kappa\equiv-\delta^2-4\alpha\chi$. The physically relevant stable fixed point is

$$x^*=\frac{\alpha-\mu+\sqrt{\alpha^2-2\alpha\mu+\mu^2+4\alpha\chi}}{2\alpha}. \tag{11}$$

The $x$ scaled population size dynamics can be thought of as analogous to the particle moving dynamics in an effective potential $V_0(x)$, seeking its minimum point, with $V_0(x)\equiv-\int\zeta(x)\,dx$ with $\zeta(x)=\chi+\delta x-\alpha x^2$ from (9). Thus, $V_0$ is given by the cubic polynomial,

$$V_0(x)=\frac{x^3\alpha}{3}-\frac{\delta x^2}{2}-x\chi.$$

We see from (11) that by increasing either $\chi$ or $\delta$, the minimum $x^*$ of $V_0$ moves to the right in the potential, thus favoring the tumor stem cell population. Such behavior is, of course, expected, since an increase of $\chi$ means an increase of the frequency in which the induced plasticity mechanism occurs, and an increase of $\delta$ is an increase of the symmetric stem cell renewal rate, both of which increase the population.

## 4. Possible consequences of a spatial structure

Traditionally, anti-tumor treatments have targeted the cells directly, removing them with surgery or killing them with radiation. Since these are local treatment methods, they often are not effective in meeting their objectives. The tumors may recur because not all cells were killed or because some cells escaped the primary tumor region where the treatments worked. Since cells compete and/or cooperate with nontumor cells and between themselves, these interactions may be better conceptualized as an evolving ecosystem (Pienta et al., 2008; Kareva, 2011).

One of the possible consequences of this way of seeing the disease is that the destruction of the tumor microenvironment can be much more effective than just extracting or killing the cells that live in it. A prime example of this situation comes from paleontology: studies analyzing the conditions that preceded mass extinctions suggest that they occurred more frequently and were more destructive when pulses of disturbances that cause extensive mortality were accompanied by perturbative pressures such as climate change. This sequence weakened and destabilized populations for several generations (Arens and West, 2008).

Motivated by these considerations, it seems promising to consider mathematical techniques originating in mathematical ecology, a well-developed branch of applied mathematics (Cantrell and Cosner, 2003; Petrovskii and Li, 2005). We are now interested in the possible effects from the incorporation of diffusion in the model. For this, let $u(x,t)$ be a population of CSCs at position $x$ at time $t$ that lives in a one-dimensional domain of length $L$. By adding a diffusion term in Eq. (9), we get

$$\frac{\partial u}{\partial t'}=D\frac{\partial^2u}{\partial t'^2}+\chi-\mu u+\alpha u(1-u)\equiv D\frac{\partial^2u}{\partial t'^2}+f(u) \tag{12}$$

where $D$ is the cell diffusion coefficient and $f(u)=\chi-\mu u+\alpha u(1-u)$. This is the deterministic partial differential equation that we will consider first. Later we will consider a stochastic version. This is a reaction diffusion equation that is typical in the population dynamics of species that interact and disperse.

Eq. (12) with $\chi=0$ is the famous Fisher (1937) equation. In this equation we analyze the effect of plasticity represented by the parameter $\chi$ on the patch size to sustain a population, similar to what is sometimes called the Kierstead–Slobodkin–Skellam (KISS) size (Skellam, 1951; Kierstead and Slobodkin, 1953). The main motivation for performing this type of analysis is related to the experimental results obtained in Quintana et al. (2008), where xenografts in immunosuppressed mice sustained surprisingly high populations of cancer stem cells. The idea here, therefore, is to identify some phenomenon related to the size of the CSC niche that may justify this result. The question is: What is the effect of transplanting a cancer stem cell population to an environment where, in theory, they will have more space to live and proliferate?

To formulate the problem mathematically, we can imagine that there is a finite domain available for the cells to develop (their niche). Beyond a certain boundary (i.e. outside the niche), there

[2] Expanding in Taylor series up to first order in $\epsilon$.

are restrictions (e.g., absence of signaling to support the cancer stem cell phenotype, normoxic conditions incompatible with the state of CSCs, adverse pH conditions, etc.) which make the survival of cancer stem cells unsustainable. Outside the niche, these cells have a tendency to differentiate into progenitor cells. Thinking of the niche as a linear domain of length $L$, our problem can be mathematically formulated as a boundary value problem with Dirichlet conditions given by (12) and

$$u(0,t')=u(L,t')=0.$$

Following Méndez et al. (2008), the population density at the steady state is given by $u(x,\infty)\approx u_m \sin(\pi x/L)$, where $u_m$ is the maximum population density at steady state for a given patch size $L$. In Méndez et al. (2008), for a function $f(u)$ in the form $f(u)=a_1u+a_2u^2+a_3u^3$, an approximation to $u_m$ is found as the real solution to the equation $\Phi(u_m,L)=0$ with

$$\Phi(u_m,L)\equiv u_m\left[\frac{3a_3}{4}u_m^2+\frac{8a_2}{3\pi}u_m+a_1-D\left(\frac{\pi}{L}\right)^2\right]. \tag{13}$$

Allowing the possibility of plasticity (represented by $\chi$), we insert a term $a_0$ in the $f(u)$ function so that $f(u)=a_0+a_1u+a_2u^2+a_3u^3$. By performing the calculations as in Méndez et al. (2008), we obtain the new function

$$\Phi_\chi(u_m,L)=\frac{4a_0}{\pi}+u_m\left[\frac{3a_3}{4}u_m^2+\frac{8a_2}{3\pi}u_m+a_1-D\left(\frac{\pi}{L}\right)^2\right]. \tag{14}$$

By solving equation $\Phi_\chi(u_m,L)=0$, we get three solutions that, when placed on the same figure, make up what we call a bifurcation diagram (if $\chi=0$).[3] For $a_0=\chi$, $a_1=\alpha-\mu$, $a_2=-\alpha$ and $a_3=0$, we consider the case of Eq. (12).

Fig. 3 shows the bifurcation diagram for $\chi=0$ (blue curve) and the curves $u_m(L)$ for $\chi=0.1$ (dotted red curve) and $\chi=0.01$ (black dashed curve). We find that the inclusion of plasticity allows small cancer stem cell populations to survive even in very small niches. Above a certain approximate critical minimum value for patch size (KISS size $L_c=\pi\sqrt{D/a_1}$), the population undergoes an abrupt increase in its size. If a small cell niche is abruptly increased to a value significantly greater than $L_c$, the CSC population will be absurdly high. This may have been the case for the xenograft cancer stem cells in immunosuppressed mice reported in Quintana et al. (2008). This may also be an answer to the question raised above.

### 4.1. Effect of noise on the bifurcation diagram

#### 4.1.1. Noise in the cancer stem cell niche

Cells growing in a tissue are not alone: they are constantly communicating with one another by sending signals through tissue that are picked up and transmitted by other cells in the medium. When thousands of cells are together, there are hundreds of thousands of these signals present every minute, all competing to be heard. All this complexity induces stochastic fluctuations in population dynamics that will hereafter be called noise.

A growing body of evidence indicates that noise is generally not detrimental to biological systems, but can be employed to generate behavioral diversity (Samoilov et al., 2005; Fange and Elf, 2006). Mechanisms involving noise are important in the development of organisms (Arias and Hayward, 2006; El-Samad and Khammash, 2006), a fact supported by experiments showing that noise is down-regulated in embryonic stem cells (Zwaka, 2006) and that fluctuations of the Nanog transcription factor predispose these cells towards differentiation (Chambers et al., 2007; Kalmar et al., 2009). In Hoffmann et al. (2008) it was suggested that the regulation of noise can be an effective strategy in stem cell differentiation. The results of the present paper suggest that high levels of noise can stimulate the development of cancer stem cells.

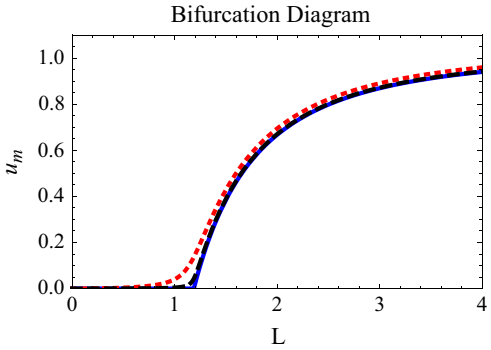


**Fig. 3.** Bifurcation diagram obtained from $\Phi_\chi(u_m,L)=0$ with $\Phi_\chi(u_m,L)$ given by Eq. (14) with $\chi=0.0$ (blue, thick line), $\chi=0.1$ (red, dotted line), $\chi=0.01$ (black, dashed line), $\mu=1$, $\alpha=8$. (For interpretation of the references to color in this figure caption, the reader is referred to the web version of this paper.)

#### 4.1.2. Modeling noise in a spatial environment

We will now reformulate the population dynamics in terms of a stochastic reaction–diffusion equation and reduce it to a deterministic equation that incorporates the systematic noise contributions (Santos and Sancho, 2001). Let us first formulate the problem in a general way and then use our model as an example.

Consider the following stochastic partial differential equation (SPDE) in the Stratonovich interpretation, with both additive and multiplicative noises:

$$\frac{\partial\phi}{\partial t}=D\nabla^2\phi+f(\phi)+\epsilon^{1/2}g(\phi)\eta(x,t)+\xi(x,t). \tag{15}$$

In the above equation, $\epsilon$ is an explicit measure of the noise strength given by $\eta(x,t)$, $\phi(x,t)$ is a field (scalar or vector) that describes the state of the system (the number of CSCs in our context) at a spatial location $x$ at time $t$, and $D$ is the diffusion coefficient. The additive noise $\xi(x,t)$ is Gaussian and white in both space and time, with zero mean and correlations given by

$$\langle\xi(x,t)\xi(x',t')\rangle=2\gamma^2\delta(x-x')\delta(t-t').$$

The multiplicative noise $\eta(x,t)$ is Gaussian, with zero mean and correlation

$$\langle\eta(x,t)\eta(x',t')\rangle=2c(|x-x'|)\delta(t-t')$$

with $c(|x-x'|)$ as the spatial correlation function. A crucial feature of (15) is that while $\eta(x,t)$ has zero mean, our new noise term $g(\phi)\eta(x,t)$ does not. If $g(\phi)$ is constant, Eq. (15) has only additive noise. In our case however, noise is coupled to the system through function $g$.

#### 4.1.3. Effective deterministic model

As mentioned above, the new noise term has nonzero mean. We define it as follows:

$$\epsilon^{1/2}\langle g(\phi)\eta(x,t)\rangle\equiv\Psi(\phi). \tag{16}$$

Adding and subtracting $\Psi(\phi)$ in (15) lead to an equivalent equation, but with zero mean noise term $R$

$$\frac{\partial\phi}{\partial t}=D\nabla^2\phi+f(\phi)+\Psi(\phi)+R(\phi,x,t) \tag{17}$$

where

$$R(\phi,x,t)=\epsilon^{1/2}g(\phi)\eta(x,t)-\Psi(\phi)+\xi(x,t). \tag{18}$$

$R(\phi,x,t)$ is related to the nonsystematic noise effect. This effect will

[3] Naturally, the name bifurcation diagram only makes sense in the absence of plasticity. This is due to the critical nature of $L_c$, which exists only for $\chi=0$. When $\chi\neq0$, the equivalent in figures will be called $u_m(L)$ curves.

be neglected (Santos and Sancho, 2001), thus leading to an effective deterministic equation

$$\frac{\partial\phi}{\partial t} = D\nabla^2\phi + f(\phi) + \Psi(\phi) \tag{19}$$

with an effective reaction term $f(\phi)+\Psi(\phi)$. $\Psi(\phi)$ can be calculated using Novikov's (1965) theorem producing

$$\epsilon^{1/2}\langle g(\phi)\eta(x,t)\rangle = \epsilon c(0)\langle g'(\phi)g(\phi)\rangle. \tag{20}$$

The deterministic *effective* model is written as

$$\frac{\partial\phi}{\partial t} = D\nabla^2\phi + f(\phi) + \epsilon c(0)g'(\phi)g(\phi). \tag{21}$$

#### 4.1.4. Application to our model

Considering the inclusion of a Gaussian noise of intensity $\sigma$ in parameter $\alpha$,[4] (by the transformation $\alpha\to\alpha+\sigma W(t)$, $W(t)$ is a Wiener process Oksendal, 2003) we get a model corresponding to Eq. (15) with $f(\phi)=\chi+(\alpha-\mu)\phi-\alpha\phi^2$ (a polynomial of degree two) and $g(\phi)=\phi(1-\phi)$. Therefore, the effective deterministic model is given by

$$\frac{\partial\phi}{\partial t} = D\nabla^2\phi + \chi + (\alpha-\mu+\sigma)\phi-(\alpha+3\sigma)\phi^2 + 2\sigma\phi^3 \tag{22}$$

or

$$\frac{\partial\phi}{\partial t} = D\nabla^2\phi + \chi + M\phi-N\phi^2 + P\phi^3 \tag{23}$$

with $M\equiv\alpha-\mu+\sigma$, $N\equiv\alpha+3\sigma$, $P\equiv2\sigma$ and $\sigma\equiv\epsilon c(0)$. Besides the renormalization in parameters $\mu$ and $\alpha$, the degree of the polynomial function to the right of (22) is lifted from two to three. The systematic contributions of the noise in the proliferation rate give rise to a cubic term in the effective reaction function. Consequently, the validity range of Eq. (23) is restricted to sufficiently small noise strengths or small densities. This does not affect our conclusions, since we are interested in the conditions for extinctions, i.e., situations where the density is indeed small. At higher densities, the model needs to be modified to include higher-order saturation effects.

It is interesting to observe the effect of $\sigma$ on the effective potential $V_{eff}(\phi)$ associated with the model without diffusion, obtained from $V_{eff}(\phi)=-\int[f(\phi)+\Psi(\phi)]\,d\phi$.

Fig. 4 shows this effect. Curves in blue, black and red (thick, dashed and dotted, respectively) have $\sigma=0, 5$ and 10, respectively. An increase in noise decreases the equilibrium population represented by the minimum of the potential, but this decrease is accompanied by the possibility of the population falling into the hole on the right with no minimum. And the larger the noise intensity, the more likely this is to occur. Cancer stem cells enjoy noise.

*The bifurcation diagram*: We can now use Eq. (14) to construct the bifurcation diagram corresponding to (23). In this case, we put $a_0=\chi$, $a_1=M$, $a_2=N$ and $a_3=P$ with $\alpha=8$, $\mu=1$.

Fig. 5 shows the bifurcation diagrams for $\chi=0$ (top of the figure) and curves $u_m(L)$ for $\chi=0.1$ (bottom). We see clearly that the noise helps cancer stem cells to survive in very small niches. The minimal patch size $L_c=\pi\sqrt{D/(\alpha-\mu+\sigma)}$ needed to sustain cell life is reduced with noise. The price to pay is related to lower values of its stationary population.

[4] We consider the inclusion of noise in this parameter by its essential importance in the population dynamics, since this parameter is associated with its nonlinear character.

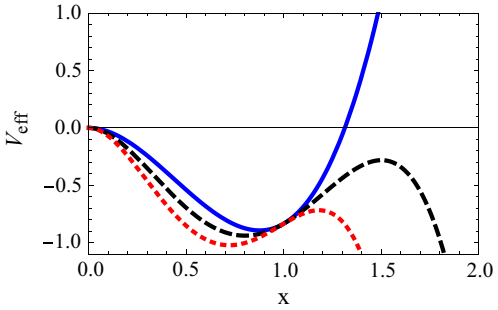


**Fig. 4.** Effect of $\sigma$ on $V_{eff}$ with $\chi=0$, $\alpha=8$, $\mu=1$. $\sigma=0$ (blue, thick line), $\sigma=5$ (black, dashed line), $\sigma=10$ (red, dotted line). An increase in the noise intensity decreases the population equilibrium but facilitates the escape of the cells to a situation where population growth is uncontrolled. (For interpretation of the references to color in this figure caption, the reader is referred to the web version of this paper.)

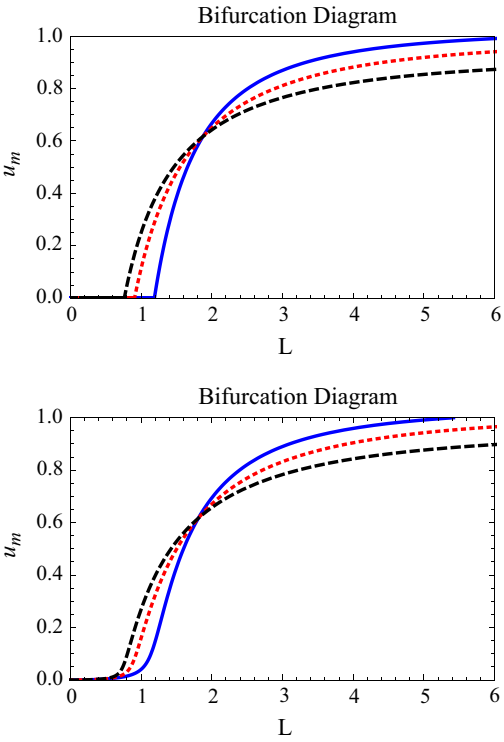


**Fig. 5.** Bifurcation diagram with $\chi=0.0$ (top) and $\chi=0.1$ (bottom), $\sigma=0.0001$ (blue, thick line), $\sigma=5$ (red, dotted line), $\sigma=10$ (black, dashed line), $\mu=1$, $\alpha=8$. Noise enables the survival of CSCs in very small niches. (For interpretation of the references to color in this figure caption, the reader is referred to the web version of this paper.)

### 4.2. The effect of diffusion in the stationary probability distribution

In this subsection we estimate the effects induced by diffusion on the stationary distribution. Let us consider the tumor as a spatially continuous medium as in the previous section, described by field variables obeying partial differential equations. We consider the reaction–diffusion equations

$$\frac{\partial\phi(\mathbf{x},t)}{\partial t} = f(\phi(\mathbf{x},t)) + D\nabla^2\phi(\mathbf{x},t) \tag{24}$$

where $\phi(\mathbf{x},t)$ is a field (scalar or vector) that describes the state of the system at a spatial location $\mathbf{x}$ at time $t$. A discretization procedure is commonly used to transform the continuous partial differential equation to be analyzed into a set of coupled ordinary differential equations, after approximating the continuous space by a lattice (García-Ojalvo and Sancho, 1999). In the case of

Eq. (24), for example, assuming a regular Cartesian lattice, the discretization leads to

$$\frac{d\phi(t)}{dt} = f(\{\phi_i\}) + \frac{D}{\Delta x^2}\sum_{j\in n(i)}(\phi_j - \phi_i) \tag{25}$$

where the sum term, which runs over the set of nearest neighbors of $i$, represents a possible choice for the discrete version of the Laplace operator and $\Delta x$ denotes the lattice spacing. The relation between the discretized field and the real one is $\phi_i(t) = \phi(i\Delta, t)$, where $i = (i_1, i_2, \ldots, i_d)$ and $d$ is the space dimension.

A lattice will be used so that the state of the system is described by a set of scalar variables $\{x_i\}$, $i = 1, \ldots, L^d$ defined on a $d$-dimensional cubic lattice with lattice points $i$. Suppose that the dynamics of the variables $x_i$ can be described by the following stochastic differential equation in the Stratonovich sense:

$$\dot{x}_i = f(x_i) + g(x_i)\xi_i - \frac{D}{2d}\sum_{j\in n(i)}(x_i - x_j). \tag{26}$$

$n(i)$ is the set of the nearest $2d$ neighbors of site $i$, and $\{\xi_i(t)\}$ are Gaussian white noises in time and space with zero mean and an autocorrelation function given by

$$\langle \xi_i(t)\xi_j(t')\rangle = \sigma^2\delta_{ij}\delta(t-t')$$

and $D$ is the diffusion coefficient. The functions $f(x_i)$ and $g(x_i)$ are $f(x_i) = \chi - \mu x_i + \alpha x_i(1-x_i)$ and $g(x_i) = x_i(1-x_i)$. Following Van den Broeck et al. (1994), and using a mean-field approximation, the stationary probability distribution at site $i$ is given by

$$P_{st}(x) = \frac{1}{Z}\exp\left[\frac{2}{\sigma^2}\int_0^x dy\,\frac{f(y) - \frac{\sigma^2}{2}g(y)g'(y) - D(y - \mathbb{E}(y))}{g(y)^2}\right] \tag{27}$$

where $Z$ is a normalization constant and

$$\mathbb{E}(y) = \langle v_i | v_j\rangle = \int y_i P_{st}(y_j|y_i)\,dy_j \tag{28}$$

represents the steady state conditional average of $y_j$ at neighboring sites $j \in n(i)$, given the value $y_i$ at site $i$. Using the Weiss mean-field approximation, neglecting the fluctuation in the neighboring sites, i.e., $\mathbb{E}(y) = \langle x\rangle$, independent of $y$, and imposing the self-consistent requirement, we obtain

$$\langle x\rangle = \int_{-\infty}^{\infty} dx\, x P_{st}(x) = F(\langle x\rangle). \tag{29}$$

We are interested in the effect of the diffusion coefficient $D$ in the stationary probability distribution of the site $i$. The maxima of $P_{st}(x)$ are obtained from $f(y) - (\sigma^2/2)g(y)g'(y) - D(y - \mathbb{E}(y)) = 0$, or

$$x^3 + \frac{x^2(2\alpha - 3\sigma^2)}{2\sigma^2} + \frac{x(2D - 2\alpha + 2\mu + \sigma^2)}{2\sigma^2} - \frac{Dm + \chi}{\sigma^2} = 0 \tag{30}$$

where we put $\mathbb{E}(y) \equiv m$. We see that $D > 0$ raises the coefficient of the linear term in $x$ and the constant term. For the cubic equation $x^3 + Bx^2 + Cx + F = 0$, the condition for having three real roots is given by (Kavinoky and Thoo, 2008)

$$\Delta \equiv \frac{q^2}{4} + \frac{p^3}{27} < 0 \tag{31}$$

with $p = C - B^2/3$ and $q = 2B^3/27 - BC/3 + F$. For $3\sigma^2 > 2\alpha$ $(B < 0)$ and $0 < m < 1$, an increase of $C$ and $F$ increases the value of $\Delta$ so that condition (31) is more difficult to achieve. In Fig. 6 (lower row) we see that an increase in the diffusion constant $D$ has the effect of hampering the transition from a unimodal to a bimodal distribution. There is competition between $\sigma$ and $D$. Fig. 6 (top left) shows the effect of increased $\sigma$ for $D = 0.1$ and Fig. 6 (top right) shows the effect of $\chi$ for $\sigma = 1.5$ and $D = 1$.

We see in Fig. 6 (top left) that for sufficiently large values of $\sigma$ bistability can occur. This bistable state can lead to the coexistence of two separate phases in space. In Zhong et al. (2008) the authors show that this type of bistability can be associated with noninfiltrative growth of a benign tumor, a case that corresponds to small noise, as well as an infiltrative type of malignant growth corresponding to intense noise. While increases in $\sigma$ stimulate bistability, increases in $D$ discourage it, as shown in Fig. 6 (bottom row).

## 5. Conclusion

We proposed a model to describe population dynamics of CSCs. Our analysis allows us to address a controversy related to the frequency of such cells in tumors. Initially, it was thought that these cells were relatively rare, comprising at most ~1% of the

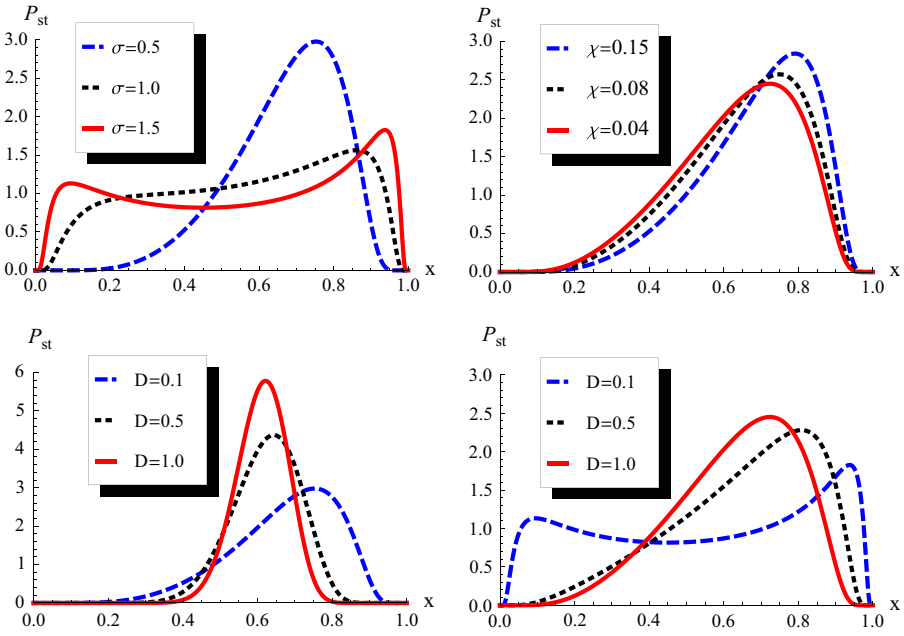


**Fig. 6.** Top left: effect of noise strength on $P_{st}$ for parameters $\alpha = 0.04$, $\mu = 0.06$, $D = 0.1$ and $\chi = 0.04$. Top right: effect of $\chi$ on $P_{st}$ for parameters $\alpha = 0.04$, $\mu = 0.06$, $D = 1$ and $\sigma = 1.5$. Bottom left: effect of $D$ on $P_{st}$ for parameters $\alpha = 0.04$, $\mu = 0.06$, $\chi = 0.04$ and $\sigma = 0.5$. Bottom right: effect of $D$ on $P_{st}$ for parameters $\alpha = 0.04$, $\mu = 0.06$, $\chi = 0.04$ and $\sigma = 1.5$.

cancer cell population. More recent experiments, however, suggest that the CSC population need not be small.

When considering the spread possibility of CSCs, we estimate the conditions to support themselves in a niche with hostile boundary conditions. Without plasticity, there is a threshold of the niche size below which the population cannot be sustained. With plasticity, this threshold is lost and cells can survive in niche, even in small populations. The inclusion of noise in case of no plasticity decreases the minimum required niche size, conspiring again in favor of CSCs.

We briefly considered a simplified model with spatial distribution in a lattice. The possibility of a bimodal stationary probability distribution was observed. Using mean-field theory, we demonstrated that diffusion ($D$) competes with noise ($\sigma$) in the construction of this bimodality. We showed that the discrepancy observed in the frequency of these cells is entirely consistent with the original hypothesis of the existence of cancer stem cells, as long as favorable conditions related to the complexity of the microenvironment are met.

## Appendix A. Rescale transforms

In this appendix we detail the rescales made throughout the main text. The first refers to Eq. (6) and the second refers to Eq. (3). The general model written in terms of the reactions is

$$
\begin{aligned}
&C \underset{k'_2/\Omega_2}{\overset{k_1}{\rightleftharpoons}} C+C\\
&P \underset{k'_4/\Omega_4}{\overset{k_3}{\rightleftharpoons}} P+P\\
&C \xrightarrow{k_5} C+P\\
&C \xrightarrow{k_6} P+P\\
&P \xrightarrow{k_7} \varnothing\\
&P \xrightarrow{k_8} C
\end{aligned}
\tag{A.1}
$$

Using the law of mass action we have

$$
\begin{cases}
\dot{C} = k_1 C\left(1-\dfrac{C}{\Omega_C}\right) - k_6 C + k_8 P\\
\dot{P} = k_3 P\left(1-\dfrac{P}{\Omega_P}\right) + k_9 C - k_{10} P
\end{cases}
\tag{A.2}
$$

with $k_9 \equiv k_5 + 2k_6$, $k_{10} \equiv k_7 + k_8$, $\Omega_C \equiv k_1/k_2$, $\Omega_P \equiv k_3/k_4$ and $k_2 \equiv k'_2/\Omega_2$, $k_4 \equiv k'_4/\Omega_4$. Using the rescale $C \equiv \Omega_C x$ and $P \equiv \Omega_P y$

$$
\begin{cases}
\dot{x} = k_1 x(1-x) - k_6 x + \dfrac{k_8 \Omega_P}{\Omega_C} y\\
\dot{y} = k_3 y(1-y) + \dfrac{k_9 \Omega_C}{\Omega_P} x - k_{10} y
\end{cases}
\tag{A.3}
$$

Using $t \equiv k_6 t'$ and $\Omega \equiv \Omega_P/\Omega_C$

$$
\begin{cases}
\dfrac{dx}{dt'} = \dfrac{k_1}{k_6} x(1-x) - x + \dfrac{k_8 \Omega}{k_6} y\\
\dfrac{dy}{dt'} = \dfrac{k_3}{k_6} y(1-y) + \dfrac{k_9}{k_6 \Omega} x - \dfrac{k_{10}}{k_6} y
\end{cases}
\tag{A.4}
$$

or

$$
\begin{cases}
x' = Ax(1-x) - x + By\\
y' = Ey(1-y) + Fx - Gy
\end{cases}
\tag{A.5}
$$

with $x' \equiv dx/dt'$, $y' \equiv dy/dt'$ and

$$
\begin{cases}
A \equiv \dfrac{k_1}{k_6}\\
B \equiv \dfrac{k_2 k_3 k_8}{k_1 k_4 k_6}\\
E \equiv \dfrac{k_3}{k_6}\\
F \equiv \dfrac{k_1 k_4 k_9}{k_2 k_3 k_6}\\
G \equiv \dfrac{k_{10}}{k_6}
\end{cases}
\tag{A.6}
$$

### A.1. Gradient system

Starting from (A.2) and carrying out the transformation $S = s_1 c$, $P = s_2 p$ and $t = s_3 \tau$, we can write

$$
\begin{cases}
\dfrac{dc}{d\tau} = k_1 s_3 c\left(1-\dfrac{s_1}{\Omega_C} c\right) - k_6 s_3 c + \dfrac{k_2 s_2 s_3}{s_1} p\\
\dfrac{dp}{d\tau} = k_3 s_3 p\left(1-\dfrac{s_2}{\Omega_P} p\right) + \dfrac{k_9 s_1 s_3}{s_2} c - k_{10} s_3 p
\end{cases}
\tag{A.7}
$$

Imposing $k_2 s_2 s_3/s_1 = k_9 s_1 s_3/s_2$, $k_6 s_3 = 1$ and $s_1 = \Omega_C$, we obtain $s_1 \equiv k_1/k_2$, $s_2 \equiv \Omega_C \sqrt{k_9/k_2}$ and $s_3 = 1/k_6$.

In this way we obtain

$$
\begin{cases}
\dfrac{dc}{d\tau} = \dfrac{k_1}{k_6} c(1-c) - c + \dfrac{\sqrt{k_2 k_9}}{k_6} p\\
\dfrac{dp}{d\tau} = \dfrac{k_3}{k_6} p\left(1-\dfrac{\Omega_C}{\Omega_P}\sqrt{\dfrac{k_9}{k_2}} p\right) + \dfrac{\sqrt{k_2 k_9}}{k_6} c - \dfrac{k_{10}}{k_6} p
\end{cases}
\tag{A.8}
$$

## References


Arens, N., West, I., 2008. Paleobiology 34, 456–471.
Arias, A.M., Hayward, P., 2006. Nat. Rev. Genet. 7, 34–44.
Armitage, P., Doll, R., 1954. Br. J. Cancer 8, 1–12.
Baker, M., 2008a. Nature 456, 553.
Baker, M., 2008b. Nature Reports Stem Cells.
Berglund, N., Gentz, B., 2006. Noise-Induced Phenomena in Slow–Fast Dynamical Systems: A Sample-Paths Approach, Probability and its Applications. Springer.
Boiko, A., Razorenova, O., van de Rijn, M., Swetter, S., Johnson, D., Ly, D., Butler, P., Yang, G., Joshua, B., Kaplan, M., et al., 2010. Nature 466, 133–137.
Bomken, S., Fišer, K., Heidenreich, O., Vormoor, J., 2010. Br. J. Cancer 103, 439–445.
Byrne, H.M., Alarcon, T., Owen, M.R., Webb, S.D., Maini, P.K., 2006. Philos. Trans. Ser A: Math. Phys. Eng. Sci. 364, 1563–1578.
Cantrell, R., Cosner, C., 2003. Spatial Ecology via Reaction–Diffusion Equations, Wiley Series in Mathematical and Computational Biology. John Wiley & Sons.
Chambers, I., Silva, J., Colby, D., Nichols, J., Nijmeijer, B., Robertson, M., Vrana, J., Jones, K., Grotewold, L., Smith, A., 2007. Nature 450, 1230–1234.
Chen, Y.Q., Jewell, N.P., Lei, X., Cheng, S.C., 2005. Biometrics 61, 170–178.
Clarke, M.F., Fuller, M., 2006. Cell 124, 1111–1115.
Dalerba, P., Cho, R.W., Clarke, M.F., 2007. Annu. Rev. Med. 58, 267–284.
Denison, T.A., Bae, Y.H., 2012. J. Control. Release, http://dx.doi.org/10.1016/j.jconrel.2012.04.014, in press.
El-Samad, H., Khammash, M., 2006. Biophys. J. 90, 3749.
Fange, D., Elf, J., 2006. PLoS Comput. Biol. 2, e80.
Fisher, R., 1937. Ann. Hum. Genet. 7, 355–369.
García-Ojalvo, J., Sancho, J., 1999. Noise in Spatially Extended Systems: With 120 Illustrations, Institute for Nonlinear Science Series. Springer-Verlag.
Gardiner, C., 2009. Stochastic Methods: A Handbook for the Natural and Social Sciences, Springer Series in Synergetics. Springer.
Grunewald, T., Herbst, S., Heinze, J., Burdach, S., 2011. J. Transl. Med. 9, 79.
Gupta, P., Chaffer, C., Weinberg, R., 2009. Nat. Med. 15, 1010–1012.
Hirsch, M., Smale, S., Devaney, R., 2004. Differential Equations, Dynamical Systems, and an Introduction to Chaos, Pure and Applied Mathematics. Academic Press.
Hoffmann, M., Chang, H.H., Huang, S., Ingber, D.E., Loeffler, M., Galle, J., 2008. PLoS One 3, e2922.
Horov, I., Pospsil, Z., Zelinka, J., 2009. J. Theor. Biol. 258, 437–443.
Ishizawa, K., Rasheed, Z., Karisch, R., Wang, Q., Kowalski, J., Susky, E., Pereira, K., Karamboulas, C., Moghal, N., Rajeshkumar, N., et al., 2010. Cell Stem Cell 7, 279–282.
Iwasaki, H., Suda, T., 2009. Cancer Sci. 100, 1166–1172.

Johnston, M., Maini, P., Jonathan Chapman, S., Edwards, C., Bodmer, W., 2010. J. Theor. Biol. 266, 708–711.
Kalmar, T., Lim, C., Hayward, P., Muñoz-Descalzo, S., Nichols, J., Garcia-Ojalvo, J., Arias, A.M., 2009. PLoS Biol. 7, e1000149.
Kareva, I., 2011. Transl. Oncol. 4, 266.
Karlin, S., Taylor, H., 2000. A Second Course in Stochastic Processes. Academic Press.
Kavinoky, R., Thoo, J., 2008. AMATYC Rev. 29, 3–8.
Kelly, P., Dakic, A., Adams, J., Nutt, S., Strasser, A., 2007. Science 317, 337.
Kierstead, H., Slobodkin, L.B., 1953. J. Mar. Res. 12, 141.
Lander, A., Kimble, J., Clevers, H., Fuchs, E., Montarras, D., Buckingham, M., Calof, A., Trumpp, A., Oskarsson, T., 2012. BMC Biol. 10, 19.
Leder, K., Holland, E., Michor, F., 2010. PloS One 5, e14366.
Marusyk, A., Polyak, K., 2010. Biochim. Biophys. Acta (BBA): Rev. Cancer 1805, 105–117.
Marusyk, A., Almendro, V., Polyak, K., 2012. Nat. Rev. Cancer, http://dx.doi.org/10.1038/nrc3261, in press.
McElwain, S., Araujo, R., 2004. Bull. Math. Biol. 66, 1039–1091. (for more information, please refer to the journal's website (see hypertext link) or contact the author).
Méndez, V., Campos, D., et al., 2008. Phys. Rev. Ser. E 77, 22901.
Morrison, S., Kimble, J., 2006. Nature 441, 1068–1074.
Nordling, C.O., 1953. Br. J. Cancer 7, 68–72.
Novikov, E., 1965. Sov. Phys.—JETP 20, 1290–1294.
Oksendal, B., 2003. Stochastic Differential Equations: An Introduction with Applications, Universitext (1979). Springer.
Perko, L., 2000. Differential Equations and Dynamical Systems, Texts in Applied Mathematics. Springer.
Petrovskii, S., Li, B., 2005. Exactly Solvable Models of Biological Invasion, Mathematical Biology and Medicine. Taylor & Francis.
Pienta, K., McGregor, N., Axelrod, R., Axelrod, D., 2008. Transl. Oncol. 1, 158.
Quintana, E., Shackleton, M., Sabel, M., Fullen, D., Johnson, T., Morrison, S., 2008. Nature 456, 593–598.
Rapp, U., Ceteci, F., Schreck, R., et al., 2008. Cell Cycle—Landes Biosci. 7, 45.
Reya, T., Morrison, S.J., Clarke, M.F., Weissman, I.L., 2001. Nature 414, 105–111.
Samoilov, M., Plyasunov, S., Arkin, A.P., 2005. Proc. Nat. Acad. Sci. USA 102, 2310–2315.
Santos, M., Sancho, J., 2001. Phys. Rev. E 64, 016129.
Sarry, J., Murphy, K., Perry, R., Sanchez, P., Secreto, A., Keefer, C., Swider, C., Strzelecki, A., Cavelier, C., Récher, C., et al., 2011. J. Clin. Invest. 121, 384.
Schatton, T., Murphy, G., Frank, N., Yamaura, K., Waaga-Gasser, A., Gasser, M., Zhan, Q., Jordan, S., Duncan, L., Weishaupt, C., et al., 2008. Nature 451, 345–349.
Schuss, Z., 2010. Theory and Applications of Stochastic Processes: An Analytical Approach, Applied Mathematical Sciences. Springer.
Shackleton, M., Quintana, E., Fearon, E., Morrison, S., 2009. Cell 138, 822–829.
Skellam, J., 1951. Biometrika 38, 196–218.
Stewart, J., Shaw, P., Gedye, C., Bernardini, M., Neel, B., Ailles, L., 2011. Proc. Natl. Acad. Sci. 108, 6468.
Tian, T., Olson, S., Whitacre, J., Harding, A., 2011. Integr. Biol. 3, 17–30.
Tomasetti, C., Levy, D., 2010. Proc. Natl. Acad. Sci. 107, 16766–16771.
Turner, C., Stinchcombe, A.R., Kohandel, M., Singh, S., Sivaloganathan, S., 2009. Cell Prolif. 42, 529–540.
Van den Broeck, C., Parrondo, J., Toral, R., 1994. Phys. Rev. Lett. 73, 3395–3398.
Vargaftig, J., Taussig, D., Griessinger, E., Anjos-Afonso, F., Lister, T., Cavenagh, J., Oakervee, H., Gribben, J., Bonnet, D., 2011. Leukemia, http://dx.doi.org/10.1038/leu.2011.250, in press.
Vermeulen, L., Sprick, M.R., Kemper, K., Stassi, G., Medema, J.P., 2008. Cell Death Differ. aop, http://dx.doi.org/10.1038/cdd.2008.20, in press.
Welte, H.R.L., Yvonne, Adjaye, James, Regenbrecht, C., 2010. Cell Commun. Signal. 8, 6.
Williams, R., Den Besten, W., Sherr, C., 2007. Genes Dev. 21, 2283.
Zapperi, S., La Porta, C.A.M., 2012. Scientific Reports 2.
Zhong, W., Shao, Y., Li, L., Wang, F., He, Z., 2008. Europhys. Lett. 82, 20003.
Zhong, Y., Guan, K., Zhou, C., Ma, W., Wang, D., Zhang, Y., Zhang, S., 2010. Cancer Lett. 292, 17–23.
Zwaka, T.P., 2006. Cell 127, 1301–1302.

Capítulo 7

# Discreteza induzindo coexistência

*Esta introdução é baseada nos resultados do artigo [6], publicado em* ***Physica A****.*

Um princípio fundamental da ecologia teórica é o "princípio da exclusão competitiva" (PEC) [59]. De acordo com este princípio, duas espécies semelhantes que competem por um recurso limitado não podem coexistir. Uma das espécies será necessariamente levada à extinção. Este princípio é apoiado por muitos modelos matemáticos, o mais famoso dos quais é o modelo de equações diferenciais de Lotka e Volterra para duas espécies concorrentes. No entanto, o princípio da exclusão competitiva não parece ocorrer na natureza, onde a alta biodiversidade é comumente observada. Esta contradição é conhecida como o *paradoxo da biodiversidade*. Por causa dos longos debates envolvidos, este paradoxo é um problema central da ecologia teórica. Várias explicações diferentes do paradoxo da biodiversidade foram apresentados, no entanto, os debates a respeito continuam.

Neste artigo [6] apresento um modelo onde a coexistência de duas espécies competitivas é induzida pela discreteza das interações. Este resultado se contrapõe ao princípio da exclusão competitiva. Mapeamos o conjunto de interações entre as espécies formulado em termos de reações, que é a descrição elementar do modelo, em um sistema de equações diferenciais parciais estocásticas que foram resolvidas numericamente. Estas equações incorporam a estocasticidade intrínseca (ruído demográfico) da dinâmica em uma aproximação contínua obtida da representação de Poisson [60]. A influência de um ruído *ambiental*, entendindo como sendo associado às variações do ambiente, também é investigada e seus efeitos são comparados aos efeitos do ruído *demográfico*. Também foram estudados os efeitos das constantes de difusão na dinâmica populacional. As principais conclusões foram:

1. Ruído ambiental favorece as populações densas, às custas das menos densas, ratificando o PEC.
2. Ruído demográfico, por outro lado, *favorece* as populações menos densas em detrimento das mais densas, contrariando o PEC.
3. As espécies mais lentas sempre sofrem os efeitos mais deletérios das flutuações estatísticas em um meio homogêneo.

Estes resultados, em particular o segundo, nos levam inevitavelmente a associar a alta diversidade observada na natureza com a discreteza das interações oriunda da finitude das populações.

Physica A 392 (2013) 5888–5897

Contents lists available at ScienceDirect

Physica A

journal homepage: www.elsevier.com/locate/physa

# Discreteness inducing coexistence

Renato Vieira dos Santos *

*Departamento de Física, Instituto de Ciências Exatas, Universidade Federal de Minas Gerais, CP 702, CEP 30161-970, Belo Horizonte, Minas Gerais, Brazil*

## HIGHLIGHTS

- We proposed a simple model that seems to violate the competitive exclusion principle.
- Demographic noise favors less dense populations at the expanse of the denser ones.
- The discontinuous character of interactions can induce coexistence.
- The slower species suffers deleterious effects of noise in a homogeneous medium.

## ARTICLE INFO

*Article history:*
Received 15 May 2013
Received in revised form 28 June 2013
Available online 5 August 2013

*Keywords:*
Additive noise and demographic stochasticity
Diffusion
Competition model
Monte Carlo simulation

## ABSTRACT

Consider two species that diffuse through space. Consider further that they differ only in initial densities and, possibly, in diffusion constants. Otherwise they are identical. What happens if they compete with each other in the same environment? What is the influence of the discrete nature of the interactions on the final destination? And what are the influence of diffusion and additive fluctuations corresponding to random migration and immigration of individuals? This paper aims to answer these questions for a particular competition model that incorporates intra and interspecific competition between the species. Based on mean field theory, the model has a stationary state dependent on the initial density conditions. We investigate how this initial density dependence is affected by the presence of demographic multiplicative noise and additive noise in space and time. There are three main conclusions: (1) Additive noise favors denser populations at the expense of the less dense, ratifying the *competitive exclusion principle*. (2) Demographic noise, on the other hand, favors less dense populations at the expense of the denser ones, inducing equal densities at the quasi-stationary state, violating the aforementioned principle. (3) The slower species always suffers the more deleterious effects of statistical fluctuations in a homogeneous medium.



## 1. Introduction

The competitive exclusion principle is one of the most fundamental principles in population biology [1]. Two species competing for a resource cannot coexist and one of the species must disappear. This principle is supported by many mathematical models, of which the Lotka–Volterra model for two competing species is the most famous. This principle has been verified in some experiments [2]. Nevertheless, discussions about the veracity of the principle persist due to the unequivocal presence of coexisting species in many ecosystems. In this paper we propose a simple toy model to study the competition between two species from the stochastic point of view. We are particularly interested in the effects of additive and demographic multiplicative noise in population dynamics.

* Tel.: +55 513133737186.
*E-mail address:* econofisico@gmail.com.

0378-4371/$ – see front matter 
http://dx.doi.org/10.1016/j.physa.2013.07.058

The dynamics of stochastic systems with agents who interact via reaction rules or have their dynamics dictated by transition rate functions can be accurately modeled by *master equations*.[1] Such equations are widely used in various fields of science, from physics, chemistry [7–9] and applied mathematics [5], to biology [3,10], ecology and epidemiology [11,12], to the social and economic sciences [13].

Stochastic models have been developed for the analysis of two distinct types of noise, internal and external [7,8,14]. In the field of quantitative ecology, such designations are commonly referred to as demographic and environmental noises, respectively [15]. External or environmental noises are the fluctuations created in an otherwise deterministic system by the application of an external random force, whose stochastic properties are supposed to be known *a priori*. This type of noise is modeled primarily by stochastic differential equations (SDE) [16,17] or Langevin equations [18,7,8]. Internal or demographic noise is modeled by master equations and caused by the fact that the system itself consist of discrete particles and it is inherent of the very mechanism through which the process evolves. Discrete systems of interacting particles often exhibit notable internal fluctuations [19].

Demographic stochasticity is known to be important in population dynamics [20]. The inclusion of stochasticity into non-linear mathematical models affects the mean dynamics. We can cite as example the ability of demographic stochasticity to excite macroscopic-scale coherent oscillations, known as quasi-cycles [21]. An extension to the spatial case where spatiotemporal patterns are induced by demographic noise was also observed [22]. Generation [23] and exacerbation [24] of the Allee effect are also consequences of the discrete character of the interactions associated with demographic noise, which can even induce survival when mean field theory indicates extinction [19]. The importance of this intrinsic noise in the microscopic dynamics of cellular systems has also been studied intensively in recent years [25], causing the appearance of a flurry of papers in this area [26]. These facts indicate a rather large effervescence in research associated with stochastic phenomena related to the inevitable discrete character of the interactions.

In this paper we study a model that in mean field theory exhibits dependence on initial conditions in steady states for two populations of species $A$ and $B$ in competition. We start by studying the model considering that the species are well mixed. Later we consider the possibility that the species may spread in a 1-dimensional space. First, we investigate the effects of the presence of additive environmental[2] noise in the relevant ordinary and partial differential equations systems. In a second step, we will investigate the effects of demographic intrinsic noise arising from discrete interactions between agents, as described by the master equation. The study is based on numerical techniques to obtain solutions of relevant stochastic differential equations, obtained as an approximation of the stochastic process as described by the master equation. All simulations were done using the software XMDS2 [27].

This paper is organized as follows: In Section 2 we describe the model. Approximation methods for master equations via diffusion processes are briefly discussed. Section 3 shows the results for the 0-dimensional case. Results for the 1-dimensional case are shown in Section 4. Diffusion effects are discussed in Sections 5 and 6 closes the paper with further discussion and conclusions. In the Appendix we present the code for one of the XMDS2 simulations.

## 2. Model

The model proposed may be described by the following sequence of reactions:

$$\begin{cases} A \xrightarrow{\alpha} A + A & B \xrightarrow{\beta} B + B \\ A + A \xrightarrow{\alpha'} A & B + B \xrightarrow{\beta'} B \\ A + B \xrightarrow{\zeta} B & A + B \xrightarrow{\xi} A. \end{cases} \tag{1}$$

The first couple of reactions in the first row refer to the birth processes of both species. The second pair describes intraspecific competition and lastly we have interspecific competition. $\alpha$ ($\beta$), $\alpha'$ ($\beta'$) and $\zeta$ ($\xi$) are parameters associated with these reactions to species $A$ ($B$) in that order.

The values used for all parameters are set to 1. Only for this parameter value is the steady state in mean-field theory dependent on the initial values of the $A$ and $B$ populations. We wondered what the effects of including noise in this particular case are. Also, this hypothesis is not as restrictive as it sounds: if $\alpha$ and $\beta$ (with $\alpha = \beta$) are small enough for us to speak of criticality and the renormalization group methods can be used, one can show that if $\zeta = \xi$ and the dimension $d \neq 0$ of the space is smaller than the critical dimension $d_c (d < d_c = 4)$, consecutive iterations of the renormalization group flow will naturally lead to the condition $\alpha' = \beta' \equiv u^* \propto 2\epsilon/3$, with $\epsilon \equiv 4 - d$ [28]. In short, we have that the species should be very similar: they have the same low rate of reproduction ($\alpha = \beta \gtrsim 0$) and equal interspecific competition rates ($\xi = \zeta$), and live on the line, in the surface, or in space.

[1] Also known as *chemical master equations* in the field of systems biology [3,4] as well as *Kolmogorov forward equations* in the mathematical literature [5,6].

[2] As the additive noise can be interpreted as arising from random fluctuations in immigration and emigration of individuals, and interpreting these processes as external to the main system, for simplicity we use the term environmental noise to designate such fluctuations.

### 2.1. From master equation to Itô equation

To evaluate the solution of the master equation, a number of approximation techniques have been proposed in the literature, such as the diffusion approximation by a Fokker–Planck equation [8], the system-size expansion method of van Kampen [7], the path integral field theory from Martin–Siggia–Rose–Janssen–de Dominicis [29–31], the Doi–Peliti field theory [32–34] and the Poisson representation [35,8].[3] The latter is particularly simple and will be used here. This method consists of obtaining a Fokker–Planck equation starting directly from reactions that describe the model. From this Fokker–Planck equation we can infer the associated Langevin equation or stochastic differential equation. Further details in Ref. [8].

## 3. 0-dimensional case

First, let us look at the simplest possible case where species are considered well mixed, which is equivalent to studying the 0-dimensional model.[4] We are interested in the case where all parameters in the reactions (1) are equal to 1. Under these conditions, we have

$$\begin{cases} \dot{\phi} = \phi - \phi^2 - \phi\psi \\ \dot{\psi} = \psi - \psi^2 - \psi\phi, \end{cases} \tag{2}$$

where the dot denotes a time derivative. Eq. (2) can be solved analytically. By setting $\Phi \equiv \phi + \psi$ and $\Psi \equiv \phi - \psi$, they can be written as

$$\begin{cases} \dot{\Phi} = \Phi - \Phi^2 \\ \dot{\Psi} = \Psi - \Psi\Phi. \end{cases} \tag{3}$$

Solving $\Phi$ equation and then solving for $\Psi$, we get

$$\Phi(t) = \frac{e^t\,(\Phi_0 + \Psi_0)}{1 + (e^t - 1)\,\Phi_0 + (e^t - 1)\,\Psi_0} \tag{4}$$

and

$$\Psi(t) = \frac{e^t\,(\Phi_0 - \Psi_0)}{1 + (e^t - 1)\,\Phi_0 + (e^t - 1)\,\Psi_0} \tag{5}$$

where we use $\Phi(0) = \Phi_0 + \Psi_0$ and $\Psi(0) = \Phi_0 - \Psi_0$. In the original variables:

$$\phi(t) = \frac{e^t\phi_0}{1 - \phi_0 - \psi_0 + e^t\,(\phi_0 + \psi_0)} \tag{6}$$

and

$$\psi(t) = \frac{e^t\psi_0}{1 - \phi_0 - \psi_0 + e^t\,(\phi_0 + \psi_0)} \tag{7}$$

with initial conditions $\phi(0) = \phi_0$ and $\psi(0) = \psi_0$. For $t \to \infty$ we obtain the stationary states

$$\begin{cases} \lim_{t\to\infty} \phi(t) = \dfrac{\phi_0}{\phi_0 + \psi_0} \\ \lim_{t\to\infty} \psi(t) = \dfrac{\psi_0}{\phi_0 + \psi_0} \end{cases} \tag{8}$$

with $\lim_{t\to\infty}[\phi(t) + \psi(t)] = 1$. Therefore the steady states depend on the initial composition of the system with constant sum $= 1$.

### 3.1. Noise in 0-dimensional model

When Eq. (2) are subjected to the action of environmental additive noise, we get:

$$\begin{cases} \dot{\phi} = \phi - \phi^2 - \phi\psi + \sigma\eta_1 \\ \dot{\psi} = \psi - \psi^2 - \psi\phi + \sigma\eta_2, \end{cases} \tag{9}$$

where $\eta_1$ and $\eta_2$ are white noise stochastic process with statistics $\langle\eta_1(t)\rangle = \langle\eta_2(t)\rangle = 0$ and $\langle\eta_1(t)\eta_1(t')\rangle = \langle\eta_2(t)\eta_2(t')\rangle = \delta(t - t')$.

[3] It was later shown that these last two methods are equivalent [36].

[4] We can also imagine that species interact in the complete graph, in the way that "everyone interacts with everyone" on the lattice.

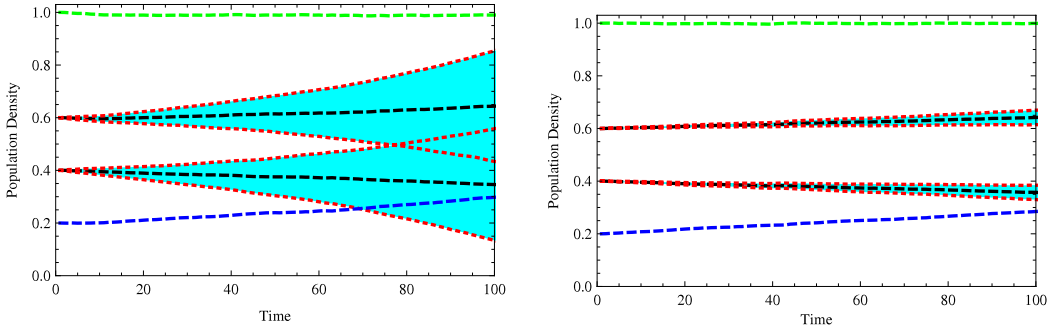


(a) Additive noise 0-dimensional model. Average of $1 \times 10^3$ Monte Carlo realizations with $\sigma = 0.1$. Black dashed lines represent the average population, shown with its red dotted lines representing 1 standard deviation from the mean.

(b) Demographic noise 0-dimensional model. Average of $1 \times 10^3$ Monte Carlo realizations with $\sigma = 0.07$. Black dashed lines represent the average population, shown with its red dotted lines representing 3 standard deviations from the mean.

**Fig. 1.** 0-dimensional SDE numerical simulations. The superior black curve represents mean $\langle\phi\rangle$ population and the inferior black curve represents $\langle\psi\rangle$ population. Superior green dashed line is the sum $\langle\phi\rangle + \langle\psi\rangle$ and inferior blue dashed line is the difference $\langle\phi\rangle - \langle\psi\rangle$. (For interpretation of the references to colour in this figure legend, the reader is referred to the web version of this article.)

Fig. 1 shows the results of simulations for the initial conditions $\phi(0) = 0.6$ and $\psi(0) = 0.4$. The upper dashed green line indicates the population sum, always constant and equal to 1. The lower blue dashed line indicates the difference in densities. We see that environmental fluctuations tend to quickly eliminate the scarcer species. Environmental fluctuations induce deleterious effects on less numerous populations favoring the more abundant species. We see from the red dotted lines, which represent 1 standard deviation from the mean, that fluctuations increase very fast, which inevitably leads to the extinction of both species. How fast this happens, will naturally depend on the noise intensity. The system reaches the absorbing state and talk about averages no longer makes sense.

Demographic noise is considered in the following equations, interpreted in the Itô sense [8][5]:

$$\begin{cases} \dot{\phi} = \phi - \phi^2 - \phi\psi + \sigma\sqrt{x(1-x)}\eta_1 \\ \dot{\psi} = \psi - \psi^2 - \psi\phi + \sigma\sqrt{y(1-y)}\eta_2. \end{cases} \tag{10}$$

$\eta_1$ and $\eta_2$ have the same statistical properties as before. When we observe Fig. 1(b) with the simulation results, we can draw identical conclusions as in the case of the additive noise. Note that the dotted red lines indicate bands of 3 standard deviations from the mean. The final conclusion of this section is that both environmental and demographic noise benefit the larger population when in competition with a less numerous population.

### 3.2. Comparison with the phenomenon of genetic drift

Let us make a comparison between the results obtained above with the phenomenon of genetic drift [37]. We will briefly discuss the phenomenon of natural selection and genetic drift.

The core difference between Natural Selection (NS) and Genetic (or allelic) Drift (GD) is the cause. Both are methods of genetic change in a population. However, one happens randomly (GD) while the other is a direct response to and environmental challenge (NS). Some examples:

Natural Selection is the mechanism by which a species changes in response to an environmental challenge. Imagine a population of brown rabbits in a field. They are breeding and being eaten occasionally by foxes until over time. Suppose that suddenly the environment changes so that the field is covered in snow. Now, the brown rabbits are highlighted and the foxes have an easy time of hunting them. Consequently, the number of brown rabbits decreases dramatically and they are threatened with extinction. White rabbits which used to be caught and eaten quickly before the snow came, are now much better adapted. As such, they are more likely to survive, breed and pass on their white genetic make up and hence more white rabbits are born—they are naturally selected by the snow and the foxes, which constitute its environment.

GD is also a change in genetic make up of a population. However it is not stimulated by the environment. Imagine our population of rabbits again. 50% of them have blue eyes and 50% have green. The eye color makes little difference to their survival chances and is just a natural variation. A newborn rabbit will statistically have a 50% chance of blue eyes and 50% chance of green eyes.

In a big population, the proportion of blue to green is likely to stay at or around 50%. However, that is not the case in a small population. Imagine there are now only 20 rabbits: 10 with blue eyes, 10 with green. Purely by chance, some of these rabbits will not breed, or some breed more often. Let us say – by chance – one green-eyed rabbit gets run over and does not breed. There are 10 blues and 9 greens. That means that there are now 53% blues and 47% greens. These proportions

[5] A factor $\sqrt{2}$ was absorbed in the constant $\sigma$.

will now have a greater impact on the subsequent generation since there are more blues, there will be a greater chance of blues appearing in the next generation and less chance of greens. This phenomenon is analogous to the phenomenon of environmental noise favoring more dense species and disfavoring the less dense shown above.

## 4. 1-dimensional case

### 4.1. Environmental noise

In this subsection we show simulations results for the 1-dimensional case with environmental noise. We are considering a 1-dimensional lattice with 128 sites uniformly distributed in the interval $(-1, 1)$. Fig. 2 shows how the population dynamics can change with variations in noise intensity. The stochastic partial differential equations (SPDE) for this case are:

$$\frac{\partial \phi}{\partial t} = D_\phi \nabla^2 \phi + \phi - \phi^2 - \phi\psi + \eta_1, \tag{11}$$

$$\frac{\partial \psi}{\partial t} = D_\psi \nabla^2 \psi + g\psi - \psi^2 - \psi\phi + \eta_2 \tag{12}$$

with the following noise properties: $\langle \eta_1(\mathbf{x}, t)\rangle = \langle \eta_2(\mathbf{x}, t)\rangle = 0$ and

$$\langle \eta_1(\mathbf{x}, t)\eta_1(\mathbf{x}', t')\rangle = \sigma^2 \delta^d(\mathbf{x} - \mathbf{x}')\delta(t - t') \tag{13}$$

$$\langle \eta_2(\mathbf{x}, t)\eta_2(\mathbf{x}', t')\rangle = \sigma^2 \delta^d(\mathbf{x} - \mathbf{x}')\delta(t - t'). \tag{14}$$

The diffusion constants are $D_\phi$ and $D_\psi$. From now on until the penultimate section we will consider $D_\phi = D_\psi = 1$.

In Fig. 2(a) we have as populations change when the noise intensity is low. We see that, within statistical fluctuations, the densities remain invariant in time. Fig. 2(b) shows the case of larger noise intensities. We see that the smaller population is more affected, while the larger population is once more benefited.

### 4.2. Demographic noise

The SPDE involving demographic noise interpreted in Itô sense are given by [8]

$$\frac{\partial \phi}{\partial t} = \nabla^2 \phi + \phi - \phi^2 - \phi\psi + \eta_1, \tag{15}$$

$$\frac{\partial \psi}{\partial t} = \nabla^2 \psi + g\psi - \psi^2 - \psi\phi + \eta_2 \tag{16}$$

with the following noise properties: $\langle \eta_1(\mathbf{x}, t)\rangle = \langle \eta_2(\mathbf{x}, t)\rangle = 0$ and

$$\langle \eta_1(\mathbf{x}, t)\eta_1(\mathbf{x}', t')\rangle = \sigma^2 \phi(\mathbf{x}, t)(1 - \phi(\mathbf{x}, t))\delta^d(\mathbf{x} - \mathbf{x}')\delta(t - t') \tag{17}$$

$$\langle \eta_2(\mathbf{x}, t)\eta_2(\mathbf{x}', t')\rangle = \sigma^2 \psi(\mathbf{x}, t)(1 - \psi(\mathbf{x}, t))\delta^d(\mathbf{x} - \mathbf{x}')\delta(t - t'), \tag{18}$$

where a factor 2 has been incorporated into the constant $\sigma^2$.

Fig. 3 shows the simulation results in one dimension using periodic boundary conditions for the case involving environmental and demographic noise. In both figures the same initial conditions were used, given by $\phi(x, 0) = 0.9$ and $\psi(x, 0) = 0.1$. We see that the effect of demographic noise is very different from environmental noise. The discrete nature of the interactions that induces demographic noise has the effect of equalizing population densities. This fact is in full contrast with the principle of competitive exclusion, which roughly states that complete competitors cannot exist [1].

*The reason for this violation can be the formation of clusters in which the nonlinear effects associated with intraspecific competition intensifies. In this case, the initially more massive species would aggregate in denser clusters and therefore tend to suffer more severe consequences. More detailed numerical simulations in higher dimensionality should be conducted for further information.*

## 5. Diffusion effects

In this section we show the effects that different values for the diffusion constants have on the dynamics. Dispersion is an important strategy that allows organisms to locate and exploit favorable habitats. Studies have already been done with the intention of studying the effects of diffusion in competition models. In Ref. [38] the authors found that species with a low dispersal rate always drive a competing species to extinction in a deterministic continuous model with a heterogeneous growth rate. A slowly dispersing species exploits favorable environments without wastefully exploring the landscape. We are talking about the so-called *cost of migration*.

Hamilton and May [39], on the other hand, considered a stochastic model in which the fast species may be preferred. In Ref. [40] the authors consider explicitly the discrete character of interactions in an agent-based model and found that

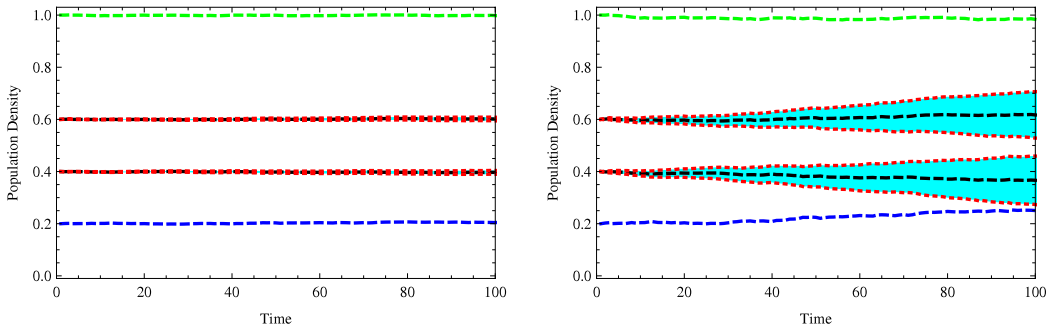


(a) 1-dimensional case with $\sigma = 0.05$. $N = 2 \times 10^4$, $1 \times 10^3$ Monte Carlo samples. Black dashed lines represent the average population, shown with its red dotted lines (not easily discernible in the scale displayed) representing 1 standard deviation from the mean.

(b) 1-dimensional case with $\sigma = 0.15$. $N = 2 \times 10^4$, $1 \times 10^3$ Monte Carlo samples. Black dashed lines represent the average population, shown with its red dotted lines representing 1 standard deviation from the mean.

**Fig. 2.** 1-dimensional SPDE numerical simulations with additive noise. Lattice has 128 sites, uniformly distributed in interval $(-1, 1)$. The superior black curve represents mean $\langle\phi\rangle$ population and the inferior black curve represents $\langle\psi\rangle$ population. Superior green dashed line is the sum $\langle\phi\rangle + \langle\psi\rangle$ and inferior blue dashed line is the difference $\langle\phi\rangle - \langle\psi\rangle$. Homogeneous initial conditions are $\phi(x, 0) = 0.6$, $\psi(x, 0) = 0.4$. Diffusion constants are unitary. (For interpretation of the references to colour in this figure legend, the reader is referred to the web version of this article.)

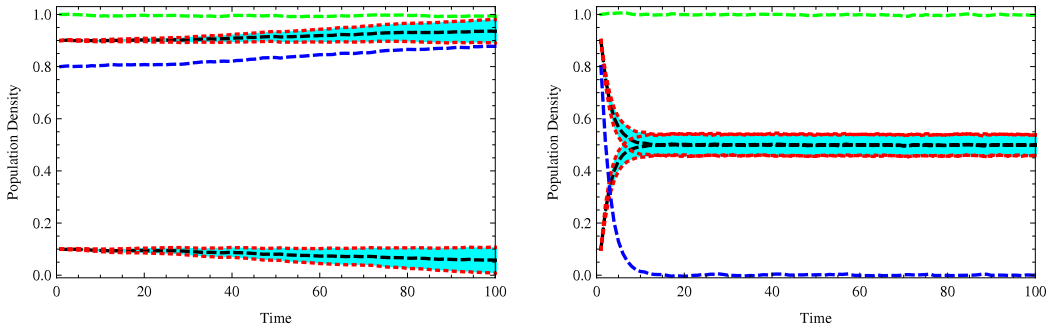


(a) Environmental noise 1-dimensional model. Average of $1 \times 10^3$ Monte Carlo realizations with $\sigma = 0.1$. Black dashed lines represent the average population, shown with its red dotted lines representing 1 standard deviation from the mean.

(b) Demographic noise 1-dimensional model. Average of $1 \times 10^3$ Monte Carlo realizations with $\sigma = 0.2$. Black dashed lines represent the average population, shown with its red dotted lines representing 10 standard deviations from the mean.

**Fig. 3.** 1-dimensional SPDE numerical simulations. Lattice has 128 sites, uniformly distributed in interval $(-1, 1)$. The superior black curve represents mean $\langle\phi\rangle$ population and inferior black curve represents $\langle\psi\rangle$ population. Superior green dashed line is the sum $\langle\phi\rangle + \langle\psi\rangle$ and inferior blue dashed line is the difference $\langle\phi\rangle - \langle\psi\rangle$. Homogeneous initial conditions are $\phi(x, 0) = 0.9$, $\psi(x, 0) = 0.1$. Diffusion constants are unitary. (For interpretation of the references to colour in this figure legend, the reader is referred to the web version of this article.)

the faster species could drive the slower one to extinction if stochastic fluctuations were large. In essence they showed that *discreteness favors faster dispersers.* In all the models mentioned above the medium in which the species lives is heterogeneous in birth rate, i.e., it depends on the position. There is a competition between *environment heterogeneity* and *interaction discreteness.* The former tends to favor the slow and the latter the fast species.

Fig. 4 presents simulation results for the case of environmental noise. Fig. 4(a) corresponds to the case with equal values for diffusion constants ($D_\phi = D_\psi = 1$) and, on the right, Fig. 4(b) shows the case with different values ($D_\phi = 1$, $D_\psi = 0.1$). All other parameters were held constant. We see that reducing the diffusion constant $D_\psi$ brings bad consequences for species *B*. For the same time interval and noise intensity, it moves more quickly to extinction. The reason for this is simple: fast dispersers smooth out fluctuations by diffusion, putting slower competitors at a disadvantage. This is due to the non-linear death rates compared to the linear birth rates in the equations. Suppose that the density of the slow species is given by $\psi(x) = \psi_0 + \eta(x, t)$ where $\langle\eta\rangle = 0$ and statistical properties (13) and (14) are valid. The total number of births in time $T$ is independent of the fluctuations,

$$\text{births} = \int_0^T \mathrm{d}t \int_0^L \psi(x)\mathrm{d}x = LT\psi_0. \tag{19}$$

Nevertheless, the total number of deaths is

$$\text{deaths} = \int_0^T \mathrm{d}t \int_0^L \psi(x)^2\mathrm{d}x = LT\left(\psi_0 + \sigma^2\right). \tag{20}$$

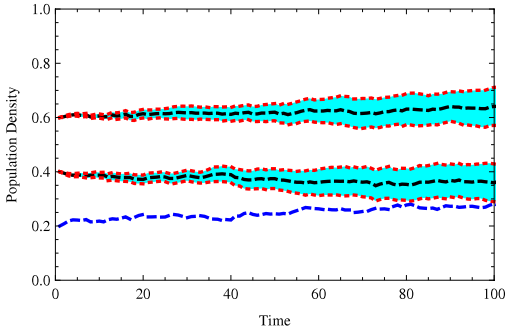


(a) Environmental noise 1-dimensional model. Average of 100 Monte Carlo realizations with $\sigma = 0.15$ and diffusion coefficients $D_\phi = 1$ and $D_\psi = 1$. Black dashed lines represent the average population, shown with its red dotted lines representing 1 standard deviations from the mean.

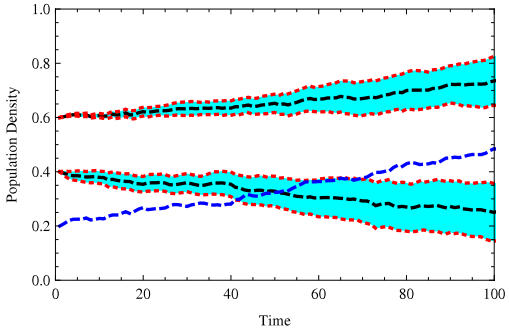


(b) Environmental noise 1-dimensional model. Average of 100 Monte Carlo realizations with $\sigma = 0.15$ and diffusion coefficients $D_\phi = 1$ and $D_\psi = 0.1$. Black dashed lines represent the average population, shown with its red dotted lines representing 1 standard deviations from the mean.

**Fig. 4.** 1-dimensional SPDE numerical simulations. Lattice has 128 sites, uniformly distributed in interval $(-1, 1)$. The superior black curve represents mean $\langle\phi\rangle$ population and inferior black curve represents $\langle\psi\rangle$ population. Inferior blue dashed line is the difference $\langle\phi\rangle - \langle\psi\rangle$. Homogeneous initial conditions are $\phi(x, 0) = 0.6$, $\psi(x, 0) = 0.4$. (For interpretation of the references to colour in this figure legend, the reader is referred to the web version of this article.)

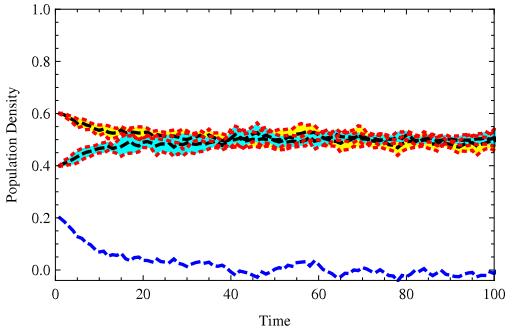


(a) Demographic noise 1-dimensional model. Average of 10 Monte Carlo realizations with $\sigma = 0.2$ and diffusion coefficients $D_\phi = 1$ and $D_\psi = 1$. Black dashed lines represent the average population, shown with its red dotted lines representing 10 standard deviations from the mean.

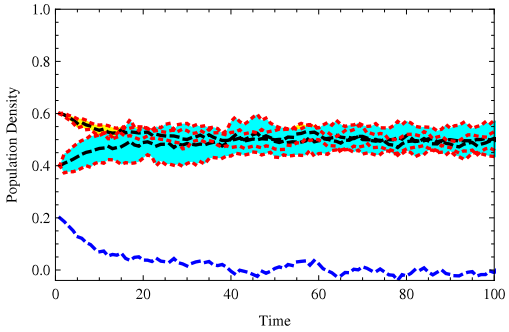


(b) Demographic noise 1-dimensional model. Average of 10 Monte Carlo realizations with $\sigma = 0.2$ and diffusion coefficients $D_\phi = 1$ and $D_\psi = 0.1$. Black dashed lines represent the average population, shown with its red dotted lines representing 10 standard deviations from the mean.

**Fig. 5.** Numerical simulations 1-dimensional SPDE. Lattice has 128 sites, uniformly distributed in interval $(-1, 1)$. The superior black curve represents mean $\langle\phi\rangle$ population and inferior black curve represents $\langle\psi\rangle$ population. Inferior blue dashed line is the difference $\langle\phi\rangle - \langle\psi\rangle$. Homogeneous initial conditions are $\phi(x, 0) = 0.6$, $\psi(x, 0) = 0.4$. (For interpretation of the references to colour in this figure legend, the reader is referred to the web version of this article.)

Fluctuations increase the death rate. As mentioned above, we expect the fluctuations of fast dispersers to be smaller, so the slow species is driven to extinction.

Fig. 5 shows the results for demographic noise. On the left is the case for equal diffusion constants and different values for diffusion constants are shown on the right, as before. The deleterious effect for the slow population is now present as an increase in fluctuations, shown in blue, compared with the fluctuations of the faster species, shown in yellow. This fact confirms the statement made above that diffusion smoothes out fluctuations. The species also tend to equalize, but the slower species now has a greater extinction probability.

## 6. Discussion and conclusion

Many theoretical models predict the competitive exclusion possibility. However, for reasons still poorly understood, competitive exclusion is not easily seen in nature and many biological systems seem to violate this principle. A well-known example is the paradox of the plankton [41]: how is it possible for a number of species to coexist in a relatively isotropic or unstructured environment all competing for the same sorts of resources? The problem is particularly acute because there is adequate evidence from enrichment experiments that natural waters, at least in the summer, present an environment that is strikingly nutrient deficient, so that competition is likely to be severe. According to the competitive exclusion principle, only a small number of plankton species should be able to coexist on these resources. Nevertheless, large numbers of plankton species coexist within small areas of open sea.

The achieved results (only for $d = 1$) seems to shed some light on this apparent paradox: *The discontinuous character of interactions can induce coexistence.* At least for situations that fit the assumptions of the proposed model. It is worth

remembering the observation about the hypothesis of many similarities between species. According to the renormalization group ideas, it is enough that the species have equal birth and interspecific competition rates and live in $0 < d < 4$ for the results to be valid. Lastly, we believe that other less restrictive models in which the discrete character of the interactions are taken into account can show more vigorously the results presented here.

**Acknowledgment**

This work is supported by CNPq, Brazil.

**Appendix. Code for demographic noise simulation**

The stochastic differential equations in XMDS2 must be written in the Stratonovich formulation [27]. All stochastic equations shown in this article are in the Itô representation. Therefore, we need to transform Itô equations in Stratonovich equations. To do this we must add the term $-\frac{1}{2}g(\phi)g(\phi)' = -\frac{\sigma}{4}(1-2\phi)$ with $g(\phi) \equiv \sigma\sqrt{\phi(1-\phi)}$ in the Itô equations [8]. The XMDS2 code for the demographic noise simulation is:

```
<?xml version="1.0" encoding="UTF-8"?>
<simulation xmds-version="2">
  <name>DIC</name>
  <author>Renato Vieira dos Santos</author>
  <description>
    Discreteness Induced Coexistence
  </description>

  <geometry>
    <propagation_dimension> t </propagation_dimension>
    <transverse_dimensions>
      <dimension name="x" lattice="128"  domain="(-1, 1)" />
    </transverse_dimensions>
  </geometry>

  <driver name="mpi-multi-path" paths="1000" />

  <features>
    <auto_vectorise />
    <validation kind="none"/>
    <benchmark />
    <error_check />
    <bing />
    <fftw />
    <globals>
      <![CDATA[
      const real alpha = 1.0;
      const real beta = 1.0;
      const real sigma = 0.2;
      const real g_A = 1.0;
      const real g_B = 1.0;
      const real h_A = 1.0;
      const real h_B = 1.0;
      const real D_A = 1.0;
      const real D_B = 1.0;
      ]]>
    </globals>
  </features>

  <noise_vector name="noiseEvolution" dimensions="x" kind="wiener" type="real"
                                          method="dsfmt" seed="314 159 276">
    <components>p_1 p_2</components>
  </noise_vector>

  <vector name="main" initial_basis="x" type="complex">
```

```
    <components>phi psi</components>
    <initialisation>
      <![CDATA[
        phi = 0.9 ;
        psi = 0.1 ;
      ]]>
    </initialisation>
  </vector>

  <sequence>
    <integrate algorithm="SI" iterations="3" interval="10" steps="100000">
      <samples>100</samples>
      <operators>
        <operator kind="ip" constant="yes">
          <operator_names>L</operator_names>
          <![CDATA[
            L = -kx*kx;
          ]]>
        </operator>
        <dependencies>noiseEvolution</dependencies>
        <integration_vectors>main</integration_vectors>
        <![CDATA[
         dphi_dt=L[phi]+(alpha*phi-g_A*pow(phi,2)-h_A*phi*psi
                +sigma*pow(g_A*phi*(1-phi),0.5)*p_1-0.25*sigma*g_A*(1-2*phi));
         dpsi_dt=L[psi]+(beta*psi-g_B*pow(psi,2)-h_B*phi*psi
                +sigma*pow(g_B*psi*(1-psi),0.5)*p_2-0.25*sigma*g_B*(1-2*psi));
        ]]>
      </operators>
    </integrate>
  </sequence>

  <output>
      <sampling_group basis="x" initial_sample="yes">
        <moments>phiR psiR sdphi sdpsi</moments>
        <dependencies>main</dependencies>
        <![CDATA[
          phiR = Re(phi);
          psiR = Re(psi);
          sdphi = Re(pow(phi,2));
          sdpsi = Re(pow(psi,2));
        ]]>
      </sampling_group>
  </output>
</simulation>
```

## References


[1] G. Hardin, et al., Science 131 (1960) 1292–1297.
[2] G. Gause, The Struggle for Existence, Dover Publications, 2003.
[3] M. Ullah, O. Wolkenhauer, Stochastic Approaches for Systems Biology, in: Interdisciplinary Applied Mathematics Series, Springer, 2011.
[4] J. Feng, W. Fu, F. Sun, Frontiers in Computational and Systems Biology, Computational Biology, Springer, 2010.
[5] S. Karlin, H. Taylor, A Second Course in Stochastic Processes, Academic Press, 2000.
[6] W. Feller, An Introduction to Probability Theory and its Applications, Vol. 2, John Wiley & Sons, 2008.
[7] N. Kampen, Stochastic Processes in Physics and Chemistry, North-Holland personal library, Elsevier, 2007.
[8] C. Gardiner, Stochastic Methods: a Handbook for the Natural and Social Sciences, in: Springer Series in Synergetics, Springer, 2009.
[9] K. Jacobs, Stochastic Processes for Physicists: Understanding Noisy Systems, Cambridge University Press, 2010.
[10] J. Freund, T. Pöschel, Stochastic Processes in Physics, Chemistry, and Biology, in: Lecture Notes in Physics, Springer, 2000.
[11] C. Mode, C. Sleeman, Stochastic Processes in Epidemiology: HIV/AIDS, Other Infectious Diseases, and Computers, World Scientific, 2000.
[12] N. Bailey, The Elements of Stochastic Processes with Applications to the Natural Sciences, in: Wiley Series in Probability and Mathematical Statistics: Applied Probability and Statistics, Wiley, 1964.
[13] D. Helbing, Quantitative Sociodynamics: Stochastic Methods and Models of Social Interaction Processes, Springer, 2011.
[14] O. Ovaskainen, B. Meerson, Trends in Ecology & Evolution 25 (2010) 643–652.
[15] D. Gravel, F. Guichard, M. Hochberg, Ecology Letters 14 (2011) 828–839.
[16] Z. Schuss, Theory and Applications of Stochastic Processes: an Analytical Approach, in: Applied Mathematical Sciences, Springer, 2010.
[17] B. Oksendal, Stochastic Differential Equations: an Introduction with Applications, in: Universitext (1979), Springer, 2003.

[18] H. Risken, The Fokker–Planck Equation: Methods of Solutions and Applications, second ed., in: Springer Series in Synergetics, Springer, 1989, third printing edition, 1996.
[19] N. Shnerb, Y. Louzoun, E. Bettelheim, S. Solomon, Proceedings of the National Academy of Sciences 97 (2000) 10322.
[20] A. Black, A. McKane, Trends in Ecology & Evolution (2012).
[21] A. McKane, T. Newman, Physical Review Letters 94 (2005) 218102.
[22] T. Butler, N. Goldenfeld, Physical Review E 84 (2011) 011112.
[23] R. Lande, Oikos (1998) 353–358.
[24] B. Dennis, Oikos 96 (2002) 389–401.
[25] J. Paulsson, Nature 427 (2004) 415–418.
[26] M. Thattai, A. Van Oudenaarden, Proceedings of the National Academy of Sciences 98 (2001) 8614–8619.
[27] G. Dennis, J. Hope, M. Johnsson, Computer Physics Communications (2012).
[28] H. Janssen, Journal of Statistical Physics 103 (2001) 801–839.
[29] P.C. Martin, E.D. Siggia, H.A. Rose, Physical Review A 8 (1973) 423–437.
[30] C. de Dominicis, Le Journal de Physique Colloques 37 (1976) 247–253.
[31] H. Janssen, Zeitschrift für Physik B Condensed Matter 23 (1976) 377–380.
[32] A. Kamenev, Keldysh and Doi-Peliti techniques for out-of-equilibrium systems, 2001.
[33] M. Doi, Journal of Physics A (Mathematical and General) 9 (1976) 1479.
[34] L. Peliti, Path Integral Approach to Birth–Death Processes on a Lattice, Technical Report, 1985.
[35] C. Gardiner, S. Chaturvedi, Journal of Statistical Physics 17 (1977) 429–468.
[36] M. Droz, A. McKane, Journal of Physics A (Mathematical and General) 27 (1994) L467.
[37] R. Der, C.L. Epstein, J.B. Plotkin, Theoretical Population Biology 80 (2011) 80–99.
[38] J. Dockery, V. Hutson, K. Mischaikow, M. Pernarowski, Journal of Mathematical Biology 37 (1998) 61–83.
[39] W. Hamilton, R. May, 1977.
[40] D.A. Kessler, L.M. Sander, Physical Review E 80 (2009) 041907.
[41] G. Hutchinson, American Naturalist (1961) 137–145.

Capítulo 8

# Conclusão

É com muito orgulho que apresento as conclusões associadas ao meu trabalho final de formação acadêmica, conquistado com muita luta e perseverança, realizado concomitantemente com a carreira docente em todos os níveis educacionais e sócio-econômicos, nas mais diversas instituições de ensino.

Uma das principais perguntas da minha linha de pesquisa pode ser formulada da seguinte forma:

Que tipo de fenômeno *emerge* nos processos biológicos em geral quando levamos em conta o *caráter discreto* das interações e a *finitude* das populações?

Esta é a pergunta relevante e é interessante conjecturar que a *discreteza* das interações nos fenômenos biológicos de modo geral parece ter um impacto profundo nos processos celulares e ecológicos. Esta afirmativa tem respaldo no fantástico desenvolvimento da física no início do século XX com o advento da *mecânica quântica*, onde o caráter discreto de muitas grandezas físicas tiveram também um enorme impacto na nossa sociedade.

Muitas quantidades em todo o mundo físico são contínuas e medidas por números reais: posição, velocidade, concentração, peso, etc. Em muitas áreas da ciência, no entanto, percebeu-se que certos padrões complexos podem ser explicados pela suposição de existência de níveis discretos subjacentes que podem ser descritos utilizando números inteiros. Em química, as diversas leis de composição de elementos, tais como "proporções definidas" e "múltiplas proporções", conhecidas por volta de 1800, levaram Dalton a formular a teoria atomista e dar uma explicação simples e elegante para todas essas leis. Por volta de 1900, Planck, Einstein, Bohr e outros perceberam que os problemas mais assustadores da (então) física moderna, como o espectro de radiação do corpo negro, a dependência universal da temperatura do calor específico de sólidos, a velocidade dos elétrons ejetados por sólidos sob radiação (efeito fotoelétrico), poderiam ser resolvidos elegantemente supondo que a energia é quantizada e varia apenas em unidades de inteiros. Em biologia, a teoria da evolução de Darwin era incompatível com a teoria da mistura de herança, até então tida como óbvia. O trabalho de Mendel, e sua redescoberta por de Vries, Correns e Tschermak por volta de 1900 (uma curiosa coincidência), restaurou a consistência matemática da evolução com a introdução do conceito de genes como o *quantum* de informação da herança genética.

Estes são apenas alguns exemplos onde os padrões complexos poderiam ser explicados simplesmente pela suposição de um nível discreto subjacente. A hipótese de descontinuidade e, especialmente, suas consequências, foi em cada um destes casos anti-intuitiva. Os organismos vivos, por outro lado, não necessitam da hipótese de descontinuidade. Mas um fato óbvio sobre eles é que os eventos de nascimento e morte mudam seu número apenas por quantidades inteiras.

A mensagem que fica com os três exemplos analisados nos artigos é que, como em muitas outras áreas da ciência, a natureza discreta da vida tem consequências importantes, que têm sido muitas vezes negligenciadas. Espero que estes resultados ajudem a disseminar na comunidade científica a necessidade de se levar em consideração a finitude das populações e a consequente natureza discreta das interações em biologia.

Apêndice A

# Mapeamento de Doi

## A.1. Introdução

Aqui começa uma sequência de apêndices que visam dar subsídios detalhados para a construção de uma teoria de campo equivalente a um dado processo estocástico descrito por uma equação mestra. Estamos falando da teoria de Doi-Peliti. O objetivo nesta seção e da próxima é descrever reações locais de criação e aniquilação de partículas se difundindo na rede ou em um meio contínuo através de um mapeamento em uma integral funcional, passando pela representação de segunda quantização utilizando a teoria de Doi-Peliti [61, 33]. Alguns exemplos de espécie única são a reação de aniquilação de pares $A+A \to \emptyset$, onde $\emptyset$ denota um componente quimicamente inerte, e a coagulação $A+A \to A$. A propagação da partícula difusiva pode ser modelada como um passeio aleatório discreto ou contínuo no tempo. Uma reação ocorre quando uma partícula se encontra suficientemente próxima de outra, onde esta proximidade, caracterizada pelo alcance da interação entre as partículas, deve ser definida *a priori*. Na rede, pode-se definir que a reação ocorre quando as partículas se encontram no mesmo sítio.

### A.1.1. Características básicas dos sistemas de reação-difusão

Um processo muito importante no estudo das transições de fase de não equilíbrio entre estados ativos e absorventes é o processo descrito pelas reações $A+A \to A$, $A \to A+A$ e $A \to \emptyset$, que ocorrem em uma rede regular $d-$dimensional. Este processo é chamado de *Percolação Direcionada* (PD) e caracteriza uma ampla classe de Universalidade. Um ponto crítico é alcançado pelo ajuste das taxas de reação $A \to (\emptyset, 2A)$. Processos mais genéricos de duas espécies, por exemplo, $A+B \to \emptyset$ requerem que tipos diferentes de partículas se aproximem para que a reação ocorra. As espécies diferentes de partículas podem ou não ter a mesma constante de difusão. Com tal generalidade disponível, é possível construir sistemas que relaxam para o equilíbrio, bem como sistemas guiados. O primeiro caso, que inclui a Percolação Direcionada, compreende tipicamente tanto as reações que aumentam o número de partículas como as que diminuem. Dependendo das combinações apropriadas das taxas de reação, a subsequente competição pode, no limite termodinâmico e em tempos longos, resultar em um estado 'ativo', caracterizado por um estado estacionário de densidade finita de partículas, bem como uma situação que evolui para uma rede vazia. Para reações que requerem a presença de pelo menos uma das partículas, o último caso constitui um estado 'inativo' ou 'absorvente' sem flutuações, estado do qual o sistema não poderá escapar nunca. A transição contínua de um estado ativo para um estado absorvente é análoga a uma transição de fase de equilíbrio de segunda ordem, e de modo similar requer o ajuste das taxas de transição como parâmetros de controle para atingir a região crítica. Como no equilíbrio, universalidade das leis de potência críticas emergem como uma consequência da divergência do comprimento de correlação $\xi$, o que induz o surgimento de invariância de escala e independência dos parâmetros microscópicos no regime crítico. Por outro lado, sistemas tais

como a reação de aniquilação de pares $A+A \to \emptyset$ são sistemas que necessariamente decaem para o estado absorvente. Nestes casos, a lei de decaimento assintótico é que é de interesse bem como o comportamento das funções de correlação no regime universal que é atingido para valores grandes da variável tempo.

### A.1.2. Teoria de Doi

Faremos uma revisão bem detalhada do mapeamento de sistemas de reação-difusão em uma teoria de campos, elaborando uma definição do sistema através de uma *equação mestra*, convertendo esta equação mestra em uma descrição em termos de operadores de *criação* e *aniquilação* correspondente, com a subsequente transposição para uma representação em *integral funcional*. É esta representação final em integral funcional que nos permitirá utilizar todo o arsenal de técnicas disponíveis em uma teoria de campos, inclusive Grupo de Renormalização (GR).

Considere um conjunto de sítios na rede denotados por $i = 1,2,3,\cdots$ onde cada sítio é ocupado por $n_1, n_2, n_3, \cdots$ partículas. Definimos $\alpha = \{n_1, n_2, n_3, \cdots\}$ como representando um estado particular da rede bem como $P(\alpha,t)$ a probabilidade de obter o estado $\alpha$ no tempo $t$. Processos dinâmicos tais como saltos de um sítio para outro, decaimentos, reações etc. irão causar uma mudança do estado $\alpha$ para o estado $\beta$, descrito por uma equação mestra caracterizada por uma taxa de transição que define a dinâmica.

$$w_{\alpha\to\beta} = \text{taxa de transição de } \alpha \text{ para } \beta$$

A dinâmica fica totalmente caracterizada através de uma equação mestra do tipo

$$\frac{d}{dt}P(\alpha,t) = \sum_{\beta}\left[w_{\beta\to\alpha}P(\beta,t) - w_{\alpha\to\beta}P(\alpha,t)\right] \tag{A.1}$$

onde as condições iniciais $P(\alpha,0)$ devem ser especificadas e a condição $\sum_{\alpha} P(\alpha,t) = 1$ deve ser satisfeita. Esta equação é parecida com a equação de Schrodinger para uma função de onda de muitas partículas já que ela é linear em $P(\alpha,t)$ e de primeira ordem na derivada temporal $d/dt$.

Agora, faremos uso de uma série de exemplos simples de aplicação da equação mestra para que, nas próximas subseções, mostrarmos como a descrição em termos de operadores de criação e aniquilação para a equação mestra é construída.

**Exemplo 1: A equação mestra para o decaimento $A \to \emptyset$.**

Considere um único sítio da rede que contém algum número de partículas idênticas. Estas partículas decaem a taxa $\lambda$. A taxa para uma transição de $n$ para $m$ partículas é

$$w_{n\to m} = \begin{cases} 0 & \text{para} \quad m \neq n-1 \\ n\lambda & \text{para} \quad m = n-1 \end{cases}$$

e a equação mestra fica

$$\frac{d}{dt}P(n,t) = \lambda\left[(n+1)P(n+1,t) - nP(n,t)\right]. \tag{A.2}$$

Esta equação mestra possui solução exata para $P(n,t)$ o que nos permite obter qualquer momento $\langle n^k\rangle \equiv \sum_n n^k P(n,t)$ ($k$ inteiro) para o processo. Em particular, seja $\rho(t) = \langle n\rangle$ a média no número de partículas no tempo $t$. Então, sem resolver a equação mestra diretamente:

$$\dot{\rho} = \sum_n n\dot{P}(n,t) = \sum_n n\left[\lambda(n+1)P(n+1,t) - \lambda nP(n,t)\right]$$

$$= \lambda \sum_n n(n+1)P(n+1,t) - \lambda \sum_n n^2 P(n,t)$$
$$= \lambda \sum_m (m-1)mP(m,t) - \lambda \sum_n n^2 P(n,t)$$
$$= -\lambda \sum_m mP(m,t) = -\lambda\rho,$$

que é o resultado que esperamos para o processo de decaimento.

**Exemplo 2: A reação $A + A \to \emptyset$.**

Novamente considere um único sítio da rede, com a regra que um par de partículas pode se aniquilar. As taxas são

$$w_{n\to m} = \begin{cases} 0 & \text{para} \quad m \neq n-2 \\ n(n-1)\lambda & \text{para} \quad m = n-2 \end{cases}$$

e a equação mestra é

$$\frac{d}{dt}P(n,t) = \lambda\left[(n+2)(n+1)P(n+2,t) - n(n-1)P(n,t)\right]. \tag{A.3}$$

**Exemplo 3: Salto entre dois sítios da rede**

Agora considere dois sítios, $i = 1,2$, com uma taxa $\Gamma$ de salto do sítio 1 para o sítio 2.

$$w_{(n_1,n_2)\to(m_1,m_2)} = \begin{cases} 0 & \text{para} \quad m_1 \neq n_1 - 1 \quad \text{ou} \quad m_2 \neq n_2 + 1 \\ n_1\Gamma & \text{para} \quad m_1 = n_1 - 1 \quad \text{e} \quad m_2 = n_2 + 1 \end{cases}$$

onde a equação mestra é

$$\frac{d}{dt}P(n_1,n_2,t) = \Gamma\left[(n_1+1)P(n_1+1,n_2-1,t) - n_1 P(n_1,n_2,t)\right]. \tag{A.4}$$

**Exemplo 4: Difusão**

Considere uma cadeia unidimensional de sítios da rede $i = 1,2,\cdots$ e permita que todas as partículas saltem para a direita ou para a esquerda com taxa $\Gamma$. A equação mestra é

$$\frac{d}{dt}P(\alpha,t) = \Gamma \sum_{\langle ij\rangle} \Big[(n_i+1)P(n_i+1,n_j-1,\cdots,t) - n_i P(\alpha,t)$$
$$+(n_j+1)P(n_i-1,n_j+1,\cdots,t) - n_j P(\alpha,t)\Big], \tag{A.5}$$

onde a soma se estende sobre pares de sítios que são primeiros vizinhos.

Definindo $\rho(x,t) = \sum_\alpha n_i P(\alpha,t)$ com $x = i\Delta x$, é possível mostrar que, para $\Delta x \to 0$ a equação (A.5) se transforma na equação de difusão unidimensional

$$\frac{\partial\rho}{\partial t} = D\frac{\partial^2\rho}{\partial x^2}$$

onde $D \equiv \Gamma(\Delta x)^2$ é a constante de difusão.

**Exemplo 5: Equação Mestra para a reação $A + A \to \emptyset$ com difusão**

O estado do sistema será caracterizado, como sempre, pela probabilidade $P(\alpha,t)$. A dinâmica estocástica é capturada através da seguinte equação mestra:

$$\frac{d}{dt}P(\alpha,t) = \frac{D}{(\Delta x)^2}\sum_{\langle ij\rangle}\Big[(n_i+1)P(\cdots,n_i+1,n_j-1,\cdots,t) - n_i P(\alpha,t)$$

$$+(n_j+1)P(\cdots,n_i-1,n_j+1,\cdots,t)-n_jP(\alpha,t)\Big]$$

$$+\lambda\sum_i\left[(n_i+2)(n_i+1)P(\cdots,n_i+2,\cdots,t)-n_i(n_i-1)P(\alpha,t)\right]. \tag{A.6}$$

onde a soma se estende sobre os pares de sítios primeiros vizinhos. O primeiro termo entre colchetes representa uma partícula saltando do sítio $i$ para o sítio $j$, incluindo tanto o fluxo de probabilidade que "entra" quanto o fluxo de probabilidade que "sai" da configuração $\alpha$ como consequência do movimento das partículas. O segundo termo corresponde aos saltos do sítio $j$ para o sítio $i$. Os fatores multiplicativos $n$ e $n+1$ são um resultado das partículas atuando independentemente. Falta especificar apenas a probabilidade inicial $P(\alpha,t=0)$. As partículas serão distribuidas em cada sítio $i$ com a distribuição de Poisson:

$$P(\alpha,0)=\prod_i\left(\frac{n_0^{n_i}}{n_i!}e^{-n_0}\right), \tag{A.7}$$

onde $n_0$ denota o número médio de partículas por sítio.

Nas próximas seções aprenderemos como representar estas e outras equações mestras em termos de operadores de criação e aniquilação. Posteriormente, este passo nos permitirá obter a formulação em integral funcional destas equações mestras.

## A.2. A representação de Doi

Modelos estocásticos clássicos de partículas podem ser reescritos em termos de operadores de criação e aniquilação familiares da mecânica quântica, como mostrado por Doi [61]. Esta representação explora o fato de que esses processos apenas mudam o número de ocupação dos sítios por um inteiro. Os microestados para qualquer processo estocástico em uma rede é dado pelos números de ocupação $\{n\}\equiv\{n_1,n_2,\cdots\}$ de cada sítio. Seja $P(\{n\},t)$ a probabilidade dos microestados no tempo $t$. Como não implementamos nenhuma restrição para ocupação dos sítios, introduzimos para cada sítio da rede $i,j,\cdots$ operadores de criação $\hat{a}^\dagger$ e aniquilação $\hat{a}$ sujeitos às relações "bosônicas" de comutação

$$[\hat{a}_i,\hat{a}_j^\dagger]=\delta_{ij},\qquad [\hat{a}_i,\hat{a}_j]=[\hat{a}_i^\dagger,\hat{a}_j^\dagger]=0. \tag{A.8}$$

Estas relações de comutação podem ser realizadas pelas seguintes relações formais

$$\hat{a}_i=\frac{\partial}{\partial a_i^\dagger}\qquad a_i^\dagger=-\frac{\partial}{\partial\hat{a}_i}. \tag{A.9}$$

A rede vazia é caracterizada por $\hat{a}_i|0\rangle=0$ para todo $i$ e em cada sítio $i$ definimos o vetor de estado $|n_i\rangle=(\hat{a}_i^\dagger)^{n_i}|0\rangle$. Para estes estados, temos:

$$\hat{a}_i|n_i\rangle=n_i|n_i-1\rangle,\qquad \hat{a}_i^\dagger|n_i\rangle=|n_i+1\rangle. \tag{A.10}$$

Podemos agora encapsular toda a informação sobre o estado $\{n\}=(n_1,n_2,\cdots)$ da rede no tempo $t$ na quantidade

$$|\phi(t)\rangle=\sum_{\{n\}}P(\{n\},t)\prod_i(\hat{a}_i^\dagger)^{n_i}|0\rangle. \tag{A.11}$$

Como consequência dessa descrição de estados em termos de um espaço de Fock em completa analogia com a descrição da mecânica quântica de muitos corpos [23], podemos escrever a evolução temporal da equação mestra em uma equação do tipo Schrodinger em tempo imaginário

$$\frac{d}{dt}|\phi(t)\rangle = -\hat{H}|\phi(t)\rangle. \tag{A.12}$$

O motivo para a realização deste procedimento é que ele permite uma descrição mais simples da dinâmica. Por exemplo, para o processo $A+A \to \emptyset$ teremos

$$\hat{H} = \Gamma \sum_{\langle ij \rangle} (\hat{a}_i^\dagger - \hat{a}_j^\dagger)(\hat{a}_i - \hat{a}_j) - \lambda \sum_i (1 - (\hat{a}_i^\dagger)^2)(\hat{a}_i)^2 \tag{A.13}$$

com a correspondente solução formal

$$|\phi(t)\rangle = e^{-\hat{H}t}|\phi(0)\rangle. \tag{A.14}$$

Para entendermos a origem da equação (A.13), seja a equação mestra para o processo $A+A \to \emptyset$ em um único sítio (A.3) dada por

$$\frac{d}{dt}P(n,t) = \lambda\left[(n+2)(n+1)P(n+2,t) - n(n-1)P(n,t)\right]. \tag{A.15}$$

Multiplicando por $|n\rangle$ e somando sobre $n$, vem:

$$\frac{d}{dt}|\phi(t)\rangle = \lambda \sum_n P(n+2,t)(n+2)(n+1)|n\rangle - \lambda \sum_n P(n,t)n(n-1)|n\rangle$$

$$= \lambda \sum_n P(n+2,t)\hat{a}^2|n+2\rangle - \lambda \sum_n P(n,t)(\hat{a}^\dagger)^2\hat{a}^2|n\rangle$$

$$= \lambda(1-(\hat{a}^\dagger)^2)\hat{a}^2 \sum_n P(n,t)|n\rangle$$

$$= \lambda(1-(\hat{a}^\dagger)^2)\hat{a}^2|\phi(t)\rangle = -\hat{H}|\phi(t)\rangle, \tag{A.16}$$

o que corresponde ao segundo termo do lado direito da equação (A.13).

Por outro lado, se lembrarmos da equação mestra para o processo de salto entre os sítios 1 e 2 (A.4)

$$\frac{d}{dt}P(n_1,n_2,t) = \Gamma\left[(n_1+1)P(n_1+1,n_2-1,t) - n_1P(n_1,n_2,t)\right], \tag{A.17}$$

multiplicando por $|n_1,n_2\rangle$ e somando em $n_1$ e $n_2$, teremos:

$$\frac{d}{dt}|\phi(t)\rangle = \Gamma \sum_{n_1,n_2} P(n_1+1,n_2-1)(n_1+1)|n_1,n_2\rangle - \Gamma \sum_{n_1,n_2} P(n_1,n_2,t)n_1|n_1,n_2\rangle$$

$$= \Gamma \sum_{n_1,n_2} P(n_1+1,n_2-1,t)\hat{a}_2^\dagger\hat{a}_1|n_1+1,n_2-1\rangle - \Gamma \sum_{n_1,n_2} P(n_1,n_2,t)\hat{a}_1^\dagger\hat{a}_1|n_1,n_2\rangle$$

$$= \Gamma(\hat{a}_2^\dagger - \hat{a}_1^\dagger)\hat{a}_1|\phi(t)\rangle. \tag{A.18}$$

Assim, o Hamiltoniano para o processo de salto do sítio 1 para o sítio 2 fica dado por

$$\hat{H}_{1\to 2} = \Gamma(\hat{a}_2^\dagger - \hat{a}_1^\dagger)\hat{a}_1. \tag{A.19}$$

Se permitirmos o salto reverso à mesma taxa do sítio 2 para o sítio 1, ficamos com

$$\hat{H}_{1\leftrightarrow 2} = \Gamma(\hat{a}_2^\dagger - \hat{a}_1^\dagger)(\hat{a}_1 - \hat{a}_2). \tag{A.20}$$

Para saltos entre todos os vizinhos da rede, a equação (A.20) se extende para

$$\hat{H}_D = \frac{D}{(\Delta x)^2}\sum_{\langle ij\rangle}(\hat{a}_j^\dagger - \hat{a}_i^\dagger)(\hat{a}_i - \hat{a}_j) \tag{A.21}$$

que é o Hamiltoniano associado à difusão das partículas na rede e corresponde ao primeiro termo do lado direito da equação (A.13) com $\Gamma \equiv \frac{D}{(\Delta x)^2}$. As equações de movimento para $P(\{n\},t)$ e seus momentos nesta representação são idênticas obviamente às que seguem diretamente da equação mestra. Porém, neste ponto podemos ver a vantagem do uso do formalismo de Doi: a equação mestra original fica complicada pela presença de fatores com $n$ e $n^2$ que estão ausentes na representação de Doi. O formalismo de "segunda quantização" fornece o palco natural para a descrição de partículas independentes que podem variar em número, podendo ser criadas e/ou destruídas.

**Múltiplas espécies:** Em reações de duas espécies de partículas, por exemplo $A+B\to\emptyset$, a equação mestra é definida em termos dos números de ocupação das partículas $A$ e $B$, $P(\{m\},\{n\},t)$. Para a representação de Doi, introduzimos operadores de criação e aniquilação distintos para cada uma das espécies: $\hat{a}_i, \hat{a}_i^\dagger, \hat{b}_i$ e $\hat{b}_i^\dagger$ e definimos o estado

$$|\phi(t)\rangle = \sum_{\{m\},\{n\}} P(\{m\},\{n\},t)\prod_i (\hat{a}_i^\dagger)^{m_i}(\hat{b}_i^\dagger)^{n_i}|0\rangle. \tag{A.22}$$

A generalização para mais de duas espécies é trivial.

**Hamiltonianos de Doi:** Em qualquer reação descrita por processos do tipo $k_1X_1 + k_2X_2 + \cdots + k_nX_n \to l_1Y_1 + l_2Y_2 + \cdots + l_mY_m$, cada processo contribui com dois termos para $\hat{H}$ da forma

$$(\text{Taxa})\,[(\text{Reagentes}) - (\text{Produto})] \tag{A.23}$$

onde

- Reagentes = operadores de criação e aniquilação para cada reagente, ordenados normalmente;
- Produto = operador de aniquilação para cada reagente, operador de criação para cada produto, ordenados normalmente.

**Exemplos:**

1. $A+A\to\emptyset$ : Temos dois reagentes iguais a $A$ que induzem o aparecimento do termo $\lambda(\hat{a}^\dagger)^2\hat{a}^2$ no Hamiltoniano, correspondente ao termo Reagentes na equação (A.23). Como não temos nenhum produto nesta reação, o termo correspondente à Produto em (A.23) será $\lambda\hat{a}^2$ de modo que o Hamiltoniano completo fica
$$\hat{H}_{A+A\to\emptyset} = \lambda[(\hat{a}^\dagger)^2\hat{a}^2 - \hat{a}^2].$$
2. $A+A\to A$ : Usando um raciocínio análogo ao usado acima, teremos
$$\hat{H}_{A+A\to A} = \lambda[(\hat{a}^\dagger)^2\hat{a}^2 - \hat{a}^\dagger\hat{a}^2].$$
3. $A\to A+A$ :
$$\hat{H}_{A\to A+A} = \lambda[\hat{a}^\dagger\hat{a} - (\hat{a}^\dagger)^2\hat{a}].$$

4. $A+B \to C$ :
$$\hat{H}_{A+B\to C} = \lambda[\hat{a}^\dagger \hat{b}^\dagger \hat{a}\hat{b} - \hat{c}^\dagger \hat{a}\hat{b}].$$

5. Salto do sítio 1 para o sítio 2:
$$\hat{H}_{1\to 2} = \Gamma[(\hat{a}_1)^\dagger \hat{a}_1 - (\hat{a}_2)^\dagger \hat{a}_1].$$

Obtemos pois, regras gerais para obtermos o Hamiltoniano de Doi para qualquer reação descrita por processos do tipo $k_1X_1 + k_2X_2 + \cdots + k_nX_n \to l_1Y_1 + l_2Y_2 + \cdots + l_mY_m$.

### A.2.1. Comparação com o método da segunda quantização da mecânica quântica

Devemos ter em mente vários fatos enquanto trabalhamos com o método da segunda quantização para os processos estocásticos clássicos discutidos aqui. Existem algumas diferenças imediatas com relação ao modo como o método é utilizado na mecânica quântica:

- Diferentemente da equação de Schrodinger, aqui não existe o fator $i$ na equação (A.14).
- O operador "quase" Hamiltoniano $(\hat{H})$ geralmente *não* é Hermitiano.
- A diferença mais importante está no cálculo dos valores esperados de operadores. O valor esperado do operador $\hat{A}$ quando o sistema está no estado $|\phi(t)\rangle$ *não* é $\langle\phi|\hat{A}|\phi\rangle$ como na teoria quântica porque $\langle\phi|\hat{A}|\phi\rangle$ é bilinear nas probabilidades $P(\{n_i\})$.
- Um observável em um processo estocástico clássico, digamos $A(\{n_i\})$, pode ser representado por um operador $\hat{A}$, que é diagonal na base de Fock, pela prescrição de substituir $a_i^\dagger \hat{a}_i$ no lugar de $n_i$.
- Para definir uma expressão para o valor esperado em termos dos operadores, precisamos definir o *estado projeção* $\langle\mathcal{P}|$ com as seguintes propriedades:
$$\langle\mathcal{P}|0\rangle = 1, \qquad \langle\mathcal{P}|\hat{a}_i^\dagger = \langle\mathcal{P}| \tag{A.24}$$
As equações acima podem ser satisfeitas definindo $\langle\mathcal{P}|$ como
$$\langle\mathcal{P}| = \langle 0|e^{\sum_i \hat{a}_i} \tag{A.25}$$
**Demonstração:** Ver apêndice B.3.
- Para um processo estocástico clássico, o valor esperado de um observável $A(\{n_i\})$ é definido como
$$\langle A\rangle = \sum_{\{n_i\}} P(\{n_i\};t)A(\{n_i\}). \tag{A.26}$$
Das propriedades do estado projeção, temos que $\langle\mathcal{P}|\prod_{\{n_i\}} a_i^{\dagger n_i}|0\rangle = 1$. Usando este fato na equação (A.26), vem

$$\begin{aligned}
\langle A\rangle &= \sum_{\{n_i\}} P(\{n_i\};t)A(\{n_i\})\langle\mathcal{P}|\prod_{\{n_i\}} a_i^{\dagger n_i}|0\rangle \\
&= \sum_{\{n_i\}} P(\{n_i\};t)\langle\mathcal{P}|A(\{n_i\})\prod_{\{n_i\}} a_i^{\dagger n_i}|0\rangle \\
&= \sum_{\{n_i\}} P(\{n_i\};t)\langle\mathcal{P}|A(\{n_i\})|n_1,n_2,\cdots\rangle \\
&= \sum_{\{n_i\}} P(\{n_i\};t)\langle\mathcal{P}|\hat{A}|n_1,n_2,\cdots\rangle
\end{aligned}$$

onde $\hat{A}$ é o operador obtido substituindo $n_i$ por $a_i^\dagger \hat{a}_i$ em $A(\{n_i\})$. É importante notar aqui que o operador $\hat{A}$ é independente dos índices $n_i$ e assim

$$\langle A\rangle = \langle\mathcal{P}|\hat{A}|\phi(t)\rangle = \langle\mathcal{P}|\hat{A}\, e^{-\hat{H}t}|\phi(0)\rangle. \tag{A.27}$$

- Colocando $\hat{A} = \mathbf{1}$ na equação (A.27) obtemos

$$\langle \mathcal{P}|\phi(t)\rangle = \langle \mathcal{P}|e^{-\hat{H}t}|\phi(0)\rangle = 1. \tag{A.28}$$

  Esta equação significa que a probabilidade total é conservada durante a evolução temporal.

- Colocando $t = 0$ na equação (A.28) obtemos

$$\langle \mathcal{P}|\phi(0)\rangle = 1. \tag{A.29}$$

  Como a equação acima e a equação (A.28) são verdadeiras para qualquer $|\phi(0)\rangle$, devemos ter

$$\langle \mathcal{P}|\hat{H} = 0. \tag{A.30}$$

- Se $\hat{H}$ for escrito na forma ordenada normal, isto é, se todos os operadores de criação $a^\dagger$ estiverem à esquerda de todos os operadores de aniquilação $\hat{a}$, então de (A.25) e de (A.30), temos que $\hat{H}$ deve ser nulo se todos os operadores $a^\dagger$ forem substituidos por 1.

### A.2.2. O deslocamento de Doi

Usando a definição do operador projeção $\langle \mathcal{P}| = \langle 0|e^{\sum_i \hat{a}_i}$ e a definição de experança de um observável dada pela equação (A.27), temos

$$\langle A\rangle = \langle 0|e^{\sum_i \hat{a}_i}\hat{A}e^{-\hat{H}t}|\phi(0)\rangle. \tag{A.31}$$

O fator $e^{\sum_i \hat{a}_i}$ pode ser comutado através dos operadores e retornar

$$\langle A\rangle = \langle 0|\hat{A}_{\text{shifted}}e^{-\hat{H}_{\text{shifted}}t}e^{\sum_i \hat{a}_i}|\phi(0)\rangle \tag{A.32}$$

onde os operadores deslocados são obtidos dos não deslocados pela substituição de $1 + a_i^\dagger$ no lugar de $a_i^\dagger$. Este passo é consequência do que foi feito no apêndice (B.3), de onde pode-se tirar a identidade $e^{\hat{a}}f(a^\dagger) = f(a^\dagger + 1)e^{\hat{a}}$. O Hamiltoniano com $\{a_j^\dagger\} \to a_j^\dagger + 1$ é conhecido como o Hamiltoniano deslocado de Doi e a vantagem deste procedimento é que o Hamiltoniano fica ordenado normalmente (todos os $a^\dagger$ à direita dos $\hat{a}$ ) e como consequência o valor da esperança é zero.

Apêndice B

# Formulação contínua em uma teoria de campos

## B.1. Representação em estados coerentes e integrais funcionais

Partindo da representação *a la* segunda quantização, uma teoria de campos pode ser obtida pelas mesmas técnicas desenvolvidas para os sistemas quânticos de muitas partículas. Uma boa discussão desses métodos, em particular sobre a representação em estados coerentes pode ser obtida em [62] assim como em [23]. Mas aqui procuraremos abordar o assunto da maneira mais autocontida possível, onde alguns dos detalhes a respeito dos estados coerentes estão disponíveis no apêndice B.2.

### B.1.1. Representação em estados coerentes

A idéia básica da construção de uma integral funcional para operadores de campo é, como no caso da mecânica quântica, segmentar a evolução temporal do (quase) Hamiltoniano em intervalos de tempo infinitesimais e absorver o máximo possível da dinâmica durante um curto intervalo de tempo em um conjunto adequadamente escolhido de auto-estados. Mas como estes auto-estados devem ser escolhidos? No contexto da mecânica quântica de uma única partícula, a estrutura do Hamiltoniano sugere uma representação em termos dos auto-estados da coordenada e do momento. Aqui, dados os Hamiltonianos convenientemente descritos em termos de operadores de criação e aniquilação, uma idéia óbvia seria procurar por auto-estados destes operadores. Tais estados existem e são chamados *estados coerentes*. Como auto-estados do operador criação não são normalizáveis [63], focaremos nos auto-estados do operador aniquilação.

Vamos denotar o estado coerente por $|\phi\rangle$, então

$$\hat{a}|\phi\rangle = \phi|\phi\rangle. \tag{B.1}$$

Uma forma possível para o estado coerente é

$$|\phi\rangle = N(\phi)\, e^{\phi a^\dagger}|0\rangle \tag{B.2}$$

onde $N(\phi)$ é uma função de $\phi$ a ser determinada. Podemos checar explicitamente que o estado dado acima

é um estado coerente:

$$\begin{aligned}
\hat{a}|\phi\rangle &= N(\phi)\,\hat{a}\,e^{\phi a^\dagger}|0\rangle \\
&= N(\phi)\left[\hat{a}, e^{\phi a^\dagger}\right]|0\rangle \qquad (\text{usamos} \quad \hat{a}|0\rangle = 0) \\
&= N(\phi)\left[\frac{\partial}{\partial a^\dagger}, e^{\phi a^\dagger}\right]|0\rangle \\
&= N(\phi)\,\phi\,e^{\phi a^\dagger}|0\rangle \\
&= \phi|\phi\rangle
\end{aligned}$$

Como a fase global do vetor de estado não tem significado, podemos escolher $N(\phi)$ real. A constante de normalização $N(\phi)$ pode ser determinada exigindo

$$\begin{aligned}
1 &= \langle\phi|\phi\rangle \\
&= N^2(\phi)\langle 0|e^{\phi^*\hat{a}}e^{\phi\,a^\dagger}|0\rangle \\
&= N^2(\phi)\left\langle 0\left|\sum_{m=0}^{\infty}\frac{\phi^*\hat{a}^m}{m!}\sum_{n=0}^{\infty}\frac{\phi^n\,a^{\dagger n}}{n!}\right|0\right\rangle
\end{aligned} \tag{B.3}$$

Para $m \neq n$,

$$\langle 0|\hat{a}^m a^{\dagger n}|0\rangle = 0.$$

Para $m = n$, temos

$$\begin{aligned}
\langle 0|\hat{a}^n a^{\dagger n}|0\rangle &= \langle 0|\hat{a}^{n-1}\,[\hat{a}, a^{\dagger n}]|0\rangle \qquad (\text{usando} \quad \hat{a}|0\rangle = 0) \\
&= \langle 0|\hat{a}^{n-1} n a^{\dagger(n-1)}|0\rangle \qquad (\text{usando} \quad (A.9)) \\
&= n\langle 0|\hat{a}^{n-1}a^{\dagger(n-1)}|0\rangle \\
&= n(n-1)\langle 0|\hat{a}^{n-2}a^{\dagger(n-2)}|0\rangle \\
&\quad\vdots \\
&= n!
\end{aligned} \tag{B.4}$$

Portanto, temos

$$\langle 0|\hat{a}^m a^{\dagger n}|0\rangle = n!\delta_{m,n} \tag{B.5}$$

Substituindo este resultado em (B.3), vem

$$\begin{aligned}
1 &= N^2(\phi)\sum_{m,n=0}^{\infty}\frac{\phi^{*m}\phi^n}{m!n!}n!\delta_{m,n} \\
&= N^2(\phi)\sum_{n=0}^{\infty}\frac{|\phi|^{2n}}{n!} \\
&= N^2(\phi)e^{|\phi|^2} \\
&\Rightarrow \quad N(\phi) = e^{-\frac{1}{2}|\phi|^2}
\end{aligned} \tag{B.6}$$

O estado coerente normalizado é então dado por

$$|\phi\rangle = e^{-\frac{1}{2}|\phi|^2+\phi a^\dagger}|0\rangle \tag{B.7}$$

#### Estado projeção

O estado projeção $\langle \mathcal{P}|$ definido em (A.25) é também um estado coerente, já que

$$\langle \mathcal{P}| = \langle 0|e^{\hat{a}} = e^{\frac{1}{2}}\langle 1| \tag{B.8}$$

onde usamos (B.7) fazendo $\phi \to 1$, ou seja, $|1\rangle = e^{-\frac{1}{2}+a^\dagger}|0\rangle$.

#### Produto interno entre dois estados coerentes

Para uso subsequente vamos calcular uma expressão para o produto interno entre dois estados coerentes $|\phi_1\rangle$ e $|\phi_2\rangle$ :

$$\begin{aligned}
\langle\phi_1|\phi_2\rangle &= \left\langle 0\middle| e^{-\frac{1}{2}|\phi_1|^2+\phi_1^*\hat{a}}e^{-\frac{1}{2}|\phi_2|^2+\phi_2 a^\dagger}\middle|0\right\rangle \\
&= e^{-\frac{1}{2}|\phi_1|^2-\frac{1}{2}|\phi_2|^2}\left\langle 0\middle| e^{\phi_1^*\hat{a}}e^{\phi_2 a^\dagger}\middle|0\right\rangle \\
&= e^{-\frac{1}{2}|\phi_1|^2-\frac{1}{2}|\phi_2|^2}\left\langle 0\middle| \sum_{m=0}^{\infty}\frac{\phi_1^{*m}\hat{a}^m}{m!}\sum_{n=0}^{\infty}\frac{\phi_2^n a^{\dagger n}}{n!}\middle|0\right\rangle \\
&= e^{-\frac{1}{2}|\phi_1|^2-\frac{1}{2}|\phi_2|^2}\sum_{m,n=0}^{\infty}\frac{\phi_1^{*m}\phi_2^n}{m!\,n!}\langle 0|\hat{a}^m a^{\dagger n}|0\rangle \\
&= e^{-\frac{1}{2}|\phi_1|^2-\frac{1}{2}|\phi_2|^2}\sum_{m,n=0}^{\infty}\frac{\phi_1^{*m}\phi_2^n}{m!\,n!}n!\,\delta_{m,n} \\
&= e^{-\frac{1}{2}|\phi_1|^2-\frac{1}{2}|\phi_2|^2}\sum_{n=0}^{\infty}\frac{\phi_1^{*n}\phi_2^n}{n!} \\
&= e^{-\frac{1}{2}|\phi_1|^2-\frac{1}{2}|\phi_2|^2}e^{\phi_1^*\phi_2} \\
\Rightarrow \langle\phi_1|\phi_2\rangle &= e^{-\frac{1}{2}|\phi_1|^2-\frac{1}{2}|\phi_2|^2+\phi_1^*\phi_2}
\end{aligned} \tag{B.9}$$

#### Resolução da identidade em termos de estados coerentes

É possível mostrar que a resolução da identidade escrita em termos do estados $\phi$ é dada por

$$\mathbf{1} = \int \frac{d^2\phi}{\pi}|\phi\rangle\langle\phi|. \tag{B.10}$$

Veja apêndice (B.2.2) para maiores detalhes.

### B.1.2. Formulação em integral funcional

Partiremos dos resultados relacionados aos estados coerentes discutidos acima a agora obteremos a formulação em integral funcional para os processos estocásticos de interesse.

#### Processo estocástico com uma única espécie em dimensão 0

Por simplicidade derivaremos primeiro a formulação em integral de caminho de um processo estocástico para uma única espécie em um único sítio da rede, evitando complicações desnecessárias na notação.

Seja $\hat{H}$ o quase-Hamiltoniano do processo. Sejam $\hat{a}$, $a^\dagger$ e $|0\rangle$ o operador aniquilação, o de criação e o estado de vácuo respectivamente. O estado do sistema é dado por (A.11)* e a evolução temporal é dada pela equação (A.12).

Para derivar a formulação em integral funcional partimos de (A.12)

$$|\psi(t)\rangle = e^{-\hat{H}t}|\psi(0)\rangle. \tag{B.11}$$

Vamos discretizar o tempo $t$ em $N$ subintervalos de comprimento $\Delta t$, i. e.

$$\Delta t = \frac{t}{N}. \tag{B.12}$$

Estamos interessados no limite $\Delta t \to 0$. Equação (B.11) pode ser escrita como

$$|\psi(t)\rangle = \lim_{\Delta t\to 0} e^{-\hat{H}N\Delta t}|\psi(0)\rangle \tag{B.13}$$

$$\begin{aligned} |\psi(t)\rangle &= \lim_{\Delta t\to 0} e^{-\hat{H}N\Delta t}|\psi(0)\rangle \\ &= \lim_{\Delta t\to 0} e^{-\hat{H}\Delta t}e^{-\hat{H}\Delta t}\cdots e^{-\hat{H}\Delta t}|\psi(0)\rangle \end{aligned} \tag{B.14}$$

Inserindo a resolução da identidade (B.10) entre cada subintervalo de tempo na equação acima, obteremos

$$\begin{aligned} |\psi(t)\rangle &= \lim_{\Delta t\to 0}\int \frac{d^2\phi_t}{\pi}|\phi_t\rangle\langle\phi_t|e^{-\hat{H}\Delta t}\int \frac{d^2\phi_{t-\Delta t}}{\pi}|\phi_{t-\Delta t}\rangle\langle\phi_{t-\Delta t}|e^{-\hat{H}\Delta t} \\ &\quad \int \frac{d^2\phi_{t-2\Delta t}}{\pi}|\phi_{t-2\Delta t}\rangle\langle\phi_{t-2\Delta t}|e^{-\hat{H}\Delta t} \\ &\quad \vdots \\ &\quad \int \frac{d^2\phi_{\Delta t}}{\pi}|\phi_{\Delta t}\rangle\langle\phi_{\Delta t}|e^{-\hat{H}\Delta t}\int \frac{d^2\phi_0}{\pi}|\phi_0\rangle\langle\phi_0|\psi(0)\rangle \\ &= \lim_{\Delta t\to 0}\mathcal{N}^{-1}\int\left(\prod_{\tau=0}^{t} d^2\phi_\tau\right)|\phi_t\rangle\langle\phi_t|e^{-\hat{H}\Delta t}|\phi_{t-\Delta t}\rangle\langle\phi_{t-\Delta t}|e^{-\hat{H}\Delta t}|\phi_{t-2\Delta t}\rangle \\ &\quad \cdots\langle\phi_{\Delta t}|e^{-\hat{H}\Delta t}|\phi_0\rangle\langle\phi_0|\psi(0)\rangle \\ &= \lim_{\Delta t\to 0}\mathcal{N}^{-1}\int\left(\prod_{\tau=0}^{t} d^2\phi_\tau\right)|\phi_t\rangle\left[\prod_{\tau=\Delta t}^{t}\langle\phi_\tau|e^{-\hat{H}\Delta t}|\phi_{\tau-\Delta t}\rangle\right]\langle\phi_0|\psi(0)\rangle \end{aligned} \tag{B.15}$$

onde $\mathcal{N}$ é a constante de normalização.

Seja $A(n)$ um observável. O operador correspondente $\hat{A}$ é definido substituindo $n$ por $a^\dagger\hat{a}$ em $A(n)$. O valor esperado é dado por (A.27) como

*Com $\psi(t)$ no lugar de $\phi(t)$.

$$\begin{aligned}\langle A\rangle &= \langle \mathcal{P}|\hat{A}|\psi(t)\rangle \\ &= e^{\frac{1}{2}}\langle 1|\hat{A}|\psi(t)\rangle \\ &= \mathcal{N}^{-1}\lim_{\Delta t\to 0}\int\left(\prod_{\tau=0}^{t} d^2\phi_\tau\right)\langle 1|\hat{A}|\phi_t\rangle\left[\prod_{\tau=\Delta t}^{t}\langle\phi_\tau|e^{-\hat{H}\Delta t}|\phi_{\tau-\Delta t}\rangle\right]\langle\phi_0|\psi(0)\rangle. \end{aligned} \tag{B.16}$$

O fator $e^{\frac{1}{2}}$ foi absorvido na constante de normalização.

Vamos agora calcular cada termo da equação (B.16) um a um. Consideremos o termo do meio:

$$\begin{aligned}\langle\phi_\tau|e^{-\hat{H}\Delta t}|\phi_{t-\Delta t}\rangle &= \langle\phi_\tau|[\mathbf{1}-\hat{H}\Delta t+O(\Delta t^2)]|\phi_{\tau-\Delta t}\rangle \\ &= \langle\phi_\tau|\phi_{\tau-\Delta t}\rangle-\langle\phi_\tau|\hat{H}|\phi_{\tau-\Delta t}\rangle\Delta t+O(\Delta t^2) \\ &= \langle\phi_\tau|\phi_{\tau-\Delta t}\rangle-\langle\phi_\tau|\hat{H}(\phi_\tau^*,\phi_{\tau-\Delta t})|\phi_{\tau-\Delta t}\rangle\Delta t+O(\Delta t^2) \\ &= \langle\phi_\tau|\phi_{\tau-\Delta t}\rangle-\hat{H}(\phi_\tau^*,\phi_{\tau-\Delta t})\langle\phi_\tau||\phi_{\tau-\Delta t}\rangle\Delta t+O(\Delta t^2) \\ &= \langle\phi_\tau|\phi_{\tau-\Delta t}\rangle[\mathbf{1}-\hat{H}(\phi_\tau^*,\phi_{\tau-\Delta t})+O(\Delta t^2)] \\ &= \langle\phi_\tau|\phi_{\tau-\Delta t}\rangle e^{-\hat{H}(\phi_\tau^*,\phi_{\tau-\Delta t})\Delta t}\end{aligned} \tag{B.17}$$

onde $\hat{H}(\phi_\tau^*,\phi_{\tau-\Delta t})$ é obtido substituindo $\hat{a}$ por $\phi_{\tau-\Delta t}$ e $a^\dagger$ por $\phi_\tau^*$ na forma ordenada normal. Usando agora o produto interno de estados coerentes (B.9),

$$\begin{aligned}\langle\phi_\tau|\phi_{\tau-\Delta t}\rangle &= e^{-\frac{1}{2}|\phi_\tau|^2-\frac{1}{2}|\phi_{\tau-\Delta t}|^2+\phi_\tau^*\phi_{\tau-\Delta t}} \\ &= e^{\frac{1}{2}(|\phi_\tau|^2-|\phi_{\tau-\Delta t}|^2)}e^{-|\phi_\tau|^2+\phi_\tau^*\phi_{\tau-\Delta t}} \\ &= e^{\frac{1}{2}(|\phi_\tau|^2-|\phi_{\tau-\Delta t}|^2)}e^{-\phi_\tau^*(\phi_\tau-\phi_{\tau-\Delta t})}\end{aligned} \tag{B.18}$$

Desta forma,

$$\begin{aligned}\prod_{\tau=\Delta t}^{t}\langle\phi_\tau|e^{-\hat{H}\Delta t}|\phi_{t-\Delta t}\rangle &= \prod_{\tau=\Delta t}^{t}\langle\phi_\tau|\phi_{\tau-\Delta t}\rangle e^{-\hat{H}(\phi_\tau^*,\phi_{\tau-\Delta t})\Delta t} \\ &= \prod_{\tau=\Delta t}^{t} e^{\frac{1}{2}(|\phi_\tau|^2-|\phi_{\tau-\Delta t}|^2)}e^{-\phi_\tau^*(\phi_\tau-\phi_{\tau-\Delta t})}e^{-\hat{H}(\phi_\tau^*,\phi_{\tau-\Delta t})\Delta t} \\ &= \left[\prod_{\tau=\Delta t}^{t} e^{\frac{1}{2}(|\phi_\tau|^2-|\phi_{\tau-\Delta t}|^2)}\right]\left[\prod_{\tau=\Delta t}^{t} e^{-\phi_\tau^*(\phi_\tau-\phi_{\tau-\Delta t})}e^{-\hat{H}(\phi_\tau^*,\phi_{\tau-\Delta t})\Delta t}\right] \\ &= e^{\frac{1}{2}\sum_{\tau=\Delta t}^{t}(|\phi_\tau|^2-|\phi_{\tau-\Delta t}|^2)}e^{-\sum_{\tau=\Delta t}^{t}[\phi_\tau^*(\phi_\tau-\phi_{\tau-\Delta t})+\hat{H}(\phi_\tau^*,\phi_{\tau-\Delta t})\Delta t]} \\ &= e^{\frac{1}{2}[|\phi_t|^2-|\phi_{t-\Delta t}|^2+|\phi_{t-\Delta t}|^2-|\phi_{t-2\Delta t}|^2+\cdots+|\phi_{\Delta t}|^2-|\phi_0|^2]} \\ &\quad\times e^{-\sum_{\tau=\Delta t}^{t}[\phi_\tau^*(\phi_\tau-\phi_{\tau-\Delta t})+\hat{H}(\phi_\tau^*,\phi_{\tau-\Delta t})\Delta t]} \\ &= e^{\frac{1}{2}(|\phi_t|^2-|\phi_0|^2)}e^{-\sum_{\tau=\Delta t}^{t}[\phi_\tau^*(\phi_\tau-\phi_{\tau-\Delta t})+\hat{H}(\phi_\tau^*,\phi_{\tau-\Delta t})\Delta t]}\end{aligned} \tag{B.19}$$

Vamos agora desenvolver um pouco o termo $\langle 1|\hat{A}|\phi_t\rangle$ na equação (B.16):

$$\begin{aligned}\langle 1|\hat{A}|\phi_t\rangle &= A(\phi_t)\langle 1|\phi_t\rangle \\ &= A(\phi_t)e^{-\frac{1}{2}1^2-\frac{1}{2}|\phi_t|^2+\phi_t} \\ &= A(\phi_t)e^{-\frac{1}{2}-\frac{1}{2}|\phi_t|^2+\phi_t} \end{aligned} \tag{B.20}$$

onde $A(\phi_t)$ é obtido substituindo 1 no lugar de $a^\dagger$ e $\phi_t$ no lugar de $\hat{a}$ no operador $\hat{A}$ escrito na forma ordenada normal.

Vamos agora desenvolver $\langle\phi_0|\psi(0)\rangle$ em (B.16) utilizando como distribuição inicial a distribuição de *Poisson*,

$$P(n,0) = \frac{\bar{n}_0^n}{n!}e^{-\bar{n}_0} \tag{B.21}$$

Primeiramente

$$\begin{aligned}|\psi(0)\rangle &= \sum_n P(n,0)|n\rangle \\ &= \sum_n \frac{\bar{n}_0^n}{n!}e^{-\bar{n}_0}a^{\dagger n}|0\rangle \\ &= e^{-\bar{n}_0}e^{\bar{n}_0 a^\dagger}|0\rangle \\ &= e^{-\bar{n}_0}|\bar{n}_0\rangle \end{aligned} \tag{B.22}$$

O próprio estado inicial $|\psi(0)\rangle$ é um estado coerente para distribuições iniciais de Poisson. Em sistemas $d-$dimensionais com difusão, é interessante notar que um processo de difusão partindo de uma distribuição de Poisson na ausência de ruído permanece uma distribuição de Poisson nos tempos subsequentes. Portanto, as flutuações estocásticas nestes sistemas descrevem apenas os *desvios da distribuição Poissoniana*. Este fato está relacionado com o surgimento de fatores negativos de origem complexa[†] nas correlações do ruído que emergem naturalmente da teoria. Veremos um exemplo desta situação posteriormente.

Agora,

$$\begin{aligned}\langle\phi_0|\psi(0)\rangle &= e^{-\bar{n}_0}\langle\phi_0|\bar{n}_0\rangle \\ &= e^{-\bar{n}_0}e^{-\frac{1}{2}|\phi_0|^2-\frac{1}{2}|\bar{n}_0|^2+\phi_0^*\bar{n}_0}. \end{aligned} \tag{B.23}$$

Substituindo as equações (B.19), (B.20) e (B.23) em (B.16) e absorvendo todas as constantes no fator de normalização, obteremos

[†]Complexo no sentido do conjunto dos números imaginários $\mathbb{Z}$.

$$
\begin{aligned}
\langle A\rangle &= \mathcal{N}^{-1}\lim_{\Delta t\to 0}\int\left(\prod_{\tau=0}^{t} d^2\phi_\tau\right) A(\phi_t)e^{-\frac{1}{2}|\phi_t|^2+\phi_t} \\
&\quad\times e^{\frac{1}{2}(|\phi_t|^2-|\phi_0|^2)}e^{-\sum_{\tau=\Delta t}^{t}[\phi_t^*(\phi_t-\phi_{\tau-\Delta t})+\hat{H}(\phi_\tau^*,\phi_{\tau-\Delta t})\Delta t]}e^{-\frac{1}{2}|\phi_0|^2+\phi_0^*\bar{n}_0} \\
&= \mathcal{N}^{-1}\lim_{\Delta t\to 0}\int\left(\prod_{\tau=0}^{t} d^2\phi_\tau\right) A(\phi_t)e^{\phi_t}e^{-|\phi_0|^2}e^{\phi_0^*\bar{n}_0} \\
&\quad\times\exp\left\{-\sum_{\tau=\Delta t}^{t}[\phi_\tau^*(\phi_\tau-\phi_{\tau-\Delta t})+\hat{H}(\phi_\tau^*,\phi_{\tau-\Delta t})\Delta t]\right\} \\
&= \mathcal{N}^{-1}\lim_{\Delta t\to 0}\int\left(\prod_{\tau=0}^{t} d^2\phi_\tau\right) A(\phi_t)e^{\phi_t}e^{-|\phi_0|^2}e^{\phi_0^*\bar{n}_0} \\
&\quad\times\exp\left\{-\sum_{\tau=\Delta t}^{t}\left[\phi_\tau^*\left(\frac{\phi_\tau-\phi_{\tau-\Delta t}}{\Delta t}\right)\Delta t+\hat{H}(\phi_\tau^*,\phi_{\tau-\Delta t})\Delta t\right]\right\} \\
&\overset{\Delta t\to 0}{=} \mathcal{N}^{-1}\int\mathcal{D}\phi\;\mathcal{D}\phi^* A[\phi(t)]e^{\phi(t)}e^{-|\phi(0)|^2}e^{\phi^*(0)\bar{n}_0} \\
&\quad\times\exp\left\{-\int_0^t dt'\left[\phi^*(t')\frac{\partial\phi(t')}{\partial t'}+\hat{H}[\phi^*(t'),\phi(t')]\right]\right\} \\
&= \mathcal{N}^{-1}\int\mathcal{D}\phi\;\mathcal{D}\phi^*\,A[\phi(t)]\exp\{-S[\phi^*,\phi]_0^t\}
\end{aligned}
\tag{B.24}
$$

onde

$$
\begin{aligned}
S[\phi^*,\phi]_0^t &= -[\phi(t_f)-|\phi(0)|^2+\phi^*(0)\bar{n}_0]+\int_0^{t_f}dt\left\{\phi^*(t)\frac{\partial\phi(t)}{\partial t}+\hat{H}[\phi^*(t),\phi(t)]\right\} \\
&= -[\phi(t_f)+\phi^*(0)\{\bar{n}_0-\phi(0)\}]+\int_0^{t_f}dt\{\phi^*(t)\;\partial_t\phi(t)+\hat{H}[\phi^*(t),\phi(t)]\}
\end{aligned}
\tag{B.25}
$$

**Pontos importantes:**

- Ao tomarmos o limite $\Delta t\to 0$, substituimos $\phi_\tau^*$ e $\phi_{\tau-\Delta t}$ por $\phi^*(t')$ e $\phi(t')$. Por isso, sempre que um termo contiver ambos $\phi^*(t')$ e $\phi(t')$, $\phi^*(t')$ deverá ser considerado estar em um tempo posterior a $\phi(t')$.
- A medida é definida como

$$
\mathcal{D}\phi\;\mathcal{D}\phi^* = \lim_{\Delta t\to 0}\prod_{\tau=0}^{t} d^2\phi_\tau. \tag{B.26}
$$

- A constante de normalização é determinada impondo $A(\phi)=1$ na equação (B.24):

$$
\begin{aligned}
1 &= \mathcal{N}^{-1}\int\mathcal{D}\phi\;\mathcal{D}\phi^*\;1\;\exp\{-S[\phi^*,\phi]_0^t\} \\
\Rightarrow\mathcal{N} &= \int\mathcal{D}\phi\;\mathcal{D}\phi^*\exp\{-S[\phi^*,\phi]_0^t\}
\end{aligned}
\tag{B.27}
$$

**Termo inicial**

A integral com relação a $\phi_0^*$ na equação (B.20) pode ser feita:

$$
\begin{aligned}
\int d\phi_0^*\;e^{-|\phi_0|^2}e^{\phi_0^*\bar{n}_0} &= \int d\phi_0^*\exp\{\phi_0^*(\bar{n}_0-\phi_0)\} \\
&= \delta(\bar{n}_0-\phi_0)
\end{aligned}
\tag{B.28}
$$

Agora a integral sobre $\phi_0$ também pode ser feita o que reforça a condição inicial no integrando. O termo $[\phi^*(0)\{\bar{n}_0 - \phi(0)\}]$ pode ser tirado da ação (B.25), já que a delta de Dirac impõe $\phi(0) = \bar{n}_0$. Porém, uma integral de caminho com o dado vínculo não é diretamente susceptível aos métodos perturbativos.

**Esquema para o cálculo perturbativo**

A parte da ação $S$ que é bilinear nos campos ($\propto \phi^*\phi$) é escolhida como "ação referência" e resolvida exatamente. Os termos restantes são tratados perturbativamente. Nos cálculos perturbativos, um termo será zero se todo $\phi$ nele não puder ser pareado com um $\phi^*$ em um tempo anterior.

Na exponencial de $\phi^*(0)\phi(0)$, todos os termos exceto o primeiro são nulos, já que não há nenhum $\phi^*$ anterior à $t = 0$. Isto é equivalente a desprezar $|\phi|^2$ na ação. Desta forma, ficamos apenas com $e^{-\bar{n}_0\phi^*(0)}$ como termo inicial.

**Termo final**

O termo $\phi(t_f)$ na ação (B.25) pode ser tratado realizando o seguinte "deslocamento" no campo:

$$\phi^*(t) = 1 + \bar{\phi}(t) \tag{B.29}$$

Desta forma,

$$\begin{aligned} \int_0^{t_f} dt\ \phi^*(t)\ \partial_t\phi(t) &= \int_0^{t_f} dt(1+\bar{\phi}(t))\partial_t\phi(t) \\ &= \phi(t_f) - \phi(0) + \int_0^{t_f} dt\ \bar{\phi}(t)\partial_t\phi(t) \end{aligned} \tag{B.30}$$

A ação em termos do campo deslocado se torna

$$S[\bar{\phi}(t),\phi]_0^{t_f} = -[\phi(0) + (1+\bar{\phi}(0))\bar{n}_0] + \int_0^{t_f} dt\{\bar{\phi}(t)\partial_t\phi(t) + \hat{H}[\bar{\phi}(t),\phi(t)]\}. \tag{B.31}$$

Mais uma vez desprezamos $\phi(0)$ da ação por não existir um $\bar{\phi}$ pareado anterior a $t = 0$. O termo $\bar{n}_0$ pode ser absorvido na constante de normalização. A ação se reduz a

$$S[\bar{\phi}(t),\phi]_0^{t_f} = -\bar{\phi}(0)\bar{n}_0 + \int_0^{t_f} dt\{\bar{\phi}(t)\partial_t\phi(t) + \hat{H}[\bar{\phi}(t),\phi(t)]\} \tag{B.32}$$

onde $\hat{H}[\bar{\phi}(t),\phi(t)]$ é obtido substituindo $1+\bar{\phi}(t)$ no lugar de $a^\dagger$ e $\phi(t)$ no lugar de $\hat{a}$.

### B.1.3. Processos estocásticos de uma única espécie em $d-$dimensões

De posse da formulação em integral de caminho para o caso de dimensão 0, não é difícil generalizar para $d$ dimensões. No apêndice (B.4) executa-se esta generalização bem como se obtém o limite contínuo da ação que fica determinada por

$$S[\bar{\phi},\phi]_0^{t_f} = -\int d^dx\ \bar{\phi}(\mathbf{x},0)\ \bar{n}_0 + \int_0^{t_f} dt \int d^dx\ \left[\bar{\phi}(\mathbf{x},t)(\partial_t - D\nabla^2)\phi(\mathbf{x},t) + \hat{H}'(\mathbf{x})\right] \tag{B.33}$$

onde $\hat{H}'(\mathbf{x})$ é a parte do Hamiltoniano que *não* corresponde à difusão.

#### Processos estocásticos de múltiplas espécies em dimensão $d$

A ação obtida em (B.84) e reproduzida na seção anterior pode ser generalizada para o caso de múltiplas espécies. Escrevendo diretamente esta generalização obteremos:

$$\begin{aligned} S[\bar{\phi}_1,\phi_1,\bar{\phi}_2,\phi_2,\cdots] &= -\int d^dx\left[\bar{\phi}_1(\mathbf{x},0)\,\bar{n}_{0,1}+\bar{\phi}_2(\mathbf{x},0)\,\bar{n})_{0,2}+\cdots\right] \\ &= +\int_0^{t_f} dt\int d^dx[\bar{\phi}_1(\mathbf{x},t)(\partial_t-D\nabla^2)\phi_1(\mathbf{x},t) \\ &+ \bar{\phi}_2(\mathbf{x},t)(\partial_d-D\nabla^2)\phi_2(\mathbf{x},t) \\ &\vdots \\ &+ \hat{H}'(\mathbf{x})] \end{aligned} \tag{B.34}$$

#### Exemplos

Neste ponto, vamos obter $H$ explícitamente para o processo de aniquilação de pares limitado por difusão, $A+A\to\emptyset$. Como o operador evolução associado (A.13) já está ordenado normalmente, obtemos diretamente

$$H(\{\phi^*\},\{\phi\}) = \frac{D}{h^2}\sum_{\langle ij\rangle}(\phi_i^*-\phi_j^*)(\phi_i-\phi_j)-\lambda\sum_i(1-(\phi_i^*)^2)\phi_i^2. \tag{B.35}$$

Tomamos o limite contínuo, substituindo diferenças finitas na rede por gradientes no espaço. A teoria de campo resultante, antes de qualquer transformação de variáveis será

$$S[\tilde{\phi},\phi] = \int d^dx\left\{-\phi(t_f)+\int_0^{t_f}dt\left[\tilde{\phi}\left(\partial_t-D\nabla^2\right)\phi-\lambda_0\left(1-\tilde{\phi}^2\right)\phi^2\right]-n_0\tilde{\phi}(0)\right\}, \tag{B.36}$$

onde $\lambda_0\equiv\lambda h^d$. Fazendo a mudança $\tilde{\phi}\to 1+\bar{\phi}$, obtemos

$$S[\bar{\phi},\phi] = \int d^dx\left\{\int_0^{t_f}dt\left[\bar{\phi}\left(\partial_t-D\nabla^2\right)\phi-\lambda_1\bar{\phi}\phi^2+\lambda_2\bar{\phi}^2\phi^2\right]-n_0\bar{\phi}(0)\right\} \tag{B.37}$$

com $\lambda_1=2\lambda_0$ e $\lambda_2=\lambda_0$.

A descrição para sistemas de múltiplas espécies requer, no nível da equação mestra, conjuntos de números de ocupação adicionais. Por exemplo, a equação mestra para a reação de aniquilação de duas espécies $A+B\to\emptyset$ emprega a probabilidade $P(\{m\},\{n\},t)$ onde $\{m\}$ e $\{n\}$ respectivamente denotam os conjuntos de números de ocupação das partículas $A$ e $B$. As partículas $A$ e $B$ se difundem na rede com constantes de difusão $D_A$ e $D_B$, possivelmente com $D_A\neq D_B$. Desenvolvendo todo o procedimento descrito acima, obteremos a seguinte ação [27]:

$$\begin{aligned} S[\bar{a},a,\bar{b},b] = \int d^dx\Bigg\{\int_0^{t_f}dt\Big[&\bar{a}\left(\partial_t-D_A\nabla^2\right)a+\bar{b}\left(\partial_t-D_B\nabla^2\right)b \\ &+\lambda_0(\bar{a}+\bar{b})ab+\lambda_0\bar{a}\bar{b}ab\Big]-a_0\bar{a}(0)-b_0\bar{b}(0)\Bigg\}. \end{aligned} \tag{B.38}$$

Generalização para múltiplas partículas é simples: para cada espécie de partícula nova, operadores da segunda quantização e campos correspondentes devem ser introduzidos. Os detalhes da reação ficam codificados na equação mestra. Com alguma prática, é simples partir diretamente da representação de Doi, como exemplificado na seção A.2.

A ação (B.38) é linear em $\bar{a}$ e $\bar{b}$. O extremo da ação com $\bar{b}=1$ é:

$$\frac{\delta S}{\delta \bar{a}} = (\partial_t - D_A\nabla^2)a + 2\lambda_0 ab - a_0\delta(t) = 0$$

e, com $\bar{a}=1$ :

$$\frac{\delta S}{\delta \bar{b}} = (\partial_t - D_B\nabla^2)b + 2\lambda_0 ab - b_0\delta(t) = 0.$$

Se $\lambda_0 = 0$, as duas equações acima nada mais são que duas equações de difusão independentes para as densidades de partículas $a$ e $b$ com condições iniciais dadas por $a(0)=a_0$ e $b(0)=b_0$.

**Relação com equações diferenciais parciais estocásticas (EDPE's)**

A teoria de campo desenvolvida acima às vezes pode ser colocada na forma de equações diferenciais parciais estocásticas, via procedimento de Martin-Siggia-Rose-Janssen-de Dominicis (MSRJD) [64, 65, 66], executado ao contrário. Ao invés de partirmos das EDPE's e obtermos uma teoria de campo equivalente, podemos partir da teoria de campo e obter as EDPE's. Considere a ação (B.38) para o processo $A+A\to\emptyset$. Exceto o termo quártico $\lambda_2\bar{\phi}^2\phi^2$, todos os termos são lineares em $\bar{\phi}$. Porém o termo quártico pode ser linearizado introduzindo o campo auxiliar $\eta$, onde

$$\exp(-\lambda_2\bar{\phi}^2\phi^2) \propto \int d\eta \exp\left(-\frac{\eta^2}{2}\right)\exp(i\eta\sqrt{2\lambda_2}\bar{\phi}\phi). \tag{B.39}$$

Substituindo esta relação na ação teremos três campos que flutuam, $\bar{\phi}$, $\phi$ e $\eta$, mas com a vantagem de a ação ser linear em $\bar{\phi}$. Além disso, realizando a integração funcional em $\mathcal{D}\bar{\phi}$

$$\int \mathcal{D}\eta\, e^{\left(-\frac{\eta^2}{2}\right)} \int \mathcal{D}\phi \int \mathcal{D}\bar{\phi}\, e^{-\int \bar{\phi}(\partial_t - D\nabla^2)\phi + 2\lambda_0\bar{\phi}\phi^2 + i\eta\sqrt{2\lambda_0}\bar{\phi}\phi}$$

cria-se uma função $\delta$ que dá origem à equação

$$\partial_t\phi = D\nabla^2\phi - 2\lambda_0\phi^2 + i\sqrt{2\lambda_0}\eta\phi, \tag{B.40}$$

onde $\eta$ representa uma variável estocástica Gaussiana com

$$\langle\eta(\mathbf{x},t)\rangle = 0$$

e

$$\langle\eta(\mathbf{x},t)\eta(\mathbf{x}',t')\rangle = -2\lambda_0\phi(\mathbf{x},t)^2\delta(\mathbf{x}-\mathbf{x}')\delta(t-t'),$$

uma EDPE com ruido complexo! É razoável que quando o número de partículas diminui, a intensidade do ruído também diminua. Este fato está expresso explícitamente nesta última equação envolvendo o ruido $\eta$ na proporcionalidade direta entre $\langle\eta\eta'\rangle$ e $\phi^2$. O aparecimento do sinal negativo para a correlação do ruído é apenas consequência do fato de $\phi$ ser complexo e, portanto, não poder ser diretamente interpretado como a densidade das partículas, como se poderia supor de início. Existe uma razão física do porquê de não podermos obter um ruido branco real neste problema. Uma dada partícula, uma vez que não aniquilada, terá "varrido" uma área ao seu redor sem qualquer partícula dentro. Desta forma, as partículas devem ser anti-correlacionadas. O campo $\phi$ como uma quantidade flutuante não é a mesma grandeza da densidade de partículas. São os valores esperados de $\phi$ e da densidade de partículas é que são os mesmos. Para vermos isso, vamos calcular a densidade média de partículas denotada por $\bar{n} \equiv \overline{\hat{a}^\dagger\hat{a}}$ :

$$\begin{aligned}
\bar{n} &= \langle 0|e^{\hat{a}}a^\dagger\hat{a}e^{-\hat{H}t}|\psi(0)\rangle \\
&= \langle 0|(1+a^\dagger)e^{\hat{a}}\hat{a}|\psi(t)\rangle \qquad \text{(usando equação } (B.11) \text{ e equação } (B.65)) \\
&= \langle 0|e^{\hat{a}}\hat{a}|\psi(t)\rangle + \langle 0|a^\dagger e^{\hat{a}}\hat{a}|\psi(t)\rangle \\
&= \langle\mathcal{P}|\hat{a}|\psi(t)\rangle \qquad \text{(usando } \langle 0|a^\dagger = 0 \text{ e equação } (A.25))
\end{aligned} \tag{B.41}$$

Agora na formulação de integral de caminho

$$\langle \mathcal{P}|\hat{a}|\psi(t)\rangle = \frac{\int \mathcal{D}\phi\ \mathcal{D}\bar{\phi}\ \phi\ e^{-S}}{\int \mathcal{D}\phi\ \mathcal{D}\bar{\phi}\ e^{-S}} = \langle\phi\rangle. \tag{B.42}$$

Portanto, $\overline{n} = \langle\phi\rangle$. Apesar de o primeiro momento para a densidade de partículas e para o campo serem iguais, isto não é necessariamente válido para momentos maiores. Por exemplo, a densidade média quadrática $\overline{n^2} \equiv \overline{(a^\dagger\hat{a})^2}$ pode ser calculada de maneira análoga ao cálculo de $\overline{n}$ :

$$\begin{aligned}
\overline{n^2} &= \langle 0|e^{\hat{a}}(a^\dagger\hat{a})^2|\psi(t)\rangle \\
&= \langle 0|e^{\hat{a}}a^\dagger \underbrace{\hat{a}a^\dagger}_{=a^\dagger\hat{a}+1} \hat{a}|\psi(t)\rangle \\
&= \langle 0|e^{\hat{a}}a^\dagger(a^\dagger\hat{a}+1)\hat{a}|\psi(t)\rangle \\
&= \langle 0|e^{\hat{a}}(a^\dagger)^2\hat{a}^2|\psi(t)\rangle + \langle 0|e^{\hat{a}}a^\dagger\hat{a}|\psi(t)\rangle \\
&= \langle\mathcal{P}|\hat{a}^2|\psi(t)\rangle + \langle\mathcal{P}|\hat{a}|\psi(t)\rangle, \qquad \text{(usando equação } (B.11)
\end{aligned} \tag{B.43}$$

ou seja,

$$\overline{n^2} = \langle\phi^2\rangle + \langle\phi\rangle.$$

De modo geral, se $\phi$ possui distribuição Gaussiana, como deve ser o caso da difusão pura, então a densidade $n$ deve possuir distribuição de Poisson. Isto é esperado, já que um passeio aleatório simples possui estatística Poissoniana. O efeito das reações é modificar isso. Em certo sentido, o "ruído" $\eta$ em (B.40) representa somente a parte física do ruído que se origina na "discreteza" dos processos de reação. Entretanto, como esta parte do ruído não pode ser verdadeiramente desmembrada do ruído físico "total" que inclui o associado à difusão, não existe necessidade para suas correlações serem positivas.

Existe uma maneira de se obter uma EDPE para a densidade de partículas. Partindo da ação (B.36), aplicamos a transformação não linear de Cole-Hopf $\tilde{\phi} = e^{\tilde{\rho}}$, $\phi = \rho e^{-\tilde{\rho}}$ tal que $\tilde{\phi}\phi = \rho$ com Jacobiano 1. Esta transformação resulta em $\tilde{\phi}\partial_t\phi = \partial_t[\rho(1-\tilde{\rho})] + \tilde{\rho}\partial_t\rho$ e, omitindo contribuições de fronteira, temos $-D\tilde{\phi}\nabla^2\phi = -D\phi\nabla^2\tilde{\phi} = -D\rho[\nabla^2\tilde{\rho} + (\nabla\tilde{\rho})^2]$ para o termo de difusão. O termo de interação fica representado por $-\lambda_0(1-\tilde{\phi}^2)\phi^2 = \lambda_0\rho^2(1-e^{-2\tilde{\rho}}) = 2\lambda_0\tilde{\rho}\rho^2 - 2\lambda_0\tilde{\rho}^2\rho^2 + \cdots$ . Vemos que o termo quadrático em $\tilde{\rho}$ tem agora sinal oposto ao que tinha antes na representação em $\tilde{\phi}$, e portanto corresponde a um ruido real, no lugar do imaginário. Porém, truncar a série em segunda ordem não é justificável e, além disso, descrever a dinâmica do sistema em termos de $\rho$ e $\tilde{\rho}$ através da transformação de Cole-Hopf tem o custo adicional da incorporação de um termo de "ruido de difusão" associado ao acoplamento não linear $-D\rho(\nabla\tilde{\rho})^2$.

Uma conclusão importante que tiramos da discussão acima é que simplesmente escrever as equações de campo médio para a reação de aniquilação e adicionar ruido Gaussiano *real*, como comumente se faz, não necessariamente retorna as EDPE's apropriadas. Outra observação é que a linearização feita em $\bar{\phi}$ requer que este campo apareça quadraticamente na ação e, portanto, apenas reações de duas partículas podem ser escritas em termos de EDPE's. Se a reação for por exemplo da forma $3A \to \emptyset$, não poderemos representar o sistema como um conjunto de EDPE's com ruido multiplicativo.

## B.2. Estados coerentes

Neste apêndice faremos uma breve revisão do conceito de estados coerentes e utilizaremos o oscilador harmônico como exemplo.

Primeiramente poderíamos nos perguntar: o que é um estado coerente? Para responder a esta pergunta, vamos primeiramente relembrar o conceito de pacote de onda de incerteza mínima. O estado de mínima energia do oscilador harmônico quântico é representado por um pacote de onda de incerteza mínima. Para

vermos isso, utilizamos as seguintes representações para os operadores posição $\hat{x}$ e momento $\hat{p}$ em termos dos operadores criação $\hat{a}^\dagger$ e destruição $\hat{a}$ :[‡]

$$x^2 = \frac{\hbar}{2m\omega}(a+a^\dagger)^2 \tag{B.44}$$

e

$$p^2 = -\frac{m\omega\hbar}{2}(a-a^\dagger)^2. \tag{B.45}$$

Como

$$\langle 0|(a+a^\dagger)(a+a^\dagger)|0\rangle = \langle 0|aa^\dagger|0\rangle = 1 \tag{B.46}$$

e

$$\langle 0|(a-a^\dagger)(a-a^\dagger)|0\rangle = -\langle 0|aa^\dagger|0\rangle = -1, \tag{B.47}$$

segue que

$$\langle x^2\rangle\langle p^2\rangle = -\frac{\hbar^2}{4}1(-1) = \frac{\hbar^2}{4}$$

e lembrando que $\langle x\rangle = \langle p\rangle = 0$, temos

$$\langle(\Delta x)^2\rangle\langle(\Delta p)^2\rangle = \frac{\hbar^2}{4}. \tag{B.48}$$

Poderíamos agora perguntar em que circunstância um estado genérico $|n\rangle$ é também representado por um pacote de onde de incerteza mínima. Correspondendo a (B.46) e (B.47) temos

$$\langle n|(a+a^\dagger)(a+a^\dagger)|n\rangle = \langle n|aa^\dagger + a^\dagger a|n\rangle = \langle n|2a^\dagger a + [a,a^\dagger]|n\rangle = 2n+1$$

e similarmente

$$\langle n|(a-a^\dagger)(a-a^\dagger)|n\rangle = -(2n+1),$$

o que implica

$$\langle(\Delta x)^2\rangle_n\langle(\Delta p)^2\rangle_n = \frac{\hbar^2}{4}(2n+1)^2 \tag{B.49}$$

e então $|n\rangle$ não é mínimo. Claramente o fato crucial para que $|0\rangle$ seja de mínima incerteza é

$$a|0\rangle = 0 \qquad \Rightarrow \qquad \langle 0|a^\dagger a|0\rangle = 0.$$

É natural esperar que outros pacotes de onda de incerteza mínima com valores esperados para $x$ e $p$ diferentes de zero sejam ainda autofunções de $a$ :

$$a|\alpha\rangle = \alpha|\alpha\rangle \tag{B.50}$$

o que implica em $\langle\alpha|a^\dagger a|\alpha\rangle = \alpha\langle\alpha|a^\dagger|\alpha\rangle = \alpha\alpha^*\langle\alpha|\alpha\rangle = |\alpha|^2$. É fácil checar que $|\alpha\rangle$ define um pacote de onde de incerteza mínima

$$\langle\alpha|(a+a^\dagger)|\alpha\rangle = (\alpha+\alpha^*)$$

$$\langle\alpha|(a-a^\dagger)|\alpha\rangle = (\alpha-\alpha^*)$$

[‡]Por simplicidade de notação omitiremos de agora em diante o chapéu ˆ dos operadores das equações.

$$\langle\alpha|(a+a^\dagger)(a+a^\dagger)|\alpha\rangle = (\alpha+\alpha^*)^2+1$$

$$\langle\alpha|(a-a^\dagger)(a-a^\dagger)|\alpha\rangle = (\alpha-\alpha^*)^2-1$$

e portanto

$$\langle(\Delta x)^2\rangle_\alpha = \langle x^2\rangle_\alpha - \langle x\rangle_\alpha^2 = \frac{\hbar}{2m\omega}$$

$$\langle(\Delta p)^2\rangle_\alpha = \langle p^2\rangle_\alpha - \langle p\rangle_\alpha^2 = \frac{\hbar m\omega}{2}$$

e, de acordo com as equações acima

$$\langle(\Delta x)^2\rangle_\alpha\langle(\Delta p)^2\rangle_\alpha = \frac{\hbar^2}{4}. \tag{B.51}$$

Assim, os estados $|\alpha\rangle$ definidos por (B.48) satisfazem a condição de incerteza mínima. Eles são chamados de *estados coerentes*.

### B.2.1. Estados coerentes na representação n

Na base $|n\rangle$ o estado coerente se escreve

$$|\alpha\rangle = \sum_n c_n|n\rangle = \sum_n |n\rangle\langle n|\alpha\rangle. \tag{B.52}$$

Como

$$|n\rangle = \frac{(a^\dagger)^n}{\sqrt{n!}}|0\rangle \tag{B.53}$$

temos

$$\langle n|\alpha\rangle = \frac{\alpha^n}{\sqrt{n!}}\langle 0|\alpha\rangle \tag{B.54}$$

e então

$$|\alpha\rangle = \langle 0|\alpha\rangle\sum_{n=0}^{\infty}\frac{\alpha^n}{\sqrt{n!}}|n\rangle. \tag{B.55}$$

A constante $\langle 0|\alpha\rangle$ é determinada por normalização como segue:

$$1 = \sum_n\langle\alpha|n\rangle\langle n|\alpha\rangle = |\langle 0|\alpha\rangle|^2\sum_{m=0}^{\infty}\frac{|\alpha|^{2m}}{m!} = |\langle 0|\alpha\rangle|^2 e^{|\alpha|^2}.$$

Resolvendo esta equação para $\langle 0|\alpha\rangle$ teremos:

$$\langle 0|\alpha\rangle = e^{-\frac{1}{2}|\alpha|^2} \tag{B.56}$$

a menos de um fator de fase. Substituindo em (B.54) obtemos a forma final:

$$|\alpha\rangle = e^{-\frac{1}{2}|\alpha|^2}\sum_{n=0}^{\infty}\frac{\alpha^n}{\sqrt{n!}}|n\rangle. \tag{B.57}$$

Uma expressão útil pode ser obtida usando a forma explícita para $|n\rangle$, equação (B.53):

$$\sum_{n=0}^{\infty} \frac{\alpha^n}{\sqrt{n!}}|n\rangle = \sum_{n=0}^{\infty} \frac{\alpha^n}{n!}(a^\dagger)^n|0\rangle,$$

que implica

$$|\alpha\rangle = e^{-\frac{1}{2}|\alpha|^2+\alpha a^\dagger}|0\rangle = e^{\alpha a^\dagger - \alpha^* a}|0\rangle. \tag{B.58}$$

### B.2.2. Ortogonalidade e relações de completeza

Vamos calcular a sobreposição entre os estados coerentes usando a equação (B.57).

$$\langle\alpha|\beta\rangle = \sum_n \langle\alpha|n\rangle\langle n|\beta\rangle = e^{-\frac{1}{2}|\alpha|^2-\frac{1}{2}|\beta|^2}\sum_n \frac{(\alpha^*\beta)^n}{n!}$$

$$= e^{-\frac{1}{2}|\alpha|^2-\frac{1}{2}|\beta|^2+\alpha^*\beta}. \tag{B.59}$$

Similarmente,

$$\langle\beta|\alpha\rangle = e^{-\frac{1}{2}|\alpha|^2-\frac{1}{2}|\beta|^2+\beta^*\alpha}. \tag{B.60}$$

Então

$$|\langle\alpha|\beta\rangle|^2 = \langle\alpha|\beta\rangle\langle\beta|\alpha\rangle = e^{-|\alpha|^2-|\beta|^2+\alpha^*\beta+\alpha\beta^*}$$

ou

$$|\langle\alpha|\beta\rangle|^2 = e^{-|\alpha-\beta|^2}. \tag{B.61}$$

Como $\langle\alpha|\beta\rangle \neq 0$ para $\alpha \neq \beta$, dizemos que o conjunto $\{|\alpha\rangle\}$ é *supercompleto*[§]. Mas ainda é possível encontrar uma relação de completeza:

$$\int d^2\alpha|\alpha\rangle\langle\alpha| = \int d^2\,\alpha e^{-|\alpha|^2}\sum_{m,n}\frac{(a^*)^n\alpha^m}{\sqrt{n!m!}}|m\rangle\langle n| \tag{B.62}$$

onde $d^2\alpha$ significa somar sobre todos os valores complexos de $\alpha$, integrando sobre todo o plano complexo. Escrevendo $\alpha$ na forma polar:

$$\alpha = re^{i\phi} \qquad \Rightarrow \qquad d^2\alpha = d\phi\,dr\,r, \tag{B.63}$$

obtemos

$$\int d^2\alpha e^{-|\alpha|^2}(\alpha^*)^n\alpha^m = \int_0^\infty dr\,r e^{-r^2}r^{m+n}\int_0^{2\pi} d\phi\, e^{i(m-n)\phi} = 2\pi\delta_{m,n}\frac{1}{2}\int_0^\infty dr^2\,(r^2)^m e^{-r^2}$$

$$= \pi m!\delta_{m,n}.$$

Usando este resultado obtemos finalmente

$$\int d^2\alpha|\alpha\rangle\langle\alpha| = \pi\sum_n |n\rangle\langle n| = \pi,$$

[§]Overcomplete

ou, equivalentemente,

$$\int \frac{d^2\alpha}{\pi}|\alpha\rangle\langle\alpha| = 1. \tag{B.64}$$

## B.3. Prova propriedade de $\langle\mathcal{P}|$

Da definição do operador projeção $\langle\mathcal{P}|$, vem

$$\langle\mathcal{P}|a_i^\dagger = \langle 0|e^{\sum_i \hat{a}_i} a_i^\dagger = \langle 0|e^{\hat{a}_i} a_i^\dagger e^{\sum_{j\neq i}\hat{a}_j}.$$

Agora,

$$\begin{aligned}
e^{\hat{a}}a^\dagger &= [e^{\hat{a}}, a^\dagger] + a^\dagger e^{\hat{a}} \\
&= \left[e^{\hat{a}}, -\frac{\partial}{\partial\hat{a}}\right] + a^\dagger e^{\hat{a}} \\
&= \left[\frac{\partial}{\partial\hat{a}}, e^{\hat{a}}\right] + a^\dagger e^{\hat{a}} \\
&= \frac{\partial}{\partial\hat{a}}e^{\hat{a}} - e^{\hat{a}}\frac{\partial}{\partial\hat{a}} + a^\dagger e^{\hat{a}} \\
&= e^{\hat{a}}\frac{\partial}{\partial\hat{a}} + e^{\hat{a}} - e^{\hat{a}}\frac{\partial}{\partial\hat{a}} + a^\dagger e^{\hat{a}} \\
&= e^{\hat{a}} + a^\dagger e^{\hat{a}} \\
\Rightarrow\quad & e^{\hat{a}}a^\dagger = (1 + a^\dagger)e^{\hat{a}}
\end{aligned} \tag{B.65}$$

Usando este resultado, temos

$$\begin{aligned}
\langle\mathcal{P}|e_i^\dagger &= \langle 0|(1 + a_i^\dagger)e^{\hat{a}_i}e^{\sum_{j\neq i}\hat{a}_j} \\
&= \langle 0|e^{\sum_i \hat{a}_i} \qquad (\text{usando} \quad \langle 0|a_i^\dagger = 0) \\
&= \langle\mathcal{P}|.
\end{aligned} \tag{B.66}$$

Além disso,

$$\langle\mathcal{P}|0\rangle = \langle 0|\left(1 + \sum_i \hat{a}_i + \cdots\right)|0\rangle = 1, \tag{B.67}$$

onde usamos $\hat{a}_i|0\rangle = 0$.

## B.4. Generalização da formulação em integral funcional para $d$ dimensões

Seja $\hat{H}$ o "quase" Hamiltoniano para o processo. Sejam $\hat{a}_i$, $a_i^\dagger$ e $|0\rangle$ o operador de aniquilação, de criação e o estado de vácuo respectivamente. O subscrito $i$ é um marcador que denota o sítio da rede.

A resolução da identidade em termos de estados coerentes para cada rede será

$$\mathbf{1} = \int \left( \prod_i \frac{d^2\phi_i}{\pi} \right) |\{\phi\}\rangle\langle\{\phi\}| \tag{B.68}$$

onde $|\{\phi\}\rangle = \otimes_i |\phi_i\rangle$. A expressão em integral de caminho análoga à equação (B.15) para o caso de dimensão 0 será

$$|\psi(t)\rangle = \lim_{\Delta t\to 0} \mathcal{N}^{-1} \int \left( \prod_{\tau=0}^{t} \prod_i d^2\phi_{i,\tau} \right) |\{\phi\}_t\rangle \left[ \prod_{\tau=\Delta t}^{t} \prod_i \langle\phi_{i,\tau}|e^{-\hat{H}\,\Delta t}|\phi_{i,\tau-\Delta t}\rangle \right] \langle\{\phi\}_0|\psi(0)\rangle \tag{B.69}$$

O operador $\hat{A}$ correspondente a um observável $A(\{n\})$ é obtido substituindo $n_i$ por $a_i^\dagger \hat{a}_i$. O valor esperado análogo a (B.16) será dado por

$$\begin{aligned} \langle A\rangle &= \lim_{\Delta t\to 0} \mathcal{N}^{-1} \int \left( \prod_{\tau=0}^{t} \prod_i d^2\phi_{i,\tau} \right) \langle\{1\}|\hat{A}|\{\phi\}_t\rangle \\ &\quad \times \left[ \prod_{\tau=\Delta t}^{t} \prod_i \langle\phi_{i,\tau}|e^{-\hat{H}\,\Delta t}|\phi_{i,\tau-\Delta t}\rangle \right] \langle\{\phi\}_0|\psi(0)\rangle. \end{aligned} \tag{B.70}$$

O termo do meio na equação de cima é dado por

$$\begin{aligned} \prod_{\tau=\Delta t}^{t} \prod_i \langle\phi_{i,\tau}|e^{-\hat{H}\,\Delta t}|\phi_{i,\tau-\Delta t}\rangle &= \exp\left\{ \frac{1}{2} \sum_i (|\phi_{i,t}|^2 - |\phi_{i,0}|^2) \right\} \\ &\quad \times \exp\left\{ -\sum_{\tau=\Delta t}^{t} \left[ \sum_i \phi^*_{i,\tau}(\phi_{i,\tau} - \phi_{i,\tau-\Delta t}) + \hat{H}(\{\phi^*_\tau\}, \{\phi_{\tau-\Delta t}\})\Delta t \right] \right\}. \end{aligned} \tag{B.71}$$

O primeiro termo em (B.70) será

$$\begin{aligned} \langle\{1\}|\hat{A}|\{\phi\}_t\rangle &= \langle\{1\}|A(\{\phi\}_t)|\{\phi\}_t\rangle \\ &= A(\{\phi\}_t)\langle\{1\}|\{\phi\}_t\rangle \\ &= A(\{\phi\}_t) \prod_i \exp\left\{ -\frac{1}{2} - \frac{1}{2}|\phi_{i,t}|^2 + \phi_{i,t} \right\} \\ &\propto A(\{\phi\}_t) \exp\left\{ \sum_i \left[ -\frac{1}{2}|\phi_{i,t}|^2 + \phi_{i,t} \right] \right\} \end{aligned} \tag{B.72}$$

Assumindo distribuição inicial como sendo *Poisson*, obtemos para o terceiro termo de (B.70):

$$\begin{aligned}\langle\{\phi\}_0|\psi(0)\rangle &\propto \prod_i \exp\left\{-\frac{1}{2}|\phi_{i,0}|^2+\phi^*_{i,0}\bar{n}_0\right\}\\ &\propto \exp\left\{\sum_i\left[-\frac{1}{2}|\phi_{i,0}|^2+\phi^*_{i,0}\,\bar{n}_0\right]\right\}\end{aligned} \tag{B.73}$$

Substituindo as equações (B.71), (B.72) e (B.73) em (B.70) e absorvendo todas as constantes no fator de normalização, teremos

$$\begin{aligned}\langle A\rangle &= \mathcal{N}^{-1}\lim_{\Delta t\to 0}\int\left(\prod_{\tau=0}^{t}\prod_i d^2\phi_{i,\tau}\right)A(\{\phi\}_t)\exp\left\{\sum_i[\phi_{i,t}-|\phi_{i,0}|^2+\phi^*_{i,0}\,\bar{n}_0]\right\}\\ &\quad\times\exp\left\{-\sum_{\tau=\Delta t}^{t}\left[\sum_i\phi^*_{i,\tau}(\phi_{i,\tau}-\phi_{i,\tau-\Delta t})+\hat{H}(\{\phi^*_\tau\},\{\phi_{\tau-\Delta t}\})\Delta t\right]\right\}\\ &= \mathcal{N}^{-1}\int\left(\prod_i\mathcal{D}\phi_i\,\mathcal{D}\phi^*_i\right)A[\{\phi(t)\}]\exp\left\{\sum_i[\phi_i(t)-|\phi_i(0)|^2+\phi^*_i(0)\bar{n}_0]\right\}\\ &\quad\times\exp\left\{-\int_0^t dt'\left[\sum_i\phi^*_i(t')\frac{\partial\phi_i(t')}{\partial t'}+\hat{H}[\{\phi^*(t')\},\{\phi(t')\}]\right]\right\}\\ &= \mathcal{N}^{-1}\int\left(\prod_i\mathcal{D}\phi_i\,\mathcal{D}\phi^*_i\right)A[\{\phi(t)\}]\exp\left\{-S[\{\phi^*\},\{\phi\}]_0^t\right\}\end{aligned} \tag{B.74}$$

onde

$$\begin{aligned}S[\{\phi^*\},\{\phi\}]_0^{t_f} &= -\sum_i[\phi_i(t_f)-|\phi_i(0)|^2+\phi^*_i(0)\bar{n}_0]\\ &+ \int_0^{t_f}dt\left[\sum_i\phi^*_i(t)\frac{\partial\phi_i(t)}{\partial t}+\hat{H}[\{\phi^*(t)\},\{\phi(t)\}]\right]\end{aligned} \tag{B.75}$$

O termo contendo $\phi(0)$ pode ser desprezado da ação já que não temos $\phi^*$ para $t<0$. Assim,

$$\begin{aligned}S[\{\phi^*\},\{\phi\}]_0^{t_f} &= -\sum_i[\phi_i(t_f)+\phi^*_i(0)\bar{n}_0]\\ &+ \int_0^{t_f}dt\left[\sum_i\phi^*_i(t)\frac{\partial\phi_i(t)}{\partial t}+\hat{H}[\{\phi^*(t)\},\{\phi(t)\}]\right]\end{aligned} \tag{B.76}$$

Deslocando o campo $\phi^*$ para $1+\bar{\phi}$, obtemos

$$\begin{aligned}S[\{\phi^*\},\{\phi\}]_0^{t_f} &= -\sum_i[\phi_i(0)+\{1+\bar{\phi}_i(0)\}\bar{n}_0]\\ &+ \int_0^{t_f}dt\left[\sum_i\bar{\phi}_i(t)\frac{\partial\phi_i(t)}{\partial t}+\hat{H}[\{\bar{\phi}(t)\},\{\phi(t)\}]\right]\end{aligned} \tag{B.77}$$

Novamente podemos descprezar o termo $\phi(0)$ e a constante e obtermos

$$S[\{\bar{\phi}\},\{\phi\}]_0^{t_f} = -\sum_i \bar{\phi}_i(0)\,\bar{n}_0 + \int_0^{t_f} dt \left[\sum_i \bar{\phi}_i(t)\frac{\partial \phi_i(t)}{\partial t} + \hat{H}[\{\bar{\phi}(t)\},\{\phi(t)\}]\right] \tag{B.78}$$

**Limite contínuo**

Obtemos o limite contínuo seguindo o seguinte esquema:

$$\begin{array}{l} \sum_i \to \int \frac{d^d x}{h^d} \\ \phi_i(t) \to h^d\ \phi(\mathbf{x},t) \\ \bar{\phi}_i(t) \to \bar{\phi}(\mathbf{x},t) \end{array} \tag{B.79}$$

onde $h$ é a constante da rede.

Vamos assumir que cada processo estocástico elementar que ocorre em cada sítio ocorra em toda a rede e que ainda haja difusão entre os sítios vizinhos. Vamos assumir ainda que as taxas de transição e de difusão são independentes dos sítios. Desta forma, o Hamiltoniano completo pode ser dividido em duas partes como segue:

$$\hat{H} = \hat{H}_{\text{difusão}} + \hat{H}_{\text{reação}}. \tag{B.80}$$

Para um sistema de uma espécie e constante de difusão $D$

$$\begin{aligned} \hat{H}_{\text{difusão}} &= D\sum_{\langle i,j\rangle}(\bar{\phi}_i - \bar{\phi}_j)(\phi_i - \phi_j) \\ &= D\int \frac{d^d x}{h^d}\{h\,\nabla\phi(\bar{\mathbf{x}})\}\cdot\{h\,\nabla\phi(\mathbf{x})\,h^d\}\} \qquad \text{(limite contínuo)} \\ &= Dh^2\int d^d x\,\nabla\bar{\phi}(\mathbf{x})\cdot\nabla\phi(\mathbf{x}) \\ &= -Dh^2\int d^d x\,\bar{\phi}(\mathbf{x})\,\nabla^2\phi(\mathbf{x}) \end{aligned} \tag{B.81}$$

onde no último passo realizamos uma integração por partes e desprezamos os termos de fronteira.

A parte de reação do Hamiltoniano pode ser escrita como

$$\begin{aligned} \hat{H}_{\text{reação}} &= \sum_i \hat{H}'_i \\ &= \int \frac{d^d x}{h^d}\,\hat{H}'(\mathbf{x}) \end{aligned} \tag{B.82}$$

onde $\hat{H}'_i$ é a parte de reação do Hamiltoniano em cada sítio $i$. Substituindo na expressão para a ação, obteremos a ação no limite contínuo

$$\begin{aligned} S[\bar{\phi},\phi] &= -\int \frac{d^dx}{h^d}\,\bar{\phi}(\mathbf{x},0)\,\bar{n}_0 \\ &+ \int_0^{t_f} dt \int \frac{d^dx}{h^d}\left[\bar{\phi}(\mathbf{x},t)\frac{\partial\phi(\mathbf{x},t)}{\partial t}h^d - Dh^{d+2}\,\bar{\phi}(\mathbf{x})\,\nabla^2\phi(\mathbf{x}) + \hat{H}'(\mathbf{x})\right] \\ &= -\int \frac{d^dx}{h^d}\,\bar{\phi}(\mathbf{x},0)\,\bar{n}_0 \\ &+ \int_0^{t_f} dt \int d^dx\left[\bar{\phi}(\mathbf{x},t)\frac{\partial\phi(\mathbf{x},t)}{\partial t} - Dh^2\,\bar{\phi}(\mathbf{x})\,\nabla^2\phi(\mathbf{x}) + \frac{1}{h^d}\hat{H}'(\mathbf{x})\right] \end{aligned} \tag{B.83}$$

Podemos redefinir todas as constantes de modo a absorver todos os fatores de $h$, e assim, obteremos finalmente a ação

$$S[\bar{\phi},\phi]_0^{t_f} = -\int d^dx\,\bar{\phi}(\mathbf{x},0)\,\bar{n}_0 + \int_0^{t_f} dt \int d^dx\left[\bar{\phi}(\mathbf{x},t)(\partial_t - D\nabla^2)\phi(\mathbf{x},t) + \hat{H}'(\mathbf{x})\right]. \tag{B.84}$$

# Referências Bibliográficas


[1] Santos, R. V. and Silva, L. M. 08 2013 *PLoS ONE* **8(8)**, e69131.
(Cited on pages i, iii, and 83.)

[2] Santos, R. V. and Silva, L. M. (2013) *Journal of Theoretical Biology* **335**, 79 – 87.
(Cited on pages i, iii, and 101.)

[3] deOliveira, M. M., Santos, R. V., and Dickman, R. (2012) *Phys. Rev. E* **86**, 011121.
(Cited on pages i, iii, 19, and 20.)

[4] Santos, R. V. and Dickman, R. (2013) *Journal of Statistical Mechanics: Theory and Experiment* **2013(07)**, P07004.
(Cited on pages i, iii, and 31.)

[5] Santos, R. V. The importance of being discrete in sex. Submitted to PLOS ONE (2013).
(Cited on pages i, iii, 53, and 54.)

[6] Santos, R. V. Discreteness induced coexistence. To appear in Physica A (2013).
(Cited on pages i, iii, and 111.)

[7] Plischke, M. and Bergersen, B. (2006) Equilibrium Statistical Physics, World Scientific Publishing Company, Incorporated, .
(Cited on page 1.)

[8] Goldenfeld, N. July 1992 Lectures On Phase Transitions And The Renormalization Group (Frontiers in Physics, 85), Westview Press, illustrated edition edition.
(Cited on page 1.)

[9] Amit, D. (1984) Field theory, the renormalization group, and critical phenomena, World Scientific, .
(Cited on page 1.)

[10] Binney, J. J., Dowrick, N. J., Fisher, A. J., and Newman, M. E. J. (1992) The theory of critical phenomena, Oxford University Press, Oxford.
(Cited on page 1.)

[11] Cardy, J. (1996) Scaling and Renormalization in Statistical Physics, Cambridge University Press, .
(Cited on page 1.)

[12] Parisi, G. (1988) Statistical Field Theory, Frontiers in PhysicsAddison-Wesley, .
(Cited on pages 1 and 2.)

[13] Mussardo, G. (2010) Statistical Field Theory: An Introduction to Exactly Solved Models in Statistical Physics, Oxford Graduate TextsOUP Oxford, .
(Cited on page 1.)

[14] vanSaarloos, W. (2003) *Physics reports* **386(2)**, 29–222.
(Cited on page 1.)

[15] McKane, A. and Newman, T. (2005) *Physical review letters* **94(21)**, 218102.
(Cited on page 1.)

[16] Butler, T. and Goldenfeld, N. (2011) *Physical Review E* **84(1)**, 011112.
(Cited on page 1.)

[17] Lande, R. (1998) *Oikos* pp. 353–358.

(Cited on page 1.)
[18] Dennis, B. (2002) *Oikos* **96(3)**, 389–401.
(Cited on page 1.)
[19] Allee, W. and Bowen, E. S. (1932) *Journal of Experimental Zoology* **61(2)**, 185–207.
(Cited on page 1.)
[20] Allee, W., Park, O., Emerson, A., Park, T., and Schmidt, K. (1949) Principles of animal ecology, WB Saunders London, .
(Cited on page 1.)
[21] Paulsson, J. (2004) *Nature* **427(6973)**, 415–418.
(Cited on page 1.)
[22] Thattai, M. and Van Oudenaarden, A. (2001) *Proceedings of the National Academy of Sciences* **98(15)**, 8614–8619.
(Cited on page 2.)
[23] Negele, J. W. and Orland, H. November 1998 Quantum Many-particle Systems (Advanced Book Classics), Westview Press, .
(Cited on pages 2, 129, and 133.)
[24] Murray, J. (2003) Mathematical Biology II: Spatial Models and Biomedical Applications, Interdisciplinary Applied MathematicsSpringer, .
(Cited on page 3.)
[25] Cantrell, R. and Cosner, C. (2003) Spatial Ecology via Reaction-Diffusion Equations, Wiley Series in Mathematical and Computational BiologyJohn Wiley & Sons, .
(Cited on page 3.)
[26] Toussaint, D. and Wilczek, F. (1983) *The Journal of Chemical Physics* **78**, 2642.
(Cited on page 3.)
[27] Tauber, U. C., Howard, M., and Vollmayr-Lee, B. P. (2005) *J Phys A-Math Gen* **38(17)**, 79.
(Cited on pages 3, 8, 9, 16, 31, and 141.)
[28] Peskin, M. and Schroeder, D. (1995) An Introduction To Quantum Field Theory, Advanced Book ProgramWestview Press, .
(Cited on pages 5, 7, and 10.)
[29] Mattück, R. (1967) A guide to Feynman diagrams in the many-body problem, European physics seriesMcGraw-Hill Pub. Co., .
(Cited on page 7.)
[30] Zinn-Justin, J. (2002) Quantum Field Theory and Critical Phenomena (International Series of Monographs on Physics), Clarendon Press, 4 edition.
(Cited on page 12.)
[31] Gustafson, K. E. July 1997 Introduction to Partial Differential Equations and Hilbert Space Methods, Dover Publications, 3 edition.
(Cited on page 16.)
[32] Cardy, J. (2006) *A+ A* **100**, 26.
(Cited on page 17.)
[33] Peliti, L. Path integral approach to birth-death processes on a lattice Technical report March 1985.
(Cited on pages 20 and 125.)
[34] Gabel, A., Meerson, B., and Redner, S. (2013) *Phys. Rev. E* **87**, 010101.
(Cited on pages 31 and 32.)
[35] Smith, J. and Dawkins, R. (1993) The Theory of Evolution, Canto SeriesCambridge University Press, .
(Cited on page 53.)
[36] Jarne, P. and Auld, J. (2006) *Evolution* **60(9)**, 1816–1824.
(Cited on page 53.)
[37] Eppley, S. and Jesson, L. (2008) *Journal of evolutionary biology* **21(3)**, 727–736.
(Cited on page 53.)
[38] Lehtonen, J., Jennions, M. D., and Kokko, H. (2012) *Trends in ecology & evolution* **27(3)**, 172–178.
(Cited on page 53.)
[39] Meirmans, S., Meirmans, P. G., and Kirkendall, L. R. (2012) *The Quarterly Review of Biology* **87(1)**,

19–40.
(Cited on page 53.)
[40] Otto, S. P. and Lenormand, T. (2002) *Nature Reviews Genetics* **3(4)**, 252–261.
(Cited on page 53.)
[41] Driessens, G., Beck, B., Caauwe, A., Simons, B. D., and Blanpain, C. August 2012 *Nature* **488(7412)**, 527–530.
(Cited on page 83.)
[42] Chen, J., Li, Y., Yu, T.-S., McKay, R. M., Burns, D. K., Kernie, S. G., and Parada, L. F. August 2012 *Nature* **488(7412)**, 522–526.
(Cited on page 83.)
[43] Ishizawa, K., Rasheed, Z., Karisch, R., Wang, Q., Kowalski, J., Susky, E., Pereira, K., Karamboulas, C., Moghal, N., Rajeshkumar, N., et al. (2010) *Cell stem cell* **7(3)**, 279–282.
(Cited on page 83.)
[44] Stewart, J., Shaw, P., Gedye, C., Bernardini, M., Neel, B., and Ailles, L. (2011) *Proceedings of the National Academy of Sciences* **108(16)**, 6468.
(Cited on page 83.)
[45] Vargaftig, J., Taussig, D., Griessinger, E., Anjos-Afonso, F., Lister, T., Cavenagh, J., Oakervee, H., Gribben, J., and Bonnet, D. (2011) *Leukemia*.
(Cited on page 83.)
[46] Sarry, J., Murphy, K., Perry, R., Sanchez, P., Secreto, A., Keefer, C., Swider, C., Strzelecki, A., Cavelier, C., Récher, C., et al. (2011) *The Journal of Clinical Investigation* **121(1)**, 384.
(Cited on page 83.)
[47] Zhong, Y., Guan, K., Zhou, C., Ma, W., Wang, D., Zhang, Y., and Zhang, S. (2010) *Cancer letters* **292(1)**, 17–23.
(Cited on page 83.)
[48] Baker, M. (2008) *Nature* **456(7222)**, 553.
(Cited on page 83.)
[49] Johnston, M., Maini, P., Jonathan Chapman, S., Edwards, C., and Bodmer, W. (2010) *Journal of theoretical biology* **266(4)**, 708–711.
(Cited on page 83.)
[50] Baker, M. (2008) *Nature Reports Stem Cells*.
(Cited on page 83.)
[51] Schatton, T., Murphy, G., Frank, N., Yamaura, K., Waaga-Gasser, A., Gasser, M., Zhan, Q., Jordan, S., Duncan, L., Weishaupt, C., et al. (2008) *Nature* **451(7176)**, 345–349.
(Cited on page 83.)
[52] Boiko, A., Razorenova, O., van deRijn, M., Swetter, S., Johnson, D., Ly, D., Butler, P., Yang, G., Joshua, B., Kaplan, M., et al. (2010) *Nature* **466(7302)**, 133–137.
(Cited on page 83.)
[53] (2011) *Nature Medicine* **17**, 278 – 279.
(Cited on page 83.)
[54] Quintana, E., Shackleton, M., Sabel, M., Fullen, D., Johnson, T., and Morrison, S. (2008) *Nature* **456(7222)**, 593–598.
(Cited on page 83.)
[55] Morrison, S. and Kimble, J. (2006) *Nature* **441(7097)**, 1068–1074.
(Cited on page 83.)
[56] Rapp, U., Ceteci, F., Schreck, R., et al. (2008) *Cell Cycle* **7(1)**, 45.
(Cited on page 83.)
[57] Chaffer, C., Brueckmann, I., Scheel, C., Kaestli, A., Wiggins, P., Rodrigues, L., Brooks, M., Reinhardt, F., Su, Y., Polyak, K., et al. (2011) *Proceedings of the National Academy of Sciences* **108(19)**, 7950.
(Cited on page 83.)
[58] Strauss, R., Hamerlik, P., Lieber, A., and Bartek, J. (2012) *Molecular Therapy*.
(Cited on page 83.)
[59] Hardin, G. et al. (1960) *Science* **131(3409)**, 1292–1297.

(Cited on page 111.)
[60] Gardiner, C. (2009) Stochastic methods: a handbook for the natural and social sciences, Springer series in synergeticsSpringer, .
(Cited on page 111.)
[61] Doi, M. (1976) *J Phys A-Math Gen* **9(9)**, 1479.
(Cited on pages 125 and 128.)
[62] Schulman, L. S. December 2005 Techniques and Applications of Path Integration, Dover Publications, .
(Cited on page 133.)
[63] Fan, H. and Wünsche, A. (2001) *The European Physical Journal D-Atomic, Molecular, Optical and Plasma Physics* **15(3)**, 405–412.
(Cited on page 133.)
[64] Martin, P. C., Siggia, E. D., and Rose, H. A. July 1973 *Physical Review A* **8(1)**, 423+.
(Cited on page 142.)
[65] Janssen, H. (1976) *Zeitschrift für Physik B Condensed Matter* **23(4)**, 377–380.
(Cited on page 142.)
[66] deDominicis, C. (1976) *Le Journal de Physique Colloques* **37(C1)**, 1–1.
(Cited on page 142.)